**Consejo Superior de Investigaciones Científicas (CSIC)**

Instituto de Ciencias de la Tierra "Jaume Almera"-ICTJA-CSIC
Departamento de Estructura, Dinámica de la Tierra y Cristalografía

**Universidad de Barcelona**
Departamento de Geodinámica y Geofísica
Programa de doctorado Ciencias de la Tierra

# Geophysical and petrological characterization of the lithospheric mantle in Iberia and North Africa

Memoria realizada por Alberto Carballo para optar al grado de
Doctor bajo la dirección de los doctores Manel Fernàndez e Ivone Jiménez Munt

Alberto Carballo González

Barcelona, 30 de Abril de 2015

Directores: Tutor:

Dr. Manel Fernàndez Ortiga Dra. Ivone Jiménez-Munt Dr. Juan José Ledo Fernández

*Si no intentamos superar nuestros límites jamás sabremos donde están.*

-Ayrton Senna-

## Agradecimientos

Por fin ha llegado este anhelado momento, un momento el cual durante estos cuatro años y medio no me atrevía ni a imaginar. Heme aquí en la dulce tesitura de trasladar los últimos agradecimientos a todo aquel que durante esta aventura que ya acaba me ha aportado algo y ha ayudado con su presencia.

Sin más dilación, desde la silla que me ha acompañado todo este tiempo (en ocasiones postrado y esclavo), quiero en primer lugar agradecerles a mis directores de Tesis, Manel e Ivone, la oportunidad de poder hacer un Doctorado y su dedicación durante todo este proceso. A Manel, el enseñarme no sólo a ser más exigente conmigo mismo sino con todo, su visión global de la geofísica compartiendo conmigo sus amplios saberes y sus discusiones sobre política para poder entender la idiosincrasia del país. A Ivone, su disponibilidad a la hora de ayudarme, sus enseñanzas en la parte más técnica de programación y su visión más pragmática de todo. Sin vuestra ayuda no hubiese sido posible. En especial quiero dar las gracias a Montse por todo lo que me ha ayudado, enseñado y apoyado. Sin ella tampoco hubiera sido posible. No quiero olvidarme de toda la gente del departamento de Estructura y Dinámica de la Tierra como Jaume, Antonio, Dani y Jordi de los que he tenido la oportunidad de aprender, gracias. También al Consejo en el que he estado trabajando estos años.

A Juanjo Ledo que aceptó la tutoría de un servidor, a la comisión de doctorado y Carles Martín Closas por seguirme durante estos años. A Javier Fullea por acoger a este humilde becario (precario) en Dublín durante casi dos fantásticos meses y por ayudarme a hacer mis primeros pinitos en FORTRAN. A Puy le debo el iniciarme en el mundillo de la geofísica y el empujón para llegar aquí. A David Pedreira que amablemente siempre me echó una mano y también a Juan Carlos Afonso por sus consejos durante estos años y sobretodo por haber desarrollado el código LitMod-2D.

En un alarde de corporativismo (guiño) quiero agradecer especialmente a toda la muchachada del Almera hacer más fácil mi estancia aquí: Xevi, Dario, Silvia, Laura, Steffi, Helena, Chusa, Guiomar, Jose, Marc, Mar, Alba, Giovanni, Mireia, Raquel, Bea, Clara y demás doctorandos que han pasado por el Almera. También a los que ya nos son doctorandos (por no decir muchachada) como Ignacio, Eduard, Sofía, David, Max, Mario, Vinyet… y a los compañeros de Máster.

Huelga decir que es necesario destacar a mis dos compañeros de despacho que han convivido conmigo en esta ardua andadura. A Lavinia, que ha llevado un camino paralelo al mío y ha padecido conmigo las sinrazones de LitMod, grazie mille (manos en posición italiana). A Globig, ese joven teutón venido de la extinta Alemania Oriental al que para describir sus andanzas harían falta dos Tesis como esta, Danke mein Kommunistisch Kamerad.

A mis amigos salmantinos de toda la vida, la vieja guardia, compañeros de fátigas y miles de batallas (y las que quedan), a Manu, Julio, Guille, Zato, Olea, Astu, Nice y Juan, muchas gracias.

A toda la gente de Barcelona que he conocido y tan buenos momentos me han dado: Anye, María, Davids, Nuria, Almen, Jeny, Dani… Y a todo el Munseñ, en nuestra memoria siempre estará la Décima (Liga). Mención aparte para Davids y Juan que me dieron cobijo y un gran recibimiento a mi llegada a la Ciudad Condal. Aquí quiero acentuar la capacidad de vuestro afilado y sibilino sarcasmo a la hora de banalizar todos los problemas, sin él no lo hubiese conseguido.

Mención especial también merece Marta, quién me soporta estoicamente en todos los momentos y que me ha dado paz en una vida de guerra.

Finalmente, quiero agradecérselo especialmente a la famila que es la que más sufre conmigo. A Cris por su apoyo incondicional e inquebratntable, y por estar siempre ahí. A mi padre por su Fé en mi y por todas las horas que ha echado conmigo tanto en el fútbol o enseñándome siempre algo. Y sobretodo, a mi madre porque es mi madre y por haberme inculcado la cultura del esfuerzo.

Muchas gracias a todos por haber formado parte de mis venturas y desventuras durante estos años y en las que he sufrido altibajos, algún tras piés e incluso hartazgo, pero creánme cuando les digo que ahora empieza a compensar.

Alberto Carballo González

Barcelona, 2015.

**Funding**

The author of this thesis benefits from a four-year JAE Pre-CP (2010-00036) fellowship from CSIC between 2010 and 2014. This thesis has been supported by the Topo-Iberia Consolider-Ingenio project and GASAM/TopoMed with reference CSD2006-0004 and CGL2008-03474-E/BTE/07-TOPO-EUROPE-FP-006, respectively.

# CONTENTS


**Prologue** IV

**Summary** V

**Thesis** 1

**Chapter 1: General introduction** 1

1.1. – Motivation and overview 3
1.2. – Methodology 9
1.3. – Geological setting 13
1.3.1. – Variscan domain 13
1.3.2. – Alpine domain 14
1.3.3. – The Central System and adjacent foreland basins 15
1.3.4. – The Betic–Rif orogen and west Mediterranean basins 16
1.3.5. – The Atlas Mountains and the Sahara platform 18
1.3.6. – Neogene and Quaternary volcanism 19
1.4. – Geophysical data 20
1.4.1. – Global geophysical data 20

**Chapter 2: The Pyrenees–Balearic Promontory–Kabyles–Tell–Atlas geo–transect** 23

2.1. – Crustal geometry from previous studies 25
2.2. – Mantle characterization and LAB depth from previous studies 27
2.3. – Results 29
2.3.1. – Lithosphere mantle structure 32
2.3.2. – Temperature and density distribution 33
2.3.3. – Mantle velocity distribution 35
2.4. – Discussion 39
2.4.1. – LAB topography 39
2.4.2. – Changes in mantle composition 41

**Chapter 3: The Cantabrian Margin geo–transect** 45

3.1. – Crustal geometry from previous studies 48
3.2. – Results 55
3.2.1. – Lithosphere mantle structure 56
3.2.2. – Temperature and density distribution 58
3.2.3. – Mantle velocity distribution 59
3.2. – Discussion 61

**Chapter 4: The Cantabrian Mountains–Central System–Betics geo–transect** 63
4.1. – Crustal geometry from previous studies 66
4.2. – Mantle characterization and LAB depth from previous studies 68
4.3. – Results 70
4.3.1. – Lithosphere mantle structure 73
4.3.2. – Temperature and density distribution 73
4.3.3. – Mantle velocity distribution 75
4.4. – Discussion 79
4.4.1. – LAB topography 79
4.4.2. – Changes in mantle composition 81
4.4.3. – Thermal and compositional sub-lithospheric anomalies 82

**Chapter 5: The Iberian Massif–Gibraltar Arc–Atlas Mountains geo–transect** 87

5.1. – Crustal geometry from previous studies 90
5.2. – Mantle characterization and LAB depth from previous studies 92
5.3. – Preliminary results 93
5.3.1. – Lithosphere mantle structure 94
5.3.2. – Temperature and density distribution 97
5.3.3. – Mantle velocity distribution 99
5.4. – Discussion 103
5.4.1. – LAB topography 103
5.4.2. – Changes in mantle composition 104
5.4.3. – Thermal and compositional sub-lithospheric anomalies 105

**Chapter 6: General Discussion** 109

6.1. – Lithosphere structure 111
6.2. – Lithospheric mantle composition 113
6.3. – Anomalous low Pn velocities 116
6.3.1. – Low Pn velocities in the west-Mediterranean basins 116
6.3.2. – Low Pn velocities in the Bay of Biscay 118
6.3.3. – Low Pn velocities beneath the Cantabrian Mountains, composition and densification of the subducting Iberian lower crust 121
6.4. – Thermal and compositional sub-lithospheric anomalies 122

**Chapter 7: Conclusions, limitations and future works** 123

**Limitations and future works** 131
**List of figures and tables** 133
**References** 143

# Prologue

This thesis is organized as a compendium of three scientific articles, published or accepted in peer-reviewed, scientific journals indexed in the "Journal Citation Report" of the Institute for Scientific Information (ISI-JCR). The three articles and one additional in preparation correspond to fourth different geo-transects and describe the lithosphere structure and mantle characterization in the Iberian plate and the western Mediterranean. The 2D models described in this thesis represent the first lithosphere structure combining a thermal and petrological approach in Iberia and in North Africa.

The three articles and the article in preparation form the core of this thesis and constitute the main scientific effort developed therein. These are:

- Carballo, A., Fernandez, M., Torne, M., Jiménez-Munt, I., Villaseñor, A., 2015a. Thermal and petrophysical characterization of the lithospheric mantle along the Northeastern Iberia geo-transect. Gondwana Research, http://dx.doi.org/10.1016/j.gr.2013.12.012.

- Pedreira, D., Afonso, J.C., Pulgar, J.A., Gallastegui, J., Carballo, A., Fernàndez, M., García-Castellanos, D., Jiménez-Munt, I., Semprich, J., 2015. Geophysical-petrological modeling of the lithosphere beneath the Cantabrian Mountains and the North-Iberian margin: geodynamic implications, Lithos (accepted).

- Carballo, A., Fernandez, M., Jimenez-Munt, I., Torne, M., Vergés, J., Melchiorre, M., Pedreira, D., Afonso, J.C., Garcia-Castellanos, D., Diaz, J., Villaseñor, A., Pulgar, J.A., Quintana, L., 2015b. From the Norht-Iberian Margin to the Alboran Basin: a lithosphere geo-transect crossing the Iberian Plate (submitted, under moderate revision).

- Carballo, A., Fernandez, M., Jimenez-Munt, I., Torne, M., Vergés, J., Melchiorre, M., Villaseñor, A. From the Iberia Variscan domain to the Alpine North Africa ranges crossing Gibraltar Arc System: a lithosphere geo-transect. (In prep.).

# Summary

In this thesis, I present a geophysical and petrological study that aims to define the lithosphere structure and the chemical variations in composition of the lithosphere mantle in the Iberian plate, the western Mediterranean and North Africa. In the last decades, several studies have been conducted to unravel the lithospheric structure of Iberia, western Mediterranean, and North Africa using a thermal approach. In this thesis I have compared these previous studies with my results. Also, the low Pn velocities measured in the western Mediterranean basins and in the Bay of Biscay are investigated. Finally, the sub-lithospheric low-velocity anomaly imaged from tomography models in the Iberian plate and North Africa and its possible correlation with the high topography observed in most of the Iberian plate and in the Atlas Mountains is studied.

The present-day lithospheric structure of Iberia and the western Mediterranean region is the result of a complex and puzzling displacement of the Iberian microplate relative to Africa and Eurasia. This movement initiated in early Cretaceous times with the northward propagation of the Atlantic Ocean, and the Alpine collision of the northward moving African plate with stable Eurasia. The succession of these tectonothermal events has probably modified the chemical composition of the lithospheric mantle, as observed at global scale, with relevant implications in the geometry of the crust–mantle and lithosphere–asthenosphere boundaries. Thereby, the present-day crustal and lithospheric mantle structure in Iberia, North Africa and the western Mediterranean is the result of compressional tectonics with collision/subduction in the former Eurasia–Iberia and in the Iberia–Africa plate boundaries, and back-arc extensional tectonics in the Neogene western Mediterranean.

The modeling in the present work is based on an integrated geophysical-petrological methodology combining elevation, gravity, geoid, surface heat flow, seismic and geochemical data. Unlike previous models proposed for the region where the density of the lithospheric mantle is only temperature-dependent, the applied methodology allows calculating seismic velocities and density in the mantle down to 400 km depth from its chemical composition through self-consistent thermodynamic calculations. The model follows a forward scheme in which the crustal and lithospheric mantle geometry, crustal rock properties and mantle chemical composition are predefined. The resulting values are then compared with the measured observables and the crust and lithospheric mantle geometry, as well as the mantle compositions, are modified within their uncertainty ranges until the residual is minimized and the best fit is obtained. The crustal structure is mainly constrained by active-source and passive-source seismic experiments as seismic reflection, wide-angle/refraction seismic profiles or receiver functions and geological cross sections; whereas the upper mantle is constrained by tomography models. This methodology allows us to reproduce the main

trends of the geophysical observables as well as the inferred P-, Pn- and S-wave seismic velocities from tomography models and seismic experiments available for the study region.

I present the crust and upper mantle structure along four geo-transects crossing the NE-Iberian Peninsula, the western Mediterranean basin and the Algeria margin; the Cantabrian margin, the Central System and the Betics orogenic belt; and the southern Central Iberian Zone, the Gibraltar Arc and the Atlas Mountains.

The first geo-transect is a new model on the present-day lithospheric structure along a 1100 km crossing the NE-Iberian Peninsula, the Western Mediterranean basin and the Algeria margin and ending at the Tell–Atlas Mountains. Original seismic data to constrain the crustal geometry come from ECORS—Central Pyrenees (ECORS Pyrenees Team, 1988), ESCI—Catalánides (Gallart et al., 1994), ESCI—Valencia (Vidal et al., 1998), Hinz (1972) and ALE-4 (an industry profile). Five lithospheric mantle compositions are considered including average Phanerozoic and lherzolitic Proterozoic in the continental mainland, and two more fertile PUM (primitive upper mantle) compositions in the Western Mediterranean basin. Also in the Saharan Platform a more depleted composition (tecton incipient or little extension) is suggested. The second profile runs from the North-Iberian Margin to the Duero Basin and it is extended southwards until the Alboran Basin in the third profile crossing the Central System, the Tagus Basin and the Betics orogenic belt. The crustal geometry in the second geo-transect is defined in more detail, and is based on previous works as Gallastegui (2000), and MARCONI-1 seismic refraction and wide-angle reflection data (Ruiz et al., in prep.). In the third geo-transect, the crustal structure in the north is taken and simplified from the second geo-transect. Southwards, I used the Toledo-Salamanca wide-angle seismic survey (Suriñach et al., 1988), the ALCUDIA deep seismic reflection profile (Martinez-Poyatos et al., 2012), the ALCUDIA2 Wide-Angle Seismic Reflection Transect (Ehsan et al., 2014), the works by Banda et al. (1993), Gallart et al. (1995), Comas et al. (1995), Carbonell et al. (1997) and several geological cross-sections (e.g., Banks and Warburton et al., 1991; Casas-Sainz and Faccenna., 2001; Casas-Sainz et al., 2009; Quintana et al., 2015; Banks and Warburton et al., 1991; Berástegui et al., 1998; Michard et al., 2002; Frizon de Lamotte et al., 2004; Platt et al., 2003 and Ruiz-Constán et al., 2012). In this case, I have considered four lithospheric mantle compositions: a predominantly average Phanerozoic in the continental mainland, two more fertile compositions in the Alboran Sea and in the Calatrava Volcanic Province, and a hydrated uppermost mantle in the North-Iberian Margin. In the fourth geo-transect, the seismic studies used are the ALCUDIA wide-angle seismic reflection transect (Ehsan, 2014), La Línea-Carmona refraction seismic experiment (Medialdea et al., 1986), RIFSIS wide-

angle seismic reflection (Gil et al., 2014), SIMA wide-angle reflection seismic experiment (Ayarza et al., 2014) and Marismas cross-section (Berástegui et al., 1998). I defined three distinct chemical lithospheric mantle domains: a predominantly average Phanerozoic composition in the continental mainland, and two rather fertile mantle compositions beneath the volcanic areas close to the Calatrava Volcanic Province and the Atlas Mountains. Mantle petrology affects the resulting density distribution and LAB (lithosphere–asthenosphere boundary) geometry and allows a direct comparison with tomography models and seismic data. The chosen compositions are compatible with the global geochemical xenolith data and the tectonothermal age of the different domains. Indeed, the different mantle compositions result in moderate differences of relevant observables as P-wave seismic velocities and densities.

The obtained LAB geometries show large variations in lithospheric mantle thickness. Deepest LABs are found below the Pyreenes, Cantabrian Mountains, Betic Cordillera and Strait of Gibraltar while the shallowest LAB is reached in the Mediterranean basins (Valencia Through, Balearic Promontory, Algerian Basin and Alboran Basin). The LAB depth beneath the Iberia Meseta is deeper than in previous studies, shallowing in the Calatrava Volcanic Province, and also beneath the Atlas Mountains as proposed from previous studies. Several processes may cause low velocities in the uppermost mantle that are not included in our modeling approach. Measured low Pn velocities can be explained by either serpentinization and/or seismic anisotropy and only partly, by transient thermal effects. I assumed that a variable thick hydrated layer, in which I have increased the water content to as much as 1%, characterizes the uppermost mantle in the Western Mediterranean basin and the Bay of Biscay regions. Anisotropy is also a possible cause of mismatch between calculated and observed seismic velocities, particularly when the fast polarity direction is perpendicular to the model transect.

Finally, our numerical approach assumes thermal steady-state and therefore tends to underestimate the temperature prevailing at shallow levels of the lithospheric mantle and overestimate it at deeper lithospheric levels in order to maintain the same buoyancy than a linear steady-state geotherm. The sub-lithospheric negative anomaly imaged in tomography models below the Iberian plate and the Atlas Mountains, is related to the high mean topography in these areas and can be partly consistent with a low-velocity/high-temperature/low-density modelled layer in the sublithospheric mantle. The negative velocity anomaly, beneath the CVP and the Atlas, which extends along the Iberian Plate, is interpreted as a positive thermal anomaly with the same composition as the sub-lithospheric mantle. The detached/torn lithospheric slab beneath

the the Gibraltar Arc is modelled as a high-velocity/high-density/low-temperature lithospheric mantle body with a negative buoyancy.

# Chapter 1: General Introduction

# 1.1. – Motivation and overview

The present lithospheric structure of the Iberian Peninsula (hereinafter referred as Iberia), the north margin of Africa and the western Mediterranean region developed from the interplay of consecutive geodynamic processes related to the Early Jurassic opening of the Betic-Rif corridor between the Central Atlantic and the Ligurian-Tethys oceans. Later on, took place the opening of the North Atlantic along the western margin of Iberia, and the Early Cretaceous opening of the Bay of Biscay and Pyrenees. Finally, the Late Cretaceous to Present convergence of Africa and Europe, triggered the total consumption of the Ligurian-Tethys Ocean. As a consequence of this protracted convergence phase, compression took place along the plates boundaries and the interior of the Iberia, resulting in the Cantabrian-Pyrenees and Gorringe-Betics-Rif-Atlas systems, and significant intraplate deformation (e.g., Dercourt et al. 1986, Banks and Warburton, 1991; Casas and Faccenna, 2002; Vergés and Fernandez, 2006; De Vicente et al., 2008).

From latest Cretaceous to Oligocene times shortening accommodated mainly along the Bay of Biscay–Pyrenees plate boundary, generating crustal-scale thrusts in the Pyrenees-Cantabrian Mountains but also in the inner part of the plate (Iberian Chain and Central System) as well as in the Betic-Rif and Atlas systems. While in north Iberia convergence was the predominant deformation mechanism lasting until the late Oligocene-Early Miocene, from Oligocene times onward, the convergence between Africa and Eurasia was responsible for coeval compression and extension along the southern and eastern Iberian margins. This convergence gave rise to the formation of the Betic–Rif orogenic system (this area encompassing the Alboran Basin, the Betic and Rif orogens, and the Gulf of Cadiz) and the Valencia Trough - Balearic Promontory - Algerian Basin system, both related to subduction and further slab retreating of the Ligurian-Tethys domains (e.g., Torne et al., 1996; Gueguen et al., 1998; Vergés and Sabat, 1999; Rosenbaum et al., 2002; Faccenna et al., 2004; Spakman and Wortel, 2004; Vergés and Fernandez, 2012). The north African margin in Algeria, presently under compression (Stich et al., 2003; Deverchere et al., 2005; Domzig et al., 2006), is formed by the piling up of metamorphic slices corresponding to the Kabylies and thrusting sheets of Mesozoic and Tertiary sediments in the Tell–Atlas region (e.g., Frizon de Lamotte et al., 2000; Mauffret, 2007).

As a result, Iberia is characterized by different geological units (e.g., Vera, 2004; Vergés and Fernàndez, 2006; Fig. 1). The western Iberia corresponds to the Variscan Iberian Massif (VIM), which is mainly made up of metasediments and granitic rocks that are Precambrian and Palaeozoic in age. In turn, the eastern Iberia is formed by thick

Mesozoic sedimentary sequences inverted during the Alpine orogeny, which may incorporate Paleozoic basement, and the associated foreland basins. The eastern and southern margins of Iberia were affected by coeval extension and compression during the Neogene, giving rise to intramontanous basins and the present Iberian-Mediterranean margin. Considerable volcanic activity, with magmas characterized by calc-alkaline and alkaline affinities, developed from Early Miocene to Pliocene and Quaternary times along the Mediterranean border, affecting onshore and offshore areas (e.g., Torres-Roldan et al., 1986; Ancochea and Nixon, 1987; Martí et al., 1992; Cebria and Lopez-Ruiz, 1995; Turner et al., 1999; Villaseca et al., 2010). The northern motion of Africa towards Europe has produced very different structures focused on a limited area: the southwestern region of the Iberian Peninsula, which underwent a long and complex geodynamic evolution, characterized by the transition from the stable Variscan Iberian Massif to the Betic-Rif orogenic system; the subsiding Alboran Basin surrounded by the Betic Orogen in the north and the Rif mountains in the south with its apex at the Gibraltar Strait; a subducting lithosphere slab beneath the Betic-Rif orogenic system; and finally, the intraplate Atlas Mountain Chain with a topography exceeding the one expected from the estimated shortening. The entire region is affected by shallow, intermediate and even deep seismic activity (Buforn and Coca, 2002; Hatzfeld and Frogneaux, 1981; Lopez Casado et al., 2001; Ramdani, 1998). Recently, some authors (e.g. Anguita and Hernán, 2000; Duggen et al., 2004; Duggen et al., 2009) claimed, that the adjacent Atlas Mountains were included in the Betic-Rif orogenic system. Volcanic activity has been widespread in Iberia and North Africa. The origin of the high topography in the Atlas in a context of limited orogenic deformation/shortening, together with observed alkaline volcanism, intermediate depth seismicity, and high heat flow are major subjects of study. Besides old Tertiary volcanism in North Africa, most of the volcanic activity is younger and took place during the Miocene (middle to late) and Pliocene and it is still ongoing. The oldest extrusive, found in the High Atlas, are basalts associated with Mesozoic rifting (Duggen et al., 2004). In the Calatrava Volcanic Province (CVP), one of the three most important areas with recent volcanic activity in the Iberian Peninsula, together with those of Olot and Cabo de Gata, the magmas are characterized by calc-alkaline and alkaline affinities, developed from Early Miocene to Pliocene and Quaternary times (e.g., Torres-Roldan et al., 1986; Ancochea and Nixon, 1987; Martí et al., 1992; Cebria and Lopez-Ruiz, 1995; Turner et al., 1999; Villaseca et al., 2010).

The superposition of all these tectonothermal episodes resulted in large lateral variations of the crust and lithospheric mantle thickness. Thereby, the present-day crustal and lithospheric mantle structure in Iberia, the western Mediterranean and N-Africa is the result of compressional tectonics with collision/subduction in the former

Eurasia–Iberia and in the Iberia–Africa plate boundaries, and back-arc extensional tectonics in the Neogene western Mediterranean. This complex tectonic evolution affected Paleozoic, Mesozoic and Tertiary domains. The succession of the tectonothermal events has probably modified the chemical composition of the lithospheric mantle as observed at global scale (e.g., Poudjom Djomani et al., 2001; Griffin et al., 2009) with relevant implications in the geometry of the crust–mantle and lithosphere–asthenosphere boundaries. Up to date however, a quantified thermal and petrophysical characterization of the lithospheric mantle in Iberia, N-Africa and western Mediterranean consistent with the tectonothermal evolution of the region has not been attempted.

Whereas the crustal structure is well defined from the numerous seismic surveys and combined seismic and gravity models (e.g., ECORS Pyrenees Team, 1988; Gallart et al., 1994; Vidal et al., 1998; Roca et al., 2004; Álvarez-Marrón et al., 1997; Ruiz et al., in prep.; Ehsan et al., 2014; Banda et al., 1993; Gil et al., 2014; Ayarza et al., 2014 and references therein), the depth to lithosphere–asthenosphere boundary (LAB) remains more uncertain due to the lack of direct observables and its more elusive definition (Eaton et al., 2009; Fischer et al., 2010). In the last decades, several studies have been conducted to unravel the lithospheric structure of Iberia and its margins using a thermal approach (e.g., Zeyen and Fernandez et al., 1994; Torne et al., 2000; Tejero et al., 2002; Ayarza et al., 2004; Fernandez et al., 2004; Roca et al., 2004; Frizon de Lamotte et al., 2004; Fullea et al., 2007; Palomeras et al., 2011; Torne et al., 2015). However, these models are based on a pure thermal approach in which the density of the lithospheric mantle is only temperature dependent and related to the density of the asthenosphere that, in turn, is considered constant everywhere (Lachenbruch and Morgan, 1990). A major caveat of this approach is the lack of full consistency with the petrophysical properties of the mantle (density and elastic parameters) and therefore, the obtained results cannot be properly compared with seismic data or tomography models. In addition, the contribution of chemical composition and phase transitions on the density and buoyancy of the lithospheric mantle and therefore, on the resulting lithospheric structure (Afonso et al., 2008; Fullea et al., 2010) are not accounted for.

Recently, Afonso et al. (2008) presented a new 2D integrated geophysical–petrological methodology that allows studying the thermal, compositional, density and seismological structure of the upper mantle down to 410 km depth. The method uses a self-consistent thermodynamic–geophysical framework, in which all relevant properties are functions of temperature, pressure, and mineral composition allowing for the incorporation of lateral compositional variations in the lithospheric mantle and for the direct comparison with seismic data and tomography models. This methodology was

further developed in 3D and applied to characterize the upper mantle structure in the Betic-Rif-Atlas system (Fullea et al., 2010).

In this thesis, I present the crust and upper mantle structure in Iberia, the Western Mediterranean and the north of Africa along four lithospheric geo-transects using the LitMod-2D finite-element code developed by Afonso et al. (2008) (Fig. 1.1). (1) The first lithospheric geo-transect along a 1100 km long profile begins with a N–S trend crossing the southern part of the Aquitanian Basin, the Pyrenees and the northern part of the Eastern Ebro Basin. Then it continues with a NNW–SSE direction to cross perpendiculary the main tectonic structures as the southern part of the Eastern Ebro Basin, the Catalan Coastal Ranges, the Valencia Trough Basin, the Balearic Promontory, the Algeria Basin, the North African margin, the Kabylies, and ending at the Tell–Atlas mountain range. (2) The second profile is a N-S crustal transect across the Central Cantabrian Mountains and the North-Iberian margin. (3) The third profile images the crust and upper mantle structure along a 1065-km-long transect, crossing the entire Iberian plate in N-S direction, by using a modified version of the LitMod-2D code (Afonso et al., 2008). To be consistent, the transect includes the second profile with a more simplified custal structure and rock properties extending towards the Central System, the Tagus (or Tajo) Basin, and the Betic Cordillera (hereinafter Betics), ending in the Alboran Basin. (4) The last profile is a ~1110-km-long geo-transect that runs from southwestern Variscan Iberian Massif in the Eurasian plate, crossing the Gibraltar Strait and the Atlas Mountains. In order to study the mantle structures of these geo-transects I combined seismological, petrological and geochemical constraints. A common observation in the Bay of Biscay, the Valencia Trough and the Algerian Basin is the low Pn-velocity values obtained in seismic experiments. With this approach, theoretical upper mantle velocities can be compared with the results of the ESCIN-4 and MARCONI-1 seismic profiles in the Bay of Biscay, which revealed P-wave velocities of 7.8-7.9 km/s beneath the Moho in the margin, being as low as 7.7-7.8 km/s in the mantle wedge above the subducting Iberian crust (Fernández-Viejo et al., 1998; Ruiz et al., 2007). In the western Mediterranean basins (Valencia Trough and Algerian Basin), the seismic experiments show low Pn-velocities which range from 7.7 to 7.95 km/s (Torne et al., 1992; Dañobeitia et al., 1992; Vidal et al., 1998; Grevemeyer, pers. comm.) and a noticeable seismic anisotropy, which amounts up to 4.5% and shows almost orthogonal fast polarization directions (FPD) in both basins (Díaz et al., 2013).

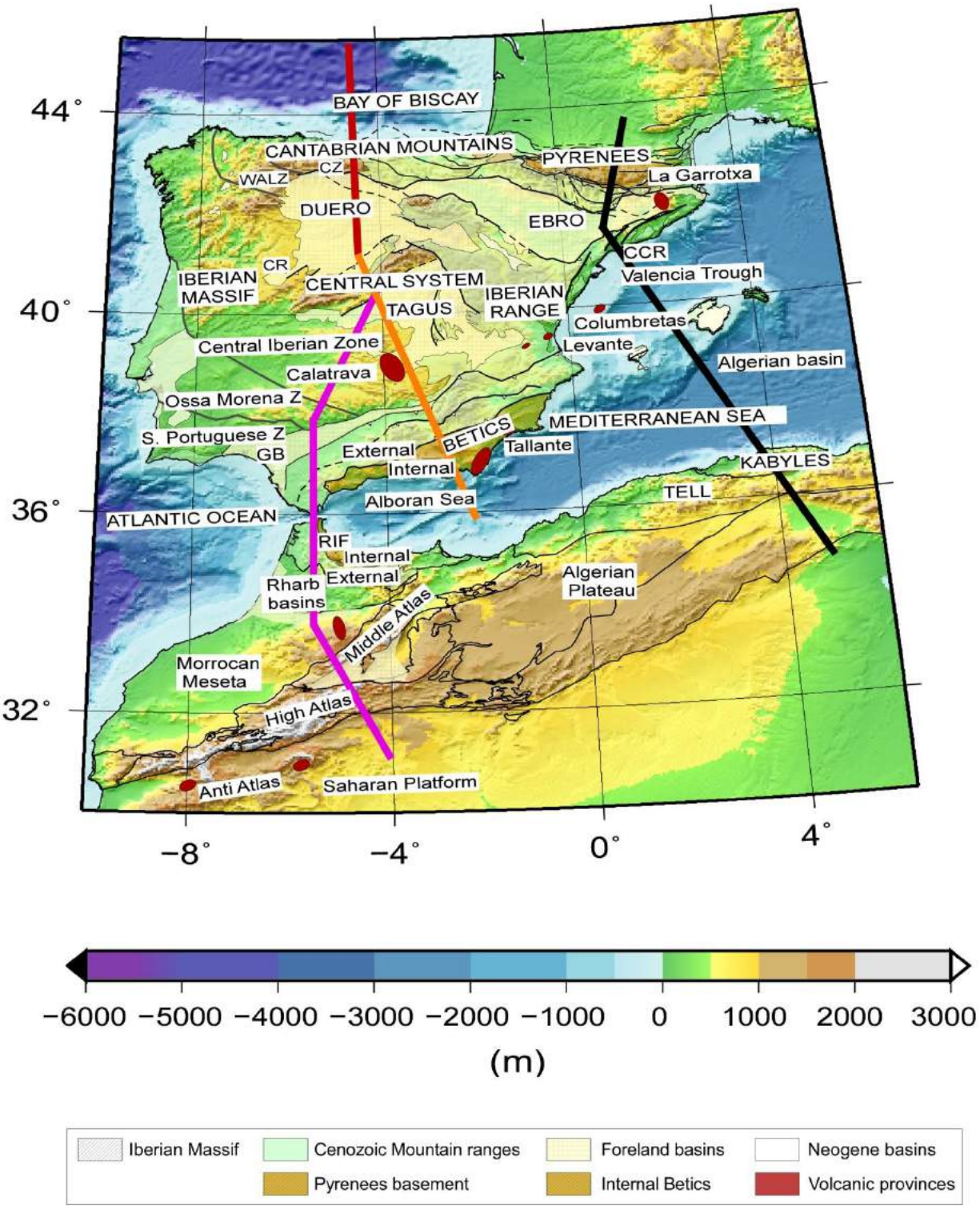


Figure 1.1: Geological map of the study area showing the principal geological domains of Iberia and North Africa. Thick lines locate the modeled transects: Black line-first geo-transect; Red line-second geo-transect; Orange line-third geo-transect and pink line-fourth geo-transect. WALZ, west Asturian-Leonese Zone; CZ, Cantabrian Zone; CCR, Catalan Coastal Ranges; CR, Ciudad Rodrigo Basin, located in the SW side of the Duero Basin; GB, Guadalquivir Basin.

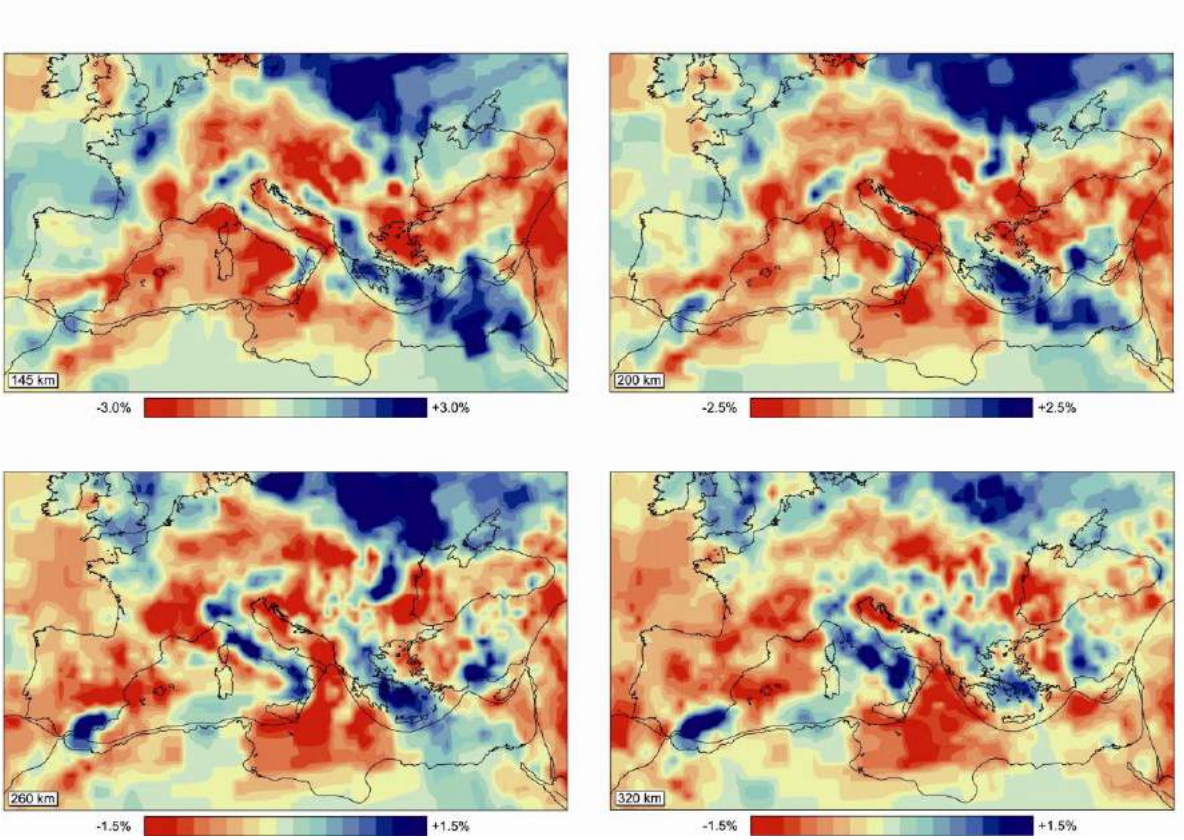


Figure 1.2: P-wave anomaly of the western-Mediterranean region from the tomography model of Villaseñor et al., 2003 for different depths (145, 200, 260 and 320). Shown are P wave seismic velocity anomalies relative to the 1-D reference model ak135 of Kennett et al. (1995). The blue anomaly under the Rif-Gibraltar-Betic (RGB) (southern Iberia) is the image of the slab. Courtesy by A. Villaseñor.

Low P-wave upper mantle velocities in extensional regions have been traditionally interpreted in terms of compositional crust–mantle transition, and underplating (e.g., Morgan and Ramberg, 1987; Collier et al., 1994; Thybo and Artemieva et al., 2014) but effects of anisotropy, thermal disequilibrium and presence of water in the uppermost mantle have not been fully considered in these basins.

Another important observation is the fast velocity anomaly beneath the westernmost Alboran Basin-Gibraltar Arc in the uppermost mantle and surrounding slower velocities below the Iberian plate and the Atlas Mountains. The fast velocity anomaly has been interpreted in terms of a lithospheric slab originated by any of the proposed mechanisms by different authors (e.g., Bezada et al., 2013; Bijwaard and Spakman, 2000; Garcia-Castellanos and Villaseñor, 2011; Calvert et al., 2000; Monna et al., 2013; Piromallo and Morelli, 2003; Schmid et al., 2008) (Fig. 1.2).

In this context, the aims of this thesis are:

(1) To investigate the lithospheric thickness variation in Iberia, in its eastern margin

and in North Africa where the geological structures have been affected by the Alpine orogeny, by combining seismological, petrological and geochemical constraints.

(2) To analyze possible variations in the composition of the upper mantle, compatible with seismic data and tomography models.

(3) To decipher the still unresolved origin of the observed low uppermost mantle Pn velocities beneath the Valencia Trough, Algerian basins and Bay of Biscay, and the range of scenarios that may explain the low seismic velocities observed beneath the crust in the continental margin.

(4) To investigate the effects of sublithospheric mantle perturbations of thermal and/or compositional origin imaged by tomography models, and to correlate them with the still unresolved high topography observed both in the Iberian plate and in the Atlas Mountains.

In summary, this thesis will help to better understand the upper mantle structure and composition of Iberia, North Africa and the western Mediterranean, and the interpretation of the mantle seismic velocity anomalies imaged by tomograghy models and seismics experiments. Also, this thesis is addressing the question of the high elevation found in the study area and their relation to the sub-lithospheric seismic anomalies imaged from the tomography models.

This thesis has been structured in seven chapters:

- The first chapter (this chapter) illustrates the motivation and the objetives and also introduces a brief review of the study area from a geological and geophysical point of view.
- The second, third, fourth and fifth chapters deal with the general results in the study area. Each chapter is dedicated to the present-day crustal and upper mantle structure resulting for each geo-transect.
- The sixth chapter is a general discussion of the results obtained from the modeled geo-transects in the context of the different geodynamic areas.
- Chapter seventh summarizes the main conclusions from the previous chapters and outlines the possible future work.

## 1.2. – Methodology

The methodology used in this work is based on the LitMod-2D code (Afonso et al., 2008), which combines geophysical and petrological data to study the crust and

upper mantle structure from a thermal, compositional, seismological and density point of view, within a self-consistent thermodynamic-geophysical framework. The code allows calculating the 2D distribution of temperature, density and mantle seismic velocities down to 400 km depth and the surface heat flow, elevation, and gravity and geoid anomalies. The model follows a forward scheme in which the crustal geometry is constrained from previous seismic studies, and the lithosphere mantle geometry and composition are changed according to the geodynamic setting, xenolith data and tomography models until the best fit is reached (Fig. 1.3).

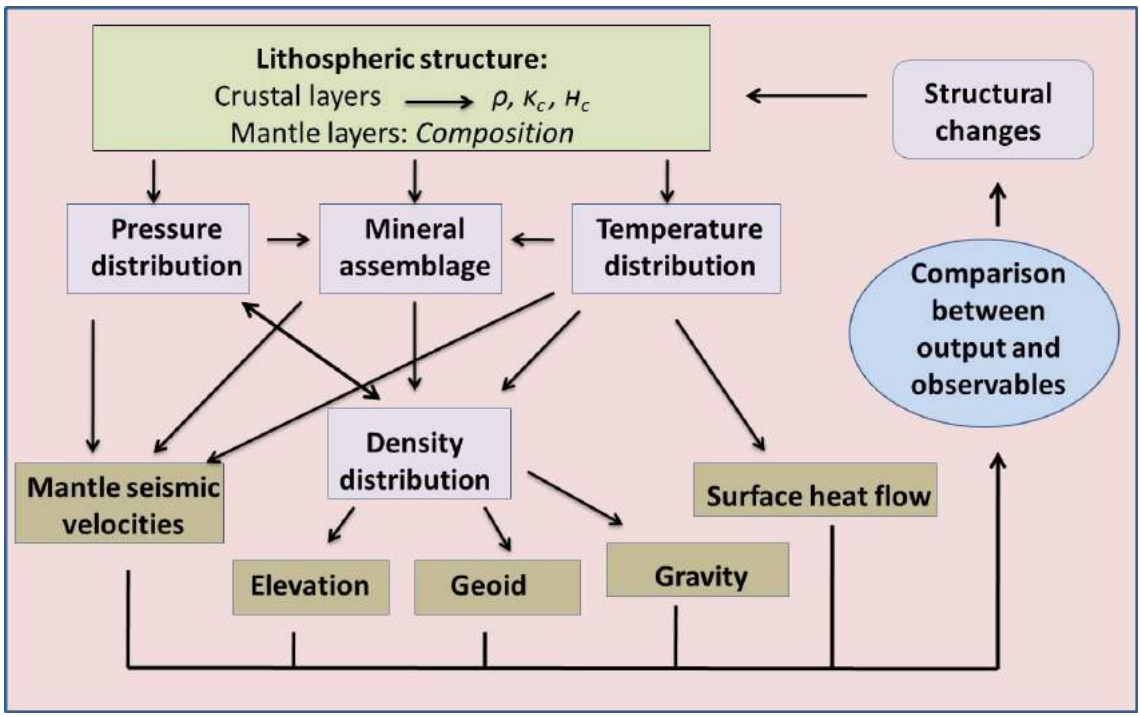


Figure 1.3: Flowchart indicating the general modeling procedure used in LitMod.

A comparison of model outputs against observed data is used to obtain a lithospheric/sublithospheric model that simultaneously fits all geophysical and petrological observables, and consequently reduces the uncertainties associated with previous thermal approaches. The different crustal and mantle bodies of the model are defined in cross-section and a mesh of triangular finite elements is automatically adjusted to fit their geometry. Each mantle body in LitMod-2D is characterized by its main oxides composition (in weight %) within the $Na_2O$-CaO-FeO-MgO-$Al_2O_3$-$SiO_2$ (NCFMAS) system. Stable mineral assemblages are determined through self-consistent thermodynamic calculations via Perplex (Connolly, 1990; Connolly, 2005) and thus, physical properties of each mineral and of the bulk mantle (density, thermal expansion coefficient, elastic parameters, and thermal conductivity) depend not only on

temperature as in previous methodologies, but also on pressure, composition, and phase changes.

Once the bulk physical properties are determined for each mantle composition, gravity, geoid, elevation, surface heat-flow and P- and S-seismic velocities are computed and compared with observations. In this work, an augmented-modified version of the Holland and Powell (1998) (revised in 2002) thermodynamic database is used, which takes into account all major phases relevant for the continental crust (Afonso and Zlotnik, 2011). Anelastic effects are computed as a function of the grain size, oscillation period, P-T conditions, and empirical parameters (Afonso et al., 2008 and references therein). In this study, I selected a grain size of 5 mm and an oscillation period of 75 s. The heat transport equation is solved by using the finite elements method in steady-state with the following boundary conditions: 0 ºC at the surface; 1330 ºC at the LAB; and no heat flow across the lateral boundaries of the model. Below the LAB, the algorithm considers a 40 km thick thermal buffer with a temperature of 1400 ºC at its base. This is done to avoid unrealistic discontinuities between a conductive thermal gradient within the lithospheric mantle and an adiabatic thermal gradient within the asthenosphere. The temperature at the base of the model (400 km) is set to 1520 ºC. The temperature gradient below the thermal buffer layer is restricted to $0.35 < dT/dz < 0.50$ ºC/km, otherwise the temperature at 400 km depth is modified accordingly (see Afonso et al., 2008 for further details). From the calculated densities for each element of the mesh, free air and Bouguer gravity anomalies in two dimensions are calculated using the algorithm for polygonal bodies of Talwani et al. (1959). The calculation of the geoid height is done following the 2.5D method outlined in Zeyen et al. (2005), such that

$$\Delta N = \frac{G.\rho}{g_0} \int_{x_1}^{x_2} \int_{y_1}^{y_2} \int_{z_1}^{z_2} \frac{1}{\sqrt{x^2 + y^2 + z^2}} dz\, dy\, dx$$

where $\Delta N$ is the geoid anomaly, G is the gravitational constant, $g_o$ is the normal gravity acceleration at the Earth's surface and x, y, and z the coordinates of the prism boundaries. According to the principle of isostasy, all regions of the Earth must have a compensation level where the pressure does not vary laterally. Here, it is assumed that the level of compensation is located at the base of the model, roughly coinciding with the 410-km discontinuity. In principle, absolute elevation is computed under the assumption of local isostasy considering a reference column corresponding to a mid-ocean ridge (Afonso et al., 2008). The final formulae that LitMod solves to obtain absolute elevation are similar to those of Lachenbruch and Morgan (1990), where the elevation above ($E_a$) and below ($E_b$) the sea level are given respectively, by

$$E_a = \int_{L_{top}}^{L_{bottom}} \frac{\rho_b - \rho_l(z)}{\rho_b} dz - \text{II}$$

$$E_b = E_a \frac{\rho_b}{\rho_b - \rho_w}$$

where $L_{top}$ is taken at the top of the column, $L_{bottom}$ is taken at the bottom of the column, $\rho_b$ (assumed constant) is the density of the mantle at 400 km depth, $\rho_l(z)$ is the depth-dependent density, $\rho_w$ is the density of seawater (=1030 kg $m^{-3}$), and II is a calibration constant.

In the second, third and fourth profiles the calculation of elevation with flexural support is incorporated. There are deviations from the local isostasy model that are compensated with a flexural isostatic model to evaluate whether they can result in significant topography misfits. Vertical loads relevant to flexure are computed from the lateral changes in lithostatic pressure at the base of the model (400 km depth) resulting from the derived crust and upper mantle structure. Note that a constant pressure at the base of the model implies that the whole transect is under perfect local isostasy. To calculate the deflection from the vertical load distribution, I use an updated version of the code tAo (Garcia-Castellanos et al., 2007). The deflection or vertical displacement of each column, associated with the vertical load, is calculated for a prescribed elastic thickness distribution $T_e$. Larger $T_e$ values smooth out larger wavelengths of these vertical displacements, reducing the misfit between the model and the observed topography. See Jiménez-Munt et al. (2010) for details about flexural calculation.

Some modifications have been incorporated to the LitMod-2D (used in the third and fourth profiles) code to improve the mantle thermal conductivity calculations and to incorporate sub-lithospheric mantle anomalies. In the first modification, the radiative contribution to lattice thermal conductivity, as described in Grose and Afonso (2013) is added. In the second modification, I consider thermal, compositional, or thermo-compositional anomalies relative to the surrounding sub-lithospheric mantle to explain seismic velocity anomalies imaged by tomography models. In the case of thermal anomalies, the code assigns to the anomalous zone(s) the same composition as given to the asthenosphere (usually Primitive Upper Mantle, PUM), and recalculates the relevant physical parameters (density, seismic velocity, phase changes, and thermal conductivity) at P and T+ΔT conditions, ΔT being the prescribed temperature anomaly relative to the surrounding mantle. When the anomaly is compositional, the code calculates the relevant physical parameters at the P-T conditions, considering the prescribed chemical composition. Thermo-compositional anomalies can be related to lithospheric mantle bodies that have been detached and sunk into the asthenosphere and therefore, having a

different temperature and composition than the surrounding asthenosphere. These sub-lithospheric anomalies can be coupled, when the density anomaly is transmitted to surface elevation, or decoupled, when density anomalies are not transmitted to surface elevation. Therefore, decoupled anomalies do not have effects on calculated isostatic topography but they do on gravity and geoid calculations.

To avoid abrupt and unrealistic discontinuities at the LAB, I have added a compositional "buffer" at the base of the lithosphere with an intermediate composition between the subcontinental lithospheric mantle and the Primitive Upper Mantle.

# 1.3. – Geological setting

For simplicity and to facilitate comprehension of the complex tectonic scenario of the study region, in this section I describe the geological characteristics of the main morphotectonic units relevant to the modeled transects in the study area. The reader is referred to Gibbons and Moreno (2002); Vera et al. (2004); and Vergés and Fernandez (2006), and references therein for a more general description of the geology of the Iberian Peninsula, North Africa and the western Mediterranean.

## 1.3.1. – Variscan domain

The Variscan Belt, represented by the Iberian massif in the study area, is the result of the collision of several continental blocks formed by the Early Paleozoic fragmentation of a Late Proterozoic supercontinent (Mc Kerrow et al., 2000). The Avalonian plate, one of the continental fragments, was accreted in Ordovician-Silurian times to the Laurentian continent (Caledonian Orogeny). Later on, in Devonian-Carboniferous times, the Armorican fragment (Matte et al., 2001) and the Gondwanan continent collided with the Avalonian border of Laurentia, resulting in the Variscan Orogenic Belt and the Late Paleozoic Pangea (Matte, 1986, 2001). The tectonic units forming the present Iberian Massif are: the Cantabrian Zone, the West Asturian Leonese Zone (WALZ), the Galicia Tras-Os-Montes Zone (GTMZ), the Central Iberian Zone (CIZ), the Ossa-Morena Zone (OMZ), and the South Portuguese Zone (SPZ). The Cantabrian Zone (CZ) and the South Portuguese Zone (SPZ) represent opposite foreland fold and thrust belts of the orogen (to the north and to the south respectively). The Galicia Tras-Os-Montes Zone, in the northwestern part of the Iberia, consists of a pile of allochthonous tectonic units with high-pressure metamorphism and rocks including

ophiolites (Arenas et al., 1986, 1997 and Ribeiro et al., 1990a). The suture is placed beneath the mafic and ultramafic complexes of this zone, and is rooted towards the Atlantic margin (Matte, 1986 and Martınez Catalan et al., 1997). In the northern and the southern boundaries of the Ossa-Morena Zone (OMZ), two contacts of probable suture character have been recognized. The suture between the OMZ and the Central Iberian Zone (CIZ) is a complex tectonic unit called the Badajoz-Cordoba Shear zone or Central Unit (Simancas et al., 2001), which includes some retroeclogites and amphibolites with oceanic chemical signature (Simancas et al., 2003). The suture between the OMZ and the SPZ (the Beja-Acebuches ophiolite) is based on the existence of a strip of oceanic amphibolites (Quesada et al., 1994) and on the accretionary prism with slices of oceanic metabasalts (the Pulo do Lobo Unit) (Silva et al., 1990).

## 1.3.2. – Alpine domain

To the North of the Iberian Peninsula, the Pyrenean fold-thrust belt is a classic example of continent–continent collision that initiated by late Senonian and ceased at middle Oligocene. With a length of about 450 km, the belt runs in an E–W direction, from the Gulf of Lyon to the E to the Gulf of Biscay to the W (see Fig. 1.1 for location). The orogen is an asymmetrical and bivergent V-shaped continental wedge, the northern wedge being formed by a series of northward directed thrusts on top of the European plate, while the southern wedge, on top of the Iberian plate, is wider and shows greater displacement and shortening. From North to South the Pyrenean orogen comprises the Aquitaine foreland basin; the North Pyrenean thrust system; the axial zone, mainly composed by metamorphic and igneous rocks; the South Pyrenean thrust system and the Ebro foreland basin (e.g., Muñoz et al., 1986; Muñoz, 1992; Vergés et al., 1995; Muñoz, 2002). At crustal and lithospheric levels, the collision caused a thickening of the crust from about 32 km beneath the Ebro Basin to almost 60 km under the axial zone of the Pyrenees, (ECORS Pyrenees Team, 1988; Torné et al., 1989) while the LAB deepens from about to 90–110 km to 140–160 km depending on authors (e.g., Zeyen and Fernandez, 1994; Pous et al., 1995; Roca et al., 2004; Gunnell et al., 2008; Campanyà et al., 2012). Coinciding with the cessation of the main compressive stage along the Pyrenees, which also resulted in the formation of the Catalan Coastal Ranges, deformation migrated to the south and south east into the Valencia Trough and Algerian Basin domains (Vergés and Sàbat, 1999). Unlike the Pyrenees, the Catalan Coastal Ranges (see Fig. 1.1 for location) do not show significant thickening either of the crust or of the lithospheric mantle.

The Cantabrian Mountains represent the westward continuation of the Pyrenees

along the northern coast of Iberia. They are characterized by south-directed thrusts and associated folds, involving the Paleozoic basement along most of the belt. North-verging structures are present in the easternmost part of the Cantabrian Mountains, continuing to the west along the North-Iberian margin. Several deformation stages affected the area from the Late Palaeozoic to the Cenozoic (Perez-Estaun and Bea, 2004; Barnolas and Pujalte, 2004; Vera et al., 2004). The oldest event that is extensively recognized is the Variscan orogeny, which resulted from the continental collision between Laurassia and Gondwana at the end of Carboniferous times (e.g., Pérez-Estaún et al., 1991; Nance et al., 2012). After the Variscan orogeny, a rifting episode took place during the Late Paleozoic-Early Mesozoic, giving rise to localized Permo-Triassic basins. This event was followed by an important period of crustal extension related to the opening of the North Atlantic Ocean and the Bay of Biscay during Late Jurassic and Early Cretaceous times, which culminated in sea-floor spreading along the western margin of Iberia in the mid to Late Cretaceous, finishing in the Campanian (A33o) (e.g., Srivastava et al., 1990; Sibuet and Collete, 1991; Fernández-Viejo et al., 2005). Finally, N-S to NW-SE compression affected the North Iberian (Cantabrian) passive continental margin, whose geometry and inherited structures conditioned the formation of a double crustal indentation and the uplift of the Cantabrian Mountains in Eocene to Oligocene times (e.g., Alonso et al., 1996; Pulgar et al., 1996; Ferrer et al., 2008). The lower crust from the Cantabrian margin is underthrusted below a detachment level and protrudes into the Iberian crust forcing the north-directed subduction of its lower half (Pulgar et al., 1996; Gallastegui, 2000; Pedreira et al., 2003, 2007).

## 1.3.3. – The Central System and adjacent foreland basins

The Central System is a linear ENE-WSW mountain chain extending along 300 km in the central part of the Iberian Peninsula. It was uplifted as a crustal pop-up during Oligocene – Miocene bounded by NE-SW-trending reverse faults (Ribeiro et al., 1990b; Banks and Warburton, 1991; Vegas et al., 1990; de Vicente and Muñoz-Martín, 2013). The uplifted basement corresponds to high-grade Upper Precambrian gneisses and Variscan granites in the western part, and to low-grade Lower Palaeozoic metasediments in the eastern part (Fernández Casals et al., 1976). The Central System is bounded by two large sedimentary basins in the central part of Iberia: the Duero Basin to the NW and the Tagus Basin to the SE. The Duero Basin began to form during the Late Cretaceous as a continental shelf of the Cantabrian Margin. During the Eocene, the northern part evolved as a foreland basin linked to the formation of the Cantabrian Mountains (Alonso et al., 1996), whereas the southern border acted as the foreland

basin of the Central System during the early Oligocene-Miocene (Capote et al., 2002). Depocentres are related to the active borders of the basin, the sedimentary thickness reaching maximum values of 2500 m (Alonso et al., 1996). The Tagus Basin is a foreland basin related to the interaction between the Alpine tectonic uplift of the Central System and the transpressive regime along the Iberian Range. The basin is filled with Late Eocene to Late Miocene continental deposits with maximum thickness of 3500 m along its NE-SW border (Gómez-Ortiz et al., 2005).

## 1.3.4. – The Betic–Rif orogen and West Mediterranean basins

The southern margin of Iberia underwent a complex tectonic evolution about which there is a very active debate (e.g., Rosenbaum and Lister et al., 2002; Faccenna et al., 2004; Spakman and Wortel, 2004; Carminati et al., 2012; Vergés and Fernandez, 2012; van Hinsbergen et al., 2014; Casciello et al., 2014; Chertova et al., 2014). According to Vergés and Fernandez (2012), the Betic–Rif orogen was formed as a consequence of SE-dipping subduction of the western domain of the Ligurian–Tethys lithosphere beneath Africa from Late Cretaceous to middle Oligocene, followed by a fast NW and W slab roll-back. In the Algerian domain, the subduction of the Ligurian-Tethys lithosphere towards the NW, and the SE- and E-directed retreating produced the opening of the Valencia Trough, the Algerian Basin, and the Tyrrhenian Sea. Many of the other models assume a unique subduction polarity of the Ligurian-Tethys lithosphere, directed to the NW and claiming for a S-, SE- and SW-directed slab retreating with a trench rotation of ~180º in the Betic segment (e.g., Rosenbaum and Lister et al., 2002; Faccenna et al., 2004; Spakman and Wortel, 2004; van Hinsbergen et al., 2014; Chertova et al., 2014) (Fig. 1.4).

Independently on the model evolution, the Betic-Rif orogen comprises several major tectonic domains: a) the Guadaquivir and Gharb forelands basins; b) the ENE–WSW trending External units, separated in Prebetic and Subbetic domains; c) the Gibraltar Flysch Units around the western side of the thrust belt; and d) the HP/LT metamorphic complexes of the Internal units. The NW and W retreat of the Ligurian-Tethys slab produced the thrusting of the Internal Betics domain over the Iberian and Maghrebian passive continental margins. In this context, the Alboran Basin formed as a back-arc basin and it is characterized by a thin continental crust in its western part, evolving towards the east to a thin continental crust modified by arc magmatism, a magmatic-arc crust, and oceanic crust in its easternmost part and towards the Algerian

Basin (Torne et al., 2000; Booth-Rea et al., 2007).

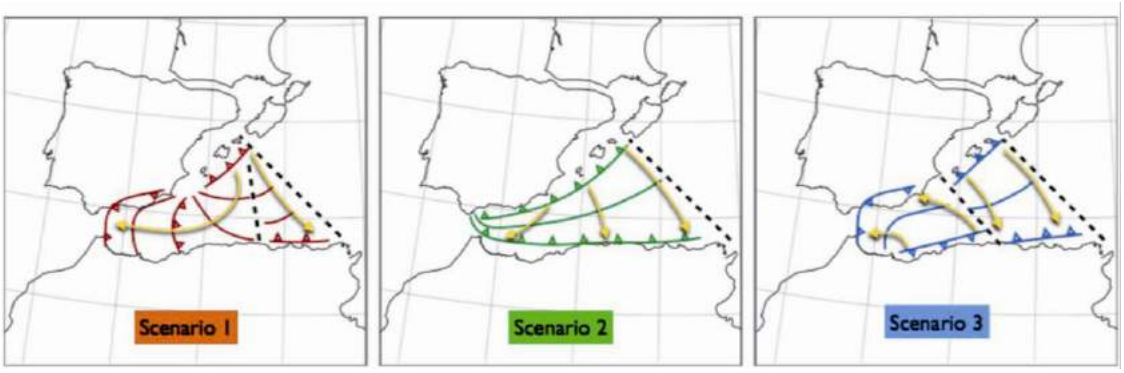


Figure 1.4: An illustration of rollback as portrayed in the three different reconstruction scenarios from Chertova et al., 2014. Scenario 1 (Spakman and Wortel, 2004) and scenario 2 (Faccena et al., 2004) assume a unique subduction polarity but start from different initial subduction zone (short and long respectively). Scenario 3 (Vergés and Fernandez, 2012) shows two opposite dipping subductions. Dashed lines represent proposed transform fault regions. The triangular zone between the transform zones of Scenario 1 depicts the lithosphere that rolls back toward the east Kabylides (Spakman and Wortel, 2004).

In the Valencia Trough and the Algerian basins, structures are related to the Tethyan subduction mainly developed between the Late Oligocene and Late Miocene (Roca et al., 2004). The crustal and lithosphere geometry is mainly the result of the south-eastward retreat of the Tethys–Maghrebides subduction zone (Doglioni et al., 1997; Carminati et al., 1998; Vergés and Sàbat, 1999). The south-eastward retreat of the slab resulted in a widespread back-arc extension which thinned the southeastern margin of the Iberian plate and caused the opening of the Valencia and Algerian basins. In the Valencia Trough Basin extension lasted from Late Oligocene to Langhian period, whereas the opening of the Algerian Basin began later (latest Early Miocene–Middle Miocene) and ended during the Tortonian, when remnants of the southern Iberia continental margin (the Kabylies) accreted with the African plate. The accretion of the Kabylies led to the development of the Tell thrust system in the northern African domain (Cavazza et al., 2004; Roca et al., 2004). Back-arc extension resulted in thinning of the crust and lithosphere mantle. In the Valencia Trough Basin the crust thins from 20 to 22 km near the Iberia coastline to 14 km at its central parts (e.g., Pascal et al., 1992; Torne et al., 1992; Gallart et al., 1994; Vidal et al., 1998), while the LAB shallows to as much as 65 to 60 km, depending on the authors (e.g., Zeyen and Fernandez, 1994; Ayala et al., 1996; Roca et al., 2004). A slight thickening of the crust and lithosphere is observed in its southeast margin, along the Balearic Promontory, where the base of the crust and LAB achieves values of about 20 and 90 km,

respectively. This thickening is partly explained by the fact that the area was affected by the orogenic activity recorded along the south-eastern passive margin of Iberia from Late Oligocene to Middle Miocene, which gave rise to the observed WNW–ENE verging folds and thrust that involve the Mesozic cover and Paleogene to Middle Miocene sediments (e.g., Sàbat et al., 1988; Roca et al., 1999). The geometry of the crust and lithosphere mantle is not so well constrained along the Algerian Basin owing to the scarcity of geophysical experiments. In the northwest part of the Algerian Basin the available seismic refraction profile of Hinz (1972) shows that the crust is partly oceanic with a thickness of about 5 km. This value is consistent with that observed in the ESCI—Valencia seismic reflection profile (Sàbat et al., 1997; Vidal et al., 1998). Roca et al. (2004) show that the LAB attains depths of about 50 km in the central parts of the basin, abruptly deepening near the African coastline to values of 175–185 km. From late Miocene, the protracted slow convergence between the African and Eurasian plates (~ 6 mm/year; Argus et al., 1989; DeMets et al., 1994) has caused intraplate compressive stresses in the whole area, which have resulted in compressive reactivation of previous faults. Active faulting combining ENE–WSW reverse faults and NW–SE right lateral strike-slip faults is particularly important in the Algerian margin as shown by numerous destructive earthquakes (El Asnam, 1980, Ms =7.3; Boumerdès, 2003, Ms = 6.7). The observed compressive deformation could indicate the development of a new African-Eurasian boundary along the Algerian margin, where the thin Algerian oceanic lithosphere is in contact with the thicker African continental lithosphere (e.g., Deverchere et al., 2005; Domzig et al., 2006).

## 1.3.5. – The Atlas Mountains and the Sahara platform

The Atlas Orogen is an intracontinental mountain belt uplifted in the foreland of the Rif and Tell Ranges, which extends more than 2000 km through Morocco, Algeria and Tunisia. The Atlas Mountains consist of two main branches, the E-trending High Atlas, with summits of 4000 m, and the NE-trending Middle Atlas, which reaches 3000 m. Foreland basins are poorly developed and the synorogenic sediments are only locally preserved, and usually are few hundred metres thick. These chains are fold-thrust belts formed during the Cenozoic from inversion of intraplate Triassic–Jurassic transtensional troughs related to convergence between Africa and Europe (Laville et al., 1977; Dutour and Ferrandini, 1985; Gorler et al., 1988; Fraissinet et al., 1988; Medina and Cherkaoui, 1991; El Harfi et al., 1996; Morel et al., 1993, 2000, etc.). In addition, rifting-related Triassic and Jurassic igneous rocks are widespread (Hailwood and Mitchell, 1971). Tectonic shortening across the Atlas Mountains is modest. Teixell et al. (2003)

calculated values ranging from 15% to 24% of the High Atlas, whereas Gomez et al. (1998) estimated it in 15% in the central Middle Atlas. Modest crustal tectonic shortening and thickening contrasts with the high topography observed suggesting a mantle contribution to uplift (Teixell et al., 2003). The internal deformation structures in the Middle Atlas are oriented NE-SW, parallel to the general trend of the chain. At its northern boundary, the Middle Atlas plunges under the Neogene sediments of the Saiss Basin, the foreland basin of the Rif orogen. The northern half of the Middle Atlas has a tabular structure only disrupted by minor normal and thrust faults (e.g., Termier, 1936; Duée et al., 1977; Fedan, 1988; du Dresnay, 1988; Charroud, 1990 and Gomez et al., 1996, 1998). The structure of the High Atlas is characterized by folds and thrusts oriented approximately NE–SW, slightly oblique to the general ENE–WSW trend of the chain (Schaer, 1987; Laville, 1985; El Kochri and Chorowicz, 1995; Teixell et al., 2003).

## 1.3.6. – Neogene and Quaternary volcanism

The presence of Neogene and Quaternary alkaline volcanism is widespread in Iberia, North Africa and western Mediterranean (see Figure 1.1). The main volcanics areas for this study are located in the Valencia Trough, Calatrava Volcanic Province, Alboran Basin and in the Atlas Mountains. In the Valencia Trough magmatism is characterized by two volcanic cycles which are clearly separated in time and by their petrological setting (Martí et al., 1992). The first volcanic cycle, being of Chattian-early Burdigalian age, is characterized by calc-alkaline andesitic and pyroclastic rocks, while the second cycle, of Tortonian to Recent age, is characterized by poorly differentiated alkali-basalts. Close to the southern border of the Tagus Basin there is the Calatrava Volcanic Province (CVP) extending over an area of 5500 $km^2$ (Ancochea, 1982). Late Miocene to Quaternary magmatism with intraplate (OIB) affinity occurring in CVP often carries nodules that provide direct information on the composition of the mantle. Geochemical and isotopic analyses of ultramafic xenoliths show a wide range of compositional heterogeneities due to both tholeiitic melts or subducted oceanic crust with metasomatic events of alkaline melts similar to the hosting lavas (LREE, Pb, Th and U enrichments in clinopyroxenes and whole rock HIMU-like signature respectively) (e.g., Cebriá and López-Ruiz, 1995; Bianchini et al., 2010; Villaseca et al., 2010). In the Alboran Basin, the extensional evolution was accompanied by broadly distributed volcanism ranging from early Oligocene tholeiitic through calc-alkaline series related to subduction, to middle-late Miocene tholeiitic through calc-alkaline and alkaline series related to lithosphere thinning (e.g., Duggen et al., 2004). In addition,

Tertiary and Quaternary alkaline volcanism (Harmand and Catagrel, 1984) has been identified in the Middle Atlas, the Moroccan Meseta, the High Plateaux, the northern part of the High Atlas, and in the Anti-Atlas. The upwelling of hot asthenospheric mantle controlled by various tectonic events (intraplate extension, rifting, slab retreat or lithospheric delamination; e.g. Carminati et al., 2012) caused partial melting at the base of the metasomatised lithosphere, and the subsequent episodic emplacement of small amounts of sodic alkaline lavas such as in the Middle Atlas and Central Morocco volcanic provinces (Bosch et al., 2014).

# 1.4. – Geophysical data

## 1.4.1. – Global geophysical data

Regional geophysical data sets (elevation, gravity, geoid height and surface heat flow; Fig. 1.5) were collected from different data sources. Elevation data come from ETOPO1 (Amante and Eakins 2009), a global elevation model of the Earth surface of 1x1-min arc resolution (Fig. 1.5a). In the study area, maximum average elevation values of about 2000 m are attained in the Pyrenees and in the Cantabrian Mountains, 1500-2000 m in the Betic Cordillera, 650 m in the Rif Cordillera and ~2700 m at the highest peak of the Middle Atlas Mountains. The Duero and Tagus basins are flat areas with average elevations of ~800 m and ~600 m, respectively. The minimum are reached in the Algerian Basin, Bay of Biscay (Cantabrian Sea) and the Alboran Sea where the ocean floor deepens to as much as -2900 m, -4500 m and -1900 m, respectively. Onshore Bouguer anomalies (Fig. 1.5b) were obtained from a recent compilation of gravity data in the Iberian Peninsula (Ayala, 2013) in the framework of the Topo-Iberia Project. Bouguer anomalies offshore and onshore in North Africa were computed from the free-air global satellite altimetry data model V16.1 (Sandwell and Smith, 1997, updated 2007) to which a full 3-D topographic correction has been applied with the software FA2BOUG (Fullea et al., 2008) using a density reduction of 2670 kg $m^{-3}$. Minimum Bouguer values of −120 mGal are achieved below the Pyrenees and Rif Mountains. Less than -100 mGal are found in the Central System, the Betic Cordillera, and the Kabylies–Tell–Atlas Mountains. Maximum values are recorded below the Valencia Trough (100 mGal), Algerian Basin (200 mGal), Bay of Biscay (300 mGal) and the Alboran Sea (100 mGal).

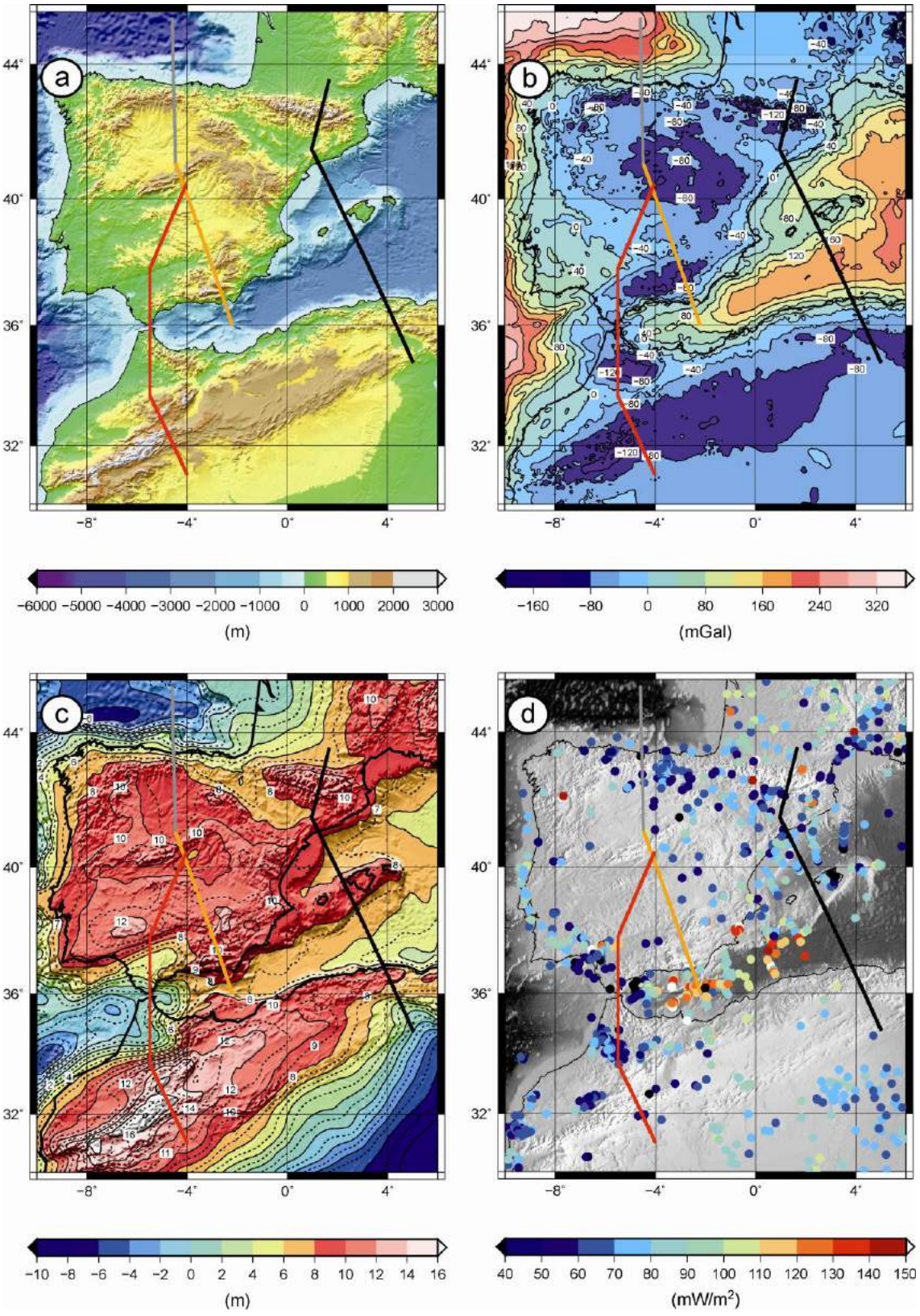


Figure 1.5: Geophysical data. a) Elevation map from ETOPO Global Data Base (V9.1) (http://www.ngdc.noaa.gov/mgg/fliers/01mgg04.html). b) Bouguer anomaly. Onshore, in the Iberian Peninsula, the Bouguer anomaly comes from Ayala (2013). Offshore and Africa Bouguer anomaly has been calculated from the free air anomaly by Sandwell and Smith (1997) using Fullea et al. (2008).

Contour interval is 40 mGal. c) Geoid anomaly map from EGM2008 Global Model (Pavlis et al., 2008). Long wavelengths (>5000 km) have been removed by subtracting spherical harmonics up to degree and order 8 from the total geoid. Contour interval is 1 m. d) Surface heat flow measurements from Fernandez et al. (1998), Marzán Blas (2000) and International Heat Flow Commission global data set for Algeria (http://www.heatflow.und.edu/index2.html). Colors of solid circles indicate heat flow values. Thick lines locate the modeled geo-transects: 1) black line; 2) grey line; 3) orange line and 4) red line.

Geoid height data (Fig. 1.5c) was taken from EGM2008 (Pavlis et al., 2008) and filtered up to degree and order 8, to retain only a residual geoid anomaly that reflects the density distribution within the lithosphere and the uppermost sub-lithospheric mantle (~400 km depth). Most of Iberia shows geoid height values between 8 and 11 m, with maximum values in the Betic Cordillera and the Tagus Basin and in the Pyrenees. In the eastern Iberia I observe values ~7 and ~5 m in the Valencia Trough and Algerian basins, respectively. The minimum geoid values are in the oceanic basins, reaching -5 m in the Bay of Biscay.

Surface heat flow data were compiled from different datasets (International Heat Flow Commission data set; Fernandez et al., 1998; and Marzán Blas et al., 2000) which also incorporates the sea-floor heat flow measurements in the Valencia Trough Basin from Foucher et al. (1992) and from Rimi et al. (2005) in Morocco. Fig. 1.5d shows the location and values of available measurements. The heat flow onshore Iberia varies between 45 and 65 $mW/m^2$. As observed the data exhibit a wide scatter around a mean value of 70–80 $mW/m^2$ in the Valencia Trough and the Balearic Promontory, with a good coverage in some areas, particularly in the Algerian Basin, Alboran Sea and onshore Algeria. Seafloor heat flow measurements carried out in the western Algeria Basin and in the Alboran Sea show values ranging from 90 to 120 $mW/m^2$ (Marzán Blas, 2000). Heat flow values exceeding 70-80 $mW/m^2$ are located at SW-Iberia (South-Portuguese Zone), NW-Iberia (Centro-Iberia Zone) corresponding to local thermal anomalies, and north Morocco and east-Algeria.

# Chapter 2: The Pyrenees–Balearic Promontory–Kabyles–Tell–Atlas geo–transect (first profile)

Most of the materials of this chapter relative to data gathering, aims, modeling technique, results and discussion, have been published in the Elsevier international journal *Gondwana Research* (Carballo et al., 2015a).

The present-day crustal and lithospheric mantle structure in NW-Iberia and the western Mediterranean is the result of compressional tectonics with collision/subduction in the former Eurasia–Iberia (Pyrenees) and in the Iberia–Africa (Tell–Atlas) plate boundaries, and back-arc extensional tectonics in the Neogene western Mediterranean. This complex tectonic evolution affected Paleozoic, Mesozoic and Tertiary domains with late-Hercynian plutonism in the Pyrenees (Michard-Vitrac et al., 1980; Fourcade and Allègre, 1981), Neogene volcanism along the Iberian–Mediterranean margin (Martí et al., 1992; Wilson and Bianchini, 1999; Lustrino et al., 2011), and generation of oceanic crust in the Algerian Basin (Sàbat et al., 1997; Vidal et al., 1998; Booth-Rea et al., 2007).

Unraveling the crust and lithosphere structure of the Alpine-Mediterranean region has been the subject, in the last decades, of numerous geological and geophysical studies that were summarized in eight regional geo-transects in the TRANSMED Atlas (Cavazza et al., 2004). In this Chapter, I present a new modeling of the TRANSMED-II geo-transect with a N–S trend crossing the southern part of the Aquitanian Basin, the Pyrenees and the northern part of the Eastern Ebro Basin. From there it continues with a NNW–SSE direction through the southern part of the Eastern Ebro Basin, the Catalan Coastal Ranges, the Valencia Trough Basin, the Balearic Promontory, the Algeria Basin, the North African margin, the Kabylies, and ending at the Tell–Atlas mountain range.

## 2.1. – Crustal geometry from previous studies

The crustal geometry is well known from the numerous deep seismic reflection and wide-angle/refraction profiles collected during the last decades (Fig. 2.1 and 2.2). The compilation of available crustal structure is summarized in the TRANSMED II transect (Roca et al., 2004). Original seismic data come from ECORS—Central Pyrenees (ECORS Pyrenees Team, 1988), ESCI—Catalánides (Gallart et al., 1994), ESCI—Valencia (Vidal et al., 1998), Hinz (1972) and ALE-4 (an industry profile) (see Fig. 2.1 for location of profiles). The Moho depth varies from 32 to 35 km beneath the Aquitanian Basin to more than 50 km in the Pyrenees and 36–32 km in the Ebro Basin and the Catalan Coastal Ranges. Towards the Valencia Trough, the Moho rises up to 16–18 km deepening to 22–25 km in the Balearic Promontory, whereas beneath the Algerian Basin the Moho lies at 10–12 km depth. In the Algerian margin, the Moho

depth increases to values of about 30 km close to the shoreline and according to Roca et al. (2004) it deepens down to 40 km depth beneath the Tell–Atlas mountains.

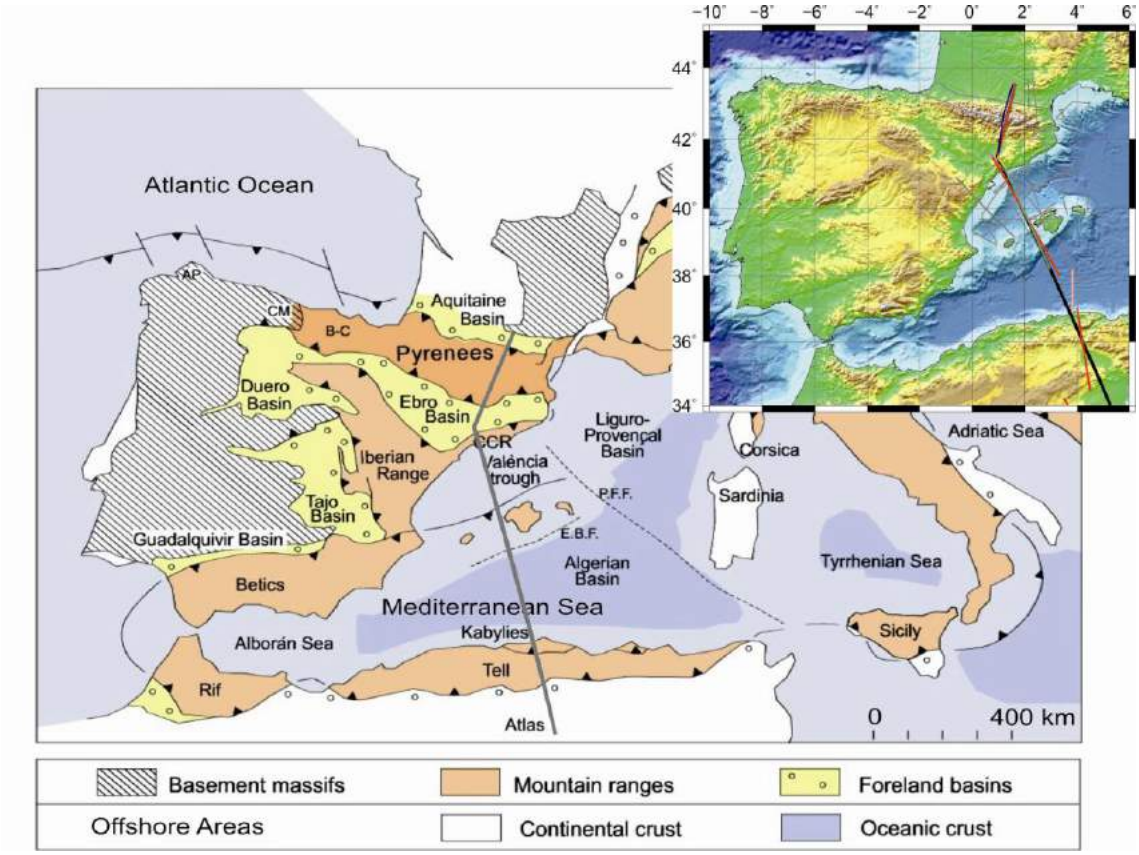


Figure 2.1: Geological map of the study area showing the principal geological domains of Iberia, Western Mediterranean and North Africa (modified from Vergés and Sàbat et al., 1999). Thick gray line locates the modeled transect. Upper right inset shows the main topography and bathymetry features of the study area in which is located: Black line-model transect; Deep blue—ECORS Pyrenees; Yellow— ESCI Catalanides; Green line—ESCI València; Pink line: ALE-4 and dark gray-other seismic experiments (Diaz et al., 2013).

The resulting crustal structure (Fig. 2.2) shows minor differences with TRANSMED-II transect. However, beneath the Kabyles–Tell–Atlas region, the modeled crust is up to 10 km thinner. In the Balearic Promontory, our results coincide with TRANSMED-II although the crust is slightly thinner with respect to Vidal et al. (1998). Density and thermal conductivity values for crustal bodies have been taken from previous studies (e.g., Fernandez et al., 1990; Torne et al., 1992, 1996; Zeyen and Fernandez, 1994). Radiogenic heat production has been taken from a global compilation carried out by Vilà et al. (2010). Parameters used in the crust are summarized in Table 2.1.

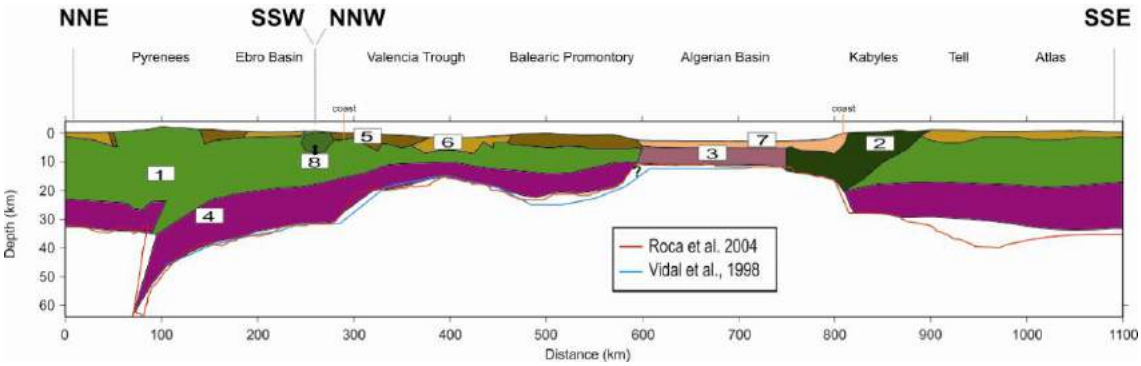


Fig. 2.2: Crustal structure along the model. Geometry of crustal bodies has been mainly taken from TRANSMED-II geotransect (Roca et al., 2004) based on ECORS—Central Pyrenees (ECORS Pyrenees Team, 1988), ESCI—Catalanides (Gallart et al., 1994), ESCI—Valencia (Vidal et al., 1998) and ALE-4 (industrial profile) seismic profiles. Blue and red lines refer to Moho depth proposed by Roca et al. (2004) and Vidal et al. (1998), respectively. Numbers denote crustal bodies summarized in Table 2.1.

| | Crust and sediments | Density ($kg/m^3$) | Heat production ($\mu W/m^3$) | Thermal conductivity ($W/(K \cdot m)$) |
|---|---|---|---|---|
| 1 | Upper crust | 2780 | 1.0 | 3.10 |
| 2 | Trans. upper crust | 2840 | 1.0 | 3.10 |
| 3 | Oceanic crust | 2950 | 0.3 | 2.50 |
| 4 | Lower crust | 2900 | 0.3 | 2.50 |
| 5 | Mesozoic sediments | 2650 | 1.0 | 2.50 |
| 6 | Cenozoic sediments | 2550 | 1.0 | 2.40 |
| 7 | Neogene sediments | 2400 | 1.0 | 2.20 |
| 8 | Tardi-hercynian plutons | 2650 | 1.2 | 2.50 |

Table 2.1. Parameters used in the first geo-transect model for the different crustal bodies.

# 2.2. – Mantle characterization and LAB depth from previous studies

The LAB beneath this geo-transect and surrounding areas has been the subject of several studies, mainly 2D modeling, integrating different geophysical data sets (e.g., Fernandez et al., 1990; Zeyen and Fernandez, 1994; Ayala et al., 1996 and 2003; Roca et al., 2004). None of these models consider pressure and compositional changes in the mantle. As pointed out by Afonso et al. (2008) the neglect of compressibility, phase changes and compositional heterogeneities could result in uncertainties in the density contrast at Moho and LAB levels and in turn in the resulting LAB depth. The assumed temperature-dependent mantle density also shows inconsistencies with tomography, xenolith and thermodynamic data. Nevertheless, as a first approach I have used the available information as a first input in our forward modeling. For instance, the works by Fernandez et al. (1990); Zeyen and Fernandez (1994) and Ayala et al. (1996, 2003)

have reported lithospheric thickening from 110 to 120 km beneath the foreland basins to as much as 150 km below the axial zone of the Pyrenees. A thickness decrease is observed towards the central region of the Valencia Trough where values of 65–60 km are reported. To the SE, along the Balearic Promontory the thickness of the lithosphere slightly increases (88–92 km), thinning towards the Algerian Basin where the LAB raises to 55 km. Towards the Algerian margin and North-Africa, Roca et al. (2004) imaged a sharp lithospheric thickening with a LAB depth exceeding 160 km. To characterize the mantle available Pn data, global and regional tomography models, and geochemical and isotopic analyses on xenolith samples were used.

Pn velocities between 7.7 and 7.9 km $s^{-1}$ have been reported by Torne et al. (1992), Vidal et al. (1998) and Grevemeyer (pers. comm.) underneath the Valencia Trough, the Balearic Promontory and the Algerian Basin coinciding with areas of attenuated continental crust and oceanic crust.

A P-wave tomography model by Piromallo and Morelli (2003) shows low velocities in the western Mediterranean basins down to 400 km depth similar to the global P-wave tomographic model of Villaseñor et al. (2003). Interestingly, these authors show relative high velocities in the North Africa margin, particularly in eastern Algeria and Tunisia (Fig. 2.3).

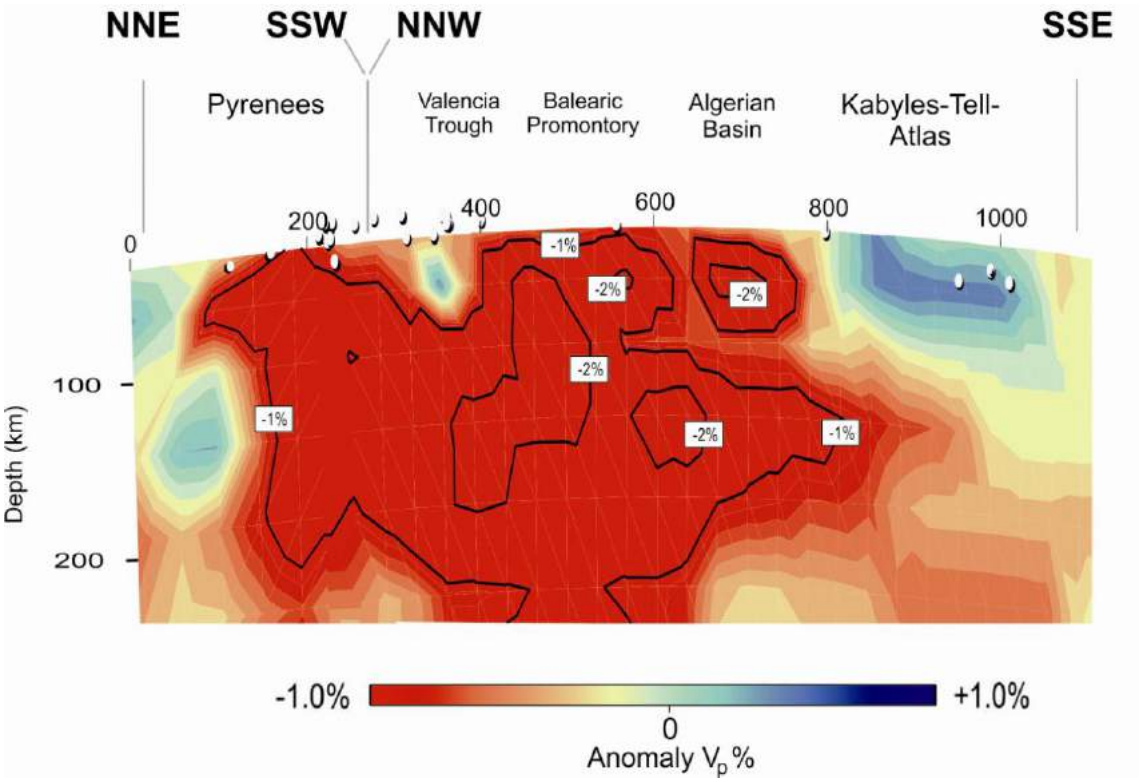


Figure 2.3: P-wave tomography model along the profile (Villaseñor et al., 2003).

The global travel-time tomography model used to compare the obtained results come from Villaseñor et al. (2003) which uses the same method described in Bijwaard et al. (1998), incorporating additional earthquakes from 1995 to 2002 and arrival times (Villaseñor et al., 2003). In total, more than 14 million arrival times from 300,000 earthquakes were reprocessed using the EHB methodology (Engdahl et al., 1998). The ray paths corresponding to these new arrival times sample, mainly, the uppermost mantle with a resolution of 0.5 x 0.5 in horizontal and 25-50 km in depth.

A regional S-wave tomography model for Europe constrained by inversions of seismic waveforms (Legendre et al., 2012) shows pronounced negative anomalies ($\Delta Vs \sim -5\%$) in the Algerian Basin at 110 km depth, the amplitude of the anomaly decreasing with depth and vanishing below 200 km depth. According to this model, the Rif–Tell–Atlas region also shows negative Vs anomalies ($\Delta Vs \sim -3\%$) at 110 km depth.

## 2.3. – Results

Mantle density has been calculated from its chemical composition whereas thermal conductivity is calculated according to Hofmeister (1999). Mineral assemblages in the lithospheric mantle have been computed using the NCFMAS approach. Figure 2.4 shows the best fitting model of the first transect. Our results shows that along the model profile, I need to consider five lithospheric mantle types, which agree with the geodynamic domains described above (Table 2.2).

In NE Iberia mainland a Proterozoic (Proton-lherzolite average, Pr_6) as proposed by Griffin et al. (2009) fits the observed geophysical data and is also in agreement with xenolith data collected by Le Roux et al. (2007). In the Valencia Trough and the Balearic Promontory the resulting mantle corresponds to a primitive upper mantle (PUM, Pm_2) as defined by Jagoutz et al. (1979) which is in agreement with the continental highly intruded nature of the lithosphere, whereas the oceanic-type Algerian Basin is characterized by a more enriched PUM-type (Pm_1, McDonough and Sun, 1995). In the Alpine domain of North Africa, which includes the continental margin and the Kabyles–Tell–Atlas region, I considered an average Phanerozoic-Tecton-type garnet-rich composition (Tc_1, Griffin et al., 2009), which differs noticeably from that obtained farther to the South corresponding to a more depleted ‘tecton incipient or little extension’ TILE composition, as already suggested by Griffin et al. (1999) (Table 2.2).

| | Mantle composition | $SiO_2$ | $Al_2O_3$ | FeO | MgO | CaO | $Na_2O$ |
|---|---|---|---|---|---|---|---|
| 9 | Pr_6 (Lherz Av.) | 45.4 | 3.7 | 8.3 | 39.9 | 3.2 | 0.26 |
| 10 | Pm_1 (Primitive uppermantle) | 45 | 4.5 | 8.1 | 37.8 | 3.6 | 0.36 |
| 11 | Pm_2 (Primitive uppermantle) | 45.2 | 4 | 7.8 | 38.3 | 3.5 | 0.33 |
| 12 | Tc_1 (Av.Tecton) | 44.5 | 3.5 | 8.0 | 39.8 | 3.1 | 0.24 |
| 13 | TILE (Tecton incipient) | 44.97 | 2.33 | 8.32 | 40.18 | 2.52 | 0.18 |

Table 2.2. Bulk mantle compositions used in the model.

As observed in Figure 2.4, calculated gravity, geoid and elevation match the observed regional trends. To account for lateral variations perpendicular to the strike of the profile, elevation, gravity, geoid and heat flow data have been projected onto the profile within a strip of 25 km half-width, whereas for heat flow data a 50 km half-width strip is used. The resulting standard deviation is plotted as error bars. Major differences in Bouguer anomaly, up to 30 mGal, are observed locally in the Kabyles Mountains probably related to local 3D crustal features not considered in our model. This misfit is also reflected in the calculated elevation reaching differences of <500m. Heat flow data is not so well constrained owing to its scarcity and associated uncertainty, particularly at the SE-half of the profile. Calculated values range from 55 to 60 $mWm^{-2}$ in the Pyrenean domain increasing steadily to 70–75 $mWm^{-2}$ in the Valencia Trough Basin and 75–80 mW $m^{-2}$ in the Algerian Basin. Towards the SE, the calculated heat flow decreases to minimum values of 50 $mWm^{-2}$ at the southeasternmost tip of the profile. Certainly, the calculated surface heat flow is consistently lower (about 15%) than measured values along the whole profile.

The main reason for this discrepancy is related to the calculated mantle thermal conductivities which have been computed using Hofmeister's P–T dependent approach (Hofmeister, 1999). Underestimation of thermal conductivity will affect essentially the calculated surface heat flow but will have minor effects on the calculated temperatures within the lithosphere and therefore on the mineral assemblages and resulting densities.

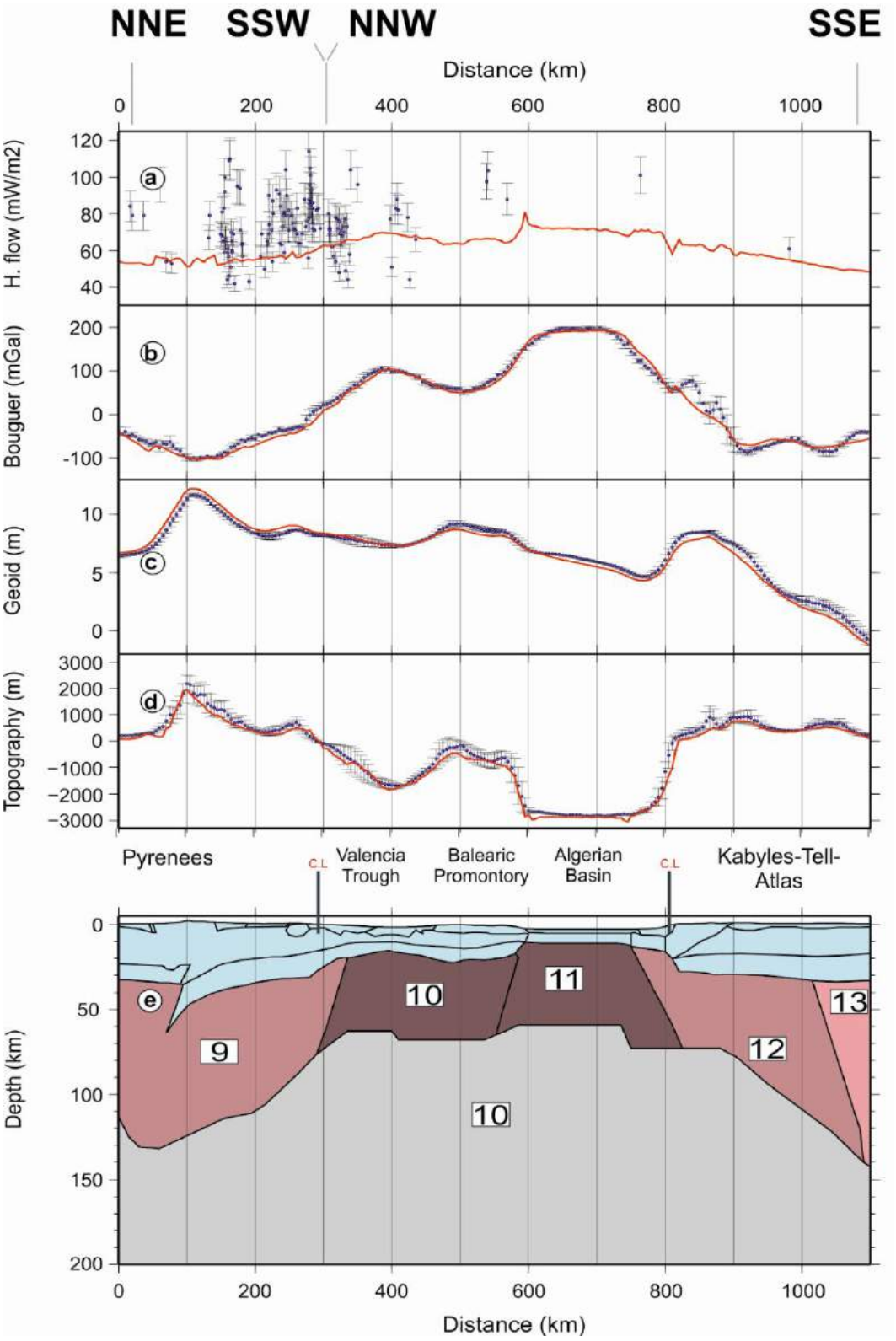


Figure 2.4: Model results (red lines) and measured data with the standard deviation of data projected onto the profile within a strip of 25 km half-width except heat flow that is projected onto a 50 km half-width strip (blue dots and vertical bars): (a) surface heat flow; (b) Bouguer anomaly; (c) geoid height; (d) elevation; (e) lithospheric structure. Crustal structure as in Fig. 2.2. Numbers in panel (e) denote mantle bodies summarized in Table 2.2. Dataset sources as in Fig. 1.3.

## 2.3.1. – Lithosphere mantle structure

Figure 2.4 shows that the LAB depth varies along the model profile reaching depths of about 130 km beneath the Pyrenean chain, about 65 and 70 km in the Valencia Trough Basin and Balearic Promontory, respectively, shallowing to as much as 60 km in the Algerian Basin. A sharp thickening is observed in the transition from the basin to the continental margin of North Africa, from where the LAB progressively deepens to reach maximum depths of 140 km at the SE tip of the profile. The resulting geometry of the LAB differs substantially from those obtained with previous models (Fig. 2.5). In the Pyrenean domain major discrepancies are observed with the results of a magneto-telluric study by Campanyà et al. (2012) where the LAB depth varies from 90 km beneath the Iberian Plate to 130 km in the Eurasian Plate. There are also differences with studies that have used similar integrated approaches. I obtain a similar lithospheric thickness to that proposed by Zeyen and Fernandez (1994) and a lower thickness than Roca et al. (2004) although our maximum thickness is slightly displaced 50 km to the North relative to these studies. Major discrepancies are observed in the style of thinning from the South Pyrenean thrust to the continental shelf of the Valencia Trough. Our results show a steady thinning of the lithosphere whereas models by Zeyen and Fernandez (1994) and Roca et al. (2004) suggest a step-like thinning resulting in differences of 15 km in the LAB depth over this region. Underneath the Neogene Mediterranean basins the calculated LAB depth is very similar to that proposed by Ayala et al. (1996, 2003) and Zeyen and Fernandez (1994). However, our results show that the LAB beneath the Valencia Trough and Balearic Promontory is 10–15 km shallower and 10 km deeper beneath the Algerian Basin than that proposed by Roca et al. (2004). From the south Algerian Basin to the Kabyles–Tell–Atlas region the lithosphere thickens in a very different style compared to TRANSMED-II (Roca et al., 2004). These authors propose a sharp thickening from 55 km to more than 160 km over a 200 km wide region, whereas our results show a more moderate steplike thickening from 60 to 140 km. Maximum differences of the LAB depth between the two models reach as much as 70 km beneath the Tell Mountains. These discrepancies are mainly related to the poorly constrained crustal thickness considered in the TRANSMED-II transect (see below) and, to a lesser extent, to the different modeling approaches.

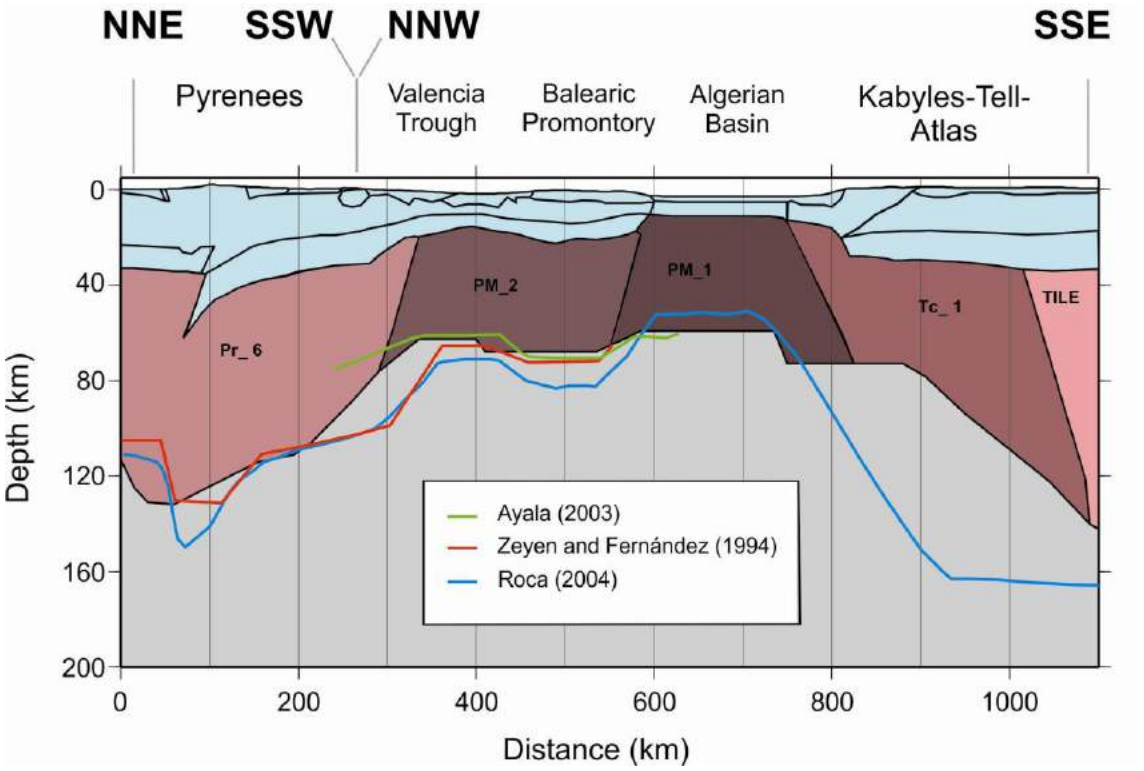


Figure 2.5: Lithosphere structure of the best fit model and mantle domains with different chemical composition (see Table 2.2). Color lines denote LAB geometries proposed in previous studies.

## 2.3.2. – Temperature and density distribution

Temperature distribution in the whole modeled domain is calculated under the assumption of steady-state thermal regime and displayed in Fig. 2.6. Thermal parameters are summarized in Table 2.1. The temperature at the crust–mantle boundary in the first model ranges from a maximum of 850 °C beneath the Pyrenees (65 km depth) to a minimum of 250 °C beneath the oceanic-type crust of the Algerian Basin, where the Moho shallows to 12 km depth. In the Pyrenean domain, average Moho temperatures are of 600–650 °C decreasing to 400–500 °C in the Valencia Trough and Balearic Promontory. In the North African region, temperatures range from 500 to 700 °C. Temperatures at the sublithospheric mantle vary from 1330 to 1400 °C in the thermal buffer increasing according to the adiabatic gradient from the base of the thermal buffer to the bottom of the model (400 km).

Densities in the crustal bodies are taken from literature and summarized in Table 2.1, whereas subcrustal densities are calculated according to mantle composition and thermodynamic formulation.

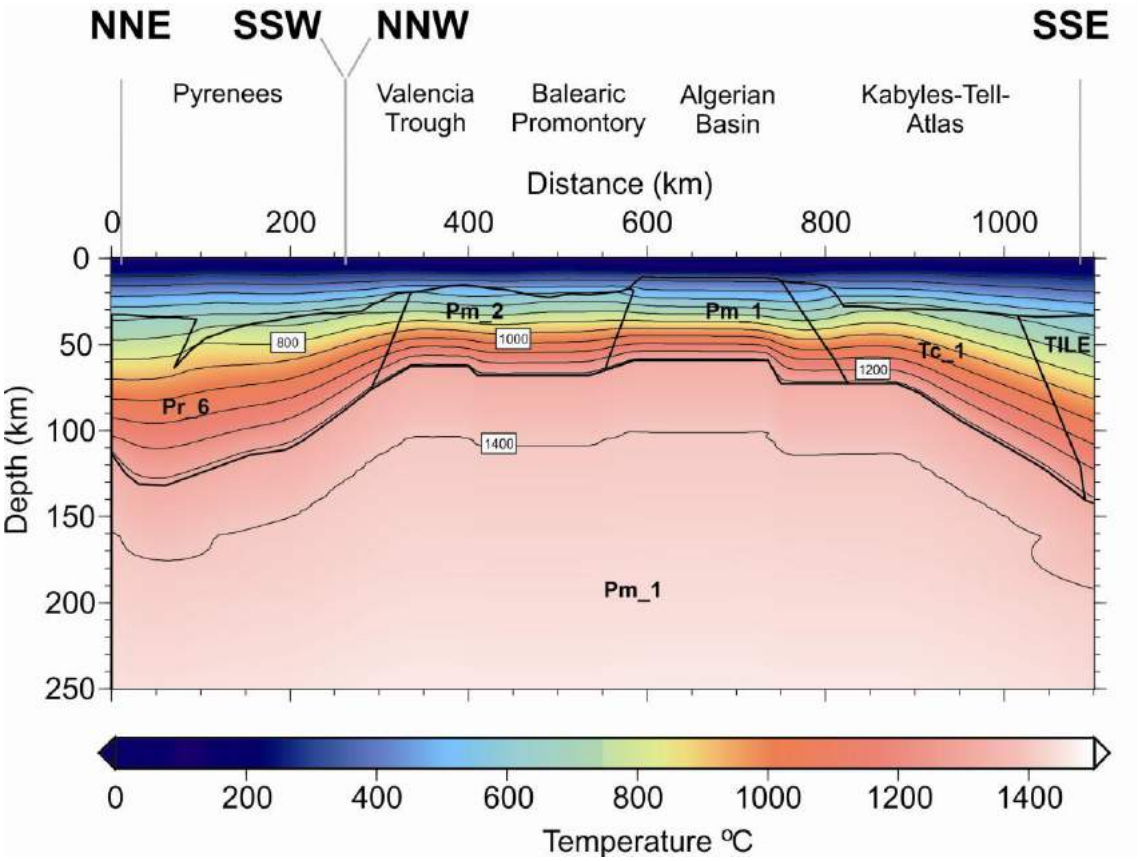


Figure 2.6: Calculated temperature distribution along the modeled transect. Contour lines every 100 °C.

Fig. 2.7 shows the mantle density distribution where within the lithosphere, the increase of density with depth by the effect of pressure generally dominates over the density decrease by thermal expansivity. However, since the base of the lithosphere is isothermal, thinner lithospheric columns are globally warmer, less dense and less sensitive to the effect of pressure than thicker ones. In the Pyrenean domain and the Atlas region densities reach values around 3350 kg $m^{-3}$ decreasing towards the Neogene extensional basins of the Mediterranean. In the Valencia Trough and the Algerian basins the lithosphere mantle density decreases from ~3320 kg $m^{-3}$ below the Moho to ~3260 kg $m^{-3}$ at the LAB. Nevertheless, in the Algerian Basin the uppermost mantle density decreases sharply to 3230 kg $m^{-3}$ related to the shallow-depth plagioclase-spinel phase transition. In contrast, beneath the Balearic Promontory and the North-Africa continental margin, a maximum density of 3320 kg $m^{-3}$ at ~50 km depth is calculated related to the spinel–garnet transition. In the North African continental margin there is a pronounced lateral density gradient with average densities increasing from 3300 kg $m^{-3}$ in the continental shelf to 3350 kg $m^{-3}$ in the Tell–Atlas region. From the LAB to the bottom of the model, density increases steadily due to the predominant effect of pressure, e.g. at 250 km depth density reaches values of 3470 kg $m^{-3}$.

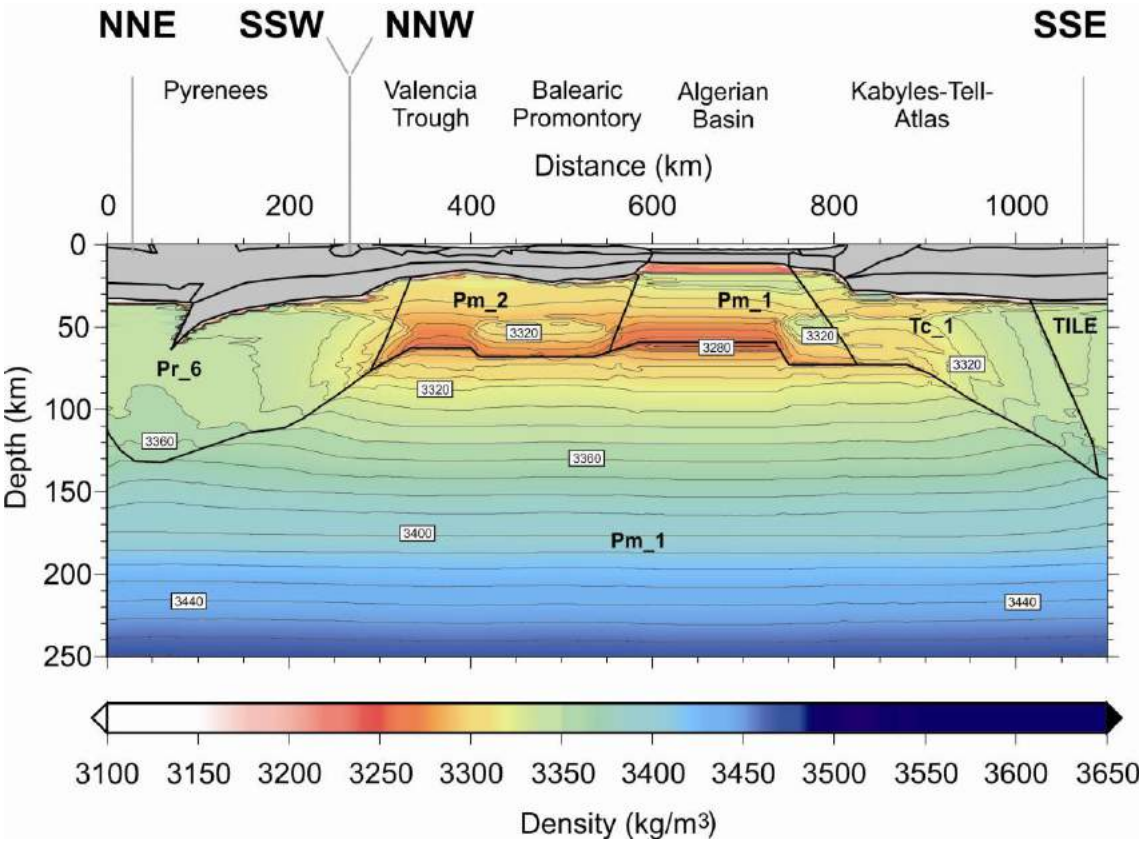


Figure 2.7: Calculated mantle density distribution along the modeled transect. Contour lines every 10 kg $m^{-3}$. Sharp density increase in the uppermost mantle beneath the Algerian Basin is related to the Pg-Sp phase transition. Sharp density increase at ~50 km depth is related to Sp–Grt phase transition.

## 2.3.3. – Mantle velocity distribution

One of the main advantages of the methodology used in this study is that LitMod allows calculating in a self-consistent way the elastic parameters of the mantle and therefore, the P and S-wave seismic velocities. Fig. 2.8a shows the calculated P-wave velocities in the mantle where low values at the LAB (7.5–7.6 km/s) are found underneath the Neogene Mediterranean basins and their continental margins.

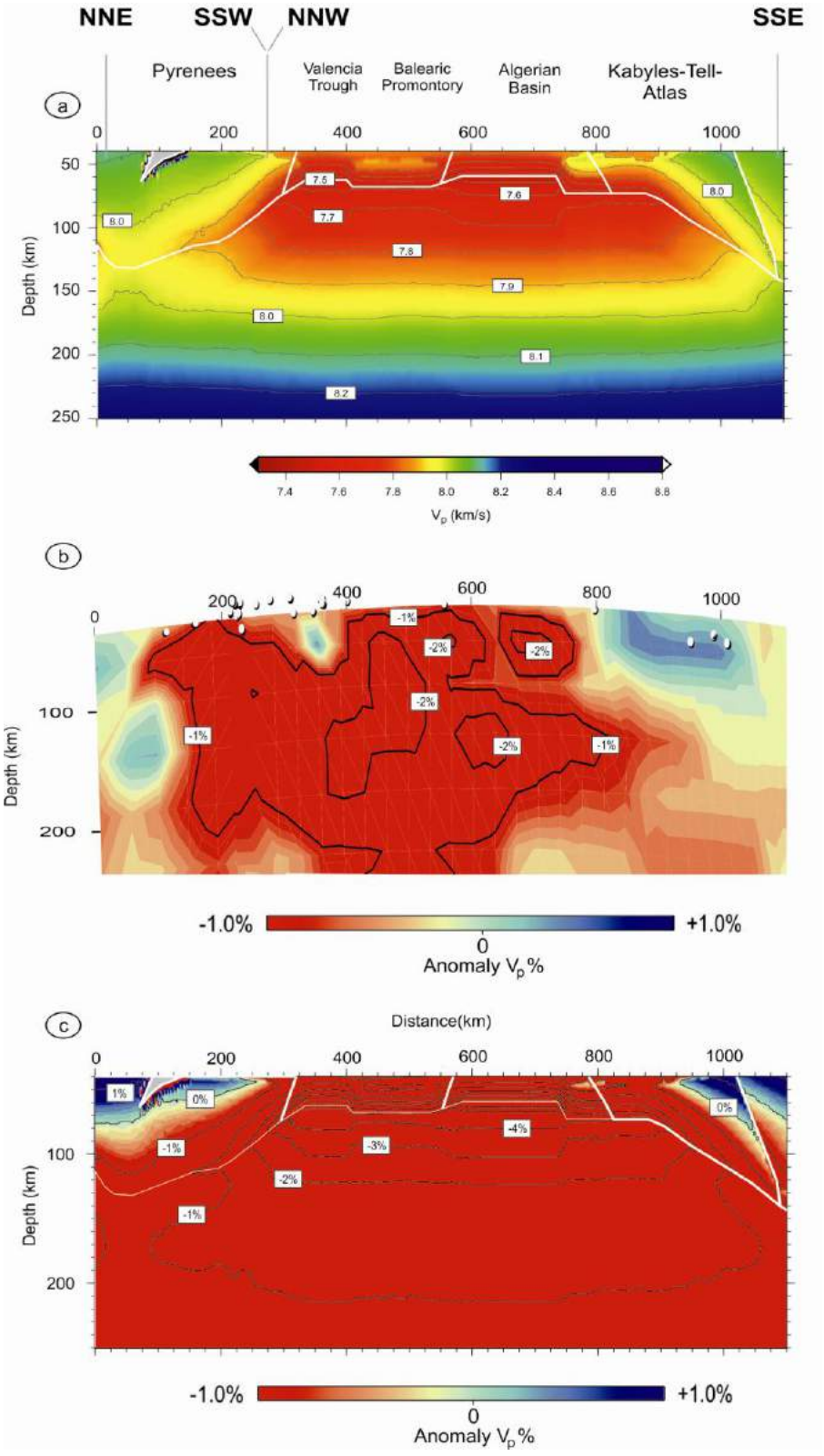


Figure 2.8: a) Calculated P-wave seismic velocities in the upper mantle (calculations extend down to 400 km depth). White solid lines indicate mantle domains with different chemical composition. b) P-wave tomography model (Villaseñor et al., 2003) and c) synthetic P-wave tomography from our model. In both cases velocity anomalies are relative to the ak135 reference model (Kennett et al., 1995). Contour lines every 1%.

The low velocity values extend down to 150 km depth and are related to the relatively high T prevailing in this part of the sublithospheric mantle. Beneath the Pyrenean and Kabyles–Tell–Atlas domains, P-wave velocities reach 8.0–8.1 km/s in the uppermost mantle decreasing slightly with depth until the LAB, defining a LVZ with variable thickness along the profile. Below 160 km depth, P-wave velocities increase with a constant gradient due to the prevailing effect of pressure. Fig. 2.8b compares the global P-wave tomographic model of Villaseñor et al. (2003) with the synthetic tomographic model obtained from our calculated P-wave velocities in the eastern lithospheric transect expressed in percentage with respect to the ak135 reference model (Kennett et al., 1995).

There is a coincidence in the low velocity zones predicted by both models though discrepancies are seen beneath the Pyrenees at depths higher than 100 km and below the Valencia Trough Basin. Also the amplitudes of the calculated low velocity anomalies are larger than those obtained in the tomographic model. The underestimation of the velocity anomalies by tomographic models based on ray theory is a well know result that is caused by the wavefront healing phenomenon (e.g. Hung et al., 2001). Therefore only the distribution and shape of the anomalies, not their amplitudes, can be meaningfully compared. In North Africa, the low resolution of the tomographic global model due to the poor coverage of available seismic stations does not allow for firm conclusions. Our results are also qualitatively consistent with the regional P-wave tomography model by Piromallo and Morelli (2003) that shows low velocities in the Western Mediterranean basins down to 400 km depth. Interestingly, these authors show relatively high velocities in the North Africa margin, particularly in eastern Algeria and Tunisia.

S-wave velocities show a similar pattern than P-wave (Fig. 2.9) with minimum values of <4.2 km/s in the sublithospheric mantle in the western Mediterranean basins. Low S-wave velocities (<4.4 km/s) extend over the sublithospheric mantle down to 200 km depth from where they increase almost linearly with depth due to the effect of pressure. Within the lithospheric mantle, S-wave velocities decrease from ~4.6 km/s in the uppermost mantle along the whole transect to 4.35 km/s in the LAB beneath the Pyrenees and the Kabyles–Tell–Atlas and <4.2 km/s beneath the Valencia Trough and the Algerian Basin. A regional S-wave tomography model for Europe constrained by inversions of seismic waveforms (Legendre et al., 2012) shows pronounced negative anomalies ($\Delta Vs \sim -5\%$) in the Algerian Basin at 110 km depth, the amplitude of the anomaly decreasing with depth and vanishing below 200 km depth. According to this model, the Rif–Tell–Atlas region also shows negative Vs anomalies ($\Delta Vs \sim -3\%$) at 110 km depth. To compare our results with this tomography model I have plotted the

resulting Vs values from Legendre et al. (2012) at different depth levels (80, 100, 150 and 200 km) according to the reference values used by these authors (Fig. 2.9). In general, our results fit well with the tomographic model although in the sublithospheric mantle our velocities are slightly higher beneath the Algeria Basin and lower beneath the Pyrenees and the Algeria margin. These small discrepancies are probably related to the thermal boundary condition used in our model that assumes a constant temperature at 400 km depth and therefore cannot account for deeper thermal anomalies.

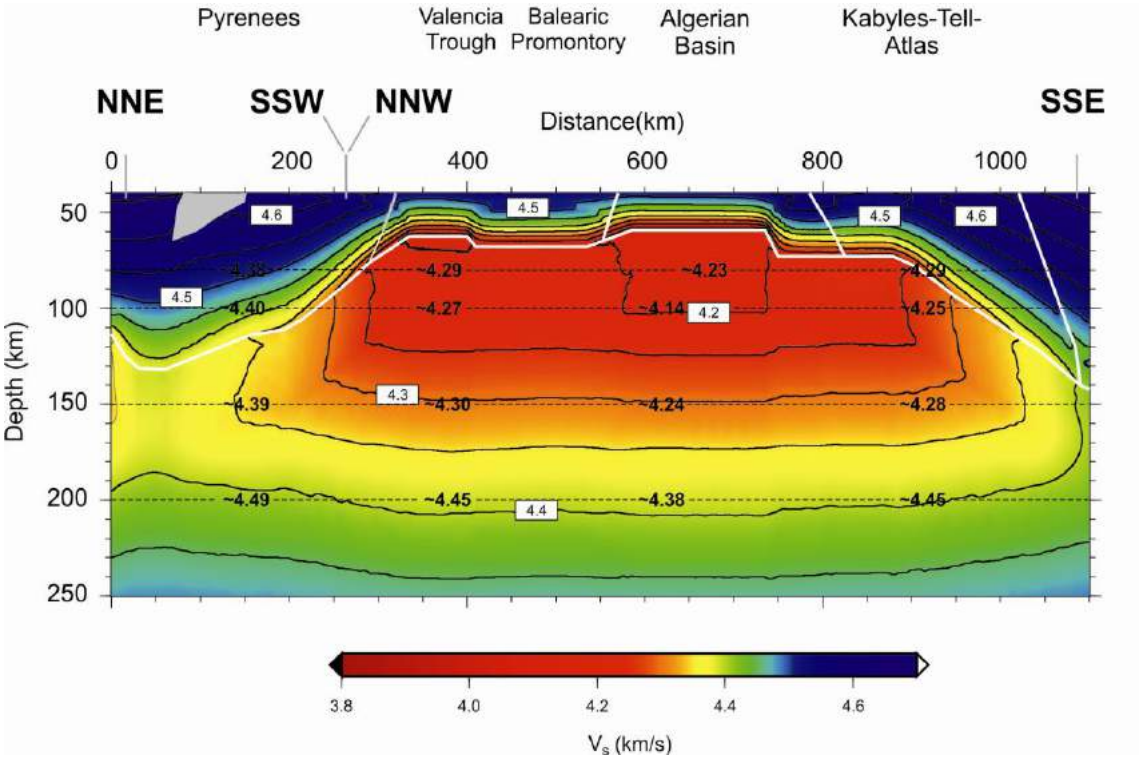


Figure 2.9: Calculated S-wave seismic velocities in the upper mantle (calculations extend down to 400 km depth). White solid lines indicate mantle domains with different chemical composition. Contour lines every 0.05 km/s. Superimposed are the S-wave velocities inferred from the regional tomography model by Legendre et al. (2012) at different depth levels. S-values have been calculated according to the reference velocities of 4.38 km/s (at 80 and 110 km), 4.39 km/s (at 150 km) and 4.45 km/s (at 200 km) (see Legendre et al., 2012).

An additional constraint on seismic mantle velocities comes from Pn velocity data. Fig. 2.10 compares the calculated P-wave velocities in the uppermost lithospheric mantle along the lithospheric transect with Pn estimates from different seismic experiments. Calculated and observed values are in agreement in the Pyrenees and in the Iberian margin of the Valencia Trough. Discrepancies arise in the Neogene Mediterranean basins amounting between 0.05 and 0.15 km/s with the exception of a local value where differences exceed 0.2 km/s. Possible explanations on these

departures between observed and modeled data as serpentinization, seismic anisotropy and/or transient thermal effects will be discussed in Chapter 6.

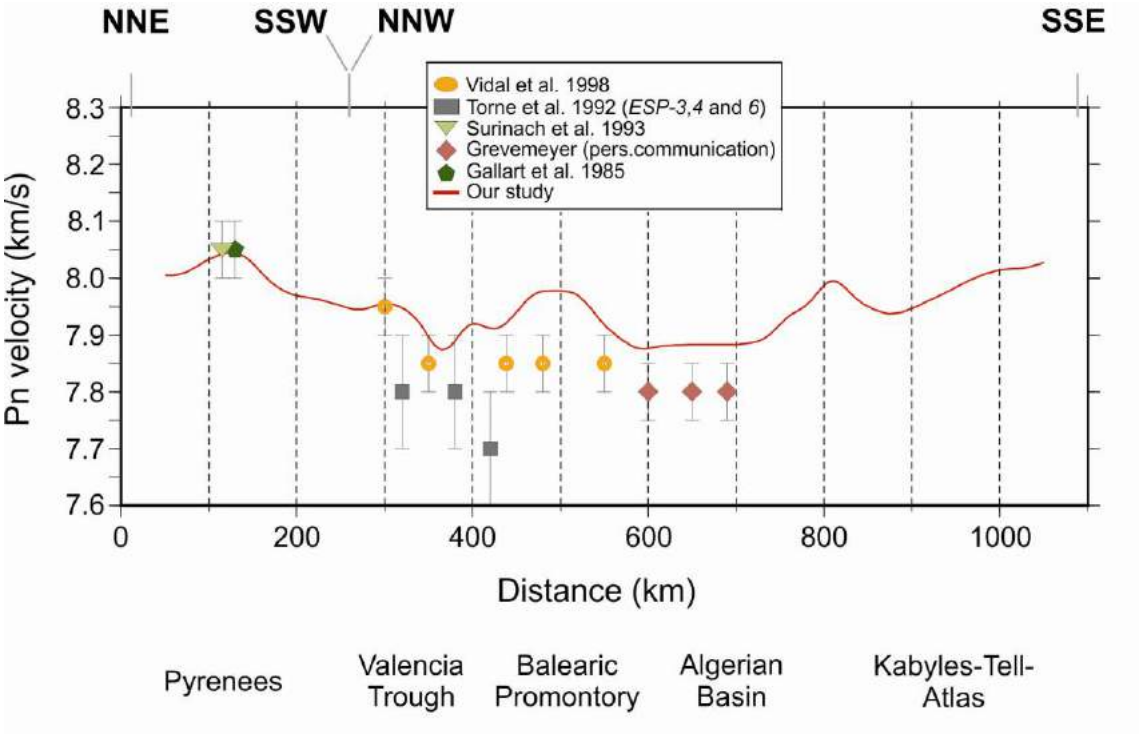


Figure 2.10: Pn velocities along the modeled transect. Red line indicates calculated Pn values. Symbols with error bars denote Pn-values from seismic experiments (see legend).

# 2.4. – Discussion

## 2.4.1. – LAB topography

As previously mentioned, the crustal structure is well constrained from the numerous seismic experiments and integrated geophysical models carried out along the studied transect with the exception of the onshore Algerian segment. However, the LAB topography relies solely on several models incorporating different datasets (e.g., Zeyen and Fernandez, 1994; Ayala et al., 1996; Ayala et al., 2003; Roca et al., 2004) and on mantle images from seismic tomography studies (e.g., Bijwaard and Spakman, 2000; Piromallo and Morelli, 2003; Villaseñor et al., 2003; Spakman and Wortel, 2004; Legendre et al., 2012). Since the obtained results have been already compared qualitatively with tomographic models, in this section I will focus on the comparison with results obtained from models using potential fields. Fig. 2.5 shows a comparison of

our results with those obtained by Zeyen and Fernandez (1994), Ayala et al. (2003) and Roca et al. (2004). Below the Pyrenees, the differences observed are of 10–20 km with a displacement to the north of the maximum thickness probably related to differences in the crustal structure just beneath the axial zone of the Pyrenees. Underneath the Ebro foreland Basin, the Catalan Coastal Ranges and the Iberian margin the LAB resulting from our model is consistently 20 km shallower than previously imaged by Zeyen and Fernandez (1994) and Roca et al. (2004) being in closer agreement with Ayala et al. (2003). Considering that the crustal structure is essentially the same as taken in previous models, the differences of the modeled LAB depth are related to the petrophysical approach I have adopted, which results in a different mantle density distribution. As mentioned, previous LAB studies by Zeyen and Fernandez (1994) and Roca et al. (2004) are based on a thermal approach in which the lithospheric mantle density is only temperature dependent and therefore, density decreases roughly linearly with depth through the thermal expansion coefficient. At difference, our modeling approach shows that in this segment of the transect (Ebro Basin–Catalan Coastal Ranges–Iberian margin) the lithosphere mantle density is nearly constant with depth and decreases laterally towards the Valencia Trough Basin with a lateral gradient of 0.25 kg $m^{-3}$ $km^{-1}$ (Fig. 2.7). The Algerian margin shows a similar lateral density gradient with increasing densities towards the Kabylies–Tell–Atlas region where a significantly thinner lithospheric mantle and a LAB depth, up to 80 km shallower than imaged by Roca et al. (2004), are proposed. This significant discrepancy is attributed to two facts: a) the already mentioned differences in the depth-density distribution between the thermal and petrophysical approaches and b) the differences obtained in the crustal thickness, which amount more than 10 km, from ca. 900 to 1000 km distance of the model transect (Fig. 2.2). The scarcity of deep seismic data in the region results in the lack of constraints on Moho depth, and our best fitting model shows a crust that is 10 km thinner than that proposed by Roca et al. (2004). As already mentioned by these authors, the onshore Algerian portion (Kabylies–Tell–Atlas) is fairly well constrained in its shallow part but poorly constrained at deep crustal levels, where no deep seismic data are available. Thus, the boundary between the upper and lower crust and the Moho geometry had to be drawn solely according to the results of previous gravity models (Mickus and Jallouli, 1999). In the Mediterranean segment of the profile the results obtained in the Valencia Trough, Balearic Promontory and Algerian Basin, fairly coincide with those obtained by Zeyen and Fernandez (1994) and Ayala et al. (2003), but differ slightly when compared with Roca et al. (2004). Discrepancies with results from these authors are of the order of 10 km attaining maximum values of 15 km in the Balearic Promontory (Fig. 2.5). The observed relative lithospheric thickening and thinning are partly attributed to the differences of the density distribution within the lithospheric

mantle related to chemical composition and the typical spinel–garnet phase transition occurring beneath the Balearic Promontory (Fig. 2.7) (see Afonso et al., 2008 for further details).

## 2.4.2. – Changes in mantle composition

As pointed out by many authors, the structure of the Earth's upper mantle in continental areas is highly heterogeneous and much of the heterogeneity is associated with the thermal and compositional structure of the lithosphere. The composition of the sub-continental lithospheric mantle (SCLM) may range from refractory dunites and harzburgites to lherzolites, depending on the degree of depletion in basaltic components through partial melting processes. These compositional heterogeneities may in turn translate in significant density differences at given P–T conditions related to compressibility, thermal expansion and phase transitions. Consequently, changes in mantle composition may affect modeling geophysical observables such as gravity, geoid, elevation, etc., since they are differentially sensitive to shallow and deep lateral density variations. The LitMod approach characterizes chemically the lithospheric mantle to calculate density, temperature distribution and seismic wave velocities; therefore we have gathered all relevant information on mantle composition derived from geochemical analyses of outcrops and/or global scale xenolith and tectonothermal age data (Table 2.2). Since some uncertainties have arised in the composition of the SCLM of the North African margin due to the lack of xenolith information, I have tested four common Tecton bulk compositions (Tc_1 to Tc_4, Griffin et al., 2009) in accordance with the average tectonic age of the crustal units in the region. All four lithospheric mantle compositions are moderately depleted when compared to PUM composition. Fig. 11a shows the calculated P-wave velocities and densities for the different mantle compositions considering a standard lithosphere with a 32-km thick crust and a LAB depth of 130 km. As seen in Fig. 11a, beneath the Sp–Gnt transition at 40–45 km depth, no major differences are detectable in terms of absolute Vp velocities (of the order of 0.03–0.035 km $s^{-1}$, between Tc_1 and Tc_4), whereas maximum differences in SCLM density are of the order of 20 kg $m^{-3}$ (between Tc_2 and Tc_4). From the four compositional models tested, only the Tc_1 composition is found to better match the medium-long wavelength part of the geophysical observables (see Fig. 4), although it should be recognized that Tc_4 and likely Tc_2 and Tc_3 could be made compatible with the geophysical observables by slightly modifying the crust and mantle lithosphere geometry.

Fig. 2.11b summarizes the compilation of absolute Vp and densities calculated

for the five compositional mantle types considered in this study with the same lithospheric structure as used in Fig. 2.11a. As observed, maximum velocity variations are of the order 0.1 km $s^{-1}$ between the PUM composition of McDonough and Sun (1995) (Pm_1) and the TILE composition of Griffin et al. (1999).

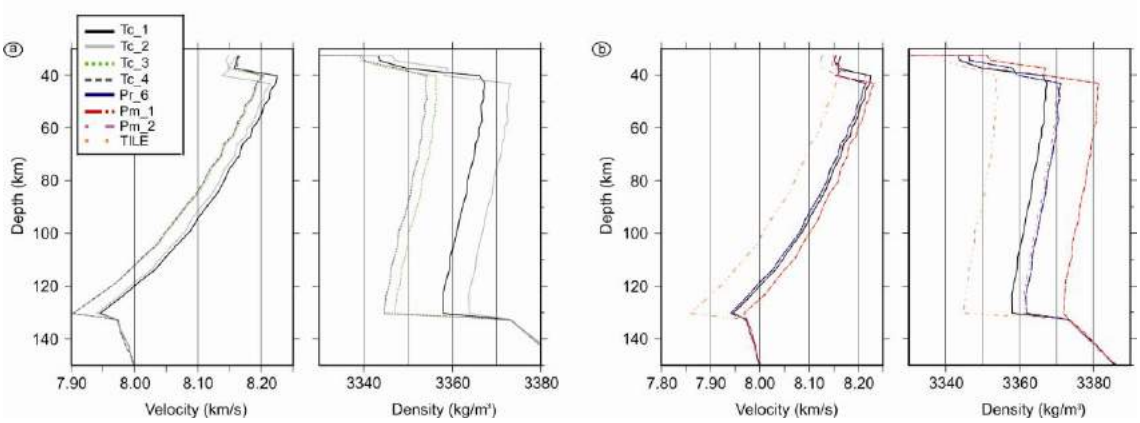


Figure 2.11: a) Depth variation of P-wave velocities (left panel) and densities (right panel) calculated for different average-Tecton mantle compositions according to Griffin et al. (2009) for a 1-D lithosphere structure consisting of 32 km thick crust and 130 km thick lithosphere. b) Same as a) for the mantle chemical compositions used in our modeled transect (see Table 2.2).

No major differences are observed in absolute Vp seismic velocities between the Proton lherzolite average type (Pr_6), the Tecton garnet type (Tc_1) and the primitive upper mantle compositions (Pm_1 and Pm_2). Results show that differences in Vp amount as much as 0.02 km $s^{-1}$ for the Pm_1 composition, which are not detectable since they fall within the range of resolution of the seismic observable. Density differences at given P-T conditions attain maximum values of 28 kg $m^{-3}$ between TILE and Pm_1; 10 to 15 kg $m^{-3}$ between TILE and Tc_1, Pr_6 and Pm_2; and between Pm_1 and Tc_1, Pr_6 and Pm_2. Differences between Tc_1, Pr_6 and Pm_2 are <5 kg $m^{-3}$, the latest being barely detectable. Although no significant differences are observed in the calculated geophysical fingerprint of the proposed compositional mantle types, these areas are characterized by different tectonic ages and histories, and therefore it is likely that the mantle has retained different compositional signatures. Our best fitting model is compatible with a bulk mantle composition corresponding to Pr_6 underneath the Pyrenees as recorded from xenolith samples. This mantle-type composition is characterized by a relatively high content on CaO and $Al_2O_3$ (3.2 and 3.7%, respectively) which may represent Phanerozoic reworking of Proterozoic to Archean crust (Griffin et al., 2009).

Widespread Neogene volcanism in the W-Mediterranean basins supports a refertilization of the former mantle and therefore it is in agreement with the PUM mantle type found in this study. In the Valencia Trough magmatism is characterized by two volcanic cycles which are clearly separated in time and by their petrological setting (Martí et al., 1992). The first volcanic cycle being of Chattian-early Burdigalian is characterized by calc-alkaline andesitic and pyroclastic rocks, while the second cycle of Tortonian to Recent age is characterized by poorly differentiated alkali-basalts. The Pm_2 mantle composition used in the Valencia Trough and Balearic Promontory is similar to that used by Fullea et al. (2010) in the western part of the Atlas region where young alkaline magmatism is also present. Seismic data show that the Algerian Basin is floored by oceanic-type crust formed during Miocene times (Booth-Rea et al., 2007) and therefore, a more enriched composition relative to Pm_2 is justified. The Pm_1 mantle-type was also selected by Fullea et al. (2010) as representative for the Alboran and Algerian basins.

In the North African margin our results are also in agreement with those obtained by Fullea et al. (2010) who concluded that a Tc_1 mantle composition produces the best regional fitting model and that this mantle type could be taken as a representative average for the whole SCLM in the Atlantic–Mediterranean transition zone. In the Sahara region I have taken a mean TILE composition to account for the transition to the West African Mobile Zone, which is characterized by largely reworked terranes including Archean/Proterozoic/Phanerozoic signatures (Begg et al., 2009). Since LitMod2D code works under a forward scheme, it is not easy to precisely assess the role the different variables have on the resulting model. Identifying mantle density with bulk composition and seismic velocities is a difficult problem due to the lack of uniqueness. Recent works by Afonso et al. (2013a, 2013b) present a complete analysis of the trade-off between temperature and compositional effects on wave velocities, the non-uniqueness of the compositional space and the dissimilar sensitivities of physical parameters to temperature and composition. In these works, the authors conclude that a wide range of compositions can equally explain multiple geophysical data. As a consequence, deep temperature anomalies $\leq$ 150 °C and compositional anomalies $\Delta$Mg#<3 are not simultaneously resolvable, being the bulk $Al_2O_3$ content a better compositional indicator than Mg#.

# Chapter 3: The Cantabrian Margin geo–transect (second profile)

This chapter includes parts relative to data gathering, aims, modeling technique, and results that have been accepted for publication in the Elsevier international journal *Lithos* (Pedreira et al., 2015), in which I participated as co-author. A simplified version of this transect is incorporated into the Cantabrian Mountains - Central System - Betics geo-transect, and therefore the discussion has been incorporated in Chapters 4 and 6.

Rifting processes within continents may result in the formation of passive margins, which may later evolve into convergent margins creating either collisional or non-collisional orogens. Recently, significant progress was made towards the understanding of the processes governing the formation and evolution of rifted margins, including the key role of structural inheritance, thermal and rheological stratification of the lithosphere and divergence velocity, among others (e.g., Pérez-Gussinyé and Reston, 2001; Huismans and Beaumont, 2007 and 2011; Manatschal et al., 2015). However, much less effort has been focused on the effects that the structure and composition of passive margins have on their subsequent tectonic inversion and their control on the architecture of mountain belts (e.g., Jammes et al., 2014; Tugend et al., 2014).

The North-Iberian (or Cantabrian) continental margin and the Cantabrian Mountains in northern Spain (Figure 3.1) are especially interesting to study these relationships for several reasons. First, the North-Iberian margin is a rare example of a margin that evolved from passive to convergent after only ~45 my of post-rift history, being one of the shortest-lived examples of passive margins worldwide (Bradley, 2008). It formed during the opening of the Bay of Biscay in the Mesozoic, and was soon affected by the convergence between the Iberian and European plates during the latest Cretaceous-Cenozoic in the framework of the Alpine orogeny. Second, its convergent stage was also aborted at an early stage of development, so that the passive margin structure can be well constrained. This is also facilitated by a good geophysical dataset available in the area. The convergent stage is also peculiar because it led to the subduction of the thickest (inner) part of the margin towards the outer margin, at the same time as the Cantabrian Mountains were uplifted from the former continental platform. The north-directed crustal root (the same polarity as in the Pyrenees) is located approximately beneath the present-day shoreline, which adds further interest to this area from the isostatic point of view.

To understand how and to which extent the particular configuration of such a young passive margin conditioned its later evolution under a convergent setting, we need a well-constrained model of the structural, thermal, geochemical and petrophysical architecture of the crust and upper mantle.

Despite the good geological and geophysical knowledge of this area, several key

issues are still poorly known. One of these issues is the nature of the basement beneath the margin. The oceanic crust with undoubtedly oceanic magnetic anomalies is present only approximately to the west of the 6ºW meridian, the remaining part of the margin being composed of thinned continental or transitional crust (Gallastegui et al., 2002; Roca et al., 2011; Ruiz, 2007; Sibuet et al., 2004). Seismic velocity-depth profiles in this ocean-continent transition reveal a high-velocity lower crust (~7.20-7.30 km/s) on top of a low-velocity upper mantle (~7.7-7.9 km/s) (Gallart et al., 1997; Fernández-Viejo et al., 1998; Ruiz et al, in prep.). These velocities can be explained either by upper mantle hydration/serpentinization (e.g., Roca et al., 2011) and/or by magma addition at the base of the crust by decompression melting during lithospheric thinning, but their relative importance remains enigmatic. This has important implications on the style of the tectonic inversion, because these two processes produce very different modifications in the rheological profile of the lithosphere.

The aim of this profile is to obtain a more reliable model of the lithospheric structure of the North-Iberian margin and the Cantabrian Mountains, using geophysical and petrological constraints.

## 3.1. – Crustal geometry from previous studies

The crustal geometry along this geo-transect is based on previous works including seismic surveys, geological cross-sections and combined geological-geophysical interpretations. This transect crosses the central Cantabrian Mountains approximately along the 4.5ºW meridian, and it is a slight modification of the model proposed by Gallastegui (2000) after the results of the MARCONI-1 seismic refraction and wide-angle reflection data (Ruiz et al., in prep.) (Fig 3.1). The geometry of the off-shore Le Danois Basin was taken from Gallastegui et al. (2002) and Cadenas (2013) and the base of the Duero Basin is based on published isobath maps constrained by a network of seismic profiles and wells (Gallastegui, 2000). Only the southernmost part of the Duero Basin, where there are no data available, has been slightly modified from those maps to fit the Bouguer anomalies. The northern limit of the Duero Basin is marked by the southern frontal structure of the Cantabrian Mountains, which has been clearly imaged by several commercial seismic lines down to ~2 s two-way travel time (TWTT). The ESCIN-2 seismic reflection profile across the central Cantabrian Mountains (Pulgar et al., 1996; 1997) provided a clear image of this structure down to 6 s TWTT, where it roots into a flat horizontal level. Beneath this level, a wedge-shaped area with strong subhorizontal reflectors is clearly identified, thinning towards the south

(orange shaded in Figure 3.2). The reflectivity of the crust beneath 6 s TWTT is highly variable, but it is clearly subhorizontal in the southern half of the profile, and north-dipping from the mountain front to the north (light blue shaded in Figure 3.2), beneath the wedge-shaped area of strong subhorizontal reflectors. The Iberian Moho shows the same dipping attitude: it is identified at 11.5-12 s TWTT beneath the Duero Basin, and starts dipping towards the north beneath the Cantabrian Mountains, down to ~15 s TWTT in the northern end of the profile (located 30 km south of the coastline). Normal-incidence ray-tracing modeling carried out by Gallastegui (2000), locates the Moho at 34 km depth beneath the Duero Basin and at 42 km depth in the northernmost point sampled by the reflections, which due to its dipping attitude, corresponds to a point at ~17 km to the south of the northern edge of the profile. However, the wide-angle reflections recorded by 7 land stations deployed in a N-S line during the acquisition of the marine ESCIN-4 profile (see location in Figure 3.1) provided clear evidence for the continuity of the Iberian Moho down to at least ~53 km.

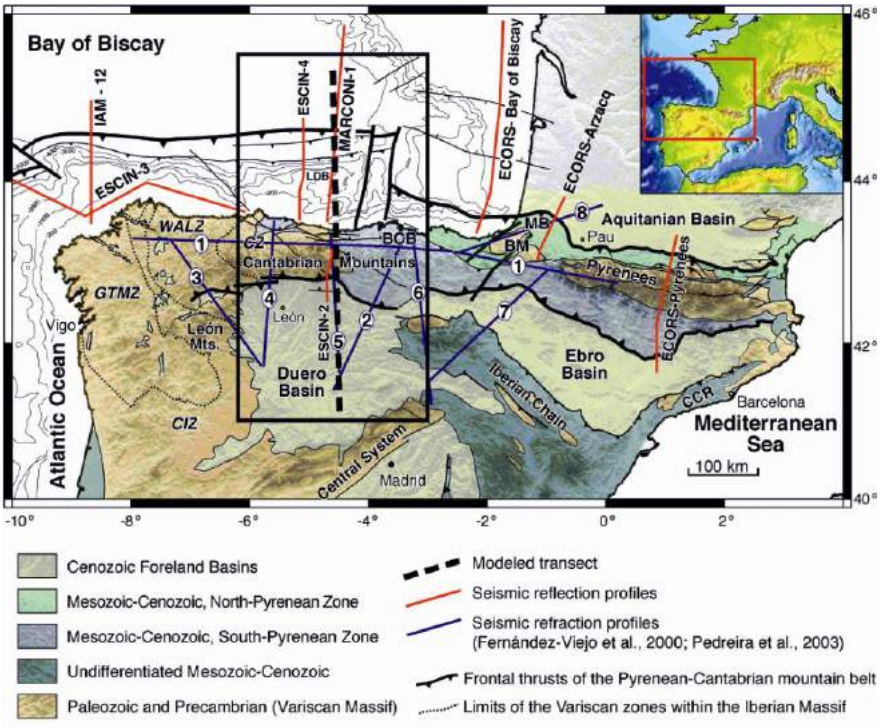


Figure 3.1: Tectonic map of the Pyrenean-Cantabrian mountain belt in north-Iberia showing the location of the modeled N-S lithospheric transect and available deep seismic profiles. BCB, Basque-Cantabrian basin; BM, Basque Massifs; CCR, Catalan Costal Ranges; MB, Mauléon basin. Acronyms in italics refer to tectonometamorphic zones within the Iberian Variscan Massif: CIZ, Central Iberian Zone; CZ, Cantabrian Zone; GTMZ, Galicia – Tras os Montes Zone; WALZ, West Asturian-Leonese Zone.

As it has been documented by Pulgar et al. (1996), Gallart et al. (1997) and

Fernández-Viejo et al. (1998), the northernmost stations (located very close to the coastline) only recorded one strong reflection, identified as the PmP beneath the Cantabrian margin (and continuing about 10-15 km inland), whereas stations to the south also imaged another strong reflection produced in a deeper, north-dipping discontinuity, interpreted to be the subducting Iberian Moho (Figure 3.2, upper-left panel). Ray-tracing modeling locates the "Cantabrian" Moho at 30 km depth beneath the coastline, uprising to ~16-18 km beneath the abyssal plain. The "Iberian" Moho, on the other hand, is located at 48-53 km depth, some 15-20 km to the south of the coastline. Wide-angle recordings of the off-shore MARCONI-1 seismic profile, located approximately along the studied transect (Figure 3.1), also provided similar results (Ruiz et al., in prep.). Therefore, both the seismic reflection profile and the wide-angle records are consistent in revealing the north-dipping attitude of the Iberian Moho, subducting beneath the margin in the same sense than in the Pyrenees, down to at least 50-55 km. Note that the limited length of the ESCIN-4 profile does not allow recording PmP reflections in the Iberian crust deeper than these values (Figure 3.2, upper left panel).

The MARCONI-1 profile is longer, but the airguns released less than half the energy used in the ESCIN-4 (Álvarez-Marrón et al., 1997; Ruiz et al., in prep.). If this root extends deeper, as proposed by Gallastegui (2000), it would be difficult to identify it due to the poor velocity contrast between eclogitized crustal rocks and mantle peridotites, and the attenuation of the seismic energy along these long-distance paths. The crustal basement beneath the Bay of Biscay is known to have been partially consumed beneath North Iberia, creating an asymmetry in the distribution of the sea-floor magnetic anomalies and an accretionary wedge at the foot of the slope (e.g., Sibuet, 2004; Vissers and Meijer, 2012). However, no evidence of subduction to the south is observed in the wide-angle records (Figure 3.2). Instead, these data point to the underthrusting of this basement and its indentation within the Iberian crust to the south, a process that can explain the same morphological features (Fernández-Viejo et al., 2012; Gallastegui et al., 2002).

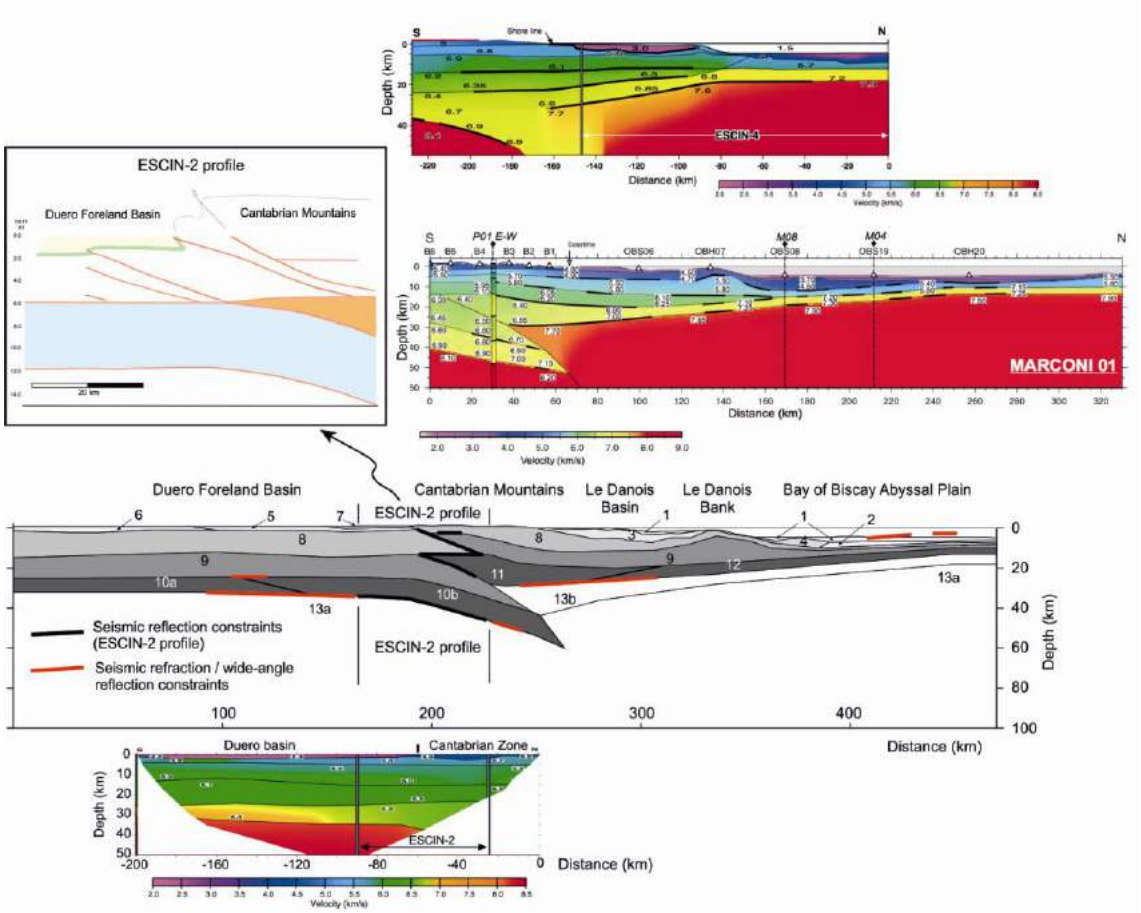


Figure 3.2: Seismic constraints used to delineate the crustal structure of the lithospheric model. Top right panels: P-wave velocity models for the ESCIN-4 and MARCONI-1 profiles (location in Figure 3.1), from Fernández-Viejo et al. (1998) and Ruiz et al. (in prep.), respectively. Superimposed on the MARCONI-1 profile there is a velocity-depth column corresponding to the intersecting E-W Profile 1 of Pedreira et al. (2003, 2007). Note the thin crust beneath the abyssal plain, with velocities of ~7.2 km/s in the lower crust (HVLC), and the velocities of 7.8-7.9 km/s in the uppermost mantle, decreasing to ~7.7 km/s in the mantle wedge above the north-Iberian crustal root (see text for details). Top left panel: record sections of seismic stations 21 (close to the coast) and 25 (near the Duero Basin), during the acquisition of the ESCIN-4 profile, taken from Gallart et al. (1997). Observe that station 21 records a clear PmP reflection denoting a sharp interface at the base of the HVLC beneath Le Danois Bank and the continental platform, gently dipping towards the south. Station 25, on the other hand, records the presence of this same interface (Bay of Biscay Moho) as south as the coastline, as well as a later PmP' phase interpreted to be produced in the north-dipping Iberian Moho. Middle panel: sketch of the crustal structure of the model with the seismic constraints superimposed: red lines mark clear seismic refraction/wide-angle reflection interfaces; black lines depict the geometrical attitude of reflectors in the ESCIN-2 profile, according to Pulgar et al. (1995) and Gallastegui (2000). Lower panel: P-wave velocity model for Profile 5 (location in Figure 3.1from Fernández-Viejo et al. (2000), showing the typical Variscan crustal structure of the crust beneath the Duero Basin, with upper, middle and lower crustal levels and a total thickness of 32-35 km. Note the increasing seismic velocities in the lower crust to the south (see text for details).

The densities considered for the different bodies of the model are listed in Table 3.1. Crustal values were mostly taken from Pedreira et al. (2007) coming from reported density determinations in rock samples or conversions from P-wave velocities (recorded along several seismic refraction/wide angle reflection profiles, as well as in boreholes). A detailed justification for all of them can be found in the aforementioned paper and references therein. However, some minor changes refering to the lower crust have been included with respect to Pedreira et al.(2007), which is now split in pieces of different densities. Beneath most of the continental margin, the density was increased from 2970 kg $m^{-3}$ to 3120 kg $m^{-3}$ to be more consistent with the high seismic velocities (~7.20 km/s) found in this zone (Figure 3.2). Away from this area of anomalously high velocities, the remaining Cantabrian/European lower crust is assumed to have a density of 2900 kg $m^{-3}$. This includes the portion that is tectonized and indented into the Iberian crust (with velocities of 6.40-6.60 km/s) and the lower crust beneath the Armorican platform.

The southern end of the modeled profile is located close to the first relieves of the Central System (Figures 3.1), where xenolith studies reveal one of the most felsic compositions worldwide for the lower crust (Rudnick and Gao, 2003; Villaseca et al., 1999). Alkaline ultrabasic dykes that intruded into the Variscan basement in early Mesozoic times carried a suite of lower-crustal xenoliths composed of felsic granulites (~95 % of the total volume) and much less abundant metapelitic granulites (~5%) and charnokites (~0.01 %).

Towards the north, this anomalous felsic end-member gives way progressively to a more mafic composition. Both felsic and mafic granulites equilibrated during the late Variscan orogeny were exhumed by the Mesozoic-Cenozoic tectonic events all along the Pyrenean-Cantabrian belt (Mendia and Ibarguchi, 1991; Vielzeuf, 1984). Similar felsic and mafic granulites were dredged from the seafloor in the northern slope of Le Danois Bank (Figure 3.3), as clasts within Early Cretaceous syn-rift conglomerates (Capdevila et al., 1980).

All these observations indicate mafic/felsic compositional layering in the lower crust all along north Iberia. Here, is assumed that the composition along the investigated profile changes laterally from “felsic” in the south (although not as felsic as in the Central System) to “intermediate” in the north. For the sake of simplicity, the Iberian lower crust is divided in only two bodies, with a zone of superposition to simulate a gradual change. In absence of further constraints, the limit was placed between them approximately following the strong gradient in seismic velocities observed in the seismic refraction profile 5 (location in Figure 3.1, P-wave velocity model in Figure

3.2).

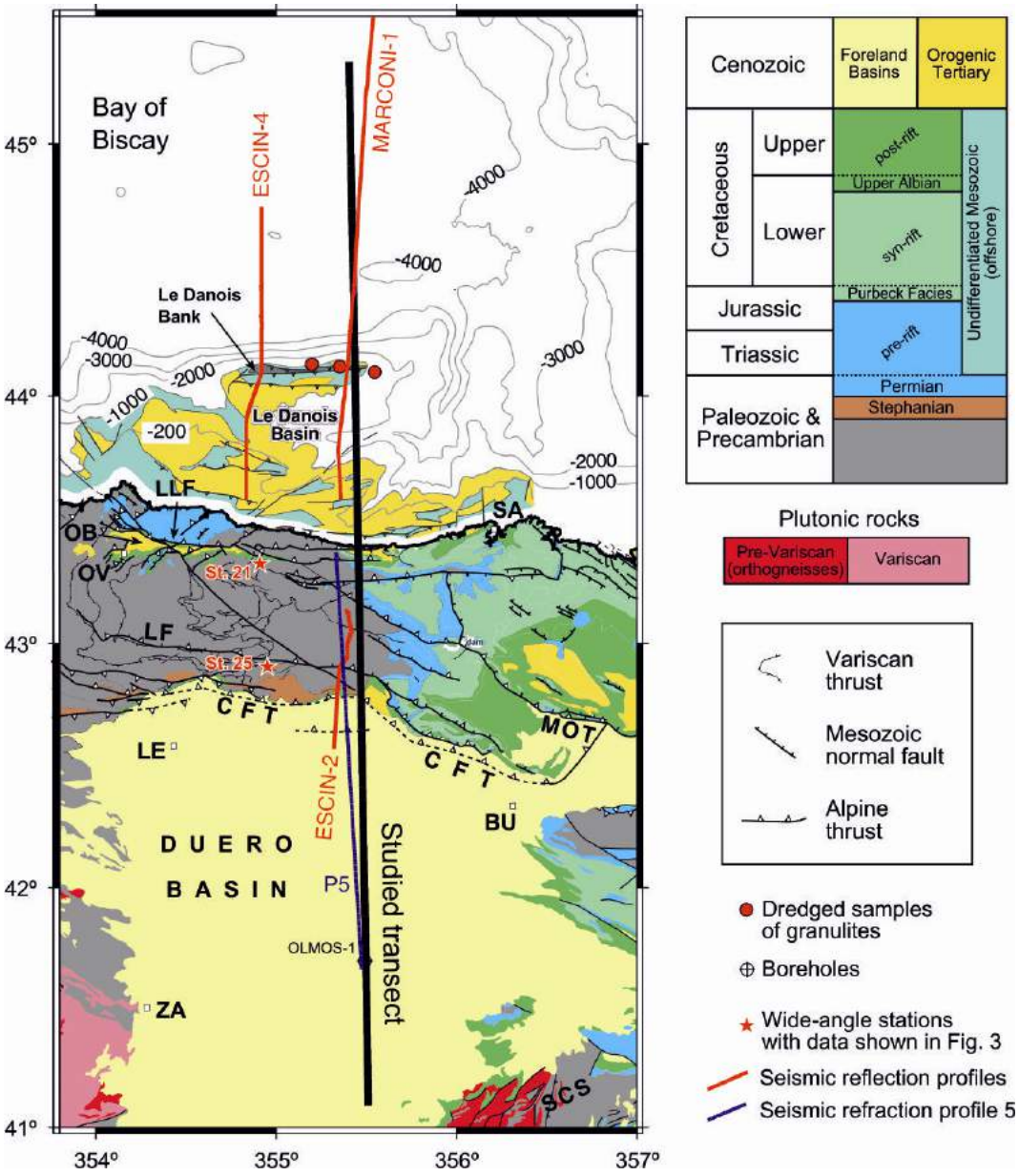


Figure 3.3: Detailed geological map of the investigated transect, modified from previous synthesis by Alonso et al. (1996), Quintana (2012), Rodríguez Fernández et al. (2004) and Gallastegui et al. (2002). Cities: BU, Burgos; LE, León; OV, Oviedo; SA, Santander; ZA, Zamora. Geological features: CFT, Cantabrian Frontal Thrust; LF, León Fault; LLF, Llanera Fault; MOT, Montes Obarenes Thrust; OB, Oviedo Basin; SCS, Spanish Central System.

Surprisingly, in spite of the more felsic composition, higher seismic velocities in the lower crust are reported near the Central System (6.8-6.9 km/s) than to the north (~6.6 km) along this profile. This observation can be at least partially explained in terms

of water content, if we assume that the lower crust is anhydrous in the south and mildly hydrated to the north. Therefore, for the "felsic" part, we consider an anhydrous mixture dominated in a 70 wt. % by the composition of the felsic granulite xenoliths from the Central System, and with a 30 wt. % contribution from the average global lower crustal composition proposed by Rudnick and Gao (2003), which is dominated by mafic granulites. For the "intermediate" composition, a 50-50% mix between these two end-members, with the addition of 2% wt. of water is considered. Forward tests have shown that this water content is enough to fit the seismic velocities, and quantities in this order are generally accepted for the lower crust (Hyndman and Shearer, 1989; Semprich et al., 2010).

Thermal conductivity and radiogenic heat production values used in this study were chosen according to different sources of information. Some of the thermal conductivity data come from measurements in wells, summarized by Fernàndez et al. (1998). For deeper parts of the crust, conductivity values are calculated based on the composition, temperature and pressure, following experimental work (Clauser and Huenges, 1995; Vosteen and Schellschmidt, 2003).

| Body | Description | Density ($kg/m^3$) | Thermal conductivity (W/(K·m)) | Heat production ($\mu W/m^3$) |
|---|---|---|---|---|
| 1 | Cenozoic in LDB and post=tectonic cover (Mid.=Up. Miocene to recent) in the abyssal plain | 2200 | 2.50 | 1.20 |
| 2 | Pre=tectonic and syn=tectonic Mesozoic= Cenozoic sediments in the abyssal plain | 2400 | 2.50 | 1.20 |
| 3 | Mesozoic in the continental platform (LDB) | 2550 | 2.50 | 1.20 |
| 4 | Accretionary wedge at the foot of the continental slope mix of sediments and basement rocks | 2550 | 2.50 | 1.50 |
| 5 | Sediments of DB (Mesozoic and mostly Tertiary) | 2460 | 2.53 | 1.20 |
| 6 | Sediments of DB (fine=grained, southern part) | 2300 | 2.53 | 1.20 |
| 7 | Sediments of DB (conglomerates northern border) | 2600 | 2.53 | 1.20 |
| 8 | Upper Crust (pre=Mesozoic basement) | 2720 | 2.40 | 1.65 |
| 9 | Middle Crust | 2860 | 2.10 | 1.00 |
| 10 | Iberian Lower Crust | b | 2.00 | 0.33-0.40 |
| 11 | European (Cantabrian)Lower Crust, except HVLC | 2900 | 2.00 | 0.33 |
| 12 | High Velocity Lower Crust in the continental margin | 3120 | 2.00 | 0.15 |
| 13 | Mantle | b | c | 0.02 |

Table 3.1. Density values and thermal properties used in this geo-transect. b, density values are dependent on the chemical composition and pressure-temperature conditions (see text and Table 3.2); c, variable thermal conductivity (pressure and temperature dependent) according to the model of Hofmeister (1999); DB, Duero basin; HVLC, High Velocity Lower Crust; LDB, Le Danois basin.

Within the mantle, as mentioned before, the effects of pressure and temperature are modelled on the bulk thermal conductivity according to the formalism in Hofmeister (1999). Radiogenic heat production is assumed to be constant within each body of the model. Crustal values come from thermal modeling studies (Brunet, 1994), measurements in samples from the area (Fernández et al., 1998; Jiménez-Díaz et al., 2012) and average values according to lithological types (Rudnick and Gao, 2003; Vilà et al., 2010). Considering the thicknesses of the crustal layers beneath the Duero Basin (2500 m for sediments and 13, 10 and 8 km for the crystalline upper, middle and lower crusts, respectively), the weighted average heat production in the whole crust is 1.11-1.12 $\mu W/m^3$. It fits well with the standard continental crust heat production of 1.03+/-(0.74-1.38) $\mu W/m^3$ proposed by Vilà et al. (2010), and lies also between the averages for Paleozoic orogens (0.96 $\mu W/m^3$) and Mesozoic-Cenozoic contractional orogenes (1.17 $\mu W/m^3$) according to Rudnick and Fountain (1995).

## 3.2. – Results

In the northern part of the Iberian plate, beneath the Moho discontinuity, the composition of the lithospheric mantle is more difficult to determine. To avoid introducing excessive complexity that is not well constrained, and taking into account that no oceanic lithosphere is expected in this part of the Bay of Biscay, a single composition for the lithospheric mantle along the transect is considered. This composition corresponds to a "tecton" (tectonothermal age of the overlying crust < 1 Ga) garnet subcontinental lithospheric mantle (type Tc_1 of Griffin et al., 2009; Table 3.2). However, this dry composition predicts P-wave velocities of ~8.1 km/s for the uppermost mantle beneath the North-Iberian margin, while seismic studies reported velocities as low as 7.7-7.9 km/s (Figure 3.2). The easiest way to explain these low velocities is to assume some degree of hydration. The presence of water allows the stabilization of hydrous phases (e.g. serpentines, amphiboles) at temperatures < ~500 ºC, causing the decrease in P-wave velocities and densities. Empirical models indicate that velocities of 7.6-7.9 km/s in the upper mantle would correspond to $H_2O$ contents of ~1-2 wt% (Carlson, 2003). Hydration of the uppermost mantle in continental margins tends to vanish with depth, creating rather complex and diffuse zones. To keep the model as simple as possible, a single body of hydrated mantle with a simple geometry (thickness of 5 km along most of the margin) and constant water content (1 wt. %) added to the Tc_1 lithospheric composition is introduced (Table 3.2).

| | Iberian lower crust | | Mantle | | |
|---|---|---|---|---|---|
| | "felsic" (south)[a] | "intermediate" (north)[b] | Lithospheric (dry)[c] | Lithospheric (hydrated)[d] | Sublithospheric[e] |
| Body | 10a | 10b | 13a | 13b | - |
| $SiO_2$ | 59.91 | 56.89 | 44.76 | 44.31 | 45.36 |
| $Al_2O_3$ | 17.25 | 16.81 | 3.52 | 3.48 | 4.49 |
| FeO | 7.83 | 7.88 | 8.05 | 7.96 | 8.11 |
| MgO | 4.64 | 5.28 | 40.04 | 39.63 | 38.10 |
| CaO | 3.98 | 5.47 | 3.12 | 3.09 | 3.58 |
| $Na_2O$ | 2.60 | 2.56 | 0.24 | 0.24 | 0.36 |
| $K_2O$ | 2.57 | 1.97 | 0.00 | 0.03 | 0.00 |
| $H_2O$ | 0.00 | 2.00 | 0.00 | 1.00 | 0.00 |

Table 3.2. Chemical composition of the Iberian lower crust and mantle along the second geo-transect. [a]Based on a mixture between the composition of the felsic granulite xenoliths from the Spanish Central System (Villaseca et al., 1999) (70 wt. %) and the average global lower crustal composition proposed by Rudnick and Gao (2003) (30 wt. %). [b]Based on an evenly mixture between the composition of the felsic granulite xenoliths from the Central System (Villaseca et al., 1999) and the average global lower crustal composition proposed by Rudnick and Gao (2003), plus 2 wt. % of water. [c]Average Tecton Garnet Subcontinental Lithospheric Mantle (Tc_1) (Griffin et al., 2009).

## 3.2.1. – Lithosphere mantle structure

Figure 3.4 shows the observed and calculated values of surface heat flow, Bouguer anomaly, geoid undulation and elevation for the lithosphere cross-section according to the constraints and assumptions described in the previous sections. The calculated response of the proposed lithospheric model fits satisfactorily the regional trends of all these observables. Lithosphere-asthenosphere boundary was introduced in the model with the simplest geometry that is able to achieve a reasonable fit of the observables (Fig. 3.4). Lithospheric thickness varies significantly along the transect: 145 km beneath the southern part of Duero Basin, 125 km beneath the northern part of the basin, 170 km under the crustal root, and 160 to 135 km (shallowing towards the north) beneath the floor of the Bay of Biscay abyssal plain. These are relatively high values, but they are necessary to avoid unrealistic elevation, geoid height and surface heat flow values with the defined crustal structure. Elevation is correctly reproduced throughout the model only when some degree of flexural support is considered (continuous line in Figure 3.4d). Theoretical elevation according to local (Airy) type of isostatic equilibrium is represented in Figures 3.4d by a dotted line. Areas where the absence of local isostatic equilibrium is more evident include the Le Danois Bank (at model distances of 300-350 km), the southern border of the abyssal plain (km 350-425)

and the zone immediately above the deepest part of the crustal root (km 250-265). Forward modeling has indicated that an effective elastic thickness of ~30 km is enough to reproduce the observed elevations. This is a reasonable value for Variscan and Alpine lithospheres according to results based on "Bouguer coherence" and "free-air admittance" methods (Pérez-Gussinyé and Watts, 2005).

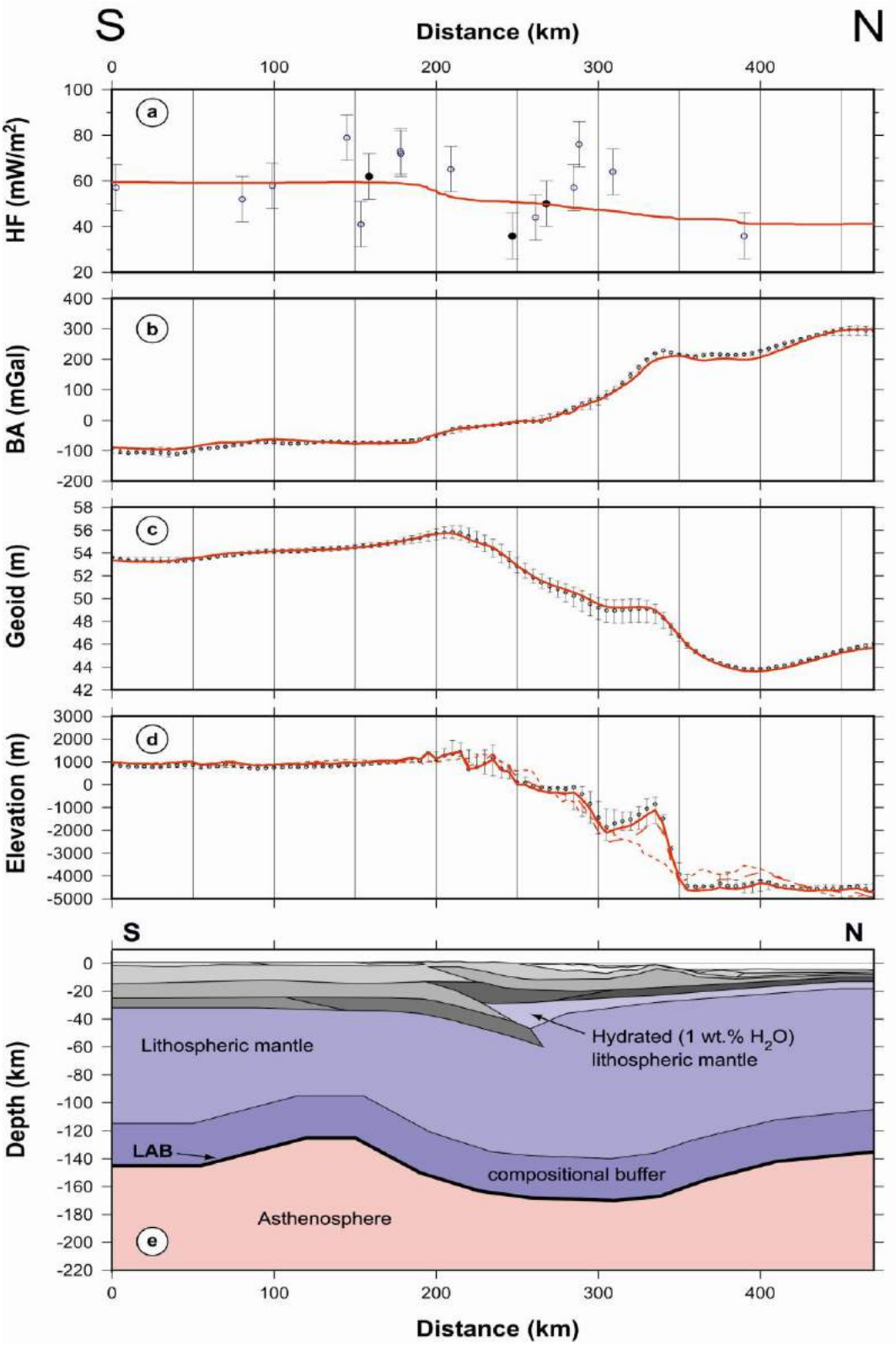

Figure 3.4: Modeling results for the Cantabrian Margin geo-transect (second profile), showing the fitting of surface heat flow (HF), Bouguer anomaly (BA), geoid and elevation. Except for heat flow values, black dots mark the observed values along the transect, and error bars represent ±1 standard deviation according to values observed 25 km to the east and to the west of the transect (grey rectangles in Figure 3.4). Heat flow values are orthogonally projected onto the section from lateral distances ≤10 km (black dots) or ≤50 km for land data and ≤100 km for marine data (blue dots). Red lines indicate the calculated responses of the model (with a Gaussian filter for the case of the surface heat flow to avoid short-wavelenght spikes). In the elevation plot, red dotted and dashed lines represent calculated elevation in the case of effective elastic thickness, Te=0 km (Airy-type isostatic equilibrium) and Te=10 km, respectively. Continuous red line represent the calculated elevation for Te=30 km (see text for details).

## 3.2.2. – Temperature and density distribution

Calculated temperatures and densities down to 225 km depth are shown in Figure 3.5.

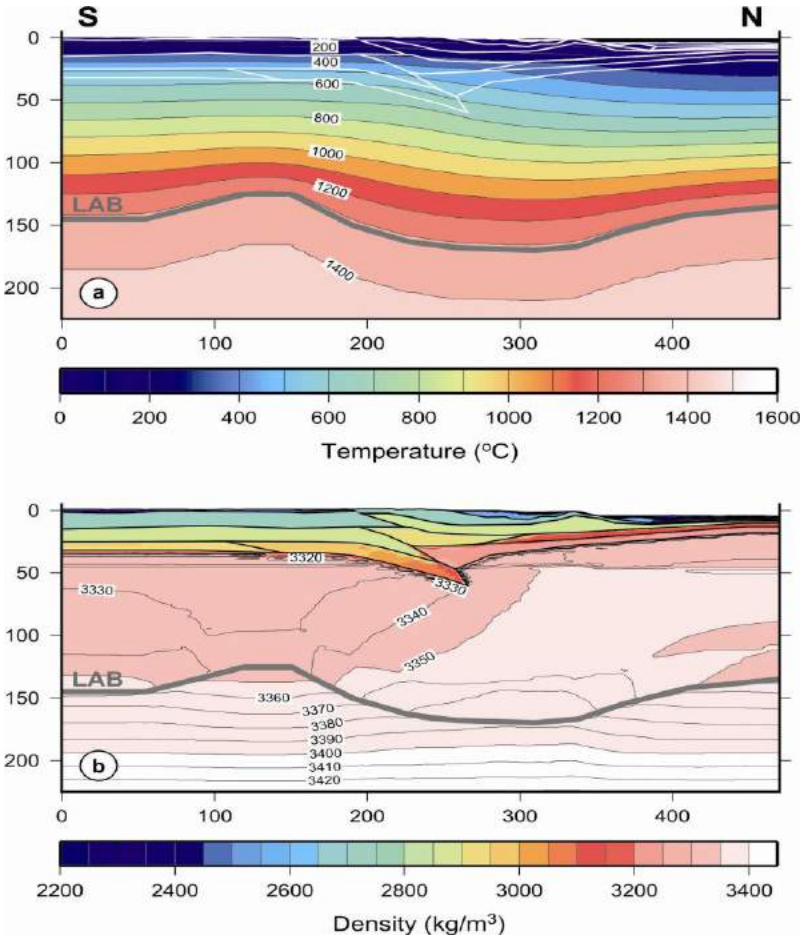


Figure 3.5: a) Thermal and b) density structure along the modeled transect. The grey bold line (LAB) represents the base of the thermal lithosphere.

Within the lithosphere, the increase of density (Fig. 3.5b) with depth by the effect of pressure generally dominates over the density decrease by thermal expansivity. However, since the base of the lithosphere is isothermal, thinner lithospheric columns are globally warmer, less dense and less sensitive to the effect of pressure than thicker ones. Density values (Figure 3.5b) vary between 3309 kg $m^{-3}$ just beneath the Iberian Moho, to 3380 kg $m^{-3}$ in the deepest part of the lithospheric root, within the compositional buffer. A density jump observed at ~45 km depth, more pronounced in the northern part of the section, corresponds to the phase change between spinel peridotites and garnet-peridotites. In the convective part of the mantle beneath the LAB, where the increase in temperature with depth is reduced to the adiabatic gradient, the stronger effect of pressure induces a steeper increment of density with depth.

## 3.2.3. – Mantle velocity distribution

P-wave velocities (Fig. 3.6), decrease towards the north as the water content increases, from an average value of 6.81 km/s in the region with felsic composition, to 6.52 km/s beneath the northern border of the Duero Basin (intermediate composition with 2 wt. % of water). These results are in close agreement with the velocity values observed along the seismic refraction/wide-angle reflection profile 5 (Figure 3.2). In the crustal root, eclogitization reactions start at ~40-45 km depth, but densification is limited due to the presence of felsic constituents and hydrated phases such as phengite. Maximum densities and P-wave velocities are 3110 kg $m^{-3}$ and 6.83 km/s, respectively.

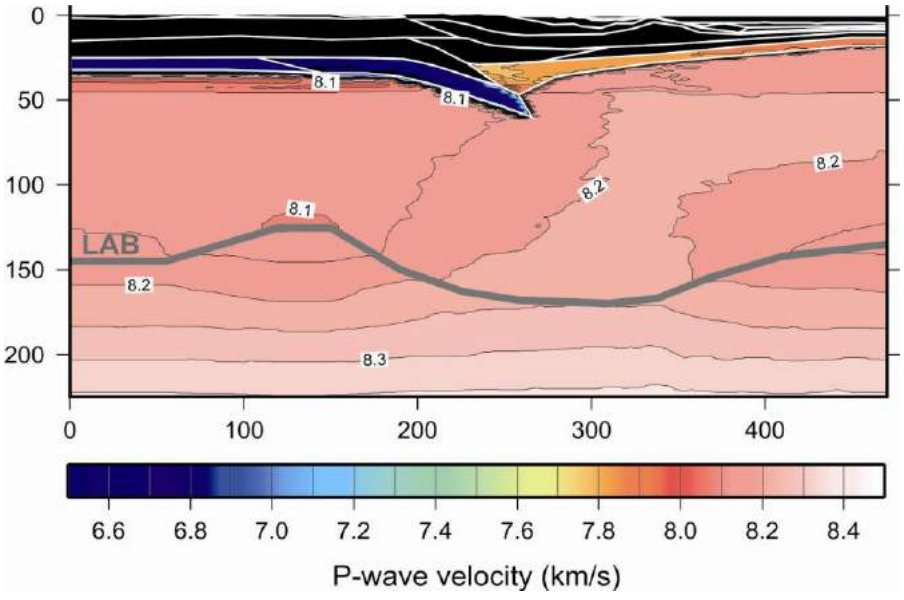


Figure 3.6: P-wave velocity structure along the modeled transect. The grey bold line (LAB) represents the base of the thermal lithosphere.

The calculated P-wave mantle velocity allows us to constrain the lithospheric structure by comparing the calculated values with published P-wave tomography models. Figure 3.8 illustrates this comparison, in which all the sections are expressed in relative perturbations of P-wave velocities with respect to the ak135 reference model (Kennett et al., 1995). Figures 3.8a and 3.8b show the structure of the studied transect from 40 to 400 km depth, according to the tomographic model of Villaseñor et al (2003), and to our model. Probably the most conspicuous feature in the tomographic slice is the low velocity anomaly located in the top-central part of the section, extending down to 90 km depth. This can be correlated with the low-velocity anomaly created in our synthetic model by the crustal root and the hydrated mantle wedge on top of it. To avoid saturation of the color scale and to facilitate this comparison, the same color palette but ranging from -2.5 to +2.5% was used. In spite of the poor resolution in the northern part of the tomographic section due to lack of seismic stations in the Bay of Biscay, the fast anomaly in the lithosphere is satisfactorily reproduced.

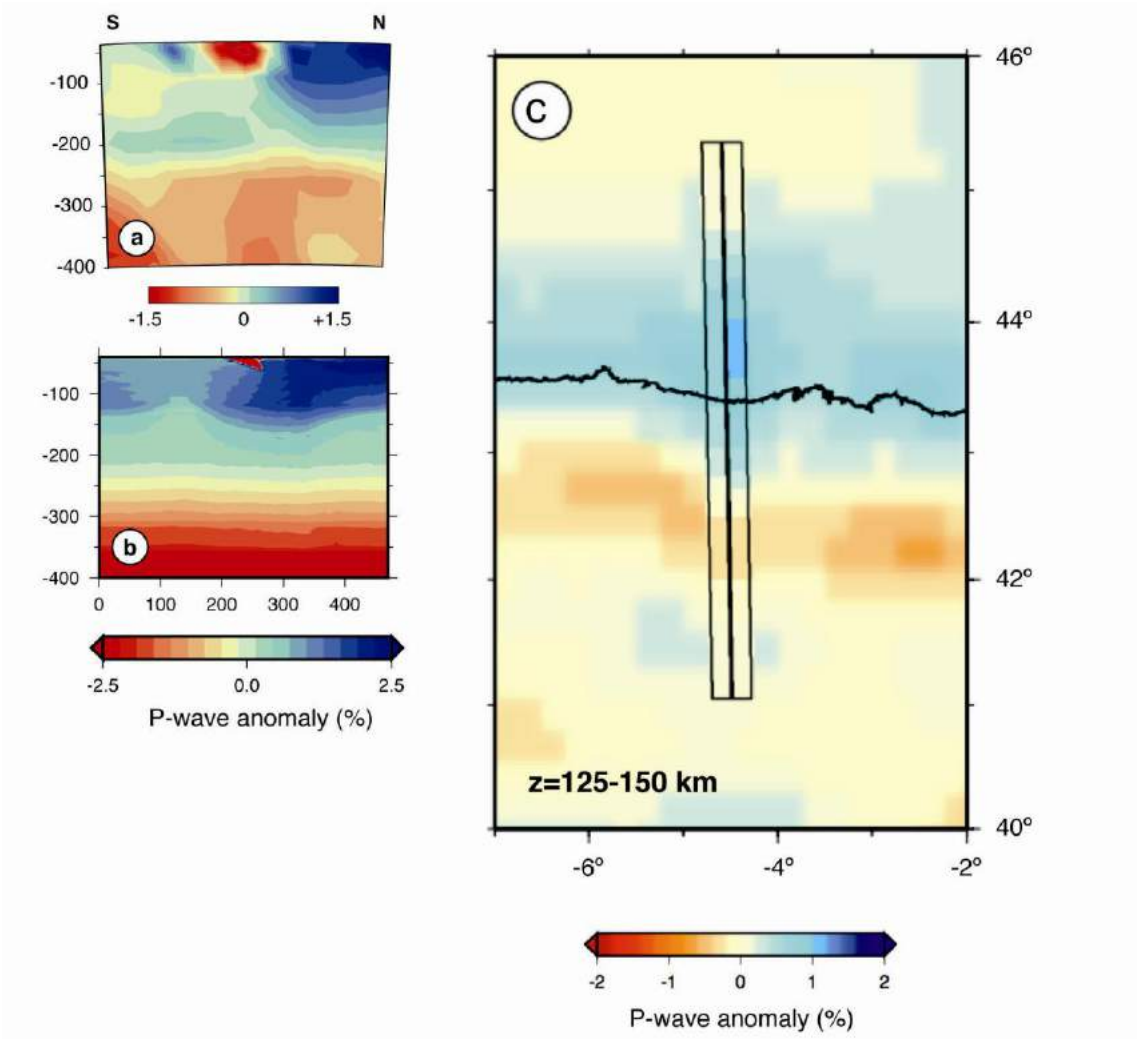


Figure 3.8: Comparison between the P-wave velocity structure calculated for the mantle along the transect

and the results of tomographic models in the same area. All plots represent percentage of velocity deviations with respect to the ak135 reference model (Kennett et al., 1995). a) vertical slice of the tomographic model of Villaseñor et al. (2003) along the studied transect. b) synthetic "pseudo-tomographic" sections, from 40 km to 400 km depth, using a wider colorbar scale (see text for details). Note in a) the low velocity anomaly located in the top-central part of the section, which can be correlated with the low-velocity anomaly created in our synthetic models by the crustal root and the hydrated mantle wedge on top of it. Note also the relatively flat surface at ~225 km depth where both types of sections show anomaly values around zero, separating a lower part with slow anomalies from an upper part with dominantly fast anomalies. c), plan view of the tomographic model of Chevrot et al. (2014), with anomalies averaged for depths between 125 and 150 km, after crustal correction. On top of this map, are plotted the calculated anomalies of the synthetic model for the same depth interval. Calculated anomalies are lowered by 0.65 % (see text for details). Note the E-W trending fast anomaly along the coast and the band to the south of relatively slow anomalies (between 42 and 43ºN) that are spatially coincident with the lithospheric root and with the area of uplifted LAB, respectively, in our model.

Calculated seismic velocities in the hydrated uppermost mantle lie in the range 7.79-7.88 km/s. These velocities fit perfectly with the values observed below the Moho in the Bay of Biscay along the ESCIN-4 and MARCONI-1 profiles, except for the southernmost edge of the mantle wedge on top of the subducting Iberian crust, where observed velocities are ~7.7 km/s (Figure 3.2).

## 3.3. – Discussion

As mentioned at the beginning of this Chapter, the Cantabrian Margin geo-transect is integrated in a simplified version into a longer geo-transect continuing in a N-S direction until the Alboran Basin. Therefore, to avoid unnecessary repetitions, the discussion relative to the obtained results in this Chapter 3 has been splitted in Chapter 4 and Chapter 6.

# Chapter 4: The Cantabrian Mountains–Central System–Betics geo–transect (third profile)

Most of the materials of this chapter relative to data gathering, aims, modeling technique, results and discussion, have been submitted for publication to the Elsevier international journal *Tectonophysics* (Carballo et al., submitted). Presently, the manuscript is under review with moderate revision.

In this Chapter, I present the crust and upper mantle structure along a 1065-km-long transect, crossing the entire Iberian plate in N-S direction (Fig. 4.1), by using a modified version of the LitMod-2D code (Afonso et al., 2008). The transect starts in the Bay of Biscay and crosses the Cantabrian Mountains, the Duero Basin, the Central System, the Tagus (or Tajo) Basin, and the Betic Cordillera, ending in the Alboran Basin. The study incorporates the large amount of recently acquired seismological data from the TopoIberia Project. An outstanding novelty of this chapter is the incorporation to the LitMod-2D methodology of sublithospheric mantle bodies with 'anomalous' temperature and/or composition, that allows for exploring the role of dynamic topography.

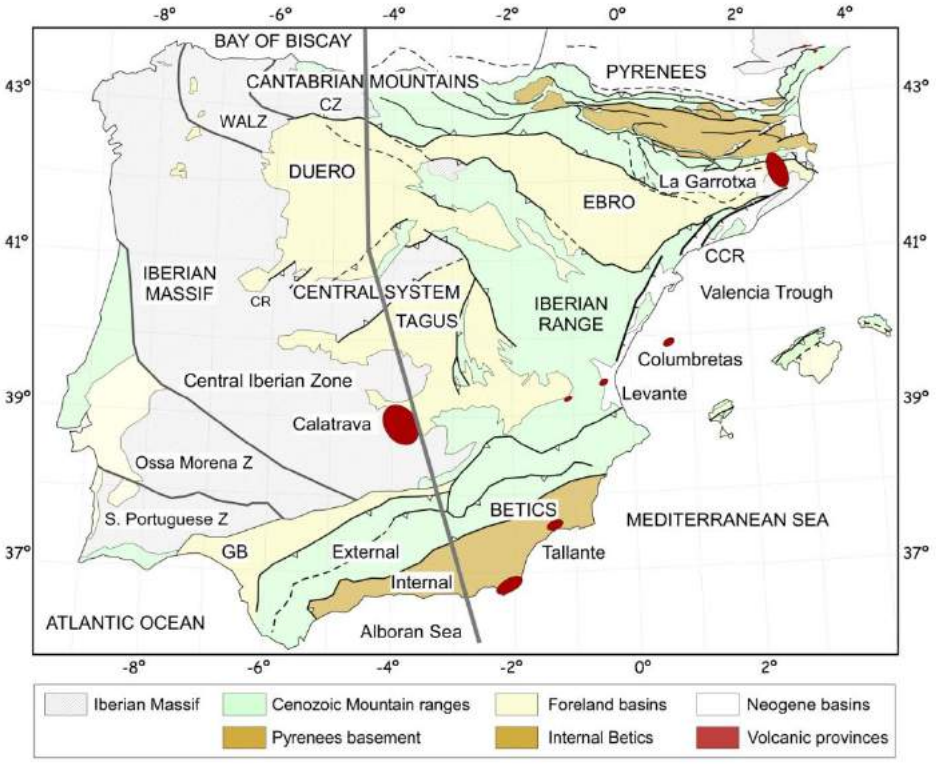


Figure 4.1: Geological map of the study area showing the principal geological domains of Iberia (modified after Vergés and Fernàndez, 2006). Thick gray line locates the modeled transect.

# 4.1. – Crustal geometry from previous studies

The crustal geometry along the geo-transect is based on previous works including seismic surveys, geological cross-sections and combined geological-geophysical interpretations (Fig. 4.2). The northern segment, from 0 to 470 km distance, coincides with the second geo-transect (Chapter 3), which is based on the same methodology. A major difference with the second geo-transect is that in the previous profile the calculations of the physical parameters of the Iberian lower crust were made using a thermodynamic approach.

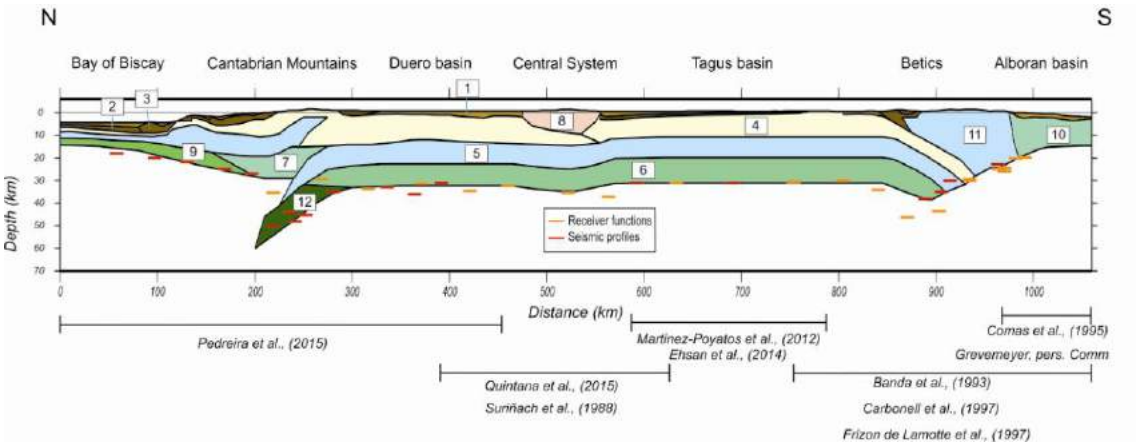


Figure 4.2: Crustal structure corresponding to the best fitting model. Different bodies have been modeled using geological cross-sections (overlaid) and seismic experiments (see text for details). Physical properties of crustal bodies are reported in Table 4.1.

In Chapter 3, a lateral change in the lower crust composition, from felsic-dry beneath the southern half of the Duero Basin, to intermediate-hydrated (2% wt. $H_2O$) northwards was considered. Consequently, the hydrated lower crust is progressively eclogitized with depth beneath the Cantabrian Mountains. In contrast, in this Chapter I consider, southwards of the Cantabrian Mountains, a lower crust with homogeneous density (and thermal properties) along the whole profile. Beneath the Cantabrian Mountains and for depths deeper than 30 km, I adopted a similar intermediate-hydrated lower crust composition, using also the thermodynamic approach in calculating the physical parameters. Another difference with Chapter 3 is the thickness of the lower crust beneath the southern half of the Duero Basin. In this profile I consider a value of 9 km, according to Suriñach et al. (1988), instead of 7 km, which was an extrapolation based on the observed thickness along a seismic refraction profile located further north (Fernández-Viejo, 2000). To constrain the crustal structure in the central segment, I used the Toledo-Salamanca wide-angle seismic survey (Suriñach et al., 1988), the ALCUDIA

deep seismic reflection profile (Martinez-Poyatos et al., 2012), the ALCUDIA2 Wide-Angle Seismic Reflection Transect (Ehsan et al., 2014) and several geological cross-sections (e.g., Banks and Warburton et al., 1991; Casas-Sainz and Faccenna, 2001; Casas-Sainz et al., 2009; Quintana et al., 2015). In the southern segment, I used seismic data from different experiments (e.g., Banda et al., 1993; Gallart et al., 1995; Comas et al., 1995; Carbonell et al., 1997) and geological cross-sections (e.g., Banks and Warburton et al., 1991; Berástegui et al., 1998; Michard et al., 2002; Frizon de Lamotte et al., 2004; Platt et al., 2003 and Ruiz-Constán et al., 2012). In addition to these data, I have also used for the whole transect the compilation of seismic data in Iberia by Diaz and Gallart (2009), and the recent receiver function data obtained in the TopoIberia project from the deployment of seismic stations (IberArray) covering the whole Iberian Peninsula (e.g., Mancilla et al., 2012, 2015).

The physical properties assigned to the sediments and the crustal layers are summarized in Table 4.1. Radiogenic heat production has been taken from a global compilation carried out by Vilà et al. (2010) and Jiménez-Díaz et al. (2012). Thermal conductivity values for crustal bodies were taken from previous studies (Fernandez et al., 1998). Within the upper crust, a body of lower density is considered for the Spanish Central System, where dominant outcrops of leucogranitic and adamellites reveal significantly lower densities than the adjacent metamorphic rocks (Gómez-Ortiz et. al., 2005).

| Bodies | Crust and sediments model | Density (kg/m3) | Heat production (μW/m3) | Thermal conductivity (W/(K · m)) |
|---|---|---|---|---|
| 1 | Tertiary and Quaternary | 2350 | 1.2 | 2.5 |
| 2 | Mesozoic sediments | 2550 | 1.2 | 2.5 |
| 3 | Accretionary prism | 2550 | 1.5 | 2.5 |
| 4 | Upper crust | 2750 | 1.65 | 2.4 |
| 5 | Middle crust | 2850 | 0.5 | 2.1 |
| 6 | Lower crust | 2950 | 0.2 | 2 |
| 7 | European Lower crust | 2900 | 0.33 | 2 |
| 8 | Central System | 2670 | 2 | 2.4 |
| 9 | High Velocity Lower Crust in the continental margin | 3120 | 0.15 | 2 |
| 10 | Neogene Extended Continental Crust of Alboran | 2900 | 0.5 | 2.5 |
| 11 | Betics domain | 2750+6*Z(km) | 1 | 2.5 |
| 12 | Subducted Iberian lower crust | a | b | 0.02 |

Table 4.1. Parameters used in the model for the different crustal bodies. a and b values are dependent on the chemical composition and pressure-temperature conditions (see text and Table 4.2).

Density values have been derived from available seismic velocities and fall within the velocity-density envelopes defined by Barton et al. (1986), Christensen and Mooney et al. (1995) and Hamilton et al. (1978). In the northern segment of the geo-transect I have used the same physical properties than in the second profile (see above) with only very minor modifications in some bodies to allow for a better integration with the rest of the data along the transect. In the mantle (and the eclogitized crustal body), mineral assemblages and physical properties are calculated by the thermodynamic module in LitMod-2D from the prescribed chemical composition and pressure-temperature conditions (Table 4.2).

## 4.2. – Mantle characterization and LAB depth from previous studies

The characterization of the mantle along the profile comes mainly from available Pn- and Sn- velocities, global and regional tomography models and geochemical and isotopic analyses on xenolith samples. Pn data have been compiled from different experiments (e.g., Díaz et al., 2013; Díaz and Gallart, 2009; and DSSWG-Alboran, 1974), showing average values of 8.0 – 8.1 km/s in Iberia mainland with maximum values of ~8.2 km/s in the southern Variscan Iberian Massif (e.g., Díaz et al., 2009; Díaz et al., 2013). Minimum Pn values of ~7.75±0.15 km/s are found in the Alboran Basin (Díaz and Gallart, 2009 and DSSWG-Alboran, 1974). Sn values have been taken from regional tomography in the Euro-Mediterranean region (Díaz et al., 2013) resulting in average velocities of ~4.6 km/s, with maximum values of 4.65 km/s near the Central System. In the northern part of the profile, beneath the North-Iberian Margin, the uppermost mantle shows anomalous low Vp velocities, with values of 7.7 – 7.9 km/s detected in seismic refraction/wide-angle reflection profiles (Fernandez-Viejo et al., 1998; Ruiz, 2007).

P-wave mantle velocities along the modelled profile are obtained from a global travel-time tomography model using the same method described in Bijwaard et al. (1998), incorporating additional earthquakes from 1995 to 2002 and arrival times (Villaseñor et al., 2003). Figure 4.3 shows the depth distribution of the P-wave velocity anomaly relative to the ak-135 model (Kennett et al., 1995). Positive anomalies, exceeding 1%, correspond to the lithospheric mantle domain beneath the North-Iberian Margin, and to the subducting Ligurian-Tethys slab beneath the Betics-Alboran region. Negative anomalies, exceeding -2%, are located beneath the Alboran Basin and the Calatrava Volcanic Province (CVP), extending down to 200 km depth. The tomography

section also shows a zone of slow P-wave velocity (-0.3% to -1%) extending from the northern end of the profile to the CVP, and from 230 km depth to the bottom of the model. A local conspicuous negative anomaly is imaged beneath the Cantabrian Mountains, which could be related to crustal thickening due to shortening. From the Cantabrian Mountains to the CVP, the lithospheric mantle does not show significant velocity anomalies.

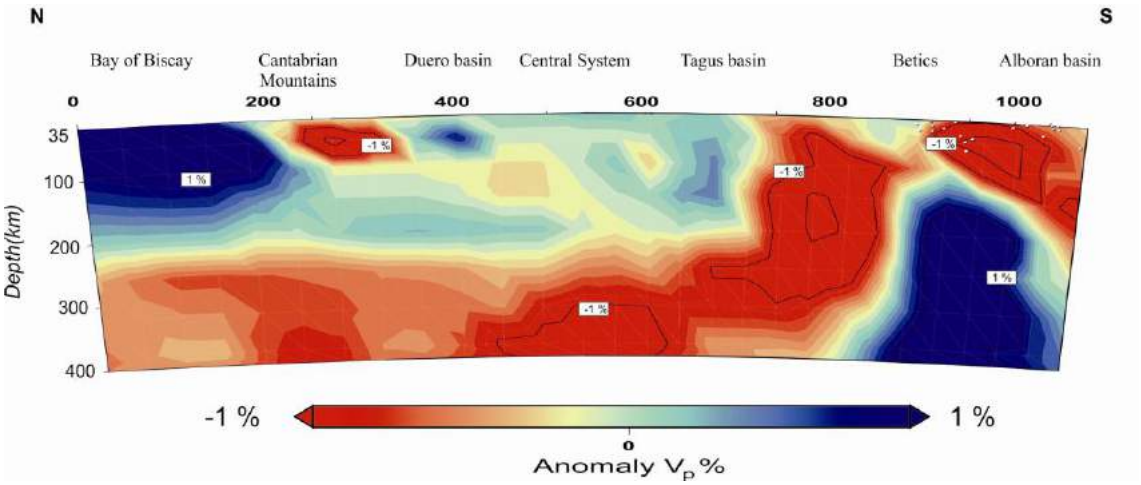


Figure 4.3: P-wave tomography model along the Cantabrian Mountains-Central System-Betics geo-transect (third profile) based on the global travel-time tomography model of Villaseñor et al. (2003).

S-wave mantle velocities are taken from a European shear wave velocity model derived from inversion of seismic shear and surface waveforms (Legendre et al., 2012). These authors show velocity anomalies relative to a regional reference model for different layers with bottom depths of 80, 110, 150 and 200 km, respectively. S-wave velocities show relatively low values (~-3%) down to 110 km depth. No significant anomalies are recorded at deeper levels, with the exception of the CVP where a conspicuous negative anomaly, exceeding -3%, from 110 to 200 km depth is identified, the maximum intensity being at 110-150 km.

Xenolith data along the modelled profile are scarce and restricted to CVP. Geochemical evidences in terms of major and trace elements of mineral phases, as well as whole rock and isotopic analyses on spinel lherzolite xenoliths show two metasomatizing events affecting the mantle beneath this central Spain area: one is related to a subduction component signature reflecting clinopyroxenes LREE, Pb, Th and U enrichments and more radiogenic whole rock compositions, while the second is related to alkaline melts, similar to the host lavas (MREE enrichments in the clinopyroxenes and HIMU signature of whole rock Sr-Nd systematics) (e.g., Cebriá and

López-Ruiz, 1995; Bianchini et al., 2010; Villaseca et al., 2010).

The geometry of the LAB beneath the Iberian Plate has been the subject of several studies integrating different geophysical data. In the northern segment of the profile the results obtained in the previous Chapter, show a maximum LAB depth of ~170 km beneath the Cantabrian Mountains, shallowing to 125-145 km below the Duero Basin. Along the central segment, LAB-depth estimates from 1D thermal modelling show values of 95-100 km beneath the Duero and Tagus basins (Jiménez-Diaz et al., 2012), which are slightly lower than those obtained by Fernandez et al. (1998, 2004), who proposed values of 110-120 km. In the southern segment, Torne et al. (2000) based on 3D gravity modelling combined with heat flow and elevation data, proposed lithospheric thickness values ranging from 140 km beneath the Betics to ~50 km in the East Alboran Basin. More recently, Fullea et al. (2010) proposed LAB-depth values of ~160 km beneath the Betics and 50-70 km beneath the East Alboran Basin based on a 3D geophysical-petrological model.

None of the previously referred models accounted for the presence of a conspicuous positive seismic velocity anomaly beneath the Betics imaged by seismic tomography and extending down to ~600 km depth (e.g., Bijwaard and Spakman, 2000; Piromallo and Morelli, 2003; Spakman and Wortel, 2004; Garcia-Castellanos and Villaseñor, 2011; Bezada et al., 2013; Monna et al., 2013). Such anomaly has been interpreted by many of the previous authors, as a retreating lithospheric slab, which is probably affected by a lateral tear propagating westwards.

# 4.3. – Results

Along the third modeled profile I have distinguished three lithospheric mantle types differing in composition according to the geological domains (Fig. 4.4). The overall composition of the lithospheric mantle along the profile falls in the lherzolitic field (Table 4.2).

| Bodies | Composition | $SiO_2$ | $Al_2O_3$ | FeO | MgO | CaO | $Na_2O$ | K2O | $H_2O$ |
|---|---|---|---|---|---|---|---|---|---|
| 12 | Eclogite | 56.89 | 16.81 | 7.88 | 5.28 | 5.47 | 2.56 | 1.97 | 2 |
| 13 | Serpentinized Tc_1 | 44.31 | 3.48 | 7.96 | 39.63 | 3.09 | 0.24 | 0.03 | 1 |
| 14 | Tc_1 (Av. Tecton) | 44.64 | 3.51 | 8.02 | 39.93 | 3.11 | 0.24 | | |
| 15 | CVP (Calatrava_65290) | 44.51 | 3.76 | 8.75 | 37.89 | 3.28 | 0.36 | | |
| 16 | Pm_1 (PUM) | 45.00 | 4.5 | 8.10 | 37.8 | 3.6 | 0.36 | | |

Table 4.2. Bulk body compositions (%) used in the geo-transect.

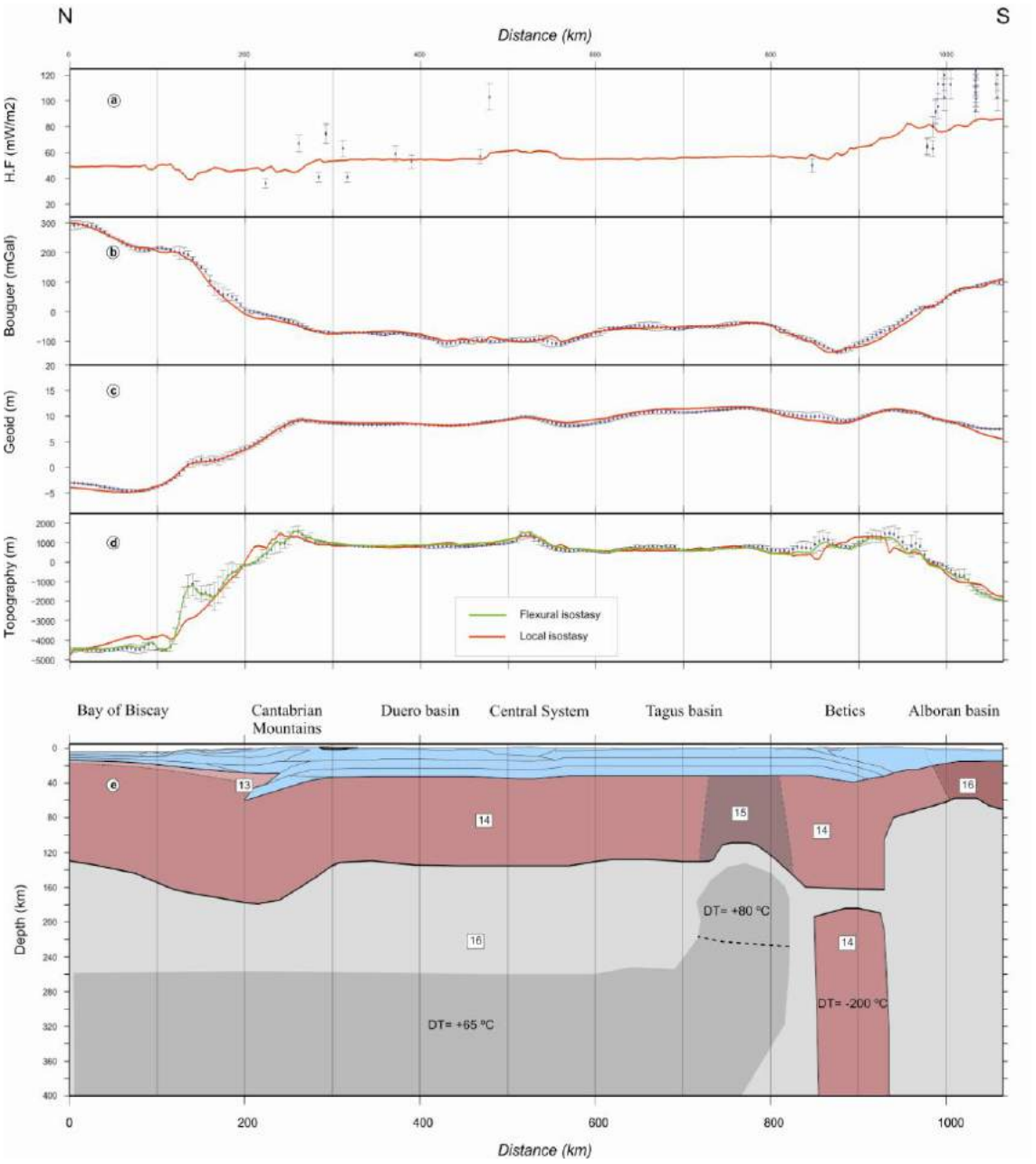


Figure 4.4: Model results (red lines), measured data with the standard deviation of data projected onto the profile within a strip of 25 km half-width (blue dots and vertical bars), coupled calculated topography (red line), and green line represent calculated elevation in the case of effective elastic thickness for the different Te (30 km, 20 and 10 km) used along the profile (see text for details): (a) surface heat flow; (b) Bouguer anomaly; (c) geoid height; (d) elevation; (e) lithospheric structure. Crustal structure like in Figure 4.2. Numbers in panel (e) denote mantle bodies summarized in Table 4.1. Dataset sources as in Figure 1.3.

Thereby, I have considered a lherzolite average (Tc_1 in Griffin et al., 2009) as

the lithospheric mantle composition prevailing in the Iberian Peninsula and the North-Iberian Margin. In the region of the Calatrava Volcanic Province, composition changes slightly towards a more fertile mantle, according to available geochemical data on xenolith samples (Table 4.2) (Villaseca et al., 2010). In the East Alboran Basin I considered a PUM composition according to Fullea et al. (2010) (Table 4.2). The North-Iberian Margin is characterized by low Pn velocities and then, I have followed the composition model proposed in Chapter 3, where a thin layer of hydrated uppermost mantle is considered (body 13, Fig. 4.4e).

The lithospheric slab below the Betics is modeled assuming a colder body with a temperature anomaly of $\Delta T$ = -200 ºC and with the same composition than the Iberian lithosphere (Tc_1). The slab is un-welded to the overlaying lithospheric mantle to simulate the lateral tearing. The sublithospheric mantle is modeled with a major-element composition representative of Primitive Upper Mantle, according to McDonough and Sun et al. (1995) (Table 4.2). To account for the low velocity layer imaged by tomography from 260 km depth to the bottom of the model, I have increased the temperature of this layer by 65 ºC along the transect, and by 80 ºC beneath the Calatrava Volcanic Province (Fig. 4.4e). Note that the geometry of the sublithospheric bodies is slightly narrower than the seismic anomalies derived from tomographic models in order to reproduce the average percentage (%$\Delta$Vp) value. The best fit model is illustrated in Figure 4.4.

Gravity and geoid show a root mean square error (rmse) of 9.2 mGal and 0.48 m, respectively. I have considered that the sub-lithospheric bodies are mechanically coupled to the lithosphere, such that the vertical stresses related to density changes within the asthenosphere are transmitted to the Earth's surface. Therefore, the density anomalies related to sub-lithospheric bodies affect not only the calculated geoid and gravity anomalies, but also the elevation. In the next section I discuss how an eventual mechanical decoupling of these anomalous sub-lithospheric bodies could affect the calculated elevation. The calculated elevation, under the assumption of local isostasy, shows local misfits of up to 1000 m in the North-Iberian Margin and of few hundred meters in the Betics and the Alboran Basin (rmse = 360 m). However, when flexural rigidity of the lithosphere is considered, the calculated elevation fits better with observations (rmse = 90 m). I have considered a variable elastic thickness, changing from Te=30 km in the northern segment of the profile (e.g., Pedreira et al., 2015), to Te=20 km in the central segment (e.g., Jiménez-Diaz et al., 2012; Ruiz et al., 2007; Gómez-Ortiz et al., 2005), and Te=10 km in the southern segment (e.g., Garcia-Castellanos et al., 2002). The calculated surface heat flow (SHF) is also in agreement with the general trend of measured values. Highest calculated SHF values correspond to

the thinned lithosphere of the Alboran Basin, although a noticeable underestimation relative to the measured values is observed. In the Iberian mainland, the calculated SHF decreases from ~60 mW/m$^2$ in the Tagus Basin to 55 mW/m$^2$ in the Duero Basin, and to ~50 mW/m$^2$ in the Cantabrian Mountains and the North-Iberian Margin.

## 4.3.1. – Lithosphere mantle structure

The calculated response of gravity, geoid and elevation match very well the observed regional trends with some local misfits (Fig. 4.4). The resulting depth of the lithosphere-asthenosphere boundary shows conspicuous lateral variations related to the main tectonic structures. Therefore, the northern Iberian margin is characterized by a LAB depth of 130-140 km in the Bay of Biscay, increasing rapidly to values of ~180 km in the Cantabrian Mountains. The central part of Iberia shows a LAB-depth of 135 km beneath the Central System decreasing slightly to values of ~130 km below the Duero and Tagus basins. The intraplate Calatrava Volcanic Province is characterized by a lithospheric thining with LAB depth values of ~110 km. The Betic orogenic system shows LAB depth values of more than 160 km beneath the Betics decreasing dramatically to around 60 km in the center of the Alboran Basin. It is worth noting that beneath the Betics there is a detached lithospheric slab reaching the bottom of the model (400 km depth).

## 4.3.2. – Temperature and density distribution

The calculated steady-state temperature distribution is shown in Figure 4.5. Within the crust, the isotherms are roughly flat, showing a slight upward deflection beneath the Southern Betics, related to the pronounced lithospheric thinning in the Alboran Basin. In contrast, the isotherms show a downward deflection in the North-Iberian Margin, related to the thin crust and low heat production in the Bay of Biscay.

The Moho temperature varies from ~200 ºC in the Bay of Biscay, to about 650 ºC in the Iberian Meseta and the Calatrava Volcanic Province, increasing to ~750 ºC beneath the Betics and the North-Iberian Margin, where the Moho depth reaches values of 40 km and 60 km, respectively. In the central part of the Alboran Basin the Moho temperature decreases to values of 500 ºC. The temperature distribution in the sub-lithospheric mantle shows the perturbations relative to the surrounding adiabatic thermal gradient prescribed in the subducting slab beneath the Betics ($\Delta T$ = -200 ºC),

and the sub-lithospheric layer located below 260 km depth that rises to less than 140 km depth beneath the CVP (ΔT = +65 and +80 ºC, respectively).

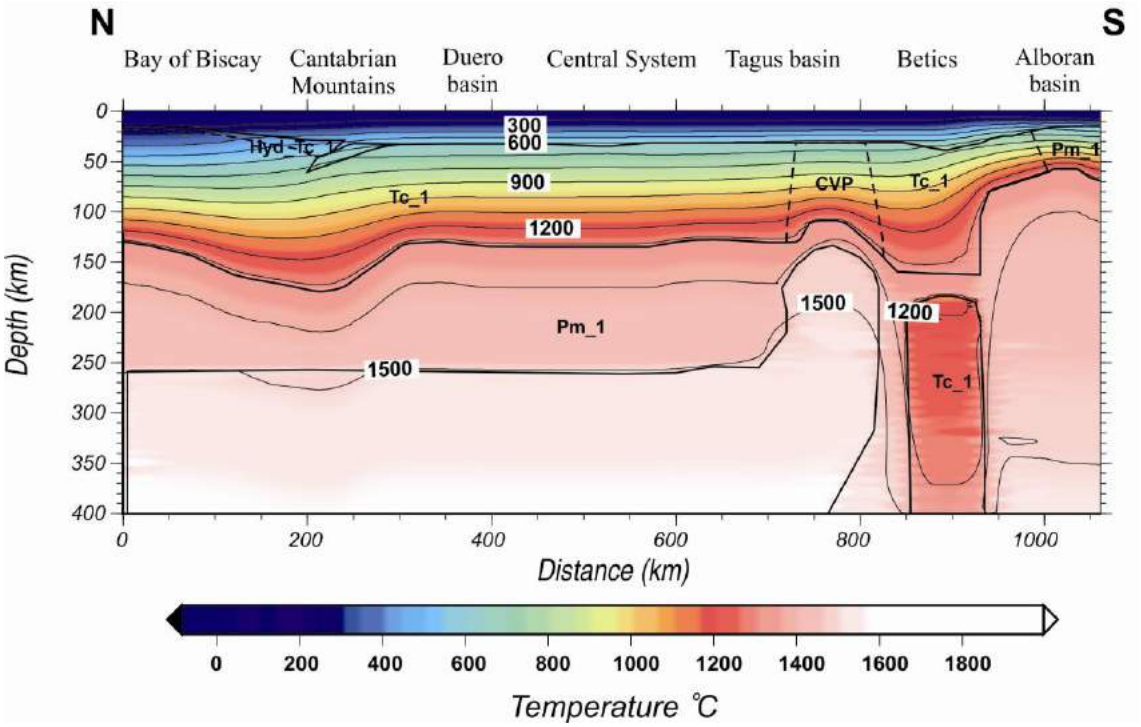


Figure 4.5: Calculated temperature distribution along the geo-transect and mantle domains with different chemical composition (see Table 4.2). Contour lines every 100 °C.

In the northern segment, the density at the crust-mantle boundary (CMB) varies between ~3320 kg/m$^3$ beneath the Cantabrian Mountains to ~3230 kg/m$^3$ in the hydrated mantle of the North-Iberian Margin (Fig. 4.6). In central Iberia the uppermost mantle density is of 3300 kg/m$^3$, decreasing to 3290 kg/m$^3$ beneath the Betics and to 3250 kg/m$^3$ beneath the Alboran Basin. The lithospheric mantle of the northern and central segments of the profile is almost isopycnic, with average densities of ~3350 kg/m$^3$ and ~3325 kg/m$^3$, respectively. Beneath the Betics, the lithospheric mantle density increases with depth from 3290 kg/m$^3$ below the Moho to 3380 kg/m$^3$ at the LAB, indicating that in this region the pressure effects on density prevail on the temperature effects due to the high Moho temperature and the consequent low thermal gradient within the lithospheric mantle. Below the Alboran Basin, the lithospheric mantle is also almost isopycnic with a density of ~3250 kg/m$^3$. Maximum lithospheric mantle densities of ~3360-3380 kg/m$^3$ are reached at the base of the lithosphere, beneath the thickened regions of the Betics and the Cantabrian Mountains, respectively. The imposed temperature anomalies in the sub-lithospheric mantle bodies translate into density anomalies of -6 kg/m$^3$ (perturbation of +60 ºC) and -9 kg/m$^3$ (perturbation of

+80 ºC), approximately. Within the slab, thermal and composition anomalies result in a positive density contrast of ~10 kg/m$^3$ at the top of the slab, vanishing with depth until the olivine-wadsleyite phase transition, with a density increase of 70 kg/m$^3$. Note that lowering the average temperature of the slab by 200 ºC produces the rising of the Ol-Wd transition from around 400 km to 390 km depth.

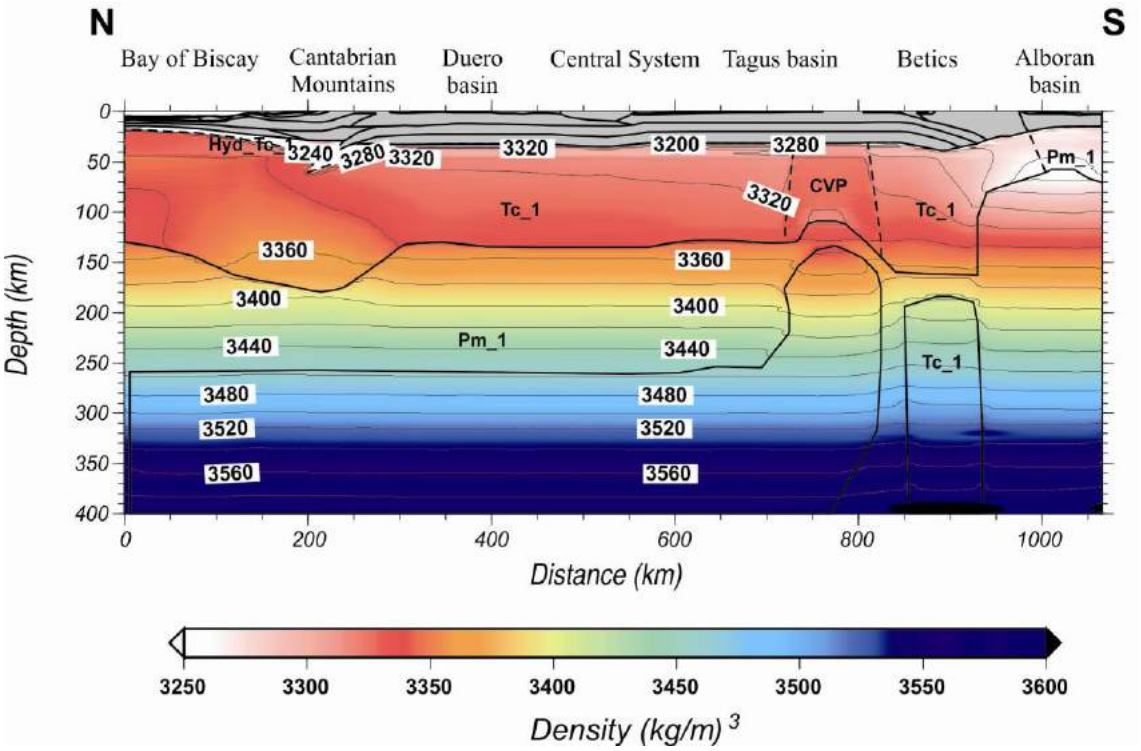


Figure 4.6: Calculated mantle density distribution along the geo- transect. Contour lines every 20 kg m$^{-3}$.

## 4.3.3. – Mantle velocity distribution

The depth-distribution of the calculated P-wave velocities within the mantle is shown in Fig. 4.7a. Most of the central Iberia shows values of 8.05 - 8.08 km/s, increasing to > 8.1 km/s in the Cantabrian Mountains and the North-Iberian Margin. The CVP shows lithosphere mantle velocities of ~8 km/s, whereas beneath the Betics, velocities increase with depth from 8.0 to 8.15 km/s. The Alboran Basin shows the lowest Vp values, ranging from 7.9 km/s, close to the Moho, to 7.6 km/s at the LAB. At sublithospheric levels, velocities are affected by the presence of bodies with prescribed anomalous temperature and composition. Therefore, the positive thermal anomalies of 65-80 ºC result in a P-wave velocity decrease of ~0.05-0.08 km/s. Within the slab, the combined effect of negative thermal anomaly (-200 ºC) and composition implies an increase of ~0.15 km/s (see also Fig. 4.11). Fig. 4.7b shows the calculated Vp anomalies

in (%) relative to a reference model consisting of a 130-km thick lithosphere and 30-km thick crust with a lithosphere mantle composition corresponding to Tc_1. Both, the global tomography (Fig. 4.3) and the synthetic tomography (Fig. 4.7b) models show very similar anomalies despite some minor misfits in their amplitude and shape.

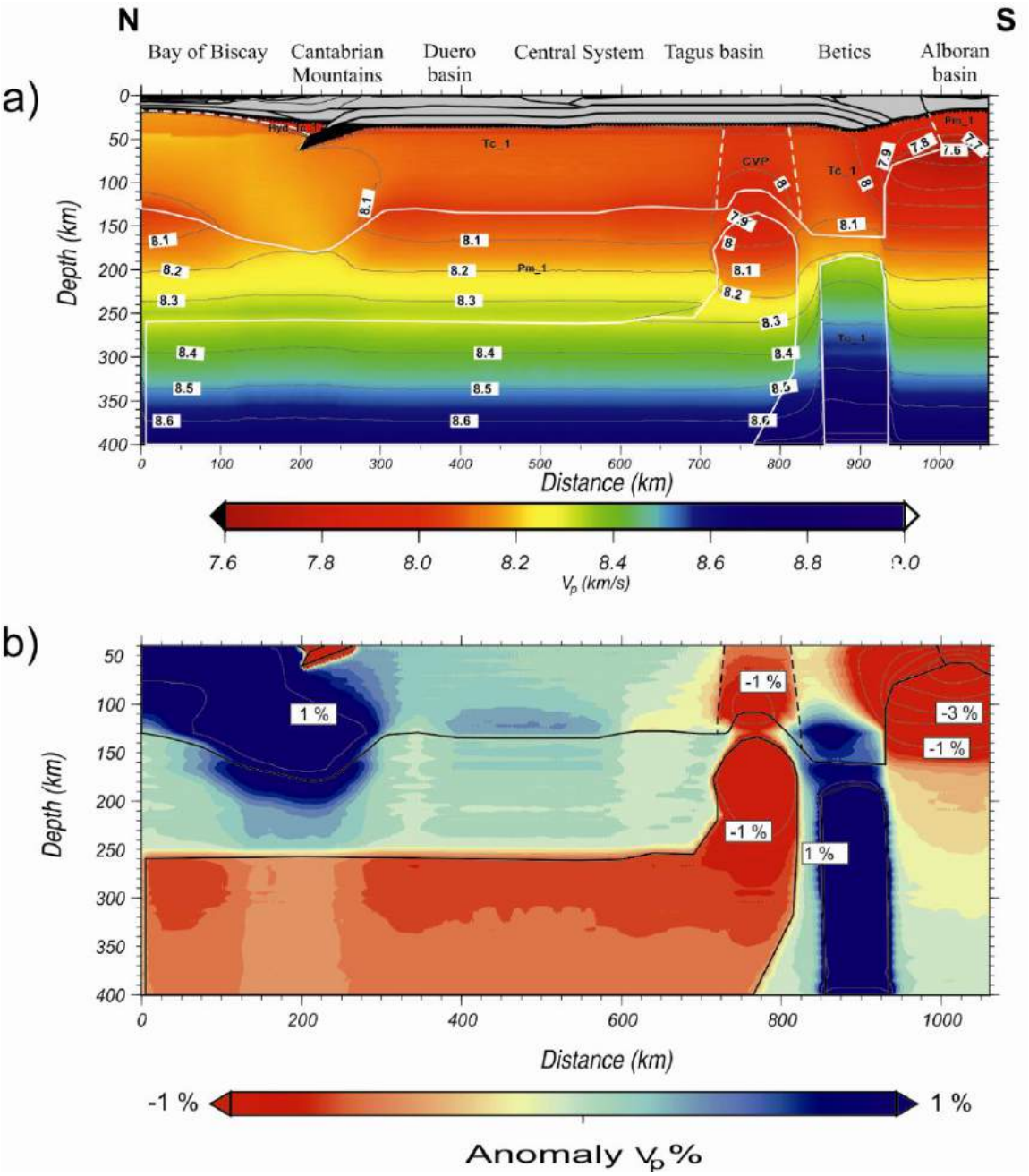


Figure 4.7: a) Calculated P-wave seismic velocities in the upper mantle down to 400 km; b) synthetic P-wave tomography from our model. In this case velocity anomalies are relative to the synthetic reference model (calculated from Vp in (%) relative to a reference model consisting of a 130 km thick lithosphere and 30-km thick crust with a lithosphere mantle composition corresponding to Tc_1) (see text). Contour lines every 1%. Compare with Figure 4.3.

Calculated S-wave velocities (Fig. 4.8) show a similar pattern than P-waves, with maximum values within the lithospheric mantle of > 4.6 km/s beneath the North-Iberian Margin and minimum values of 4.2-4.4 km/s beneath the Alboran Basin. A low velocity zone with Vs<4.45 km/s, extending from some km above the LAB to 220 km depth, is clearly depicted along the profile except beneath the Cantabrian Mountains and the Betic Cordillera. At sub-lithospheric levels, the positive thermal anomaly of 65-80 ºC translates into a Vs decrease of 0.1–0.12 km/s, whereas the combined compositional and negative thermal anomaly of -200 ºC in the subducting slab implies a Vs increase of 0.08 km/s.

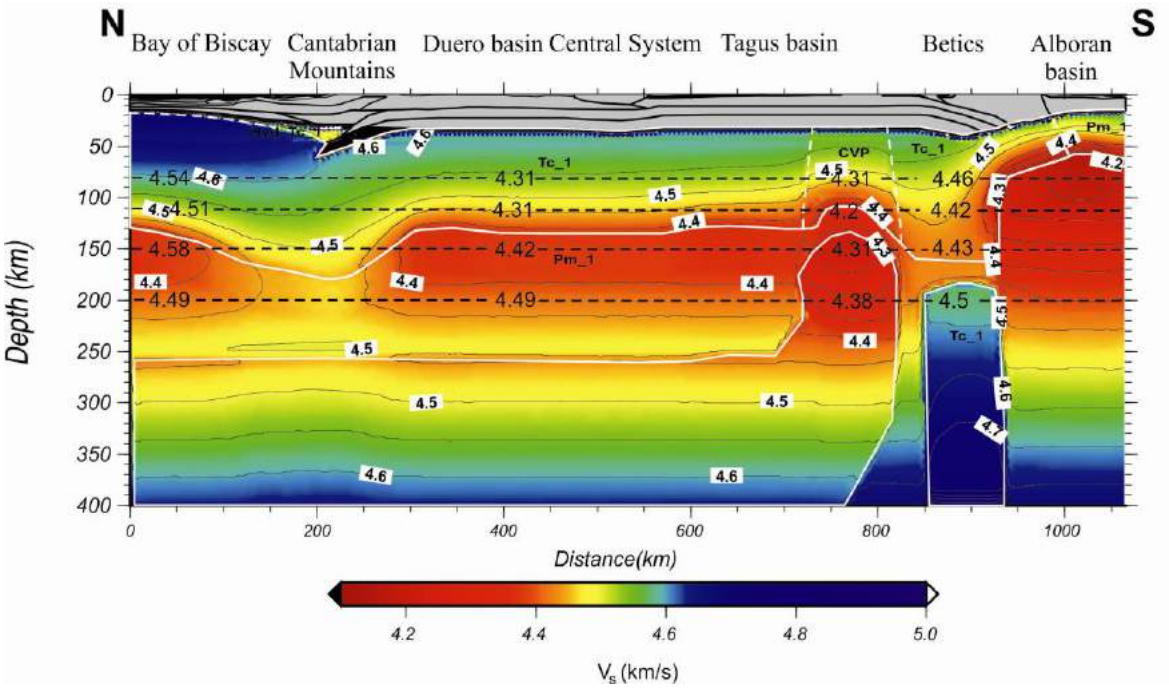


Figure 4.8: Calculated S-wave seismic velocities in the upper mantle down to 400 km depth. Contour lines every 0.05 km/s. Superimposed are the S-wave velocities inferred from the regional tomography model by Legendre et al. (2012) at different depth levels. S- values have been calculated according to the reference velocities of 4.38 km/s (at 80 and 110 km), 4.39 km/s (at 150 km) and 4.45 km/s (at 200 km) (see Legendre et al., 2012).

Figure 4.8 compares the calculated S-wave velocities with the Vs values obtained at different depth levels from the regional tomography model of Legendre et al. (2012). As mentioned before, only a qualitatively comparison of the lateral velocity variations down to 200 km depth can be made. Although the obtained results reproduce maximum lithosphere mantle velocities beneath the North-Iberian Margin and the Betic Cordillera, and minimum velocities in the CVP, there is a major discrepancy in the predicted velocity-depth variation. The main qualitative difference is that, according to

Legendre et al. (2012), the velocity tends to increase with depth following the ak-135 reference model and therefore, these authors do not image the sub-lithospheric low velocity zone except in the CVP. However, recent studies carried out in Iberia and the westernmost Mediterranean region, based on ambient noise and ballistic finite-frequency Rayleigh wave tomography, show an almost continuous low velocity zone except beneath the Cantabrian (not sampled) and Betic orogens (Palomeras et al., 2014).

Figure 4.9 compares of the calculated P- and S-wave velocities in the uppermost lithospheric mantle with Pn and Sn estimates from different seismic experiments taking into account the reported uncertainties in the experimental determinations. The calculated Pn and Sn values are the averaged velocities within the first 15 km of the uppermost mantle and the associated standard deviation. The calculated Pn velocity values fit with most of the available data except in the Betics and the Alboran Basin, where Diaz and Gallart (2009) have proposed values of 8.2±0.05 km/s 7.75±0.15 km/s, respectively. The calculated Sn velocity values show a similar trend than available data (Diaz et al., 2013) although with slightly lower magnitudes.

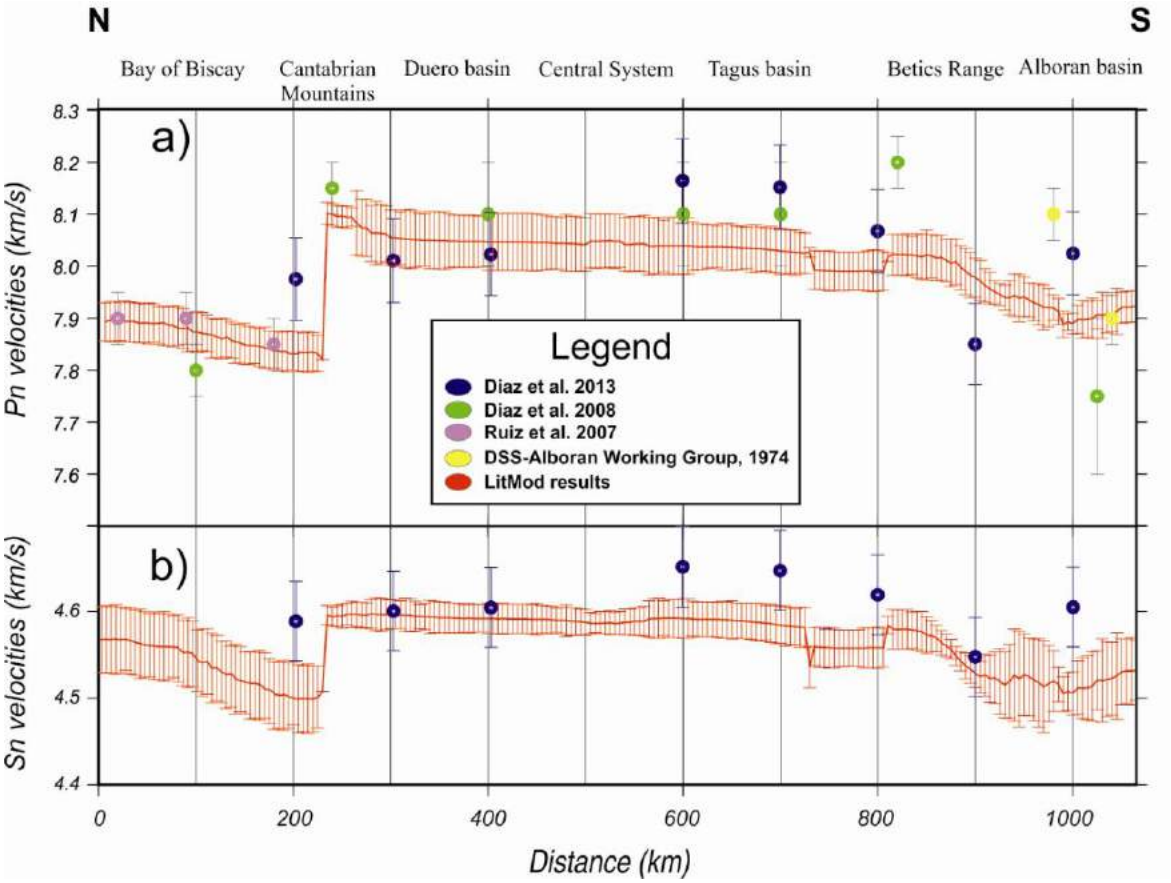


Figure 4.9: a) Pn velocities along the geo-transect. Red line indicates calculated Pn values with the associated standard deviation of the first 15 km of the uppermost mantle. Circles with error bars denote Pn-values from seismic experiments (see legend); b) Sn velocities along the modeled transect. Red line indicates calculated Sn values. Symbols with error bars denote Sn-values from Diaz et al., 2013.

# 4.4. – Discussion

## 4.4.1. – LAB topography

The calculated topography of the lithosphere-asthenosphere boundary relies on the considered crustal structure (geometry and parameters), on mantle images from seismic tomography studies, and on the compositions of the lithospheric and sub-lithospheric mantle. The modeled crustal structure is based on available data from seismic experiments and integrated geophysical models carried out close to the studied transect. Similarly, several works have investigated the lithospheric structure of Iberia using different methodological approaches. Here, I focus on the comparison of the calculated LAB-depth along the studied transect with those proposed from previous studies. Figure 4.10 compares the LAB depth obtained from different models.

In the northern segment of the transect, I used a very similar model to that corresponding to the second lithosphere profile (see above, Chapter 3). Consequently, the LAB depths obtained are very similar being 10-15 km deeper in thid third profile under the North-Iberian Margin and southern Duero Basin regions, and about 20 km shallower beneath the crustal root of the Cantabrian Mountains (Fig. 4.10).

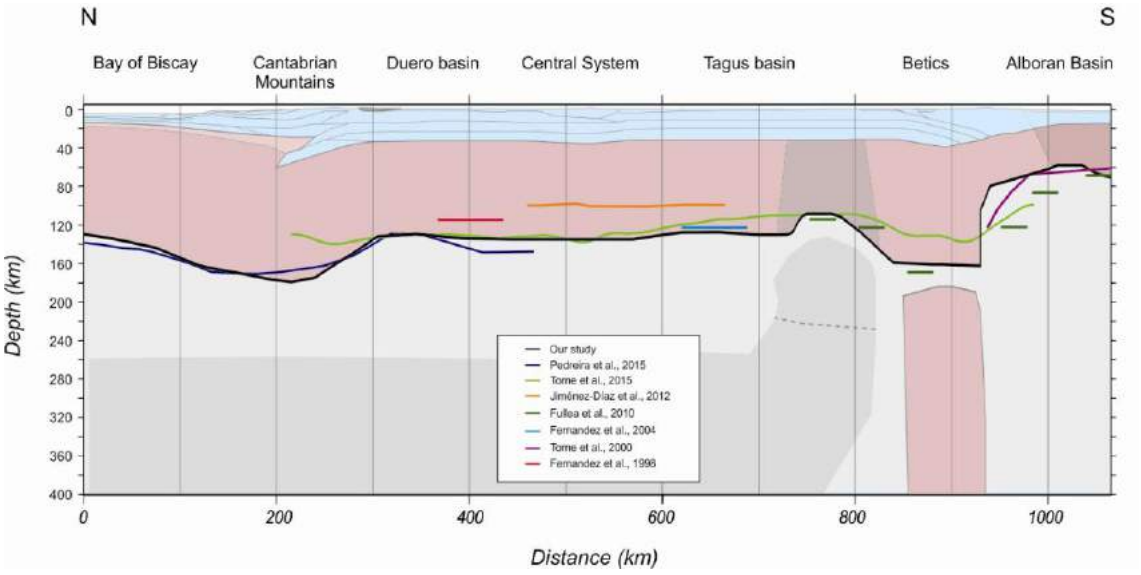


Figure 4.10: Calculated topographies of the lithosphere-asthenosphere boundary from different models.

These differences in the LAB-depth can be mainly attributed to small differences in the calculated mantle thermal conductivity and in the geometry and density of the lower crust. The mantle thermal conductivity in the Cantabrian Margin geo-transect (Chapter 3) is based on Hofmeister et al. (1999), whilst in the present profile the radiative contribution described in Grose and Afonso (2013) is considered. In addition,

in the second transect a 7-9 km thick lower crust beneath the Duero Basin with a density depending on composition and P-T conditions is considered. In this profile, I used a homogeneous lower crust along the whole transect with a constant density of 2950 kg/m$^3$ and a thickness of ~9 km beneath the Duero Basin.

A similar integrated geophysical-petrological approach was also used to image the 3D lithospheric structure in the Atlantic-Mediterranean transition region by Fullea et al. (2010). In their model, the LAB depth varies from < 70 km in the Alboran Basin to 150-170 km beneath the Betics and ~110 km in the Iberian Massif and thus it is consistently deeper than in our model (Fig. 4.10). These differences are related to: i) the crustal structure, which in the case of Fullea et al. (2010) was simpler; ii) the above mentioned calculation of the mantle thermal conductivity; and iii) the presence of the detached/torn lithospheric slab beneath the Betics, which is not considered in Fullea et al. (2010).

Many of the studies carried out in Iberia concerning the lithosphere structure and LAB-depth are based on a 'pure thermal approach'. Following this approach, Fernandez et al. (1998) and Jiménez-Díaz et al. (2012) proposed lithospheric thickness values of about 100±10 km beneath the Duero and Tagus basins, and the Central System. Both studies were based on 1D modelling of surface heat flow and elevation data. Integrated 2D lithospheric modelling combining heat flow, gravity, geoid, and elevation data gave a slightly thicker lithosphere below the Tagus Basin, with a LAB depth of 120 km (Fernandez et al., 2004). A 3D modelling of the lithosphere of the Alboran Basin and surroundings, combining elevation, surface heat flow and gravity data, yielded LAB-depth values of ~60 km in the central part of the basin, and >130 km beneath the Betics (Torne et al., 2000). Finally, a recent 1D study combining elevation, geoid data, and thermal analysis, further constrained by 3D gravity modelling over the whole Iberian Peninsula shows a similar lithospheric thickness trend than our work but with LAB-depth differences in the Cantabrian Mountains and in the Betics (Torne et al., 2015). According to these authors, the LAB lies at >140 km in the Cantabrian Mountains, ~130 km in the Duero and northern Tagus basins, shallowing southwards to <110 km in the CVP, and deepening again to >140 km beneath the Betics.

An inherent limitation of the thermal approach is that the density of the lithospheric mantle is assumed to be only temperature dependent, and that the underlying asthenosphere has a constant density everywhere. Consequently, the density within the lithospheric mantle decreases with depth according to the thermal expansion coefficient and therefore, the LAB cannot be effectively constrained by seismic or petrological models. Nevertheless, although the absolute LAB-depth values can differ

from a geophysical-petrological approach, the main trends will be comparable as far as the predominant effect on lateral density variations is related to temperature rather than to pressure and/or composition (see Tunini et al., 2015 for a thorough discussion).

## 4.4.2. – Changes in the mantle composition

The lithospheric mantle, along the modelled transect, also shows lateral changes in composition. According to the availability of geochemical analyses on xenoliths and/or volcanic samples, I have considered a homogeneous composition in the Iberian mainland, with the exception of the Calatrava Volcanic Province (CVP). The dominant composition corresponds to the Average Tecton garnet sub-continental lithospheric mantle (Tc_1) (Griffin et al., 2009), which has also been proposed for the second geo-transect (Chapter 3) along the Cantabrian margin and in Fullea et al. (2010) in the Betics.

The Calatrava Volcanic Province shows recent volcanism defining a second compositional domain. Spinel lherzolite xenoliths from the Cenozoic CVP provide a direct sampling of the shallow lithospheric mantle beneath this area (Villaseca et al., 2010). Calatrava xenoliths are lherzolites estimated to originate from depths of 35-50 km. They are richer in clinopyroxene and poorer in orthopyroxene than other Iberian mantle xenolith suites, being slightly or moderately depleted relative to primordial mantle. The absence of harzburgites in the studied suites of the CVP reflects the very low degrees of partial melting (F) that have affected this portion of mantle (< 10%) (Villaseca et al., 2010). Low F are inferred also by the trace element contents of clinopyroxenes and by the low Cr# [calculated as Cr/(Cr+Al)] of the spinels, allowing to speculate that the mantle beneath CVP has a composition very close to that of a fertile mantle. A composition of a mantle, depleted by a very low partial melting event (1.5%), estimated by the HREE contents of the clinopyroxenes was chosen to characterize the CVP mantle (Villaseca et al., 2010). The change in the lithospheric mantle composition in the CVP results in a shallower LAB since the density contrast with respect to Tc_1 is about ~11 kg/m$^3$.

In the lithospheric mantle beneath the Alboran Basin I have considered a PUM composition (McDonough and Sun 1995), as proposed by Fullea et al. (2010). This composition was also considered in the first profile for the Algerian Basin (Chapter 2). Compared to Tc_1, a PUM composition results in a higher density and a lower P-wave velocity at the uppermost mantle levels. This lower velocity is related to the higher content in plagioclase of PUM relative to Tc_1, which is particularly noticeable at the

Pg stability field. Finally, in the North-Iberian Margin I have also modified the mantle composition by considering a hydrated uppermost mantle, with 1% water content (see below). Mantle hydration results in partial serpentinization and the consequent reduction of P-wave velocities as measured in seismic experiments (see Pn velocities discussion in Chapter 6).

## 4.4.3. – Thermal and compositional sub-lithospheric anomalies

Seismic velocity anomalies at sub-lithospheric levels, imaged from tomography models in the Iberian plate along the N-S lithospheric transect, suggest the presence of bodies with different temperature and/or composition than in the surrounding PUM sub-lithospheric mantle. I interpreted the positive velocity anomaly along the N-S Iberian lithospheric mantle profile, exceeding 1% ΔVp beneath the Betics, as a detached/tore lithospheric slab with a temperature 200 ºC lower than the surrounding sub-lithospheric mantle, and a Tc_1 composition corresponding to the Iberian mantle lithosphere. The negative velocity anomaly, exceeding -2% ΔVp beneath the CVP, and extending along the central and northern segments of the profile down to 260 km depth, is interpreted as a positive thermal anomaly with a ΔT = 65-80 ºC and the same composition as the sub-lithospheric mantle.

Figure 4.11 shows the depth variation of Vp along selected vertical profiles to illustrate the influence of temperature, phase changes and chemical composition. The resulting graphics clearly show the Vp increase at ~40 km depth related to the plagioclase-spinel transition amounting <0.05 km/s, except in the Cantabrian Mountains where Pg-Sp transition superposes to the change from hydrated to dry mantle. In this case, the increase in Vp amounts 0.32 km/s. The Vp increase related to the compositional change at the LAB is also very conspicuous, especially in regions with thin and ‘hot’ lithospheric mantle (Figs. 4.11b and 4.11c). The Vp decrease related to anomalous high temperature in the sub-lithospheric mantle (Figs. 4.11a, b, c) amounts ~0.06 km/s for ΔT=65 ºC and ~0.09 km/s for ΔT=80 ºC (Fig. 4.11c). The combined thermal and compositional effect of the lithospheric slab implies a Vp increase of ~0.125 km/s between 200 km and 280 km depth, being of ~0.1 km/s at higher depths due to the high-pressure orthopyroxene phase change. Finally, the P-T conditions within the lithospheric slab cause the rise of the exothermic olivine-wadsleyite mineral phase transition to 385 km depth and then, a Vp increase of ~0.31 km/s (Fig. 4.11d).

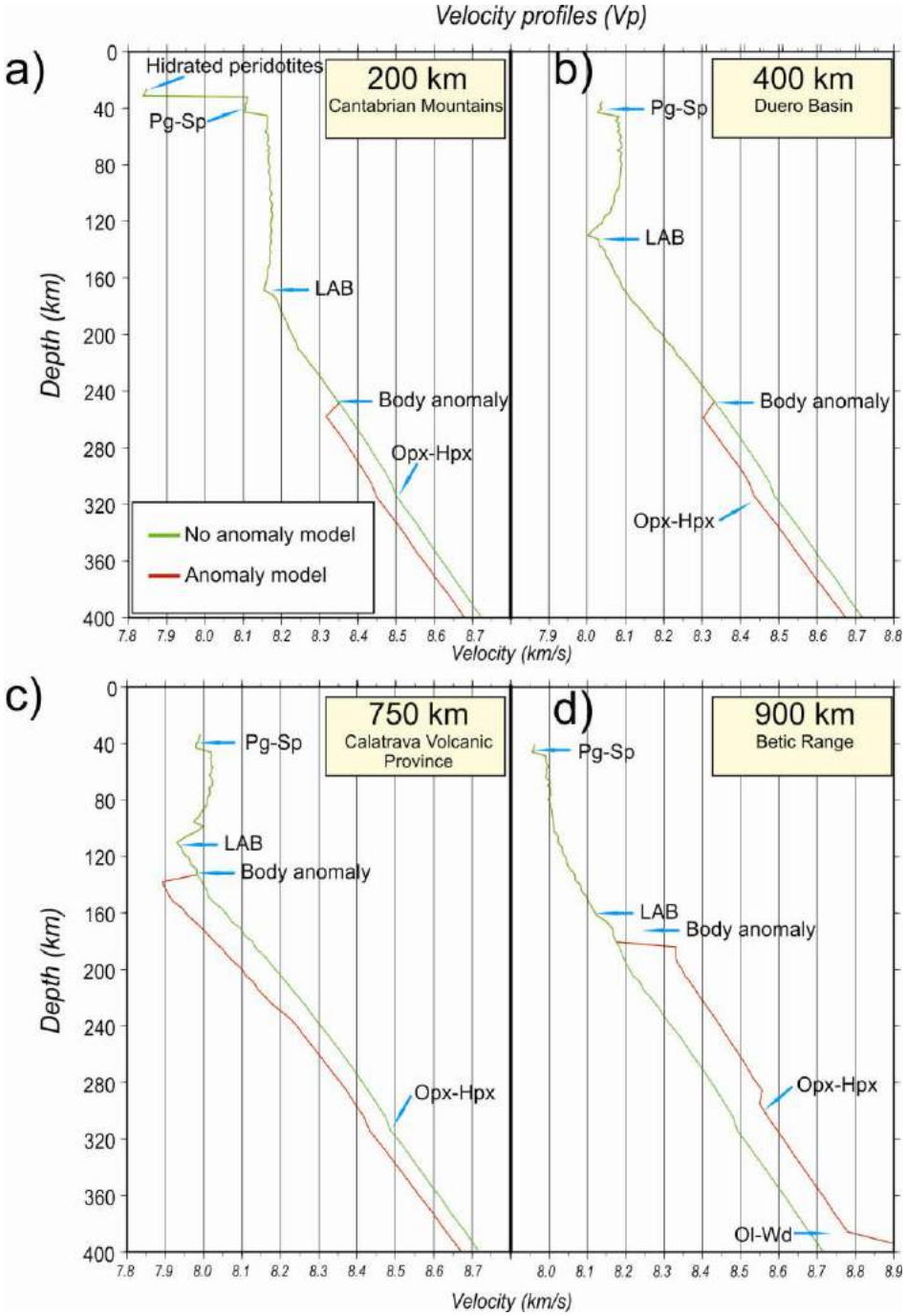


Figure 4.11: Depth variation of P-wave velocities calculated in the preferred model along the profile (at 200, 400, 750 and 900 km distance) for model with the sub-lithospheric anomalous body (red line) and model without the anomlalous body (green line). Arrows denote the lithosphere-asthenosphere boundary (LAB) and the following phase transitions: Pg-Sp, plagioclase-spinel; Opx-Hpx, orthopyroxene-high-pressure magnesian pyroxene.

Changes in chemical composition, phase transitions, and P-T conditions, translate into density changes as shown in Fig. 4.12. The density increase related to a

compositional change through the LAB, from Tc_1 to PUM, amounts ~20 kg/m$^3$; whereas that related to the olivine-wadsleyite transition within the subducting slab, usually at 400 km depth, amounts ~70 kg/m$^3$. The positive sub-lithospheric thermal anomaly implies a decrease in density of -6 kg/m$^3$ in the northern and central segment of the profile, and of -10 kg/m$^3$ beneath the CVP. The combined effect of temperature and composition in the lithospheric slab produces a density increase of 8 kg/m$^3$ at its top, vanishing with depth until the olivine-wadsleyite phase transition.

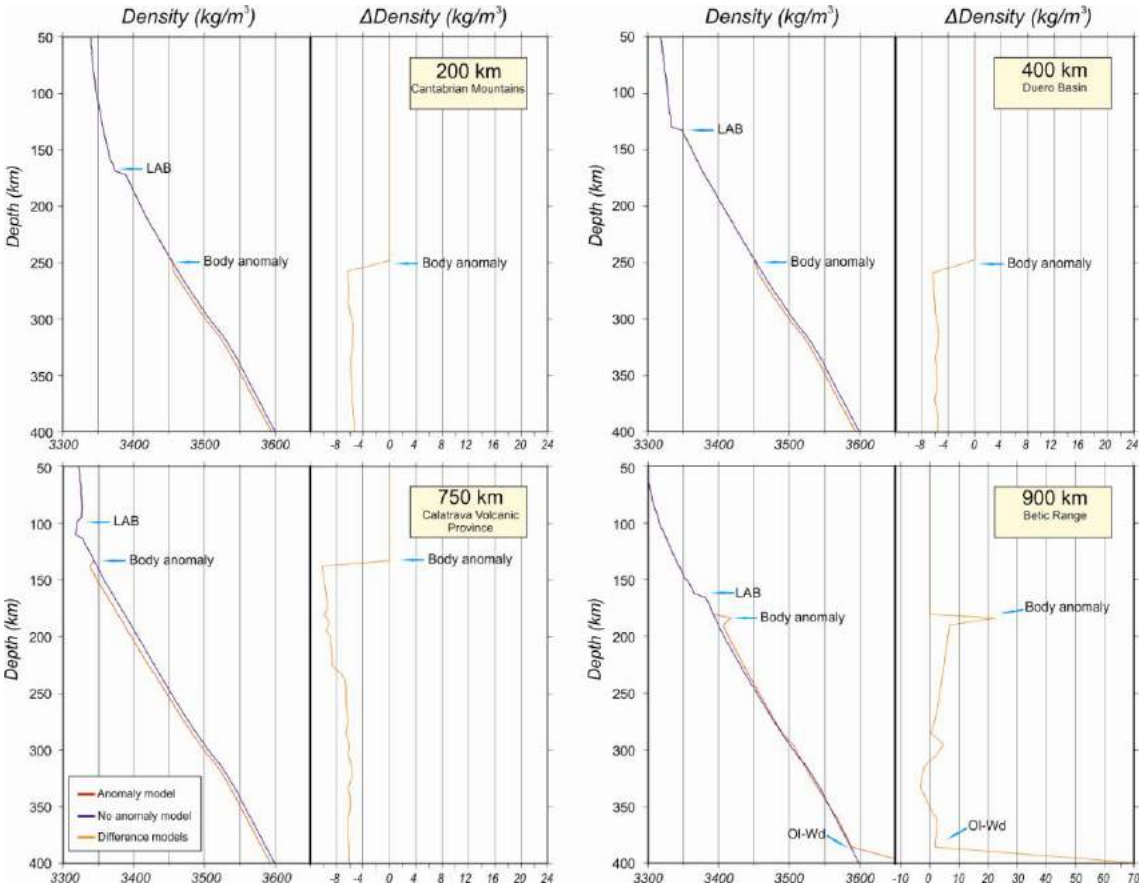


Figure 4.12: Depth variation of mantle density calculated in the preferred model along the profile (at 200, 400, 750 and 900 km distance) for model with asthenospheric anomaly and model without asthenospheric anomaly.

I have calculated the contribution of the sub-lithospheric anomalous bodies on elevation when vertical stresses related to asthenosphere density changes are not transmitted to the Earth's surface (decoupled mode). In this case, topography equals to that calculated without anomalous bodies, though their influence on potential fields would remain. Figure 4.13 illustrates the difference between elevation calculated considering coupled and decoupled anomalous sub-lithospheric bodies. The topography

perturbation caused by these bodies could be partly attenuated by viscous deformation within the low-viscosity asthenosphere, and partly by regional isostasy due to lithosphere rigidity. The lower the wavelength of the anomaly is the higher the attenuation of the topography perturbation. Therefore, an accurate estimation of the role of sub-lithospheric mass-anomalies on topography requires dynamic calculations and accurate constitutive equations. According to our results, the maximum topography perturbation related to the higher temperature of the asthenospheric body is around +340 m along the northern and central segments of the profile, rising to +470 m in the Calatrava Volcanic Province (Fig. 4.13). This deep and long wavelength density anomaly, imaged by tomography models as a relatively low velocity layer, could be the responsible for the high mean elevation of Iberia, which exceeds 600 m above sea level. The topography contribution related to the slab beneath the Betics is of about -300 m, due to the combined effect of its lower temperature, which vanishes with depth, and to the olivine-wadsleyite phase transition occurring near the bottom of the slab. Interestingly, trying to fit the decoupled elevation makes difficult fitting the measured gravity and geoid.

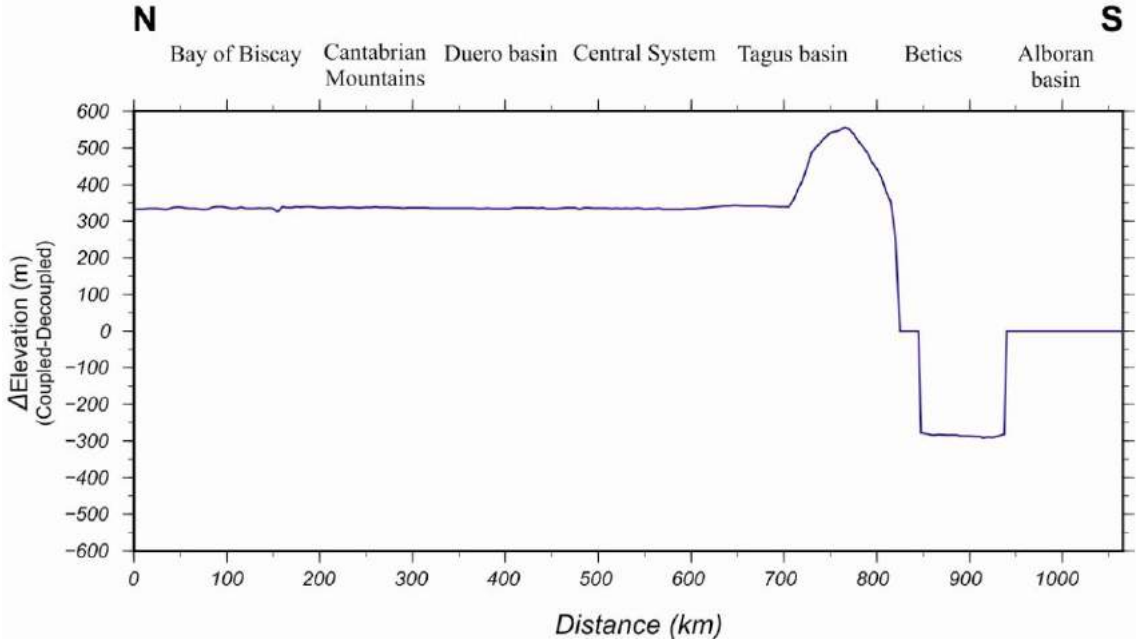


Figure 4.13: Difference between the elevations calculated considering coupled and decoupled anomalous sub-lithospheric bodies.

We must also consider the possible contribution of horizontal compressional stresses between Iberia–Africa and Eurasia to the average height anomaly of Iberia. Compressional stresses transmitted to the interior of the Iberian plate leading to most of

the topographical features of the Iberian Peninsula occurring during Oligocene–Lower Miocene times (De Vicente et al., 2009). Whether these far-field compressional stresses are only responsible for localized deformation related to crustal thrusting and flexural downwarding or, they produced long-wavelength lithospheric folding and increase of the average elevation, is not yet solved.

# Chapter 5: The Iberian Massif–Gibraltar Arc–Atlas Mountains geo–transect (fourth profile)

This Chapter forms part of a work in progress and therefore, I am showing the aims, gathering of data and method as definitive sections but the obtained results must be considered as preliminary. Likewise, I am including a tentative discussion section that can vary in the near future according to new results. This material will be included in a research article to be submitted for publication in the near future to an international journal.

In this chapter I have modelled a ~1100-km-long profile that runs from the Eurasian Plate to the African Plate crossing the southwestern Variscan Iberian Massif, the apex of the Betic-Rif orogenic system thorugh the Gibraltar Strait, and the Atlas Mountains (Fig.5.1).

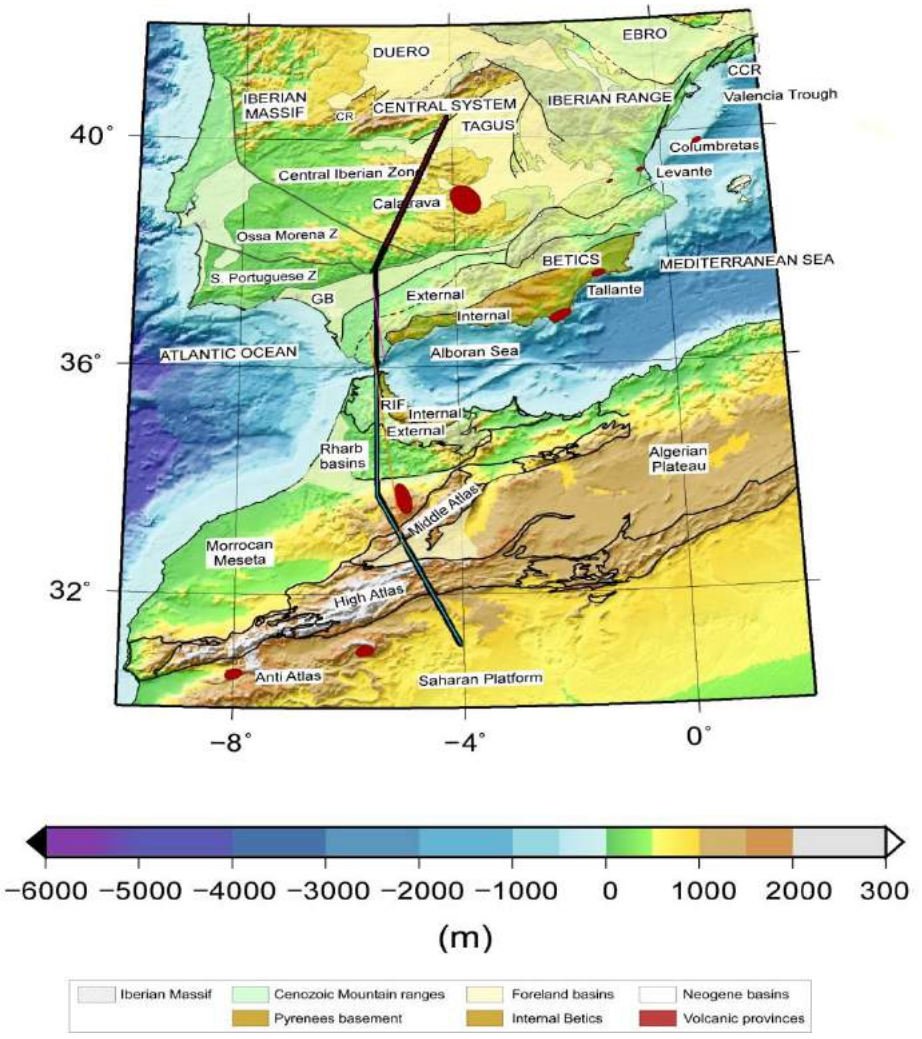


Fig. 5.1: Geological map of the study area showing the principal geological domains of the study area. Thick black line locates the modeled transect. Thin lines locates the seismics experiments: Red line- ALCUDIA wide-angle (Ehsan, 2014); Pink line- La Línea-Carmona (Medialdea et al., 1986); RIFSIS wide-angle (Gil et al., 2014); and SIMA wide-angle (Ayarza et al., 2014).

The main aim of this Chapter is to study the lateral changes in the crustal and lithospheric structure occurring in: i) the Variscan Iberian Massif, characterized by an old and tectonothermal stable lithosphere including the collisional suture zone in the Ossa Morena Zone; ii) The Betic-Rif domain developed roughly simultaneously with the NE- to E-wards rollback of a SE-dipping subduction of the segmented Ligurian-Tethys under the Africa margin; and iii) the Atlas Mountains, an intracontinental orogenic belt related to the Cenozoic-to-present convergence between Eurasia and Africa. The orientation of the geo-transect coincides with recently acquired deep seismic data under the umbrella of the TopoIberia project, which allows for a very good constraint on the resulting lithospheric model. The results of this Chapter will be included in an article in preparation.

# 5.1. – Crustal geometry from previous studies

Several studies including seismic reflection, wide-angle/refraction seismic profiles, receiver functions, magneto-tellurics and geological cross sections addressed the deep structure of the Iberia-Africa plate boundary in the Betic-Rif orogenic system and surrounding areas (Figure 5.1).

Original seismic data come from ALCUDIA wide-angle seismic reflection transect in the Variscan Iberian Massif (Ehsan, 2014), La Línea-Carmona refraction seismic experiment in the Betics (Medialdea et al., 1986), RIFSIS wide-angle seismic reflection in the Rif (Gil et al., 2014), SIMA wide-angle seismic reflection experiment across the Atlas (Ayarza et al., 2014) and the Marismas cross-section in the western Betics (Berástegui et al., 1998). In addition, I considered also the recent receiver function data obtained in the TopoIberia project from the deployment of seismic stations covering the whole Iberian Peninsula (e.g., Mancilla et al., 2012 and 2015). The crustal structure resulting from these seismic and geological data is summarized in Fig. 5.2. The northern segment, from 0 to 280 km distance, coincides with the ALCUDIA wide-angle seismic reflection profile and it is dividing the crust in three layers. To constrain the crustal structure between the north and the central segments, and due to the lack of seismic profiles, I have used the Marismas cross-section (Berástegui et al., 1998) and data from receiver function. In the central and south segments, from ~430 km to 1100 km, the crustal structure is relatively well defined by the RIFSIS (Gil et al., 2014), SIMA (Ayarza et al., 2014) and La Línea-Carmona (Medialdea et al., 1986) refraction seismic experiments. Major observations derived from the seismic experiments in the Atlas Mountains are the low velocity – low density found in the lower crust, and the differences in the Moho depth with respect to previous works

(Ayarza et al., 2014 and Gil et al., 2014). The Moho depth varies from 31-35 km beneath the Iberian Massif to more than 45 km in the Rif and ~31 km in the Rharb (or Gharb) Basin. Towards the Atlas Mountains, the Moho depth reaches up to ~40 km shallowing to ~35 km in the Saharan Platform.

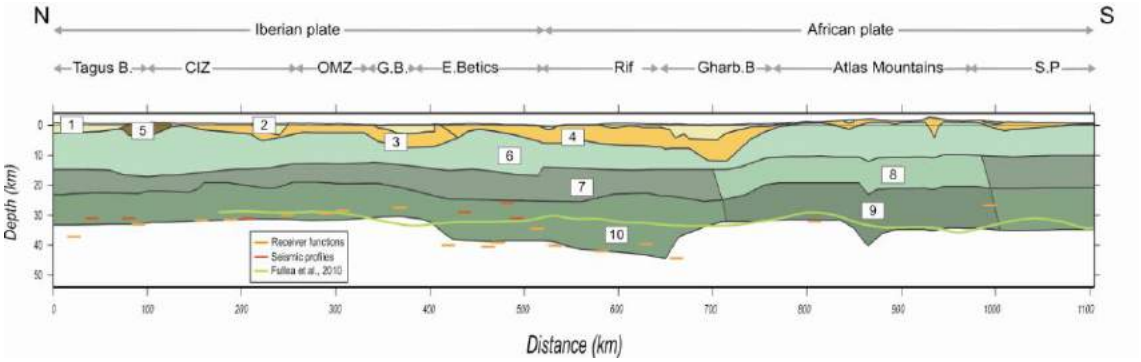


Figure 5.2: Crustal structure corresponding to the best fitting model. Different bodies have been modeled using geological cross-sections and seismic experiments (see text for details). Physical properties of crustal bodies are reported in Table 5.2. CIZ, Central Iberian Zone; OMZ, Ossa Morena Zone; GB, Guadalquivir Basin; S.P, Sharan Platform.

Pysical parameters used for crustal bodies are summarized in Table 5.1.

| Bodies | Crust and sediments model | Density (kg/m$^3$) | Heat Production (μW/m$^3$) | Thermal Conductivity (W/K·m) |
|---|---|---|---|---|
| 1 | Neogene and Quaternary | 2300 | 1 | 2.4 |
| 2 | Cenozoic sediments | 2520 | 1 | 2.4 |
| 3 | Mesozoic sediments | 2600 | 1 | 2.4 |
| 4 | Mesozoic sediments Africa | 2650 | 1 | 2.4 |
| 5 | Granitoids | 2670 | 1.65 | 2.5 |
| 6 | Upper crust | 2750 | 1.65 | 2.5 |
| 7 | Middle crust | 2850 | 0.5 | 2.1 |
| 8 | Middle crust Atlas | 2800 | 0.5 | 2.1 |
| 9 | Lower crust Atlas | 2850 | 0.3 | 2 |
| 10 | Lower crust | 2950 | 0.3 | 2 |

Table 5.1. Parameters used in the model for the different crustal bodies in the fourth model.

Density values have been taken from available seismic experiments and derived from the velocity-density envelopes defined by Barton et al. (1986), Christensen and Mooney et al. (1995) and Hamilton et al. (1978). Thermal conductivity values for crustal bodies have been taken from previous studies (e.g., Torne et al., 1992, 1996; Zeyen et al., 2005; Teixell et al., 2005). Radiogenic heat production has been taken from a global compilation carried out by Vilà et al. (2010).

## 5.2. – Mantle characterization and LAB depth from previous studies

The mantle characterization along the profile comes mainly from available Pn- and Sn- velocities, global and regional tomography models, and geochemical and isotopic analyses on xenolith samples. Pn and Sn values have been taken from regional tomography in the Euro-Mediterranean region (Díaz et al., 2013) and show constant average values of 8.0 km/s and ~4.6 km/s, respectively. Minimum of Pn and Sn values of 7.8 km/s and 4.3 km/s, respectively, are proposed near the Atlas by Makris et al. (1985).

P-wave mantle velocities along the modelled profile are from a global travel-time tomography model using the same method described in Bijwaard et al. (1998), incorporating additional earthquakes from 1995 to 2002 and arrival times (Villaseñor et al., 2003). P-wave velocity anomalies expressed in percentage with respect to the ak135 reference model (Kennett et al., 1995) are shown in Figure 5.3.

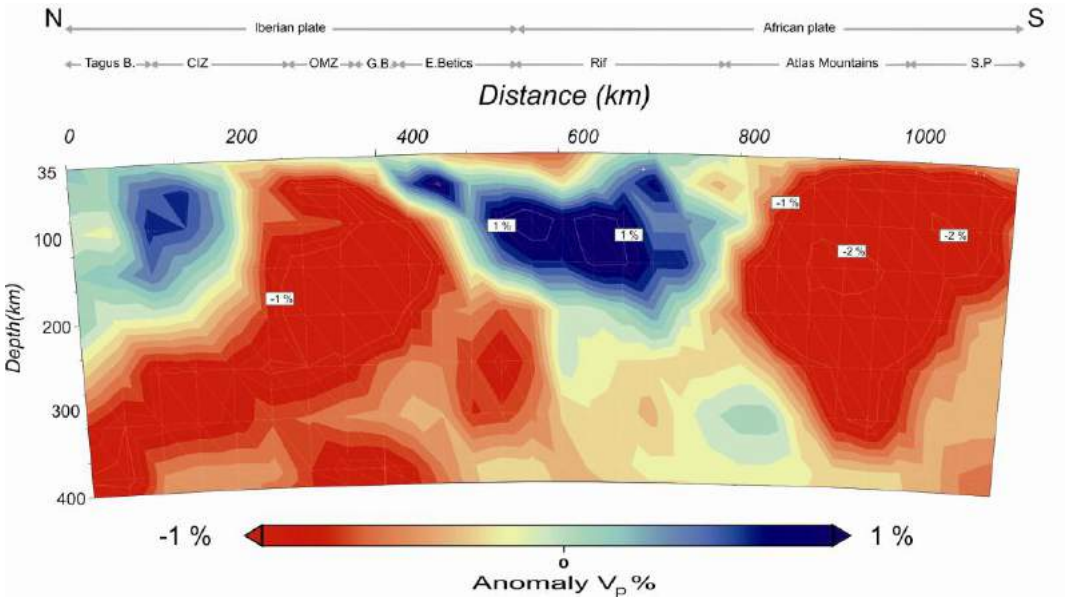


Figure 5.3: P-wave tomography model along the Iberian Massif-Arc of Gibraltar-Atlas Mountains (fourth profile) based on the global travel-time tomography model of Villaseñor et al. (2003).

Positive anomalies, exceeding 1%, correspond to the subducting slab beneath the Gibraltar Arc. The tomography section also shows a zone of fast P-wave velocity (0.3% to 1%) beneath the Tagus Basin. Negative anomalies are located beneath the OMZ and the Atlas, extending down to 400 km depth.

S-wave mantle velocities are derived from a 3D shear-wave velocity model estimated from inversion of Ambient Noise Tomography data (Gaite et al., 2014). Fast S-wave velocities coincide with the pronounced lithospheric thickening in the subducting slab beneath the Gibraltar Arc, whereas lower S-wave velocities characterize the regions with a thin lithosphere as the CIZ-OMZ and the Atlas Mountains. Xenolith data along the modelled profile are scarce and restricted to the Calatrava Volcanic Province (CVP), close to the geo-transect and affected by the same velocity anomaly in the lithosphere mantle, and in the Atlas Mountains. As explained in Chapter 4, the CVP is characterized by an enriched mantle component (Bosch et al., 2014) and the spinel lherzolite xenoliths show two metasomatizing events related to a fertile mantle (e.g., Cebriá and López-Ruiz, 1995; Bianchini et al., 2010; Villaseca et al., 2010). In the Atlas Mountains the lithosphere mantle xenoliths correspond to fertile lherzolites and less abundant harzburgites that show depletion processes followed by metasomatic enrichment, resulting in more fertile lherzolites but also in less abundant harzburgites. Both origins have often been attributed to the partial melting of asthenospheric mantle forming either deep-seated plumes (Wilson and Downes, 1992, 2006; Wilson and Bianchini, 1999) possibly emanating from a deep superplume (Forte et al., 2010); or uprising "splash plumes" (Davies and Bunge, 2006) due to the accumulation of subducted oceanic slabs during the Mesozoic closure of the Tethys ocean (Lustrino and Wilson, 2007; Faccenna and Becker, 2010; Lustrino et al., 2011; Carminati et al., 2012).

## 5.3. – Preliminary results

The geometry of the LAB beneath the Iberian Plate, Gibraltar Arc, Atlas Mountains and surrounding areas has been the subject of several studies integrating different geophysical data sets, mainly using 2D modeling (Fernandez et al., 2004; Zeyen et al., 2005; Teixell et al., 2005; Jiménez-Munt et al., 2011), Vs tomography (Palomeras et al., 2014) and 3D lithospheric model (Fullea et al., 2010; Torne et al., 2015). These studies provide information in the Variscan Belt and in North Africa. Most of these models do not consider pressure and compositional changes in the mantle, except that by Fullea et al., (2010). Nevertheless, as a first approach I used the available information as input for our forward modeling. For instance, the study of Fullea et al. (2010) has reported a maximum lithospheric thickness of 240 km beneath the Rif. A decrease in litospheric thickness is assumed towards the Rharb Basin where values of 140 km to 80 km, are reported (e.g., Jiménez-Munt et al., 2011; Fullea et al., 2010; Teixell et al., 2005). To the N, along the OMZ the lithosphere is about 100-120 km thick and reaches 120 km towards the Tagus Basin (Fernandez et al., 2004; Torne et al.,

2015). Results from Rayleigh wave tomography (Palomeras et al., 2014) reveal similar trends as the thermophysical models but with shallower LAB depth values. Their estimated LAB depth ranges from 40 to 75 km from the Tagus Basin to OMZ, dipping south in the Gibraltar Strait where the results are not clear. A thinner lithosphere of about 50 km thickness is mapped below the Atlas. It is worth to note that some of these profiles as those by Fernandez et al. (2004), Zeyen et al. (2005), Teixell et al. (2005), and Jiménez-Munt et al. (2011) do not follow the same orientation than the modelled geo-transect presented in this chapter. Therefore, the comparison of the calculated LAB depth with previous studies requires some caution and is particularly helpful from the qualitatively point of view.

## 5.3.1. – Lithosphere mantle structure

The best fitting model corresponding to the crustal structure depicted above is illustrated in Figure 5.4. Along the model profile I distinguish three lithospheric mantle types, which agree with the geological domains and xenolith samples.

The composition of the sub-lithospheric mantle is assumed to correspond to a primitive upper mantle (PUM) according to McDonough and Sun (1995). The overall composition of the lithospheric mantle along the profile falls in the lherzolitic field and thereby, I considered a lherzolite average (Tc_1) (Table 5.2) except in the CVP (Villaseca et al., 2010) and in the Atlas (Natali et al., 2013), where composition are slightly changed towards more fertile mantles, according to available geochemical data on xenolith samples. Additionally, both areas are characterized by low P-wave velocities suggesting an anomalous lithospheric mantle.

| Bodies | Composition | $SiO_2$ | $Al_2O_3$ | FeO | MgO | CaO | $Na_2O$ |
|---|---|---|---|---|---|---|---|
| 11 | Tc_1 (Av. Tecton) | 44.64 | 3.51 | 8.02 | 39.93 | 3.11 | 0.24 |
| 12 | CVP (Calatrava_65290) | 44.51 | 3.76 | 8.75 | 37.89 | 3.28 | 0.36 |
| 13 | Atlas_average | 44.08 | 3.28 | 8.73 | 41.14 | 2.59 | 0.22 |
| 14 | Pm_1 (PUM) | 45.00 | 4.5 | 8.10 | 37.8 | 3.6 | 0.36 |

Table 5.2. Chemical compositions (%) of mantle bodies used in the model.

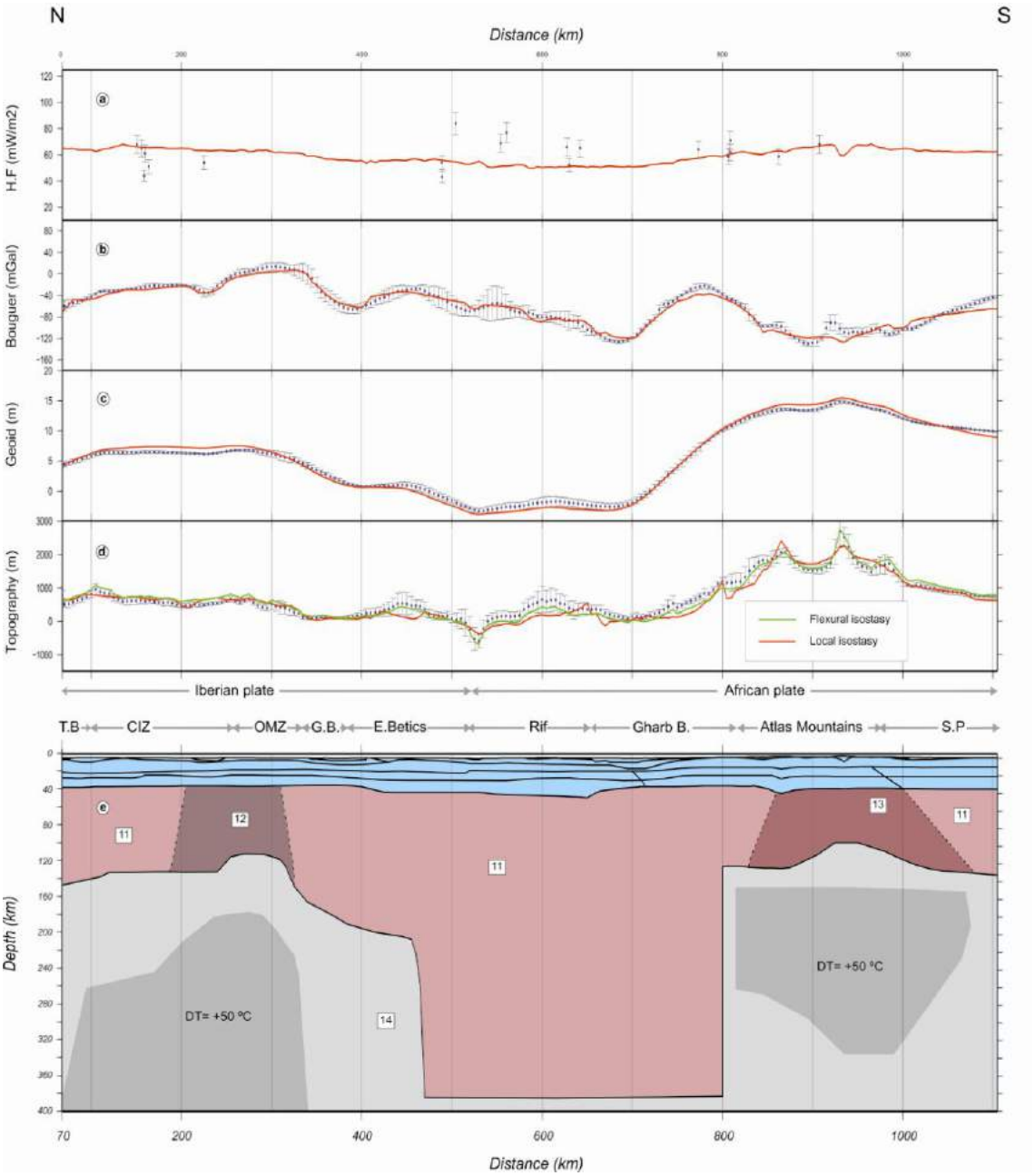


Figure 5.4: Model results (red lines), measured data with the standard deviation of data projected onto the profile within a strip of 25 km half-width (blue dots and vertical bars): (a) surface heat flow; (b) Bouguer anomaly; (c) geoid height; (d) elevation and coupled calculated topography under local isostasy (red line) and under regional isostasy with elastic thickness varying between 20 and 10 km (green line); (e) lithospheric structure. Crustal structure like in Fig. 5.2. Numbers in panel (e) denote mantle bodies summarized in Table 5.2. Dataset sources as in Fig. 1.3.

In order to reproduce the low velocity regions imaged by tomography I increased the temperature below Iberia and the Atlas Mountains by 50 ºC. These anomalously hot mantle regions are delimited by two sublithospheric bodies following a

procedure similar to Chapter 4.

In general, gravity and geoid anomalies match the major observed trends along the profile. Local misfits in the Bouguer anomaly (~20 mGal) are noticed at the southern edge of Rharb Basin and in the Sahara Platform, probably related to border effects in the end of the model. The observed surface flow, ranging between 40 and 80 $mW/m^2$, is consistent with the calculated heat flow trend. Geoid shows small misfits of about 2 meters and 1 meter in the CIZ and in the Atlas Mountains, respectively. Note that the calculated elevation under the assumption of local isostasy shows also local misfits. However when flexural rigidity of the lithosphere is considered, the calculated elevation fits well with observations. The elastic thickness considered in this work varies along the transect from Te=20 km in the Tagus Basin to the Rif Mountains, decreasing to Te=10 km in the Atlas Mountains, according to Pérez-Gussinyé and Watts (2005).

The LAB depth varyies from about 130 km beneath the CIZ to about 110 km in the OMZ and deepens to near 400 km beneath the central part of the profile where the lithospheric slab is presumed. It is worth to note that P-wave tomography along the profile (Fig. 5.3) shows the high velocity anomaly beneath the Gibraltar Strait, reaching a depth of ~200 km. However, the lithospheric slab is arcuated following the Betic-Rif orogen and therefore dips southwards beneath the Betics, and eastwards beneath the Gibraltar Strait. Figure 5.5 shows an E-W tomography cross-section through the Gibraltar Strait and the position of the modelled N-S profile. As seen in this figure, the uppermost part of the slab (100 km depth) is located to the west of the profile, in the Gulf of Cadiz region, whereas the deepest part (until 670 km depth) is located to the east of the profile, in the Alboran Basin. To account for 3D effects derived from this complex geometry, I consider that the slab in the 2D modelled section extends down to the base of the model, actually to 380 km depth to avoid problems with the boundary conditions. Finally, a sharp lithospheric mantle thinning is observed beneath the Atlas with a LAB depth of ~95 km that increases progressively to maximum depths of 130 km at the SE tip of the profile.

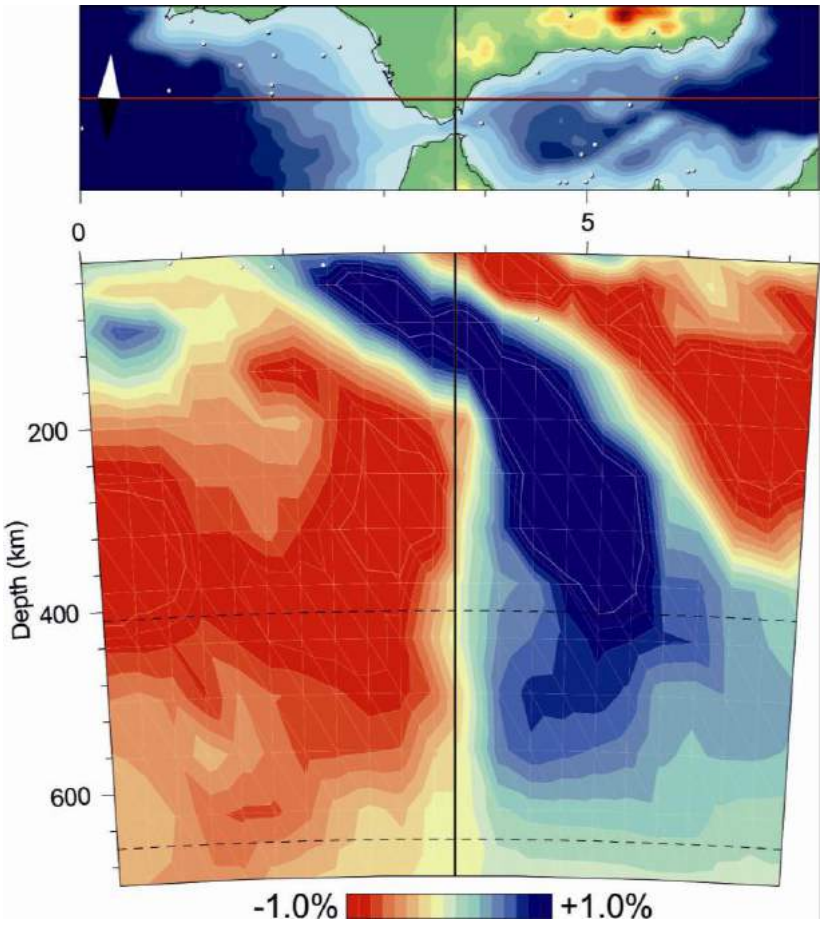


Figure 5.5: East to west tomographic cross-section based on the tomographic model of Villaseñor et al. (2003). Black line shows the location of the Iberian Massif-Arc of Gibraltar-Atlas Mountains geo-transect.

## 5.3.2. – Temperature and density distribution

The temperature distribution in the entire modeled domain is displayed in Fig. 5.6. The CIZ-OMZ is characterized by upward deflection of the isotherms with a Moho temperature of about ~600 °C. The calculated Moho temperature increases from 550 ºC in the Rif, with a crustal thickness exceeding 45 km, to 700 ºC in the Atlas, where the Moho deepens to ~40 km depth. This difference in the Moho temperature is related to the strong lateral variation of the LAB depth, which amounts ~300 km between both chains. Farther south, the Moho temperature decreases to 650 ºC in the Saharan Platform. The lithospheric mantle thinning affecting the southern part of the CIZ-OMZ and the Atlas Mountains deflects the isotherms upwards, especially near the lithosphere-asthenosphere boundary. The temperature distribution in the sub-lithospheric mantle shows strong lateral variations related to the prescribed thermal perturbations beneath

the Calatrava Volcanic Province and the Atlas Mountains that increase the temperature by 50 ºC relative to the surrounding mantle, and the presence of a subducting lithospheric slab, with a temperature between 1150 and 1300 ºC at 200-400 km depth.

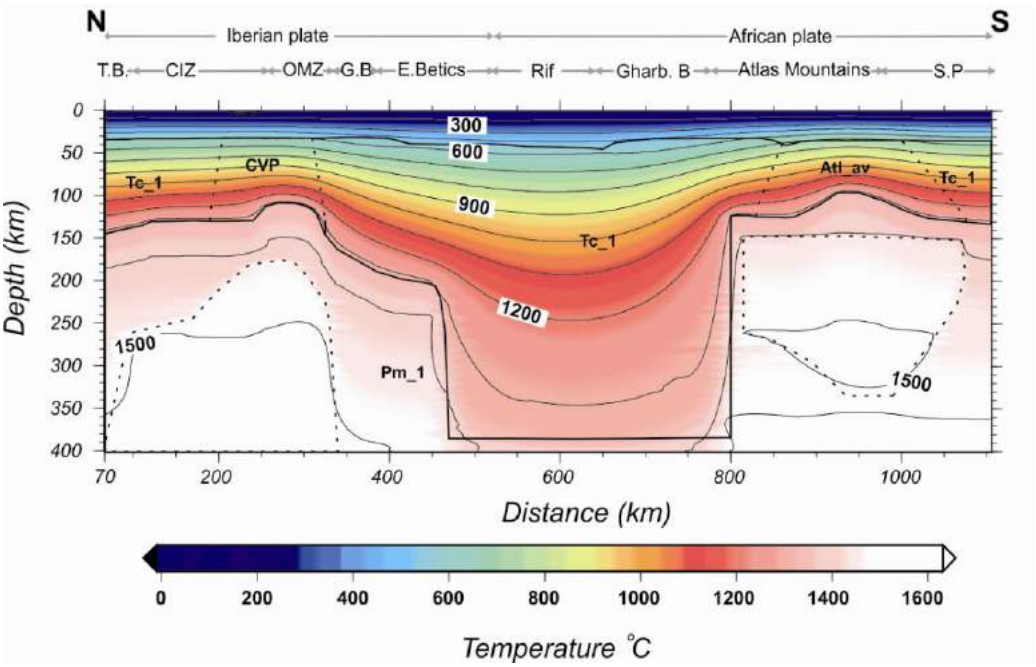


Figure 5.6: Calculated temperature distribution along the Iberian Massif-Arc of Gibraltar-Atlas Mountains geo-transect and mantle domains with different chemical composition (see Table 5.2). Contour lines every 100 °C.

The calculated mantle density distribution is shown in Fig. 5.7. In the Variscan Iberian Massif, the lithospheric mantle density increases with depth from <3320 kg/m$^3$ beneath the Moho to 3340 kg/m$^3$ at the LAB in the northernmost segment of the profile (CIZ), whereas the CVP region is essentially isopicnic due to the lithospheric thinning affecting this region and to the different chemical composition. Similar density values are calculated in the Atlas region, where the LAB also shows densities similar to the uppermost mantle (3320 kg/m$^3$). In the central segment of the profile (Betic-Rif orogenic system), the lithospheric mantle density shows a clear increase ewith depth, from 3320 kg/m$^3$ beneath the Moho to >3580 kg/m$^3$ in the LAB at 380 km depth. The density increase is not linear being less pronounced at the first 200 km depth. Interestingly, beneath ~280 km depth the density keeps almost constant horizontally despite the differences in temperature and composition between the anomalous sublithospheric bodies (ΔT=50ºC, PUM composition), the sublithospheric mantle, and the subducting slab (ΔT~ -150ºC, and Tc_1 composition). This indicates that, in this case, all the geophysical observables related to density loose sensitivity at depths higher than 300 km and therefore, the LAB topography is mainly constrained by the calculated

seismic velocities.

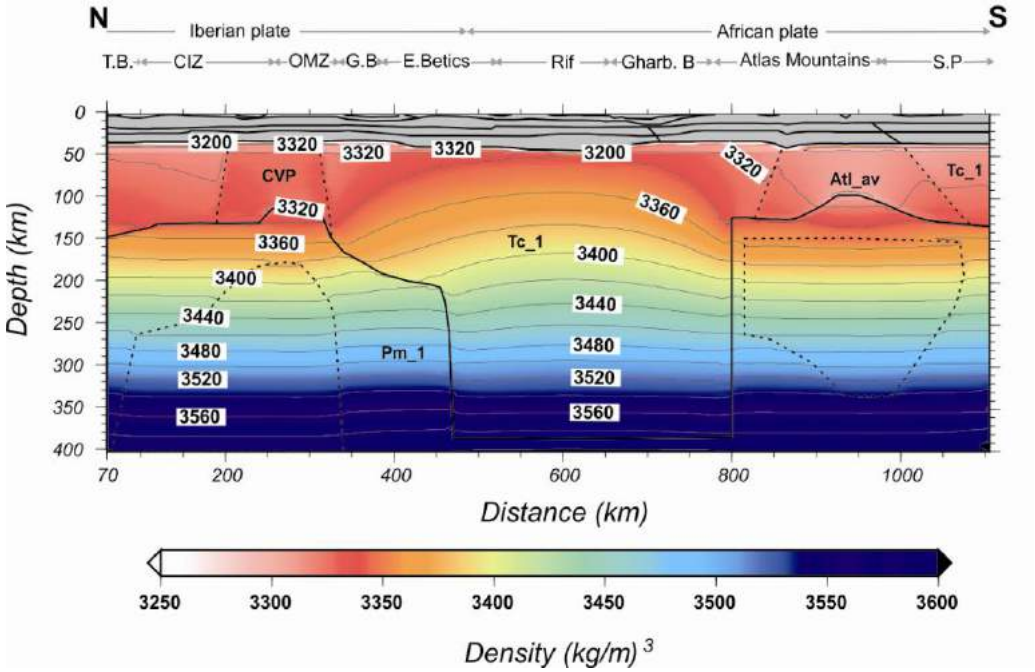


Figure 5.7: Calculated mantle density distribution along the Iberian Massif-Arc of Gibraltar-Atlas Mountains geo-transect. Contour lines every 20 kg $m^{-3}$.

## 5.3.3. – Mantle velocity distribution

Velocity variations related to compositional changes are smaller than those related to temperature and lithospheric thickness variations as it is observed along the modelled geo-transect.

Fig. 5.8a shows the calculated P-wave velocities in the mantle where the most outstanding feature is the large lateral velocity variations within the lithospheric mantle related to the differences in the LAB depth between the Betic-Rif orogenic system and the surrounding Iberian and north-Africa regions. The lithospheric mantle velocity in the CIZ and OMZ is < 8.1 km/s, with minimum values of < 8.0 km/s close to the LAB beneath the regional with chemical affinities to the CVP. Similar values (< 8.1 km/s) are calculated in the Atlas Mountains and the Sahara Platform, with minimum values of < 7.9 km/s close to the LAB beneath the Atlas Mountains. The low Vp values at the LAB (<8 km/s) underneath the OMZ and the Atlas Mountains are related to the shallower LAB and the change in mantle composition, defining a local low-velocity zone (LVZ). In contrast, P-wave velocities in the Betic-Rif orogenic system and surrounding foreland basins increase steadily from ~8.1 km/s in the uppermost mantle to > 8.7 km/s

in the LAB at ~380 km depth. In the sublithospheric mantle regions where we have imposed a thermal perturbation of 50 ºC, P-wave velocities decrease relative to the surrounding mantle by ~0.4 km/s.

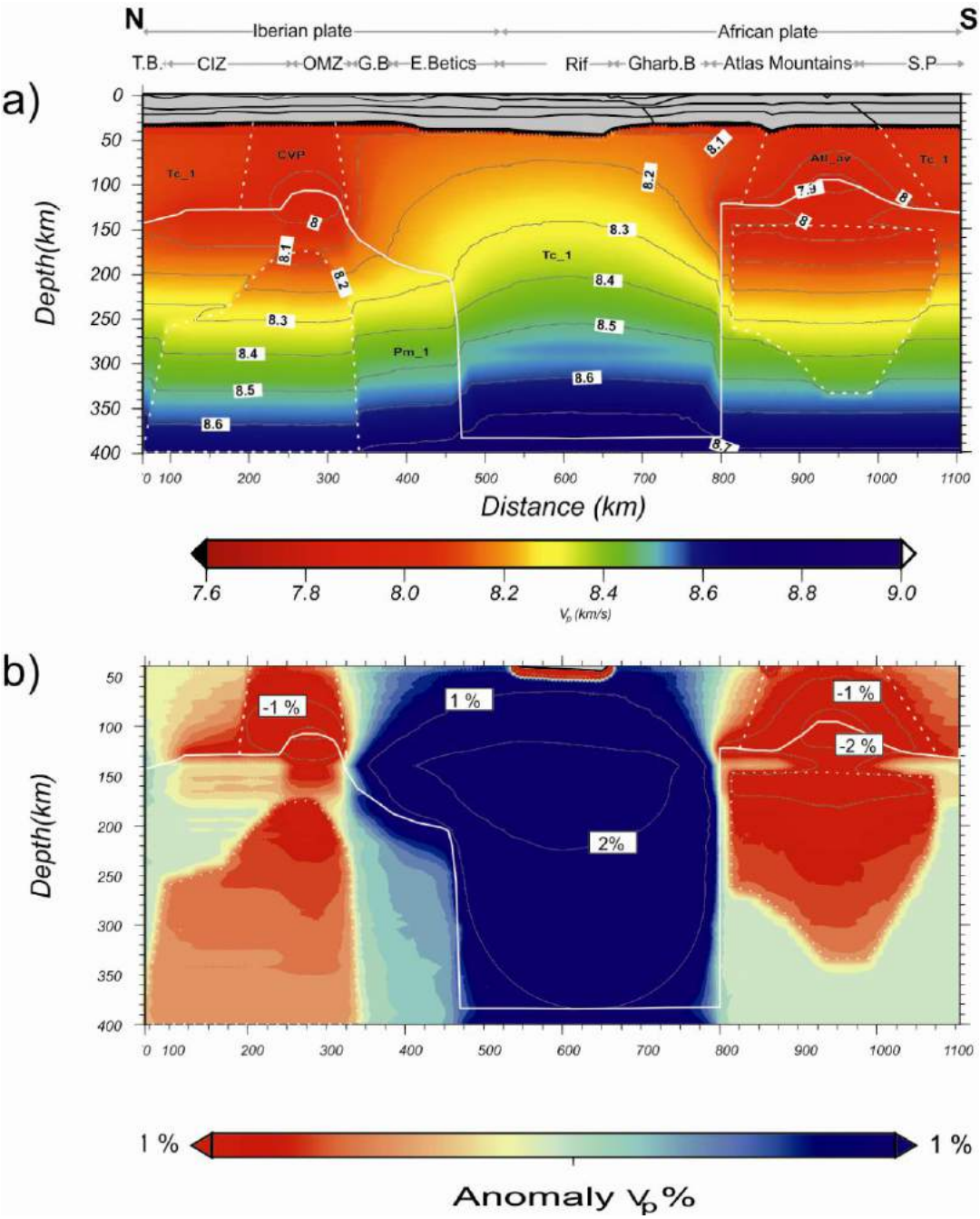


Figure 5.8. a) Calculated P-wave seismic velocities in the upper mantle down to 400 km; b) synthetic P-wave tomography from our model. In this case velocity anomalies are relative to the synthetic reference model (reference model consisting of a 130-km thick lithosphere and 30-km thick crust with a lithosphere mantle composition corresponding to Tc_1.) (see text). Contour lines every 1%. Compare with Figure 5.2.

Fig. 5.8b shows the resulting synthetic tomographic model calculated from Vp in

(%) relative to a reference model consisting of a 130-km thick lithosphere and 30-km thick crust with a lithosphere mantle composition corresponding to Tc_1. The comparison of this synthetic tomography with the global P-wave tomography model by Villaseñor et al. (2003) shown in Fig. 5.3 show coincidences in the slow and fast velocity regions predicted by both models although there are discrepancies with the amplitudes. The remarkable difference related to the shape of the fast velocity anomaly is due to strong the 3D geometry of the subducting slab, as mentioned in previous sections.

Calculated S-wave velocities show a similar pattern than P-wave with minimum values of < 4.35 km/s extending over the sub-lithospheric mantle in the OMZ and the Atlas Mountains (Fig. 5.9a), whereas in the uppermost mantle the S-wave velocities increase to ~4.6 km/s in both cases. Beneath the Betic-Rif orogenic system, uppermost mantle S-wave velocities are close to 4.65 km/s and keep approximately constant until 300-km depth. Vs values exceeding 4.7 km/s are calculated at the base of the subducting slab. The calculated Vs show a comparable pattern, in terms of fast/slow regions in the first 80 km depth, with the regional S-wave tomography model of the study area proposed by Gaite et al. (2014) from seimic ambient noise.

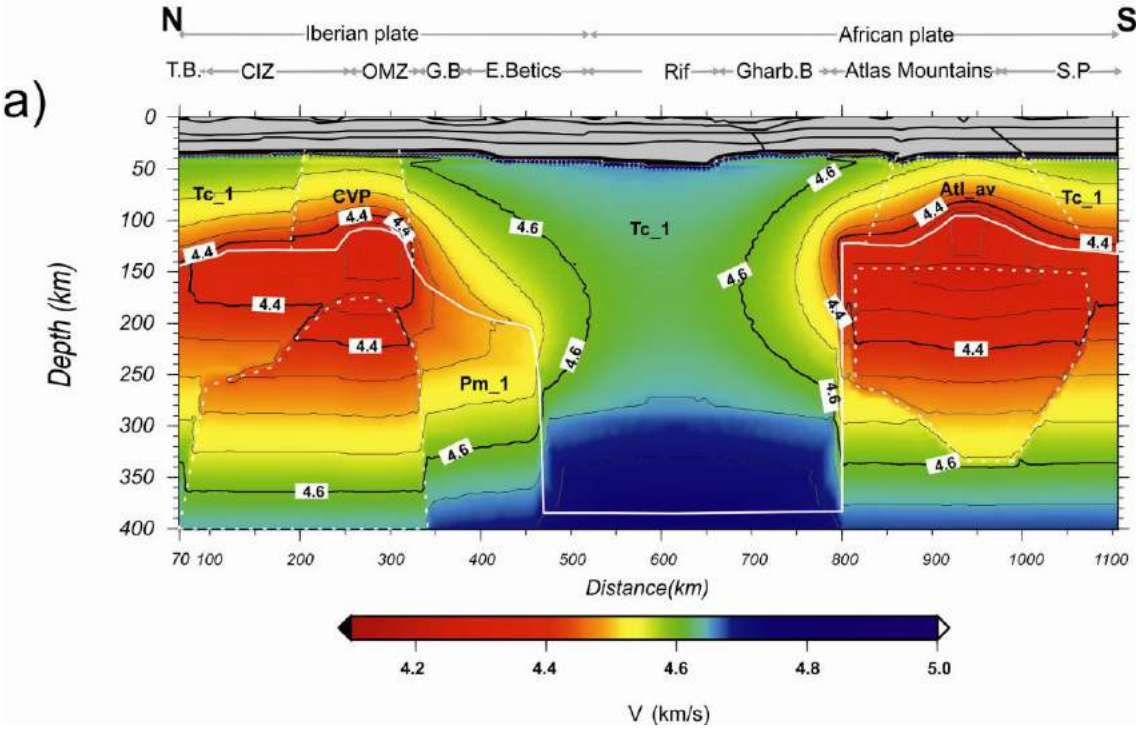


Figure 5.9: Calculated S-wave seismic velocities in the upper mantle down to 400 km depth. Contour lines every 0.05 km/s.

Pn and Sn velocity data are an additional constraint on seismic mantle velocities. Fig. 5.10 compares the calculated P-wave and S-wave velocities in the uppermost lithospheric mantle with Pn and Sn estimates from Diaz et al. (2013) from 200 km to 800 km horizontal distance along the profile, taking into account the mentioned uncertainties in the experimental methods.

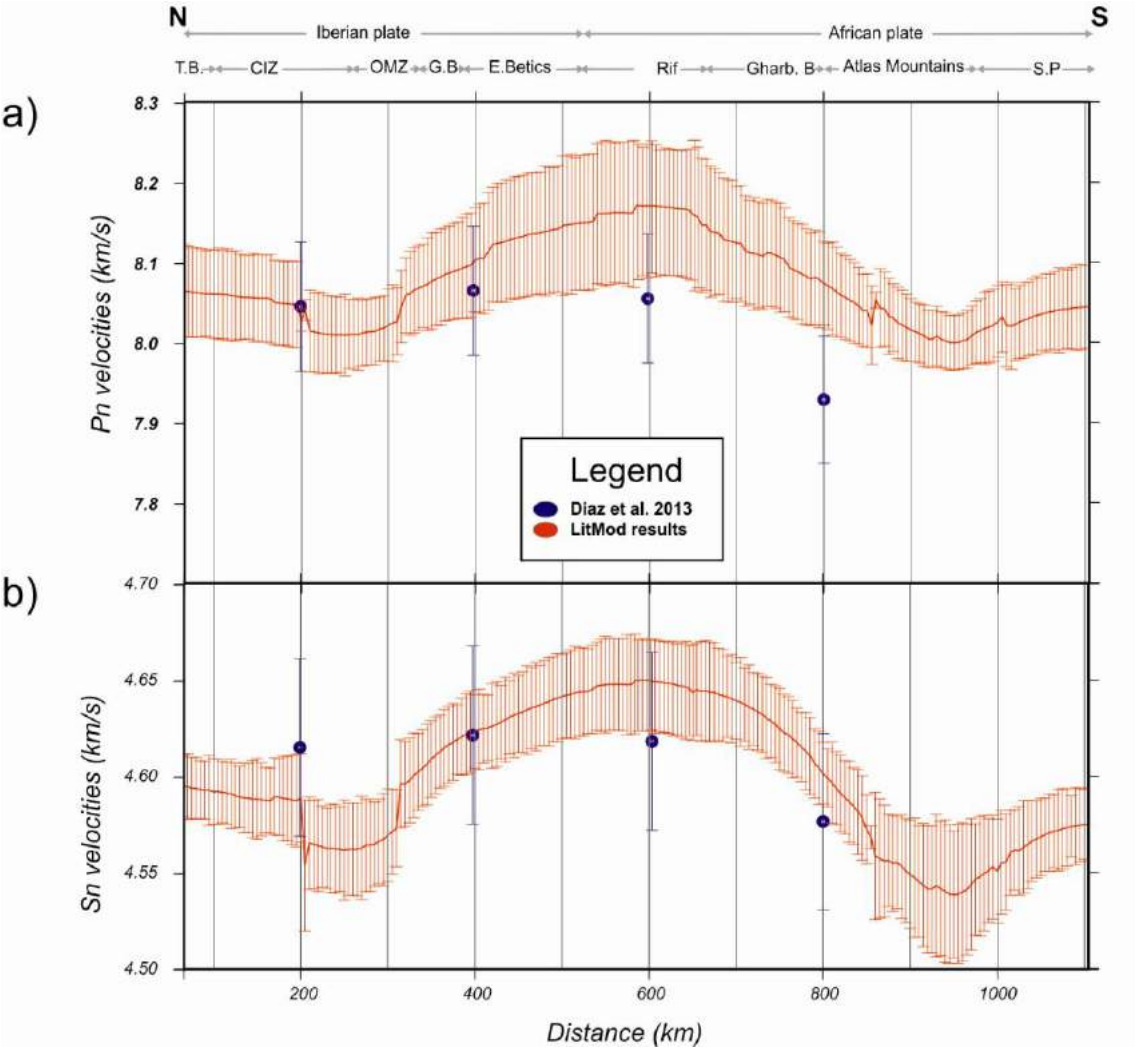


Figure 5.10: a) Pn velocities along the modeled transect. Red line indicates calculated Pn values. Circles with error bars denote Pn-values from seismic experiments (see legend); b) Sn velocities along the modeled transect. Red line indicates calculated Sn values. Symbols with error bars denote Sn-values from Diaz et al. (2013).

Calculated and observed Pn and Sn values are in good agreement along this section of the modelled geo-transect. Calculated Pn velocities increase from ~8.05 km/s in OMZ to >8.1 km/s beneath the Rif. The values decrease again to about ~8.05 km/s in the Atlas Mountains, where the lithosphere mantle is thin and different in composition.

Calculated Sn velocity values show similar trends than those proposed by Diaz et al. (2013), ranging from ~4.6 km/s below the OMZ to 4.65 km/s below the Rif, with minimum values beneath the Atlas (>4.55 km/s).

# 5.4. – Discussion

## 5.4.1. – LAB topography

Figure 5.11 compares the resulting LAB topography from Iberia to North Africa with previous studies as Fernandez et al. (2004), Zeyen et al. (2005), Teixell et al. (2005), Fullea et al. (2010), Jiménez-Munt et al. (2011), Palomeras et al. (2014) and Torne et al. (2015). Note that the orientation of the Fernandez et al. (2004), Zeyen et al. (2005), Teixell et al. (2005) and Jiménez-Munt et al. (2011) profiles do not coincides exactly with the geo-transect presented in this chapter, being comparable only some segments of these profiles.

Underneath the CIZ-OMZ the modelled LAB topography is consistently ~10 km deeper than those obtained from previously models (e.g., Fernandez et al., 2004; Fullea et al., 2010; Torne et al., 2015). Farther south, beneath the Guadalquivir Basin and the western External Betics, the model by Torne et al. (2015) predicts a noticeably shallower LAB, with differences exceeding 50 km. Across the apex of the Gibraltar Arc, previous models propose LAB depth values between 170 and 240 km in clear contrast with the ~400 km inferred from this study. In the African segment of the profile the results obtained in the Southern part of the Rharb Basin, fairly coincide with those obtained by Zeyen et al. (2005). Discrepancies with results from these authors are of the order of 20 km in the Atlas Mountains, and up to 30 km in the Saharan Platform. Jimenez-Munt et al., (2011) propose a minimum LAB depth of ~80 km, in contrast to ~95 km, as inferred from our model. Minor discrepancies are found along the rest of the profile. According to Teixell et al. (2005), the LAB lies at ~75 km depth in the Atlas Mountains, deepening southwards to <100 km in the Sahara Platform. The main reason for the encountered differences in the calculated LAB depth from different models are: 1) differences in the modelling approaches; 2) differences in the crustal geometry and densities; 3) differences in the exact location of the profiles; and probably most important 4) the no incorporation of the subducted slab and sublithospheric mantle bodies in the previous models. Finally, the LAB depth inferred from Rayleigh wave tomography by Palomeras et al. (2014) shows very shallow values along the whole profile and particularly, beneath the Rharb Basin and the Atlas Mountains, where the

proposed LAB is only some kilometers (5-15 km) beneath the Moho. It must be noted however, that these authors define the LAB depth as the depth of the maximum negative shear velocity gradient lying below the fast lid and therefore, tends to shallow the LAB depth when compared to the thermal definition.

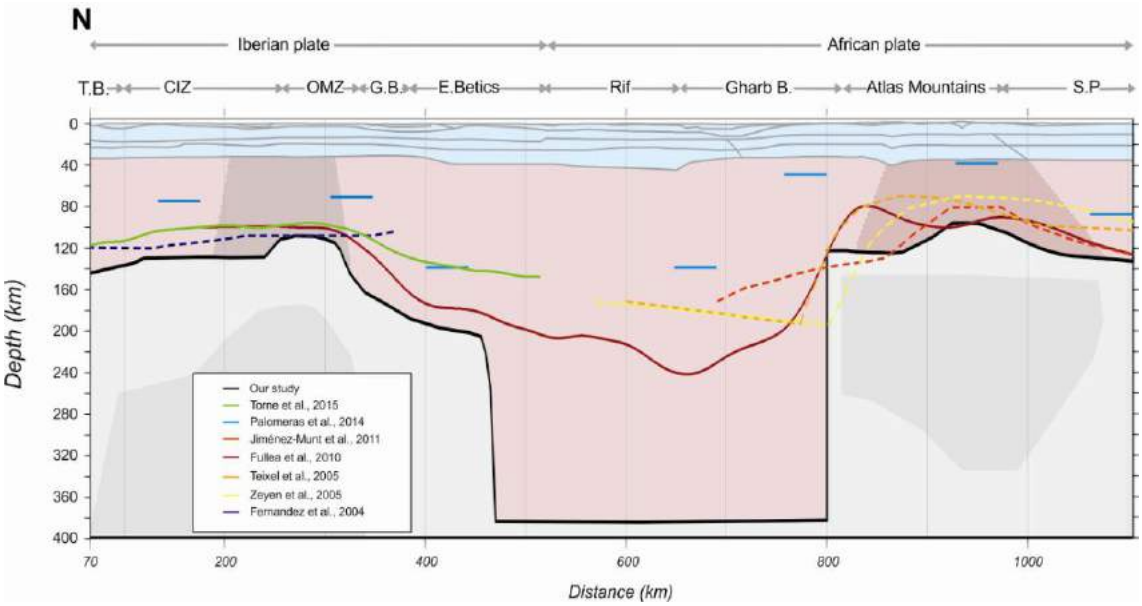


Figure 5.11: Calculated topographies of the lithosphere-asthenosphere boundary from different models. Dashes lines correspond to profiles that not coincide with the direction of the Iberian Massif-Arc of Gibraltar-Atlas Mountains geo-transect. CIZ, Central Iberian Zone; OMZ, Ossa Morena Zone; GB, Guadalquivir Basin; S.P, Sharan Platform.

## 5.4.2. – Changes in the mantle composition

In this fourth profile a homogeneous composition in the Iberian mainland and the North Africa, with the exception of the CIZ-OMZ and the Atlas Mountains has been considered. Since Iberia and north-Africa has undergone the Variscan and Alpine tecthonothermal events, a dominant Phanerozoic composition was taken for most of the model region, which corresponds to the Average Tecton garnet proposed by Griffin et al. (2009).

Negative P-wave anomalies in the lithosphere mantle imaged from tomography models (Figures 1.2 and 5.3) suggest a different compositional origin in the CIZ-OMZ along the geo-transect, probably related to the Calatrava Volcanic Province which is located close to the profile. Thereby, I characterized this section of the profile with a composition derived from a spinel lherzolite xenolith (Villaseca et al., 2010) originated at depths of 35-50 km in the Cenozoic CVP. The composition of this lithospheric mantle portion is moderately depleted relative to the PUM due to a very low partial

melting event (1.5%) and coincides with that considered in the N-S geo-transect in Chapter 4 (Table 5.2).

In the Atlas Mountains the resulting lithospheric mantle composition is an average of the xenoliths samples proposed in Natali et al. (2013), where peridotite samples are lherzolites (Table 5.2). These peridotites represent a lithospheric mantle section variably depleted by extraction of basic melts, and show a clear HIMU signature. According to Raffone et al. (2009) an upward migration of asthenospheric melts with HIMU-like isotopic signatures melts during late Cretaceous times has percolated in the overlying lithospheric mantle. Upwelling of hot asthenospheric mantle controlled by various tectonic events, caused the partial melting of the base of this metasomatised lithospheric mantle (Bosch et al., 2014). Consequently, some lherzolites recording the effects of melt percolation were only partially affected by metasomatism. Other lherzolites and more refractory mantle sectors (i.e. harzburgites) progressively approached chemical equilibrium with the migrating melt and were extensively re-fertilize (Raffone et al., 2009). The abundance of extensively re-fertilize samples and Fe-rich wehrlites relative to the first type of samples suggests that wide sectors of the mantle beneath the NE-SW volcanic alignment consist of rejuvenated lithosphere. Since the xenolith mantle composition varies from more depleted to less depleted composition, an average of all xenoliths samples is more realistic than choosing one of them. The change in the lithospheric mantle composition in both CIZ-OMZ and Atlas Mountains results in a shallower LAB in both cases, since the density contrast with respect to Tc_1 is about ~9.2 kg/m$^3$ and ~6.85 kg/m$^3$ respectively.

## 5.4.3. – Thermal and compositional sub-lithospheric anomalies

Figure 5.3 displays anomalous P-wave seismic velocities in the asthenosphere extending from the Tagus Basin to the Strait of Gibraltar and below the Atlas Mountains and the Saharan Platform. This anomalous seismic velocities imaged from tomography models are also interpreted here as a positive thermal anomaly with a $\Delta T$=50 ºC in OMZ and in the Atlas Mountains. The sublithospheric mantle composition is considered to be homogeneous along the whole profile and corresponding to the PUM.

To illustrate the influence of chemical composition, phase changes and temperature, I show the vertical P-wave velocity variation at four sites located along the profile (Figure 5.12). As observed, plagioclase-spinel transition at ~40 km depth,

increase the Vp by about 0.05 km/s, except in the Rif Mountains where the crust is too thick (~45 km) for allowing this mineral phase change. Figures 5.12a, b, and d show a decrease in the Vp amounting 0.04-0.06 km/s related to the sub-lithospheric anomalous temperature (ΔT = 50 ºC). The mineral phase change from orthopyroxene to high-pressure magnesian pyroxene can be recognized at depths of 290-315 km depending on the site.

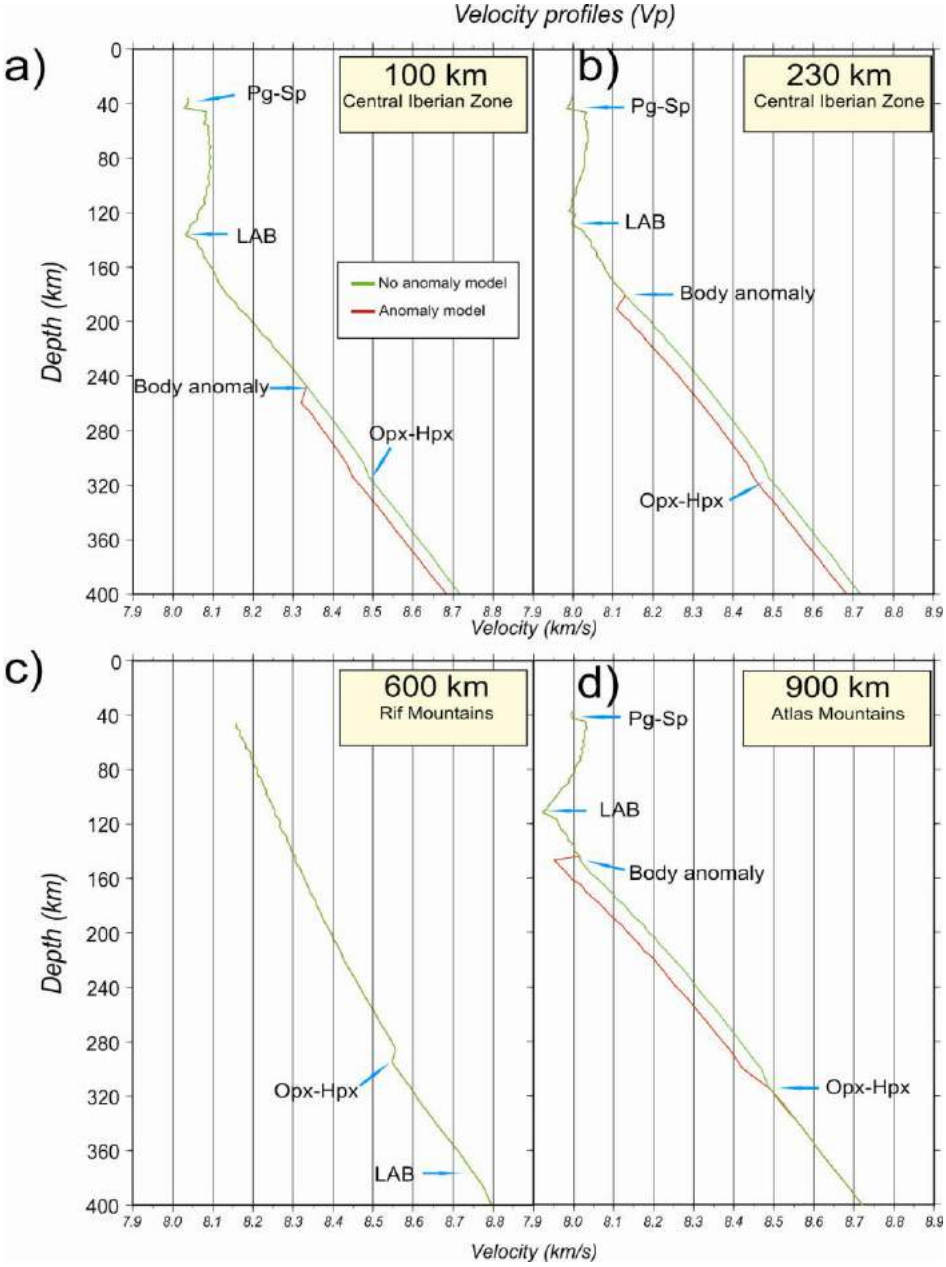


Figure 5.12: Depth variation of P-wave velocities calculated in the preferred model along the profile (in sites located at 100, 230, 600 and 900 km horizontal distance) for model with the sub-lithospheric anomalous body (red line) and model without the anomlalous body (green line). Arrows denote the lithosphere-asthenosphere boundary (LAB) and the following phase transitions: Pg-Sp, plagioclase-spinel; Opx-Hpx, orthopyroxene-high-pressure magnesian pyroxene.

Figure 5.13 illustrates the calculated densities along selected vertical profiles. The resulting density decrease related to the anomalous high temperature in the sub-lithospheric mantle amounts ~6 kg/m$^3$ and ~4 kg/m$^3$; whereas the density increase related to the compositional change at the LAB, from Tc_1 to PUM, amounts ~20 kg/m$^3$.

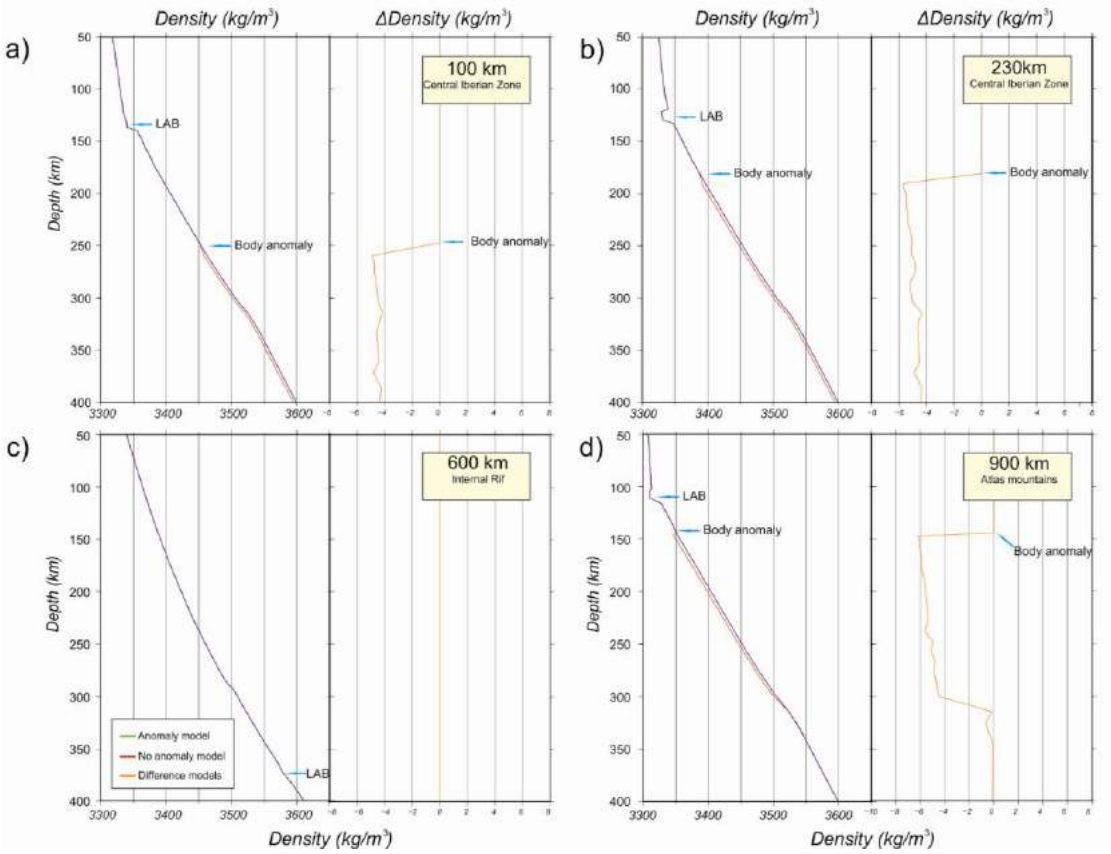


Figure 5.13: Depth variation of mantle density calculated in the preferred model along the profile (in sites located at 100, 230, 600 and 900 km horizontal distance) for model with asthenospheric anomaly and model without asthenospheric anomaly.

The calculated contribution of the high temperature sub-lithospheric bodies on the topography with respect to a decoupled model, in which the density changes in this anomalous bodies are not transmitted to the Earth‘s surface, is shown in Figure 5.14. As explained in Chapter 4, the influence of sub-lithospheric perturbations in the decoupled model remains on all the geophysical observables except in the calculated topography. Therefore, the maximum contribution to elevation related to anomalous sub-lithospheric bodies is of 330 and 300 m in the CIZ-OMZ and the Atlas Mountains, respectively.

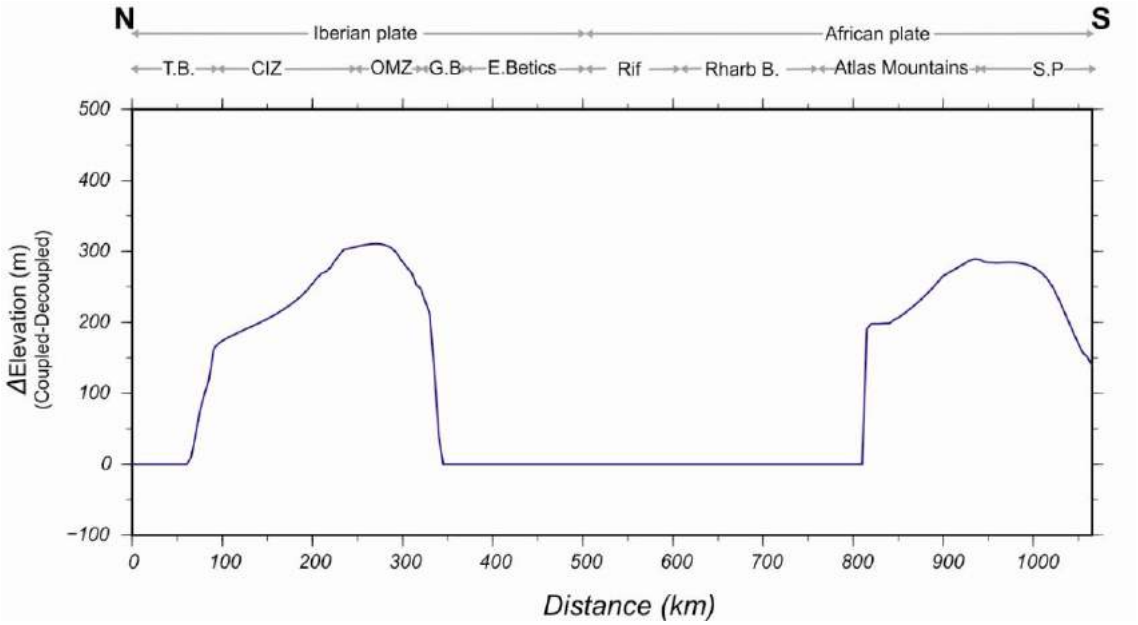


Figure 5.14: Difference between the elevations calculated considering coupled and decoupled anomalous sub-lithospheric bodies.

# Chapter 6: General Discussion

# 6.1. – Lithosphere structure

The modeled geometry of the lithosphere-asthenosphere boundary relies on the considered crustal structure (geometry and parameters), on the mantle images from seismic tomography studies, and on the compositions of the lithospheric and sub-lithospheric mantle of the study area. The crustal structure is based on numerous studies from seismic experiments and integrated geophysical models carried out in the vicinity of the studied transects. Here, I focus on the comparison of our proposed LAB-depth in the different domains.

*Northern Alpine domain – The Cantabrian Mountains and Pyrenees*

In the northern part of the study area, the crustal structure is well constrained from numerous seismic experiments carried out crossing the Cantabrian Mountains and the Pyrenees. The resulting lithospheric mantle geometry depicts a pronounced lithospheric thickening in both areas (Fig 6.1) but with some differences of up to 45 km. The crustal roots beneath both ranges show similar depths, whereas the elevation is slightly higher in the Pyrenees. The reason for a thicker lithosphere (~45 km) beneath the Cantabrian Mountains than in the Pyrenees is unclear. Some of the causes could be: i) The geoid shows differents signals between the two mountains, being highly asymmetric in the Cantabrian Mountains where it decreasing towards the Cantabrian Sea by ~12 m, meanwhile, the Pyrenees have a symmetric positive signal of ~5 m. ii) The major contribution of the total difference in the elevation in the Cantabrian Mountains of about 6000 meters (from -4500 meters to more than 1500 meters) meanwhile in the Pyrenees is about 2000 meters. iii) The differences on the mantle thermal conductivity calculation, since in the first profile (Pyrenees) is based on Hofmeister et al. (1999), whilst in the Cantabrian model incorporates the radiative contribution described in Grose and Afonso (2013). iv) The small contribution of the depth-density distribution within the lithospheric mantle related to chemical composition, since the density is higher in the Pyrenees (Pr_6) than in the Cantabrian Mountains (Tc_1) (see below). Probably the calculated mantle thermal conductivity and chemical composition are minor contributions on the final lithosphere thickness variations, more related to the total changes in the elevation.

*Southern Alpine domain – The Betic-Rif orogenic system*

This area encompasses the Alboran Basin, the Betic and Rif orogens, and the Gulf of Cadiz, a zone related to subduction and further slab retreating of the Ligurian-Tethys domain (e.g., Rosenbaum et al., 2002; Faccenna et al., 2004; Spakman and Wortel et al., 2004; Vergés and Fernandez, 2012). Several studies (e.g., Garcia-

Castellanos and Villaseñor, 2011; Fig 1.2) suggest the occurrence of a lithospheric slab below the Betics-Rif domain down to approximately 600 km depth. Both modelled profiles 3 and 4 (Fig. 4.3 and Fig 5.3) show the lithospheric slab deepening to the base of the model (it is worth to note that in the fourth profile, the methodology does not allow a deeper lithosphere slab). However, the main difference between the two profiles is that the slab is detached below the Eastern Betics (profile 3 in Chapter 4) and it is still attached in the Western Betics and Rif Mountains (profile 4 in Chapeter 5), which is in agreement with tomography models. Anyhow the lateral size of the modeled slab appears different due to the orientation of the profiles crossing the 3D structure.

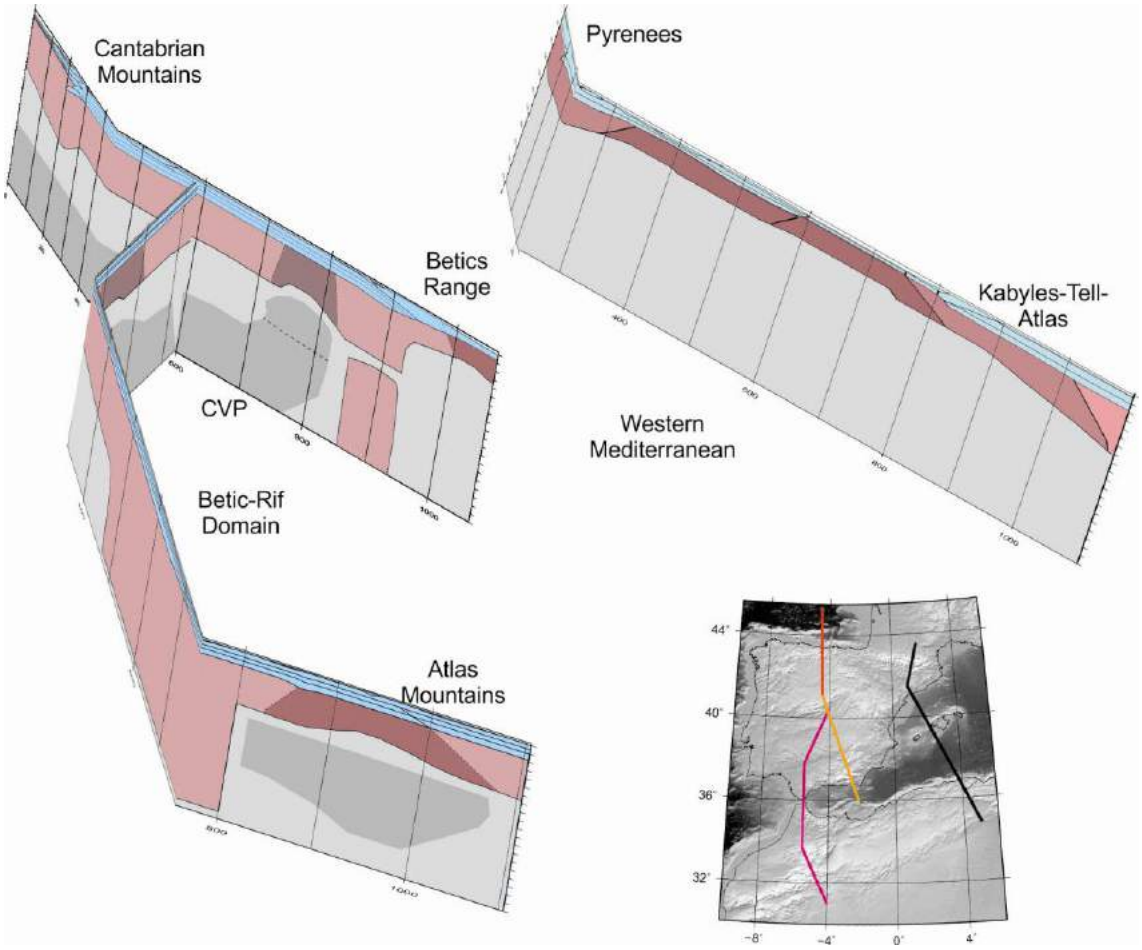


Figure 6.1: Schematic crust and upper mantle cross-sections of Iberia and North Africa of the four modeled geo-transects (second geo-transect is integrated in the third lithosphere profile). Lower right inset shows the location of the fourth geo-transects in the study area.

*Continental basins – Duero, Tagus and Ebro basins*

Duero and Tagus basins are large sedimentary basins located in the central part of the Iberian Peninsula bounding the Central System, whereas the Ebro Basin is the

foreland basin of the Pyrenees in the northeast of Iberia. The main feature in the Duero and Tagus basins is the relatively high elevation which is reflected in the calculated LAB topography of about ~135 km depth and ~125 km depth respectively. The LAB resulting from our models below the CVP are 15 km shallower than in other parts of the Tagus Basin and the two profiles (3 and 4) show the same results. The lithosphere thickness in the Ebro Basin is ~110 km, clearly dipping to the north.

*Marine domains – Valencia Trough, Algerian Basin and Bay of Biscay*

The Valencia Trough continental crust underwent thinning with large alkaline magmatic intrusions and volcanism. The Bay of Biscay crust was also extended and intruded. In the Algerian Basin, the back-arc extension produced the generation of new oceanic crust. LAB depth varies reaching values of about 130 km beneath the Bay of Biscay, about 65 km the Valencia Trough Basin and shallowing to as much as 60 km in the Algerian Basin. These differences in the LAB-depth can be mainly related to the age of the last tectono-thermal event when extension took place: first in the Bay of Biscay during the Late Jurassic-Early Cretaceous; subsequently the Valencia Trough Basin extension began in the Late Oligocene and ended during the Langhian period; and finally the opening of the Algerian Basin lasted from latest Early Miocene–Middle Miocene to Tortonian period.

*Intraplate ranges – Central System and High Atlas Mountains*

The Central System is the most prominent elevation in the interior (intraplate) of the Iberian Peninsula extending for more than 300 km. The High Atlas Mountains is a branch of the Atlas Mountains extending from the Atlantic to Tunisia. Although both ranges are intraplate mountains, they have a different origin. The Central System is interpreted as a symmetric pop-up that was uplifted during the Oligocene and the Miocene. In other hand, the structure of the High Atlas resulted from the tectonic inversion of a Mesozoic extensional basin, genetically related to the opening of the Atlantic and Tethys Ocean. Significant differences also appear when comparing our resulting LAB below these areas, indicating a flat LAB below the Central System reaching depths of about 135 km, whereas underneath the Atlas Mountains the lithosphere thins very sharply to ~95 km depth.

## 6.2. – Lithospheric mantle composition

Mineral assemblages in the lithospheric mantle have been computed using the

NCFMAS major oxides approach. I have considered several mantle compositions on the basis of global scale xenolith and tectonothermal age data, and available petrological studies on local mantle xenoliths. In this section, I discuss the lateral composition variation of the lithospheric mantle in the different domains. Figure 6.2 summarizes all the compositions used in this thesis.

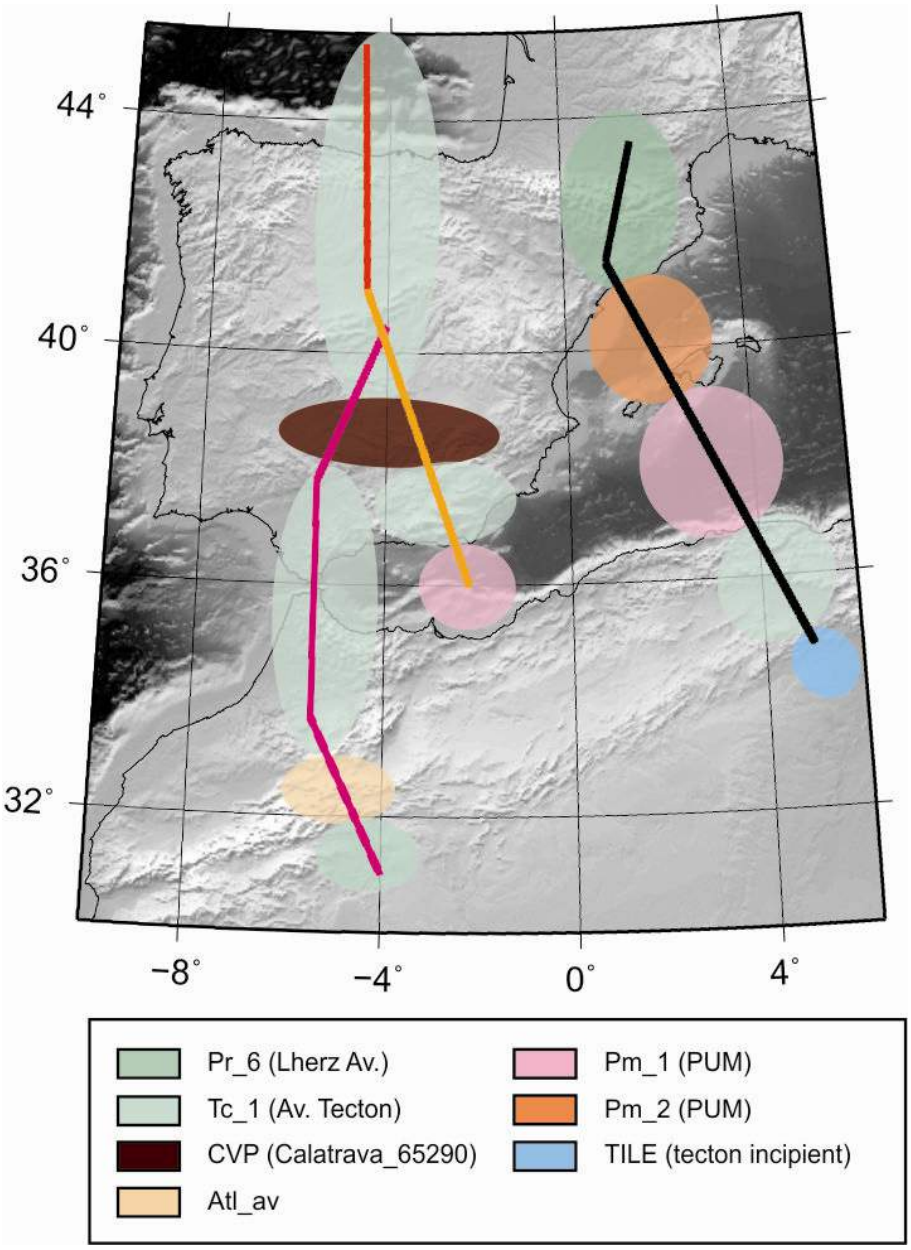


Figure 6.2: Topographic map of the study area showing the lithospheric mantles compositions used in this thesis. Thick lines locate the modeled transects: Black line-first geo-transect; Red line-second geo-transect; Light orange line-third geo-transect and pink line-fourth geo-transect. Chemical compositions described in Table 2.2, Table 3.2, Table 4.2 and Table 5.2.

*Northern Alpine domain – The Cantabrian Mountains and Pyrenees*

Two different lithospheric mantle compositions have been considered for the Cantabrian Mountains and the Pyrenees (body 9 in Table 2.2, and body 14 in Table 4.2). The lithospheric mantle composition of the Pyrenees is a lherzolite average (Pr_6) that corresponds to a local mantle xenolith suite. In the Cantabrian Mountains the lithosphere mantle composition is Average Tecton garnet (Tc_1) (Griffin et al., 2009), which has also been proposed in others areas of Iberia (e.g. Fullea et al., 2010) and it is a Phanerozoic average composition. Density differences at given P-T conditions attains maximum values of 3.6 kg $m^{-3}$ between Pr_6 and Tc_1 lithospheric mantle compositions (Fig. 2.11b). Also, differences in terms of absolute P-wave velocities are negligible between Pr_6 and Tc_1. The effects of this density contrast of these two similar compositions (Pr_6 and Tc_1) could be made compatible with the geophysical observables with small changes in the mantle lithosphere geometry in both models.

*Southern Alpine domain – The Betic-Rif orogenic system*

In the lithospheric mantle beneath the Betics and the Rif a Phanerozoic composition (Tc_1) is consistent with all the observables. This Phanerozoic average composition was also proposed by Fullea et al., 2010 in the same domain. It must be noted, that a denser composition like Tc_2 would be also compatible with the geophysical observables resulting in a slightly shallower LAB. Figure 2.11a shows that differences in Vp and densities amount as much as 0.02 km $s^{-1}$ and 5.2 kg $m^{-3}$ respectively, being the latest barely detectable.

*Continental basins – Duero, Tagus and Ebro basins*

Underneath the Duero and Tagus basins a Tc_1 lithospheric mantle composition fits well all observables, meanwhile in the Calatrava Volcanic Province a more fertile composition is needed. Global tomography (Fig 1.2) displays low velocities characterizing the lithospheric mantle below the CVP. This strong low velocity anomaly is extending towards the southwest and northeast of Iberia at 145 km depth whereas, higher velocities characterize the lithosphere below other parts of Iberia suggesting a different mantle composition relative to surroundings areas. Also, chemical analyses on xenolith samples seem to suggest that the CVP mantle has a composition very close to that of a fertile mantle. Therefore, I have extended this lithospheric mantle composition along this low velocity anomaly resulting in a smaller buoyancy and a lower P-wave velocity as imaged by tomography models. The Ebro basin is characterized with the same lithospheric mantle composition than the Duero and Tagus basins.

*Marine domains – Valencia Trough, Algerian Basin and Bay of Biscay*

Whereas in the Bay of Biscay the extension ended in the Early Cretaceous, the tectono-thermal age in the W-Mediterranean basins is younger and consistent with the presence of Neogene volcanism. A low velocity anomaly in the lithosphere mantle is imaged below the W-Mediterranean basins with a sharp lateral variation in comparison to most parts of Iberia. The most remarkable feature in the Bay of Biscay is a positive velocity anomaly coinciding with the adjacent areas suggesting a change in the lithosphere mantle composition. In consequence, the considered mantle chemical compositions in the W-Mediterranean basins are more fertile than in the Bay of Biscay and the Iberia mainland.

*Intraplate ranges – Central System and Atlas Mountains*

Very differents features are found among these intraplate ranges. The Atlas Mountains show Tertiary and Quaternary alkaline to peralkaline magmatism synchronous with tectonic compression and a strong low velocity anomaly observed from the tomography model. Consequently, I have characterized the lithosphere mantle with a more fertile composition in agreement to local xenolith samples. In contrast, the Central System lacks of post-Mesozozic volcanic manifestations and seismic velocity anomalies and, therefore, I used the same lithospheric mantle composition (Tc_1) than in the surrounding regions.

## 6.3. – Anomalous low Pn velocities

### 6.3.1. – Low Pn velocities in the west-Mediterranean basins

Anomalous low Pn velocities (Fig. 2.10) between 7.7 and 7.9 km $s^{-1}$ have been reported by Torne et al. (1992), Vidal et al. (1998) and Grevemeyer (pers. comm.) in the uppermost mantle underneath the Valencia Trough, the Balearic Promontory and the Algerian Basin, coinciding with areas of attenuated continental and oceanic crust. As observed in Fig. 6.3 Pn-velocities calculated from this study vary from 7.9 km/s underneath the Valencia Trough area increasing to almost 8.0 km/s below the Balearic Promontory while along the Algerian Basin velocities decrease again to 7.9 km/s. These values are consistently higher than those obtained by seismic experiments, even considering the uncertainties commonly associated with seismic experiments (±0.1 km/s). Thereby, the calculated P–T conditions in the W-Mediterranean basins together

with composition changes in the lithospheric mantle do not suffice to explain the measured Pn velocities. Several processes may cause low velocities in the uppermost mantle that are not included in our modeling approach. Among these, I have considered the presence of small amounts of hydrous phase in the uppermost mantle, anisotropy, and transient thermal effects related to the opening of the Western Mediterranean. The effects of these processes on the calculated Pn velocities are summarized in Fig. 6.3. The presence of a hydrated uppermost mantle or serpentinization cannot be ruled out in view of the lithosphere thinning particularly beneath the Algerian Basin. Therefore I have assumed that a variable thick hydrated layer in which I have increased the water content to as much as 1% characterizes the uppermost mantle in the region. Fig. 6.3 shows the influence on the velocities of a hydrated layer that increases its thickness from 2 km underneath the Valencia Trough slightly thickening towards the Algerian Basin to as much as 4 km, and with a variable water content varying from 1% in the Valencia Trough area to 0.3% in the Algerian Basin.

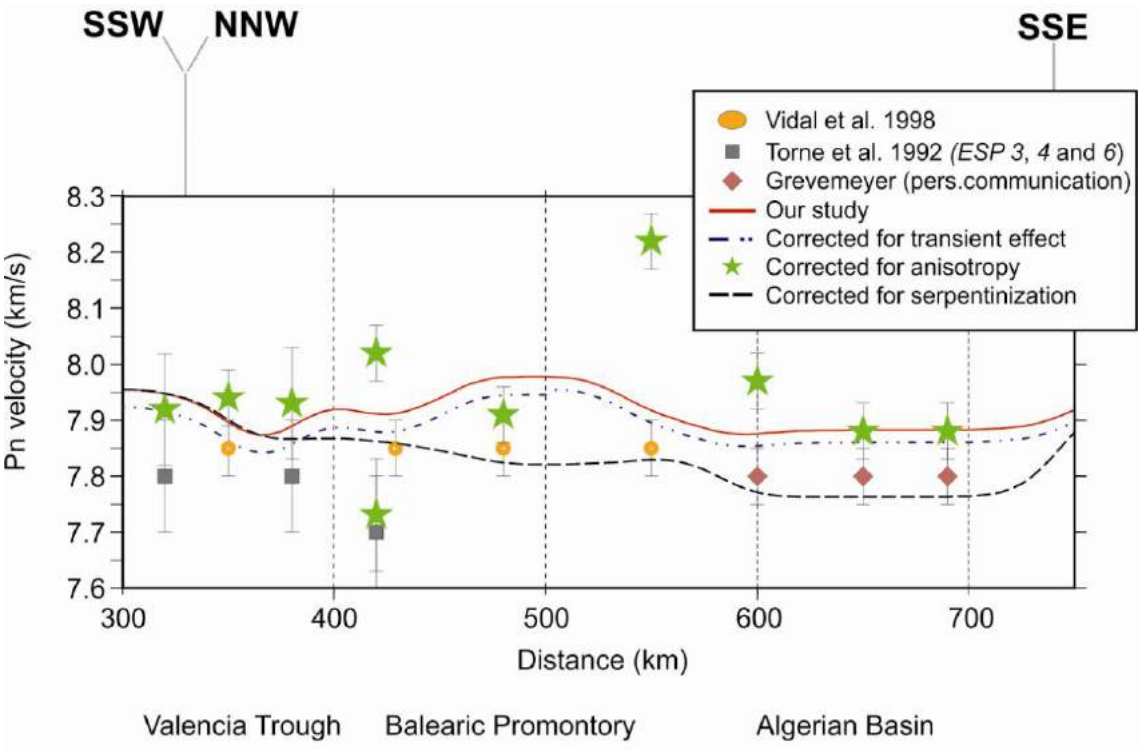


Figure 6.3: Pn velocities along the W-Mediterranean segment of the modeled transect. Circles with error bars denote Pn values from seismic experiments (see Fig. 3.10 for data sources). Red solid line denotes calculated values from our model. Stars with error bars denote Pn values from seismic experiments corrected for anisotropy effects. Blue dotter line denotes calculated values corrected for thermal transient effects. Stippled black line denotes calculated values incorporating serpentinization. See text for details.

As observed, the presence of a hydrated uppermost mantle (dashed line in Fig. 6.3) allows fitting the calculated Pn velocities with those obtained from seismic experiments with maximum differences of the order 0.025 km/s. Anisotropy is also a possible cause of mismatch between calculated and observed seismic velocities particularly when the fast polarity direction is perpendicular to the model transect. According to Díaz et al. (2013), anisotropic effects account for velocity variations ranging from minimum values of less than 0.075 km/s in the Algerian Basin to 0.3 km/s in the Balearic Promontory with the fast axis showing a predominantly E–W orientation in the Valencia Trough region switching to a NNE–SSW orientation in the Algerian Basin (see Fig. 9 of Díaz et al., 2013).

Keeping in mind these considerations, the corrected velocities obtained from seismic experiments lay well within the calculated average values with the exception of the SE margin of the Valencia Trough and the Balearic Promontory, in which differences may reach locally more than 0.3 km/s. Our numerical approach assumes thermal steady-state and therefore tends to underestimate the temperature prevailing at shallow levels of the lithospheric mantle and overestimate at deeper lithospheric levels in order to maintain the same buoyancy to that obtained from a linear steady-state geotherm. The temperature departures from steady-state geotherms can be easily calculated by considering instantaneous lithospheric thinning with a given beta-factor and occurring at a prescribed time according to McKenzie (1978). Maximum transient thermal effects are expected in the Algerian Basin where I have considered an extension factor of $\beta=5$ to simulate generation of oceanic lithosphere and t = 17 Ma, resulting in a temperature difference of $\Delta T \approx 80$ K. This $\Delta T$ translates to a $\Delta Vp = -0.04$ km/s when a typical temperature derivative of $\partial Vp/\partial T = -0.5 \times 10-4$ km $s^{-1}$ $K^{-1}$ for garnet peridotite is applied (Afonso et al., 2010). Fig. 6.3 shows that the thermal transient effect on Pn velocities is too small to account for misfits between measured and calculated P-wave velocities in the uppermost mantle. Low Pn velocities in the western-Mediterranean can be explained by either seismic anisotropy, or moderate serpentinization in the first 3-4 km of the uppermost mantle related to the crustal extension. However, transient thermal effects cannot explain the low Pn velocities measured. A combination of the three processes is also plausible.

## 6.3.2. – Low Pn velocities in the Bay of Biscay

Calculated seismic velocities in the hydrated uppermost mantle north of the Cantabrian Mountains and Bay of Biscay lie in the range 7.79-7.88 km/s. These

velocities fit perfectly with the Pn velocities measured values below the Bay of Biscay along the ESCIN-4 and MARCONI-1 profiles, except for the southernmost edge of the mantle wedge on top of the subducting Iberian crust, where measured velocities are ~7.7 km/s (Figure 3.2). Forward tests have indicated that in this small area, a water content of 2 wt. % is necessary to fit the observed velocities. The average density for the hydrated mantle layer is 3236 kg $m^{-3}$. The temperature is low enough to allow for serpentinization reactions (T<550 ºC, Figure 3.6), but the small quantities of water available are consumed in this case by other hydrated phases such as clinoamphibole, chlorite, phlogopite and talc. According to Früh-Green et al. (2004), early phases of hydration are commonly marked by the alteration of primary Opx to form talc- and/or amphibole-bearing ± chlorite assemblages, like the ones predicted in our model.

One of the questions that arise from the above discussion is the possible relationship between dehydration of the subducting greenschist/amphibolitic Iberian lower crust and the hydration of the upper mantle wedge located immediately on top of it. Water released could potentially rise as vapour phase and be incorporated into the structure of hydrous minerals in a shallower and colder part of the mantle. Figure 6.4a and 6.4b show the amount of free water (water that is not incorporated into mineral structures) as a function of pressure and temperature, for the compositions of the subducting lower crust and the hydrated upper mantle, respectively, assuming thermodynamic equilibrium. Superimposed on these graphs, we have marked the range of pressure-temperature conditions that are found inside these bodies in the model. As observed, the root preserves all the water into the structure of hydrous minerals. Therefore, other sources of water supply must be involved.

The effect of partial melting in the subducted lower crust represents another possible source of water. As these melts can potentially rise into the mantle wedge, become water-saturated as they decompress, and expel free water. We have calculated the amount of partial melt expected for the composition of the lower crust according to the melt model of Holland and Powell (2001) and White et al. (2001). As observed in Figure 6.4a, no partial melt (or negligible amounts) are expected for the pressure-temperature conditions inside the crustal root. If any melt was formed, it would be very far from the critical percentage necessary to migrate and rise (~20% after Arzi, 1978). Therefore, partial melting of the subducting lower crust can be ruled out in this case as a major supplier of water into the mantle.

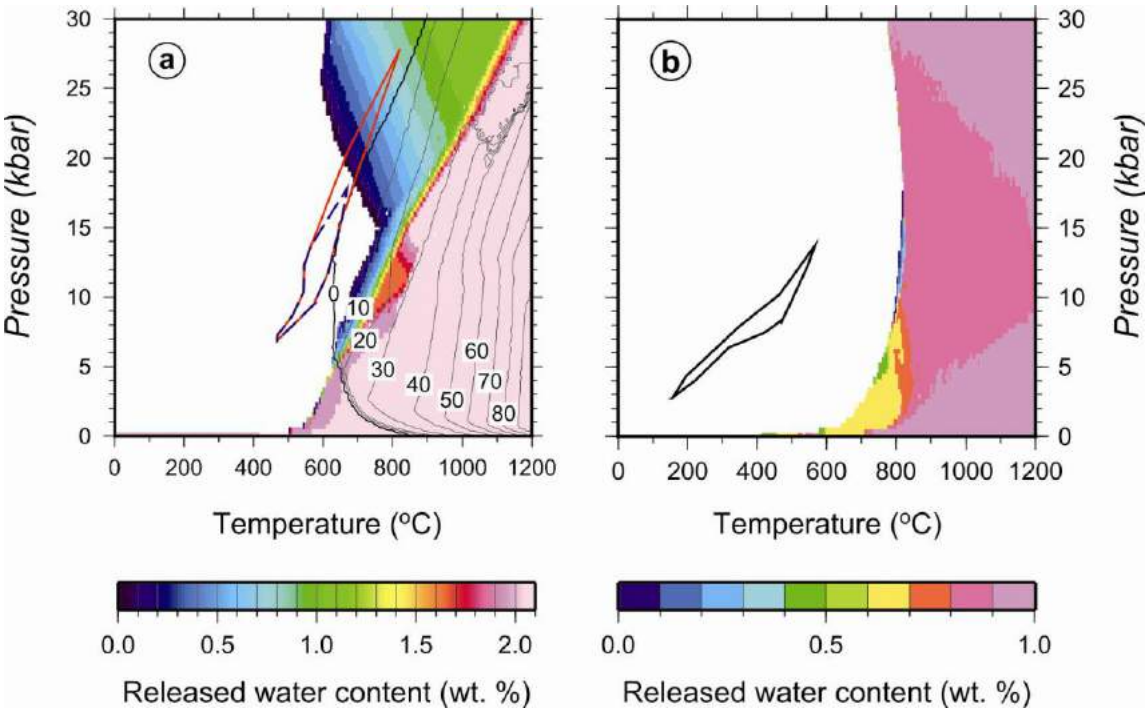


Figure 6.4: Schematic illustration of the water balance between the dehydrated subducting lower crust and the overlying hydrated mantle wedge. a) In colors: released water (in wt. %) of the subducting Iberian lower crust calculated using Perple_X (Connolly, 2009; 2005) according to the "intermediate" composition listed in Table 2.2. In black contours: percentage of partial melt for the same compostion, according to the model of Holland and Powell (2001) and White et al. (2001). The superimposed blue and red outlines mark the pressure-temperature conditions for the piece of Iberian lower crust with that composition, for model. b) Same type of diagram but for the body of hydrated upper mantle, with 1 wt.% of $H_2O$ in its composition (Table 2.2). As observed, this body keeps the 100% of the structural water unless heated up to more than ~700 ºC.

On the other hand, apart from the mantle wedge located immediately on top of the subducting Iberian crust, mildly hydration of the uppermost mantle seems to be also necessary all along the Bay of Biscay in order to explain the relatively low P-wave velocities of 7.8-7.9 km/s observed beneath the HVLC. From all the above analysis we conclude that the hydration of the upper mantle must be essentially related to infiltration of water from the seafloor during the Mesozoic rifting episode that lead to the formation of the Bay of Biscay.

## 6.3.3. – Low Pn velocities beneath the Cantabrian Mountains, composition and densification of the subducting Iberian lower crust

Two important assumptions are considered when modeling the density structure of the Iberian lower crust and mantle: first, the assumption of thermodynamic equilibrium under thermal steady-state conditions, and second, the specific chemical composition. The steady-state assumption can be considered reasonable in this case, since the last important thermal event (Late Cretaceous volcanism) ended at ~85 Ma. After that, the building of the Pyrenean-Cantabrian belt occurred at a low convergence rate (~2.5 mm/yr on average) and ended at ~16-20 Ma (Alvarez-Marrón et al., 1997; Beaumont et al., 2000; Gallastegui, 2000). Regarding the assumption of thermodynamic equilibrium that is usually valid for the mantle, it must be emphasized that it may be less reliable under the low temperatures prevailing in the crust, especially under anhydrous conditions. However, since the analysis is restricted to the lower crust, and especially focused in the transformations that occur in the root at depths >40 km and temperatures above ~600 ºC, the equilibrium assumption is reasonable. Outside the crustal root, the Iberian lower crust, with 2 wt. % $H_2O$ in our models, would be composed of hydrous greenschist-amphibolitic assemblages, according to the prevailing P-T conditions (686-988 MPa and 467-579 ºC). Under these conditions, several hydrous phases may easily coexist if some water is available, meaning that the thermophysical properties of the subducting portion of the lower crust (with 2 wt. % $H_2O$) would evolve from starting hydrous greenschist-amphibolitic assemblages.

There are, however, some implications in the case of generalized granulite preservation, derived from the fact that granulites are nominally anhydrous rocks. If water is not present, reproducing the observed variations in P-wave velocities of the Iberian lower crust with granulitic compositions would imply a strong increase of mafic components towards the south, contrary to what it is suggested by the geological evidence and the decrease in the Poisson's ratio in this direction. Another implication of the generalized granulitic composition for the lower crust is that densification of the root by eclogitization processes would be greatly hampered, as these reactions are catalyzed by fluids (Rubie, 1990; Austrheim et al., 1997; Engvik et al., 2001; Bjørnerud, 2002). The final consequence is that this granulitic lower crust, even if it were completely mafic, would be more buoyant in the deepest part of root than the amphibolitic (and then eclogitized) lower crust (Christensen and Mooney, 1995).

## 6.4. – Thermal and compositional sub-lithospheric anomalies

Seismic tomography models show the presence of different velocity anomalies at sub-lithospheric levels probably related to bodies with different temperature and/or composition than in the surrounding PUM sub-lithospheric mantle in the study area (Fig 1.2). In the Betic-Rif Domain, the positive sub-lithospheric velocity anomaly is consistently imaged by tomographic models as a subducting lithospheric slab, but the origin of the large negative anomaly in their surroundings areas, remains to date relatively unknown. In the western part of the Betic-Rif Domain the subducting slab is still attached and was reproduced with a thick lithosphere mantle extending down to near 400 km depth. However, to the East, the subducting slab is progressively detached from the lithosphere and sinking into the mantle. The un-attached slab is modelled with a temperature contrast of -200 ºC, relative to sub-lithospheric mantle, with the same lithospheric mantle composition than in the eastern part of the Betic-Rif Domain (Tc_1). A negative velocity anomaly is imaged from tomography models at shallower depths (down to 200 km depth) exceeding -2% ΔVp beneath the CVP and in the Atlas Mountains, and extending towards the Mediterranean. This high negative seismic anomaly decreases from west to southeast of Iberia. Consequently with the amplitude variation of the velocity anomaly, different thermal positive anomalies have been adopted with the same composition as the sub-lithospheric mantle.

# Chapter 7: Conclusions, limitations and future works

Along this work, I have presented four lithosphere geo-transects crossing Iberia, the western Mediterranean and North Africa based on the LitMod-2D approach. The approach integrates geopotential, lithostatic and thermal equations and, unlike previous models carried out in the region, incorporates petrophysical and geochemical data of the mantle down to 400 km depth. The main contribution of these models is the calculation of temperatures, densities, and seismic velocities (Vp and Vs) in the upper mantle as a function of prevailing P–T conditions, and chemical compositions and therefore mineral assemblages and phase transitions. Results are compared with gravity, geoid, elevation, surface heat flow and also with xenolith and seismic data and tomography models (Vp and Vs seismic mantle velocity). These different geophysical observables are simultaneously fitted, thus reducing the uncertainties associated with the modeling of these observables alone or in pairs.

Structure of the lithospheric mantle in Iberia, western Mediterranean and North Africa obeys to a complex plate reorganization since Jurassic times in which, the main tectonic episodes are (Fig. 7.1): a) Initiation of rifting in the Central Atlantic ocean and the Africa–Iberia–Eurasia plate boundary; b) Opening of the Alpine and Ligurian-Tethys oceanic domains and initiation of rifting in the North-Atlantic; c) Opening of the North-Atlantic and Valais ocean and eastern escape of Iberia and early Alpine subduction; d) Pyrenean orogeny with successive phases of initiation of shortening, Paleocene quiescence and restart of Pyrenean and Alpine orogeny; e) Atlas orogeny and subduction of the Ligurian-Tethys oceanic domain; and f) Trench retreat in the Alboran, Tyrrhenian and Pannonian domains.

The four geo-transects are in agreement with geophysical observables, geological data and seismic tomography models. The results show lateral variation in the present-day lithosphere mantle structure in Iberia, western Mediterranean and North Africa in terms of crustal and mantle thickness, temperature and mantle density distributions, and mantle compositions. Thermal sub-lithospheric perturbations are recognized and they show variations in the shape and amplitude along the study area.

The presence of compositional lithospheric mantle heterogeneities is mandatory to reduce the residuals between measured and calculated regional observables such as gravity, geoid, elevation and regional tomography models. I used a predominant Phanerozoic average mantle composition in the continental part of the study area and in the Bay of Biscay, except in the volcanics areas where more fertile lithospheric mantles was considered. Also, in the W-Mediterranean basins I have considered a more fertile composition than in Iberia and North Africa mainlands.

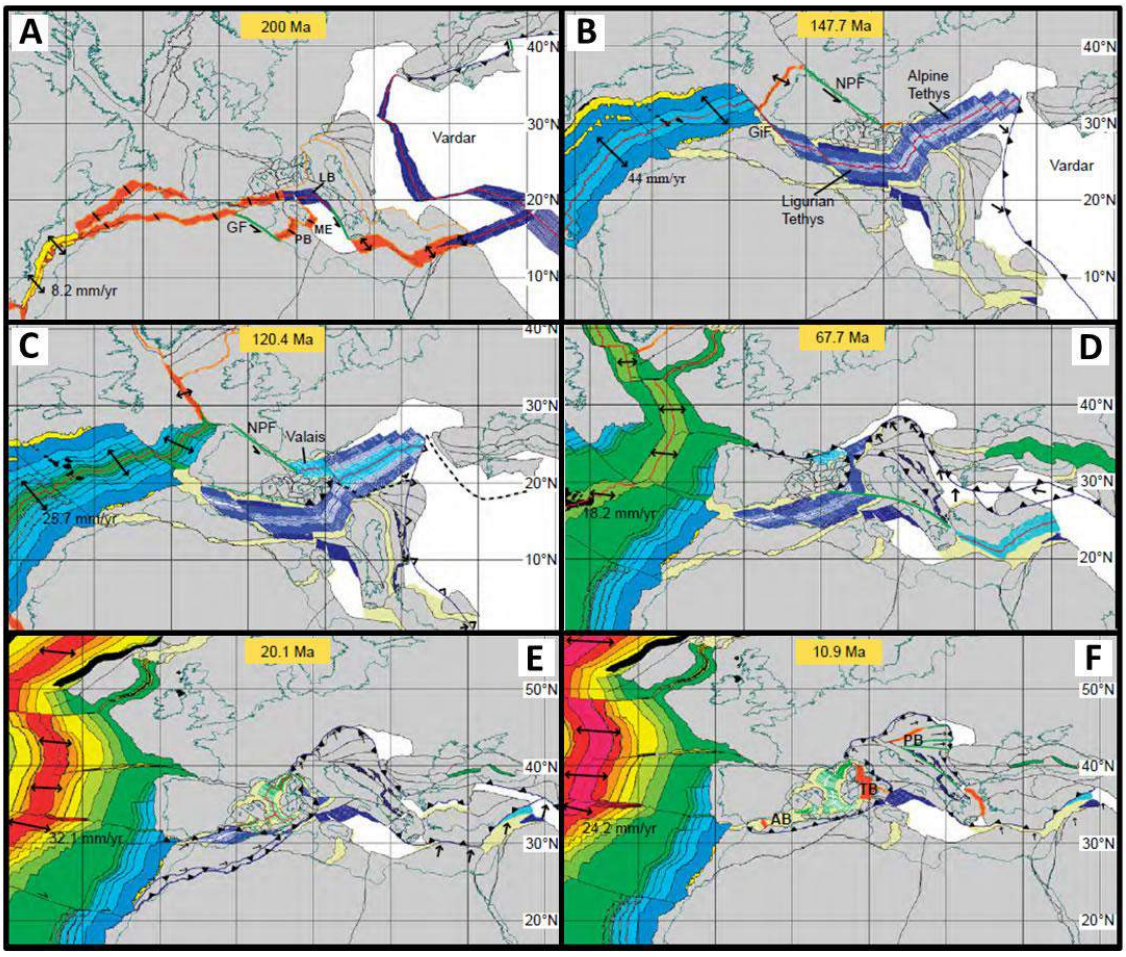


Figure 7.1: Plate tectonic maps showing the evolution of Africa, Iberia and Europe from early Jurassic to late Miocene according to Schettino and Turco (2010). Adapted from Schettino and Turco (2010).

The main conclusions arising from the presented study along each profile are:

***a) First profile, The Pyrenees-Balearic Promontory-Kabyles-Tell-Atlas***

The resulting lithospheric structure along this profile shows large variations in crust and lithospheric mantle thickness. At crustal level, our results confirm previous findings in that relative maximum crustal thickness is attained in the Pyrenees (up to 60 km), the Balearic Promontory (25 km) and the Kabyles–Tell–Atlas mountains (30–35 km), whereas relative minimum values are found in the Valencia Trough (16 km) and the Algerian Basin (10 km). At mantle lithosphere level, I observe that the LAB depth varies from 130 km beneath the Pyrenees to 65 km in the Valencia Trough, 70 km in the Balearic Promontory and 60 km in the Algerian Basin. A sharp thickening is obtained towards the N-African margin, the LAB deepening to 140 km

beneath the Tell–Atlas Mountains.

Major differences with respect to previous works are found beneath the Tell Mountains where our modeled crust is 10 km thinner (30 km Moho depth) than proposed in the TRANSMED-II geotransect. The LAB geometry shows also conspicuous differences with some of the previous works, particularly beneath the Ebro Basin and Catalan Coastal Ranges where our LAB is up to 20 km shallower and beneath the Algerian margin and the Kabyles–Tell–Atlas region where our lithosphere is up to 80 km thinner, with maximum thicknesses located underneath the Saharan platform.

I have distinguished five mantle domains according to its chemical composition inferred from xenolith data and/or tectonothermal age. In the emerged continental mainland I used a predominant Phanerozoic average mantle composition though in NE-Iberia I used a lherzolitic Proterozoic mantle. In the W-Mediterranean basins I used a PUM composition distinguishing between the highly extended and intruded Valencia Trough and Balearic Promontory and the more enriched lithospheric mantle of the oceanic Algerian Basin and the underlying asthenosphere.

The low Pn velocities recorded from seismic experiments in the W-Mediterranean basins can be explained by either moderate serpentinization in the first 3–4 km of the uppermost mantle, or seismic anisotropy. Transient thermal effects do not suffice to explain the measured Pn velocities. Evidently a combination of the three processes is also plausible.

***b) Second profile, The Cantabrian Margin***

The Iberian lower crust is assumed to change its composition from dominantly felsic in the south to intermediate and hydrated (2 wt. %) in the area that will form the crustal root. The deepest part of the root is eclogitized, but it keeps all the water in the structure of hydrated minerals. Partial melt in the subducting lower crust is not expected, or it may occur in negligible amounts. If any melt was formed, it would be far from the critical percentage necessary to migrate and rise.

Low seismic velocities beneath the Bay of Biscay Moho and in the mantle wedge above the crustal root is explained by the addition of 1 wt% of water percolated from the seafloor during the formation of the margin in the Mesozoic. Water input from dehydration reactions in the subducting lower

crust is ruled out.

Assuming a composition typical for "tecton" garnet subcontinental lithospheric mantle (Griffin et al., 2009), the thickness of the thermal lithosphere varies from 125-145 km south of the Cantabrian Mountains, to 170 km beneath the crustal root and 135-140 km beneath the central part of the Bay of Biscay. More enriched compositions such as those of some Pyrenean mantle xenoliths or the Primitive Upper Mantle were tested and allow a reduction of the lithospheric thickness of only ~5 km.

The upper mantle is interpreted to be serpentinized during the formation of the margin in the Mesozoic and later intruded by decompression melts generating a gabbroic underplating and a new seismic Moho at its base. We emphasize that the role of magmatism in ocean-continent transitions may be significant even in "non-volcanic margins". During the Alpine convergence, these petrophysical transformations promoted the underthrusting and indentation to the south of the lower crust from the necking and hyperthinned domains (with the new gabbroic additions). This process is genetically linked to the uplift of the Cantabrian Mountains and the formation of a crustal root down to at least ~60 km depth, with an estimated crustal shortening of ~98 km.

***c) Third profile, The Cantabrian Mountains-Central System-Betics***

This geo-transect shows large variations in crust and lithospheric mantle thicknesses. The LAB depth beneath the North-Iberian Margin is 130-140 km increasing to 180 km under the Cantabrian Mountains. The central part of Iberia shows a LAB-depth of 135 km decreasing to ~130 km beneath the Duero and Tagus basins and reaching only ~100 km around the Calatrava Volcanic Province. The LAB depth increases again below the Betics to about 160 km and decreases sharply to around 60 km in the Alboran Basin.

I propose 4 mantle domains, which agree with their chemical composition inferred from their geodynamic setting and tectonothermal age. In the Cantabrian Sea I consider a hydrated (1 wt. % $H_2O$) Phanerozoic (Tc_1) uppermost mantle whereas in the continental mainland I use a predominant Phanerozoic average (Tc_1) mantle composition. A more fertile lithospheric mantle close to PUM is considered to underlie the Calatrava Volcanic Province, whilst beneath the Alboran Basin, I use a PUM composition like in the underlying asthenosphere.

Beneath the Betic Cordillera, I consider a detached/torn lithospheric slab characterized by a Phanerozoic composition (Tc_1), and a temperature anomaly of -200 ºC relative to the surrounding sub-lithospheric mantle, which is interpreted as corresponding to the Ligurian-Tethys slab. Along the northern and central segments of the profile, I have considered a sub-lithospheric thermal anomaly of +65 ºC extending from 260 km of depth to the bottom of the model. In the Calatrava Volcanic Province, this anomaly might reach +80 ºC in the uppermost sub-lithospheric mantle at depths between 240 and 120 km.

Topography perturbations related to the low velocity-high temperature asthenospheric anomaly amount +340 m along the northern and central segments of the Iberian plate along this profile, rising to +470 m in the Calatrava Volcanic Province. The detached/torn lithospheric slab beneath the Betic Cordillera generates a topography perturbation of -300 m, due to its higher average density as a consequence of its lower temperature and the rising of the olivine-wadsleyite transition.

The high mean topography of the Iberian Peninsula can be partly explained by buoyancy induced by the low-velocity/low-density/high-temperature layer from 260 km depth consistent with seismic velocity anomalous region imaged by tomography models. Mechanical coupling of these density anomalies with the overlying lithosphere seem to be necessary to explain the topography and potential field data over the area.

***d) Fourth profile, The Iberian Massif-Gibraltar Arc-Atlas Mountains***

The obtained LAB geometry in this lithosphere transect shows large variations in lithospheric mantle thickness. The LAB beneath the Tagus basin is at 145 km depth, and it decreases to the OMZ down to 110 km. Lithospheric thickness over 350 km is observed in the Strait of Gibraltar and Rif Mountains, which is in agreement with the seismic tomography models. The LAB depth is shallow (95 km depth) beneath the Atlas Mountains, and it deepens to 130 km underneath the Saharan Platform.

I distinguished three lithospheric mantle domains with differences in chemical composition in accordance with xenolith data and/or tectonothermal age. I used a predominant Phanerozoic average (Tc_1) mantle composition in the continental mainland along the profile. Heterogeneities related to recent volcanism and mantle metasomatism are

found in the Calatarava Volcanic Province and the Atlas Mountains. Their chemical signature is close to the fertile PUM, which represents the chemistry of the underlying asthenosphere.

A thermal anomaly of +50 below the OMZ-CIZ and the Atlas Mountains has been imposed, in order to adjust the low seismic velocities imaged by the tomography models. The related topography caused by this low-velocity/low-density/high-temperature perturbation amounts up to 330 m in the CIZ-OMZ and 300 m in the Atlas Mountains. This buoyant sub-lithospheric body could be the responsible to the the high mean elevation in these zones.

In the South Alpine domain, the LAB depth difference from West to East is compensated by an un-attached lithospheric slab in the eastern Betics. This feature also affects the density and temperature distribution beneath the Moho showing differences of 80 $kg/m^3$ and 200 ºC respectively. The detached/torn lithospheric slab is characterized by a Phanerozoic composition (Tc_1), as the above lithosphere mantle, and a temperature anomaly of -200 ºC relative to the surrounding sub-lithospheric mantle. It is interpreted as the Ligurian-Tethys lithosphere mantle. The negative thermal perturbation related to the detached/torn lithospheric slab beneath the eastern Betics (-300 m of associated topography) is not observed in western Betics where the the slab is attached to overlying the lithosphere mantle. In the North Alpine domain, the variations in the LAB geometries from the Pyrenees to the Cantabrian Mountains is mainly attributed to the total difference in the elevation, which is higher in the Cantabrian Margin.

The resulting LAB from integrated geophysical-petrological methodology used in this thesis is systematically deeper than in others thermal approaches. Though the mantle compositions cannot be resolved univocally, the chosen compositions are compatible with the global geochemical xenolith data and the tectonothermal age of the different domains included in the modeled transect. Indeed, the different mantle compositions result in moderate differences in relevant observables as P-wave seismic velocities and densities. However, the density distribution within the lithospheric mantle, which incorporates pressure, temperature and phase transition effects, differs substantially from that expected from a pure thermal approach and is responsible for the major differences in the obtained LAB geometry.

In summary, this Thesis has provided new insights on the present-day lithosphere structure of the Iberia, western Mediterranean and North Africa, consistently with geological and geophysical data, and seismic tomography models. Hopefully, this

work will help to understand better the upper mantle structure and its contribution in the present configuration of Iberia, North Africa and the western Mediterranean.

# Limitations and future works

The technique used in this thesis has proven to be a valuable tool for the characterization of the lithosphere structure from the thermal, compositional and seismological point of view.

A major limitation is that this numerical approach assumes thermal steady state and conductive heat transfer and then it is not sensitive to mantle flow and/or thermal recovery related to ongoing mantle deformation. The presented results are constrained by the simultaneous fitting of a set of "instantaneous" density-dependent observables such as gravity, geoid and elevation, and then results must be considered as a snapshot of the present-day density distribution related to active tectonic processes. A transient thermal model could improve the calculated temperature and density distribution, but the vertically averaged density anomaly must remain similar to yield similar topography. The differences on temperature distribution due to transient effects could affect the potential fields, mainly the geoid since it depends on the density moment, and in a higher way to the calculated mantle seismic velocities.

Anyway, the steady-state assumption can be considered reasonable in the northern and central Iberian Peninsula, since the last important thermal event (Late Cretaceous volcanism) ended at ~85 Ma. After that, the building of the Pyrenean-Cantabrian belt occurred at a low convergence rate (~2.5 mm/yr on average) and ended at ~16-20 Ma. This assumption is less valid in the western Mediterranean basins, where most of deformation occurred during Neogene times, and in the Betic-Rif System due to the presence of a slab with a tearing process. A fully transient thermal approach requires a more sophisticated numerical approach and, more importantly, a deep knowledge of the past and ongoing geodynamic processes and particularly the timing of these processes.

A second strong assumption used in this methodology is the local isostasy. Some regions of Iberia are probably not under local isostasy, being supported mostly by regional isostasy. Therefore, I account for the rigidity of the lithosphere to calculate lithostatic equilibrium (flexural isostasy) using an updated version of the code tAo (Garcia-Castellanos et al., 2007). Regional isostasy has been incorporated to the LitMod-2D methodology in profiles 2, 3 and 4 although the resulting lithospheric

structure along the Pyrenees-Balearic Promontory-Kabyles-Tell-Atlas will not differ substantially by flexural effects.

In addition to regional isostasy, during my PhD Thesis two more improvements have been developed and included to the LitMod2D code and applied to the third and fourth geo-transects: i) better calculation of mantle thermal conductivity including the radiative contribution, following the formulation by Grose and Afonso (2013) and; ii) incorporation of sub-lithospheric thermal and/or compositional anomalies, to better reproduce the seismic tomography models.

Finally, the assumption of a homogeneous composition of the sub-lithospheric mantle is at the moment highly questioned. Probably, the possibility of including changes in the sub-lithospheric chemical composition is something to be developed in the near future.

Concerning to the study area and bearing in mind the mentioned limitations and improvements already done, the future work should consider the application of LitMod-3D in its forward and inversion schemes incorporating surface waves as a new constraint, which constitutes one of the best sources of information for retrieving absolute Vs values in the lithosphere and sublithospheric upper mantle.

# List of figures and tables

**Figure 1.1.** Geological map of the study area showing the principal geological domains of Iberia and North Africa. Thick lines locate the modeled transects: Black line-first geo-transect; Red line-second geo-transect; Orange line-third geo-transect and pink line-fourth geo-transect. WALZ, west Asturian-Leonese Zone; CZ, Cantabrian Zone; CCR, Catalan Coastal Ranges; CR, Ciudad Rodrigo Basin, located in the SW side of the Duero Basin; GB, Guadalquivir Basin. 7

**Figure 1.2.** P-wave anomaly of the western-Mediterranean region from the tomography model of Villaseñor et al., 2003 for different depths (145, 200, 260 and 320). Shown are P wave seismic velocity anomalies relative to the 1-D reference model ak135 of Kennett et al. (1995). The blue anomaly under the Rif-Gibraltar-Betic (RGB) (southern Iberia) is the image of the slab. Courtesy by A. Villaseñor. 8

**Figure 1.3.** Flowchart indicating the general modeling procedure used in LitMod. 10

**Figure 1.4.** An illustration of rollback as portrayed in the three different reconstruction scenarios from Chertova et al., 2014. Scenario 1 (Spakman and Wortel, 2004) and scenario 2 (Faccena et al., 2004) assume a unique subduction polarity but start from different initial subduction zone (short and long respectively). Scenario 3 (Vergés and Fernandez, 2012) shows two opposite dipping subductions. Dashed lines represent proposed transform fault regions. The triangular zone between the transform zones of Scenario 1 depicts the lithosphere that rolls back toward the east Kabylides (Spakman and Wortel, 2004). 17

**Figure 1.5.** Geophysical data. a) Elevation map from ETOPO Global Data Base (V9.1) (http://www.ngdc.noaa.gov/mgg/fliers/01mgg04.html). b) Bouguer anomaly. Onshore, in the Iberian Peninsula, the Bouguer anomaly comes from Ayala (2013). Offshore and Africa Bouguer anomaly has been calculated from the free air anomaly by Sandwell and Smith (1997) using Fullea et al. (2008). Contour interval is 40 mGal. c) Geoid anomaly map from EGM2008 Global Model (Pavlis et al., 2008). Long wavelengths (>5000 km) have been removed by subtracting spherical harmonics up to degree and order 8 from the total geoid. Contour interval is 1 m. d) Surface heat flow measurements from Fernandez et al. (1998), Marzán Blas (2000) and International Heat Flow Commission global data set for Algeria (http://www.heatflow.und.edu/index2.html). Colors of solid circles indicate heat flow values. Thick lines locate the modeled geo-transects: 1) black line; 2) grey line; 3) orange line and 4) red line. 21

**Figure 2.1.** Geological map of the study area showing the principal geological domains of Iberia, Western Mediterranean and North Africa (modified from Vergés and Sàbat et al., 1999). Thick gray line locates the modeled transect. Upper right inset shows the main topography and bathymetry features of the study area in which is located: Black line-model transect; Deep blue—ECORS Pyrenees; Yellow— ESCI Catalanides; Green line—ESCI València; Pink line: ALE-4 and dark gray-other seismic experiments (Diaz et al., 2013). 26

**Figure 2.2.** Crustal structure corresponding to the best fitting model. Geometry of crustal bodies has been mainly taken from TRANSMED-II geotransect (Roca et al., 2004) based on ECORS—Central Pyrenees (ECORS Pyrenees Team, 1988), ESCI—Catalanides (Gallart et al., 1994), ESCI—Valencia (Vidal et al., 1998) and ALE-4 (industrial profile) seismic profiles. Blue and red lines refer to Moho depth proposed by Roca et al. (2004) and Vidal et al. (1998), respectively. Numbers denote crustal bodies summarized in Table 2.1. 27

**Figure 2.3.** P-wave tomography model along the profile (Villaseñor et al., 2003). 28

**Figure 2.4.** Model results (red lines) and measured data with the standard deviation of data projected onto the profile within a strip of 25 km half-width (blue dots and vertical bars): (a) surface heat flow; (b) Bouguer anomaly; (c) geoid height; (d) elevation; (e) lithospheric structure. Crustal structure the same than Fig. 2.1. Numbers in panel (e) denote mantle bodies summarized in Table 2.2. Dataset sources as in Fig. 1.3. 31

**Figure 2.5.** Lithosphere structure of the best fit model and mantle domains with different chemical composition (see Table 2.2). Color lines denote LAB geometries proposed in previous studies. 33

**Figure 2.6.** Calculated temperature distribution along the modeled transect. Contour lines every 100 °C. 34

**Figure 2.7.** Calculated mantle density distribution along the modeled transect. Contour lines every 10 kg $m^{-3}$. Sharp density increase in the uppermost mantle beneath the Algerian Basin is related to the Pg-Sp phase transition. Sharp density increase at ~40 km depth is related to Sp–Grt phase transition. 35

**Figure 2.8**. a) Calculated P-wave seismic velocities in the upper mantle (calculations extend down to 400 km depth). White solid lines indicate mantle domains with different chemical composition. b) P-wave tomography model (Villaseñor et al., 2003) and c) synthetic P-wave tomography from our model. In both cases velocity anomalies are relative to the ak135 reference model. Contour lines every 1%. 36

**Figure 2.9.** Calculated S-wave seismic velocities in the upper mantle (calculations extend down to 400 km depth). White solid lines indicate mantle domains with different chemical composition. Contour lines every 0.05 km/s. Superimposed are the S-wave velocities inferred from the regional tomography model by Legendre et al. (2012) at different depth levels. S-values have been calculated according to the reference velocities of 4.38 km/s (at 80 and 110 km), 4.39 km/s (at 150 km) and 4.45 km/s (at 200 km) (see Legendre et al., 2012). 38

**Figure 2.10.** Pn velocities along the modeled transect. Red line indicates calculated Pn values. Symbols with error bars denote Pn-values from seismic experiments (see legend). 39

**Figure 2.11.** a) Depth variation of P-wave velocities (left panel) and densities (right panel) calculated for different average-Tecton mantle compositions according to Griffin et al. (2009) for a 1-D lithosphere structure consisting of 32 km thick crust and 130 km thick lithosphere. b) Same as a) for the mantle chemical compositions used in our modeled transect (see Table 2.2). 42

**Figure 3.1.** Tectonic map of the Pyrenean-Cantabrian mountain belt in north-Iberia showing the location of the modeled N-S lithospheric transect and available deep seismic profiles. BCB, Basque-Cantabrian basin; BM, Basque Massifs; CCR, Catalan Costal Ranges; MB, Mauléon basin. Acronyms in italics refer to tectonometamorphic zones within the Iberian Variscan Massif: CIZ, Central Iberian Zone; CZ, Cantabrian Zone; GTMZ, Galicia – Tras os Montes Zone; WALZ, West Asturian-Leonese Zone. 49

**Figure 3.2.** Seismic constraints used to delineate the crustal structure of the lithospheric model. Top right panels: P-wave velocity models for the ESCIN-4 and MARCONI-1 profiles (location in Figure 3.1), from Fernández-Viejo et al. (1998) and Ruiz et al. (in prep.), respectively. Superimposed on the MARCONI-1 profile there is a velocity-depth column corresponding to the intersecting E-W Profile 1 of Pedreira et al. (2003, 2007). Note the thin crust beneath the abyssal plain, with velocities of ~7.2 km/s in the lower crust (HVLC), and the velocities of 7.8-7.9 km/s in the uppermost mantle, decreasing to ~7.7 km/s in the mantle wedge above the north-Iberian crustal root (see text for details). Top left panel: record sections of seismic stations 21 (close to the coast) and 25 (near the Duero Basin), during the acquisition of the ESCIN-4 profile, taken from Gallart et al. (1997). Observe that station 21 records a clear PmP reflection denoting a sharp interface at the base of the HVLC beneath Le Danois Bank and the continental platform, gently dipping towards the south. Station 25, on the other hand, records the presence of this same interface (Bay of Biscay Moho) as south as the coastline, as well as a later PmP' phase interpreted to be produced in the north-dipping Iberian Moho. Middle panel: sketch of the crustal structure of the model with the seismic constraints superimposed: red lines mark clear seismic refraction/wide-angle reflection interfaces; black lines depict the geometrical attitude of reflectors in the ESCIN-2 profile, according to Pulgar et al. (1995) and Gallastegui (2000).

Lower panel: P-wave velocity model for Profile 5 (location in Figure 3.1from Fernández-Viejo et al. (2000), showing the typical Variscan crustal structure of the crust beneath the Duero Basin, with upper, middle and lower crustal levels and a total thickness of 32-35 km. Note the increasing seismic velocities in the lower crust to the south (see text for details). 51

**Figure 3.3.** Detailed geological map of the investigated transect, modified from previous synthesis by Alonso et al. (1996), Quintana (2012), Rodríguez Fernández et al. (2004) and Gallastegui et al. (2002). Cities: BU, Burgos; LE, León; OV, Oviedo; SA, Santander; ZA, Zamora. Geological features: CFT, Cantabrian Frontal Thrust; LF, León Fault; LLF, Llanera Fault; MOT, Montes Obarenes Thrust; OB, Oviedo Basin; SCS, Spanish Central System. 53

**Figure 3.4.** Modeling results for the Cantabrian Margin geo-transect (second profile), showing the fitting of surface heat flow (HF), Bouguer anomaly (BA), geoid and elevation. Except for heat flow values, black dots mark the observed values along the transect, and error bars represent ±1 standard deviation according to values observed 25 km to the east and to the west of the transect (grey rectangles in Figure 3.4). Heat flow values are orthogonally projected onto the section from lateral distances ≤10 km (black dots) or ≤50 km for land data and ≤100 km for marine data (blue dots). Red lines indicate the calculated responses of the model (with a Gaussian filter for the case of the surface heat flow to avoid short-wavelenght spikes). In the elevation plot, red dotted and dashed lines represent calculated elevation in the case of effective elastic thickness, Te=0 km (Airy-type isostatic equilibrium) and Te=10 km, respectively. Continuous red line represent the calculated elevation for Te=30 km (see text for details). 57

**Figure 3.5.** a) Thermal and b) density structure along the modeled transect. The grey bold line (LAB) represents the base of the thermal lithosphere. 58

**Figure 3.6.** P-wave velocity structure along the modeled transect. The grey bold line (LAB) represents the base of the thermal lithosphere. 59

**Figure 3.7.** Comparison between the P-wave velocity structure calculated for the mantle along the transect and the results of tomographic models in the same area. All plots represent percentage of velocity deviations with respect to the ak135 reference model (Kennett et al., 1995). a) vertical slice of the tomographic model of Villaseñor et al. (2003) along the studied transect. b) synthetic "pseudo-tomographic" sections, from 40 km to 400 km depth, using a wider colorbar scale (see text for details). Note in a) the low velocity anomaly located in the top-central part of the section, which can be correlated with the low-velocity anomaly created in our synthetic models by the crustal root and the hydrated mantle wedge on top of it. Note also the relatively flat surface at ~225 km depth where both types of sections show anomaly values around zero, separating a lower part with slow anomalies from an upper part with dominantly fast anomalies. c), plan view of the tomographic model of Chevrot et al. (2014), with anomalies averaged for depths between 125 and 150 km, after crustal correction. On

top of this map, are plotted the calculated anomalies of the synthetic model for the same depth interval. Calculated anomalies are lowered by 0.65 % (see text for details). Note the E-W trending fast anomaly along the coast and the band to the south of relatively slow anomalies (between 42 and 43ºN) that are spatially coincident with the lithospheric root and with the area of uplifted LAB, respectively, in our model. 60

**Figure 4.1.** Geological map of the study area showing the principal geological domains of Iberia (modified after Vergés and Fernàndez, 2006). Thick gray line locates the modeled transect. 65

**Figure 4.2.** Crustal structure corresponding to the best fitting model. Different bodies have been modeled using geological cross-sections (overlaid) and seismic experiments (see text for details). Physical properties of crustal bodies are reported in Table 4.1. 66

**Figure 4.3.** P-wave tomography model along the Cantabrian Mountains-Central System-Betics geo-transect (third profile) based on the global travel-time tomography model of Villaseñor et al. (2003). 69

**Figure 4.4.** Model results (red lines), measured data with the standard deviation of data projected onto the profile within a strip of 25 km half-width (blue dots and vertical bars), coupled calculated topography (red line), and green line represent calculated elevation in the case of effective elastic thickness for the different Te (30 km, 20 and 10 km) used along the profile (see text for details): (a) surface heat flow; (b) Bouguer anomaly; (c) geoid height; (d) elevation; (e) lithospheric structure. Crustal structure like in Figure 4.2. Numbers in panel (e) denote mantle bodies summarized in Table 4.1. Dataset sources as in Figure 1.3. 71

**Figure 4.5.** Calculated temperature distribution along the geo-transect and mantle domains with different chemical composition (see Table 4.2). Contour lines every 100 °C. 74

**Figure 4.6.** Calculated mantle density distribution along the geo- transect. Contour lines every 20 kg $m^{-3}$. 75

**Figure 4.7.** a) Calculated P-wave seismic velocities in the upper mantle down to 400 km; b) synthetic P-wave tomography from our model. In this case velocity anomalies are relative to the synthetic reference model (calculated from Vp in (%) relative to a reference model consisting of a 130 km thick lithosphere and 30-km thick crust with a lithosphere mantle composition corresponding to Tc_1) (see text). Contour lines every 1%. Compare with Figure 4.3. 76

**Figure 4.8.** Calculated S-wave seismic velocities in the upper mantle down to 400 km depth. Contour lines every 0.05 km/s. Superimposed are the S-wave velocities inferred from the regional tomography model by Legendre et al. (2012) at different depth levels. S- values have been calculated according to

the reference velocities of 4.38 km/s (at 80 and 110 km), 4.39 km/s (at 150 km) and 4.45 km/s (at 200 km) (see Legendre et al., 2012). 77

**Figure 4.9.** a) Pn velocities along the geo-transect. Red line indicates calculated Pn values with the associated standard deviation of the first 15 km of the uppermost mantle. Circles with error bars denote Pn-values from seismic experiments (see legend); b) Sn velocities along the modeled transect. Red line indicates calculated Sn values. Symbols with error bars denote Sn-values from Diaz et al., 2013. 78

**Figure 4.10.** Calculated topographies of the lithosphere-asthenosphere boundary from different models. 79

**Figure 4.11.** Depth variation of P-wave velocities calculated in the preferred model along the profile (at 200, 400, 750 and 900 km distance) for model with the sub-lithospheric anomalous body (red line) and model without the anomlalous body (green line). Arrows denote the lithosphere-asthenosphere boundary (LAB) and the following phase transitions: Pg-Sp, plagioclase-spinel; Opx-Hpx, orthopyroxene-high-pressure magnesian pyroxene. 83

**Figure 4.12**. Depth variation of mantle density calculated in the preferred model along the profile (at 200, 400, 750 and 900 km distance) for model with asthenospheric anomaly and model without asthenospheric anomaly. 84

**Figure 4.13.** Difference between the elevations calculated considering coupled and decoupled anomalous sub-lithospheric bodies. 85

**Figure 5.1.** Geological map of the study area showing the principal geological domains of the study area. Thick black line locates the modeled transect. Thin lines locates the seismics experiments: Red line- ALCUDIA wide-angle (Ehsan, 2014); Pink line- La Línea-Carmona (Medialdea et al., 1986); RIFSIS wide-angle (Gil et al., 2014); and SIMA wide-angle (Ayarza et al., 2014). 89

**Figure 5.2.** Crustal structure corresponding to the best fitting model. Different bodies have been modeled using geological cross-sections and seismic experiments (see text for details). Physical properties of crustal bodies are reported in Table 5.2. CIZ, Central Iberian Zone; OMZ, Ossa Morena Zone; GB, Guadalquivir Basin; S.P, Sharan Platform. 91

**Figure 5.3.** P-wave tomography model along the Iberian Massif-Arc of Gibraltar-Atlas Mountains (fourth profile) based on the global travel-time tomography model of Villaseñor et al. (2003). 92

**Figure 5.4.** Model results (red lines), measured data with the standard deviation of data projected onto the profile within a strip of 25 km half-width (blue dots and vertical bars): (a) surface heat flow; (b) Bouguer anomaly; (c) geoid height; (d) elevation and coupled calculated topography under local isostasy (red line) and under regional isostasy with elastic thickness varying between 20 and 10 km (green line); (e) lithospheric structure. Crustal structure like in Fig. 5.2. Numbers in panel (e) denote mantle bodies summarized in Table 5.2. Dataset sources as in Fig. 1.3. 95

**Figure 5.5.** East to west tomographic cross-section based on the tomographic model of Villaseñor et al. (2003). Black line shows the location of the Iberian Massif-Arc of Gibraltar-Atlas Mountains geo-transect. 97

**Figure 5.6.** Calculated temperature distribution along the Iberian Massif-Arc of Gibraltar-Atlas Mountains geo-transect and mantle domains with different chemical composition (see Table 5.2). Contour lines every 100 °C. 98

**Figure 5.7.** Calculated mantle density distribution along the Iberian Massif-Arc of Gibraltar-Atlas Mountains geo-transect. Contour lines every 20 kg $m^{-3}$. 99

**Figure 5.8.** a) Calculated P-wave seismic velocities in the upper mantle down to 400 km; b) synthetic P-wave tomography from our model. In this case velocity anomalies are relative to the synthetic reference model (reference model consisting of a 130-km thick lithosphere and 30-km thick crust with a lithosphere mantle composition corresponding to Tc_1.) (see text). Contour lines every 1%. Compare with Figure 5.2. 100

**Figure 5.9.** Calculated S-wave seismic velocities in the upper mantle down to 400 km depth. Contour lines every 0.05 km/s. 101

**Figure 5.10.** a) Pn velocities along the modeled transect. Red line indicates calculated Pn values. Circles with error bars denote Pn-values from seismic experiments (see legend); b) Sn velocities along the modeled transect. Red line indicates calculated Sn values. Symbols with error bars denote Sn-values from Diaz et al. (2013). 102

**Figure 5.11.** Calculated topographies of the lithosphere-asthenosphere boundary from different models. Dashes lines correspond to profiles that not coincide with the direction of the Iberian Massif-Arc of Gibraltar-Atlas Mountains geo-transect. CIZ, Central Iberian Zone; OMZ, Ossa Morena Zone; GB, Guadalquivir Basin; S.P, Sharan Platform. 104

**Figure 5.12.** Depth variation of P-wave velocities calculated in the preferred model along the profile (in sites located at 100, 230, 750 and 900 km horizontal distance) for model with the sub-lithospheric anomalous body (red line) and model without the anomlalous body (green line). Arrows denote the lithosphere-asthenosphere boundary (LAB) and the following phase transitions: Pg-Sp, plagioclase-spinel; Opx-Hpx, orthopyroxene-high-pressure magnesian pyroxene. 106

**Figure 5.13.** Depth variation of mantle density calculated in the preferred model along the profile (in sites located at 100, 230, 750 and 900 km horizontal distance) for model with asthenospheric anomaly and model without asthenospheric anomaly. 107

**Figure 5.14.** Difference between the elevations calculated considering coupled and decoupled anomalous sub-lithospheric bodies. 108

**Figure 6.1.** Schematic crust and upper mantle cross-sections of Iberia and North Africa of the four modeled geo-transects (second geo-transect is integrated in the third lithosphere profile). Lower right inset shows the location of the fourth geo-transects in the study area. 112

**Figure 6.2.** Topographic map of the study area showing the lithospheric mantles compositions used in this thesis. Thick lines locate the modeled transects: Black line-first geo-transect; Red line-second geo-transect; Light orange line-third geo-transect and pink line-fourth geo-transect. Chemical compositions described in Table 2.2, Table 3.2, Table 4.2 and Table 5.2. 114

**Figure 6.3.** Pn velocities along the W-Mediterranean segment of the modeled transect. Circles with error bars denote Pn values from seismic experiments (see Fig. 3.10 for data sources). Red solid line denotes calculated values from our model. Stars with error bars denote Pn values from seismic experiments corrected for anisotropy effects. Blue dotter line denotes calculated values corrected for thermal transient effects. Stippled black line denotes calculated values incorporating serpentinization. See text for details. 117

**Figure 6.4.** Schematic illustration of the water balance between the dehydrated subducting lower crust and the overlying hydrated mantle wedge. a) In colors: released water (in wt. %) of the subducting Iberian lower crust calculated using Perple_X (Connolly, 2009; 2005) according to the "intermediate" composition listed in Table 2.2. In black contours: percentage of partial melt for the same compostion, according to the model of Holland and Powell (2001) and White et al. (2001). The superimposed blue and red outlines mark the pressure-temperature conditions for the piece of Iberian lower crust with that composition, for model. b) Same type of diagram but for the body of hydrated upper mantle, with 1 wt.% of $H_2O$ in its composition (Table 2.2). As observed, this body keeps the 100% of the structural water unless heated up to more than ~700 ºC. 120

**Figure 7.1.** Figure 7.1: Plate tectonic maps showing the evolution of Africa, Iberia and Europe from early Jurassic to late Miocene according to Schettino and Turco (2010). Adapted from Schettino and Turco (2010). 126

**Table 2.1.** Parameters used in the first geo-transect model for the different crustal bodies. 27

**Table 2.2.** Bulk mantle compositions used in the model. 30

**Table 3.1.** Density values and thermal properties used in this geo-transect. b, density values are dependent on the chemical composition and pressure-temperature conditions (see text and Table 3.2); c, variable thermal conductivity (pressure and temperature dependent) according to the model of Hofmeister (1999); DB, Duero basin; HVLC, High Velocity Lower Crust; LDB, Le Danois basin. 54

**Table 3.2.** Chemical composition of the Iberian lower crust and mantle along the second geo-transect. [a]Based on a mixture between the composition of the felsic granulite xenoliths from the Spanish Central System (Villaseca et al., 1999) (70 wt. %) and the average global lower crustal composition proposed by Rudnick and Gao (2003) (30 wt. %). [b]Based on an evenly mixture between the composition of the felsic granulite xenoliths from the Central System (Villaseca et al., 1999) and the average global lower crustal composition proposed by Rudnick and Gao (2003), plus 2 wt. % of water. [c]Average Tecton Garnet Subcontinental Lithospheric Mantle (Tc_1) (Griffin et al., 2009). 56

**Table 4.1.** Parameters used in the model for the different crustal bodies. a and b values are dependent on the chemical composition and pressure-temperature conditions (see text and Table 4.2). 67

**Table 4.2.** Bulk body compositions (%) used in the geo-transect. 70

**Table 5.1.** Parameters used in the model for the different crustal bodies in the fourth model. 91

**Table 5.2.** Chemical compositions (%) of mantle bodies used in the model. 94

# References

Afonso, J.C., Fernández, M., Ranalli, G., Griffin, W.L., Connolly, J.A.D., 2008. Integrated geophysical-petrological modeling of the lithosphere and sublithospheric upper mantle: Methodology and applications. Geochem. Geophys. Geosyst. 9, Q05008. doi:10.1029/2007GC001834.

Afonso, J.C., Ranalli, G., Fernandez, M., Griffin, W.L., O'Reilly, S.Y., Faul, U., 2010. On the Vp/Vs–Mg# correlation in mantle peridotites: implications for the identification of thermal and compositional anomalies in the upper mantle. Earth and Planetary Science Letters 289, 606–618.

Afonso, J.C., Zlotnik, S., 2011. The subductability of the continental lithosphere: the before and after story, in Arc-continent collision. Frontiers in Earth Sciences edited by D. Brown & P.D. Ryan, 53-86, doi:10.1007/978-3-540-88558, Springer.

Afonso, J.C., Fullea, J., Griffin, W.L., Yang, Y., Jones, A.G., Connolly, J.A.D., O'Reilly, S.Y., 2013a. 3D multi-observable probabilistic inversion for the compositional and thermal structure of the lithosphere and upper mantle I: a priori information and geophysical observables. Journal of Geophysical Research Solid Earth 118, 2586–2617. http://dx.doi.org/10.1002/jgrb.5012423.

Afonso, J.C., Fullea, J., Yang, Y., Connolly, J.A.D., Jones, A.G., 2013b. 3D multi-observable probabilistic inversion for the compositional and thermal structure of the lithosphere and upper mantle II: general methodology and resolution analysis. Journal of Geophysical Research Solid Earth 118, 1650–1676. http://dx.doi.org/10.1002/jgrb.50123.

Alonso, J.L., Pulgar, J.A., García-Ramos, J.C., Barba, P., 1996. Tertiary basins and Alpine tectonics in the Cantabrian Mountains (NW Spain). In: P.F. Friend and C.J. Dabrio (Editors), Tertiary Basins of Spain. Cambridge University Press, Cambridge, pp. 214-227.

Álvarez-Marrón, J., Rubio, E., Torne, M., 1997. Subduction-related structures in the North Iberian margin, Journal of Geophysical Research: Solid Earth, 102(B10), 22497–22511.

Amante, C., Eakins, B.W., 2009. ETOPO1 Arc-Minute Global Relief model: Procedures, Data Sources and Analysis, NOAA Technical Memorandum NESDIS NGDC-24, 19 pp. Available at: http://www.ngdc.noaa.gov.

Anguita, F., Hernan F., 2000. The Canary Islands origin: a unifying model, J. Volcanol. Geotherm. Res., 103 (1-4), 1-26.

Ancochea, E., Ibarrola, E., 1982. Caracterización geoquimica del vulcanismo de la región volcánica central española. Bol.R.Soc.Esp.Hist.Nat. (Geol.) 80,57-88.

Ancochea, E., Nixon, P. H., 1987. Xenoliths in the Iberian peninsula. In: NIXON, P.H (ed.) Manlle Xenoliths. Wiley, Chichester, 119-124.

Arenas, R., Gil Ibarguchi, J. I., Gonzalez Lodeiro, F., Klein, E., Martínez-Catalán, J. R., Ortega Girones, E., de Pablo Macia, J. G., Peinado, M., 1986. Tectonostratigraphic units in the complexes with mafic and related rocks of the NW of the Iberian Massif, Hercynica, 2, 87 – 110.

Arenas, R., Abati, J. Martínez-Catalán, J. R., Díaz García, F., Rubio Pascual, F. J., 1997. P-T evolution of eclogites from the Agualada Unit (Ordenes Complex, northwest Iberian Massif, Spain): Implications for crustal subduction, Lithos, 40, 221 – 242.

Argus, D.F., Gordon, R.G., Demets, C., Stein, S., 1989. Closure of the Africa–Eurasia–North America plate circuit and tectonics of the Gloria fault. Journal of Geophysical Research 94, 5585–5602.

Arzi, A.A., 1978. Critical phenomena in the rheology of partially-molten rocks. Tectonophysics 44:1953–1958.

Austrheim, H., Erambert, M., Engvik A. K., 1997. Processing of crust in the root of the Caledonian continental collision zone: The role of eclogitization, Tectonophysics, 273(1-2), 129–153.

Ayala, C., Pous, J., Torné, M., 1996. The lithosphere–asthenosphere boundary of the Valencia trough (western Mediterranean) deduced from 2D geoid and gravity modeling. Geophysical Research Letters 22, 3131–3134.

Ayala, C., Torne, M., Pous, J., 2003. The lithosphere–asthenosphere boundary in the western Mediterranean from 3D joint gravity and geoid modelling: tectonic implications. Earth and Planetary Science Letters 209, 275–290.

Ayala, C., 2013. A new compilation of gravity data over the Iberian Peninsula and surrounding areas. Internal Report TopoIberia project (Consolider-Ingenio) IGME (20 pp.).

Ayarza, P., Carbonell, R., Teixell, A., Palomeras, I., Martí, D., Kchikach, A., Harnafi, M., Levander, A., Gallart, J., Arboleya, M., Alcalde, J., Charroud, M., Amrhar, M., 2014. Crustal thickness and velocity structure across the Moroccan Atlas from long

offset wide-angle reflection seismic data: The SIMA experiment. Geochemistry, Geophysics, Geosystems., 10.1002/2013GC005164.

Banda, E., Gallart, J., Garcia-Duenas, V., Danobeitia, J.J., Makris, J., 1993. Lateral variation of the crust in the Iberian Peninsula. New evidence from the Betic Cordillera. Tectonophysics 221, 53–66.

Banks, C.J., Warburton, J., 1991. Mid-crustal detachment in the Betic system of southeast Spain. Tectonophysics, 191:275-289.

Barnolas, A., Pujalte, V. (eds), 2004. La Cordillera Pirenaica. In: J.A. Vera (ed). Geología de España, SGE-IGME, Madrid, pp. 231-343.

Barton, P.J., 1986. The relationship between seismic velocity and density in the continental crust - a useful constraint? Geophysics Journal Roy Astron Society 87:195-208.

Beaumont, C., Muñoz, J.A., Hamilton, J., Fullsack, P., 2000. Factors controlling the Alpine evolution of the central Pyrenees inferred from a comparison of observations and geodynamical models. Journal of Geophysical Research 105, 8121–8145.

Begg, G., Griffin, W.L., Natapov, L.M., O'Reilly, S.Y., Grand, S., O'Neill, C.J., Poudjom-Djomani, Y., Deen, T., Hronsky, J., Bowden, P., 2009. The lithospheric architecture of Africa: seismic tomography, mantle petrology and tectonic evolution. Geosphere 5, 23–50. http://dx.doi.org/10.1130/GES00179.1.

Berástegui, X., Banks, C.J., Puig, C., Taberner, C., Waltham, D., Fernandez, M., 1998. Lateral diapiric emplacement of Triassic evaporites at the southern margin of the Guadalquivir Basin, Spain. In: Mascle, A., Puigdefabregas, C., Luterbacher, H., Fernandez, M. (Eds.), Cenozoic Foreland Basins of Western Europe. Geological Society Special Publications 134, pp. 49-68.

Bezada, M.J., Humphreys, E.D., Toomey, D.R., Harnafi, M., Dávila, J.M., Gallart, J., 2013. Evidence for slab rollback in westernmost Mediterranean from improved upper mantle imaging. Earth and Planetary Science Letters 368, 51–60.

Bianchini, G., Beccaluva, L., Bonadiman, C., Nowell, G., Pearson, G., Siena, F., Wilson, M., 2010. Mantle Metasomatism by Melts of HIMU Piclogite Components: New Insights from Fe-lherzolites Xenoliths (Calatrava Volcanic District, Central Spain). In: Coltorti, M., Gregoire, M., Downes, H. (Eds.), Petrological Evolution of the European Lithospheric Mantle: From Archaean to Present Day: London

Geological Society, Special Publications, 337, pp. 107–124.

Bjørnerud, M. G., 2002. Processes leading to eclogitization (densification) of subducted and tectonically buried crust. Journal of Geophysical Research, 107(B10), 2252, doi:10.1029/2001JB000527.

Bijwaard, H., Spakman, W., Enghdal, E.R., 1998. Closing the gap between regional and global travel time tomography. Journal of Geophysical Research 103, 30055-30078.

Bijwaard, H., Spakman, W., 2000. Non-linear global p-wave tomography by iterated linearized inversion. Geophysical Journal International 141, 71–82.

Booth-Rea, G., Ranero, C.R., Martínez-Martínez, J.M., Grevemeyer, I., 2007. Crustal types and Tertiary tectonic evolution of the Alborán Sea, western Mediterranean. Geochemistry, Geophysics, Geosystems 8, 1–25. http://dx.doi.org/10.1029/2007GC001639.

Bosch, D., Maury, R.C., El Azzouzi, M.h., Bollinger, C., Bellon, H., Verdoux, P., 2014. Lithospheric origin for Neogene-Quaternary Middle Atlas lavas (Morocco): clues from trace elements and Sr–Nd–Pb–Hf isotopes. Lithos 205, 247–265.

Bradley, D. C., 2008. Passive margins through earth history. Earth Sci. Rev., 91, 1–26.

Brunet, M. F., 1994. Subsidence in the Parentis Basin (Aquitaine, France): Implications of the thermal evolution, in Hydrocarbon and Petroleum Geology of France, edited by A. Mascle, pp. 187–198. Special Publication of the European Association of Petroleum Geologists, v. 4, Springer-Verlag.

Buforn, E., Coca, P., 2002. Seismic moment tensor for intermediate depth earthquakes at regional distances in Southern Spain. Tectonophysics 356, 49–63.

Cadenas, P., López-Fernández, C., Gallastegui, J., Fernández-Viejo, G., 2013. Seismic interpretation of the Cantabrian platform around “Le Danois Bank”, Bay of Biscay. Conference: VIII Congreso Geológico de España, Volume: Geotemas, Volumen 13, pp 1702-1705

Calvert, A., Sandvol, E., Seber, D., Barazangi, M., Roecker, S., Mourabit, T., Vidal, F., Alguacil, G., and Jabour, N., 2000. Propagation of regional seismic phases (Lg and Sn) and Pn velocity structure along the Africa-Iberia plate boundary zone. Geophysical Journal International, 142, 384-408.

Campanyà, J., Ledo, J., Queralt, P., Marcuello, A., Liesa, M., Muñoz, J.A., 2012. New

geoelectrical characterisation of a continental collision zone in the West-Central Pyrenees: constraints from long period and broad band magnetotellurics. Earth and Planetary Science Letters 333–334, 112–121.

Capote, R., Insua Arévalo, J.M., Martínez-Díaz, J.J., Martín-González, F., Tsige, M., 2002. La Sierra de Cártama: Pliegue con actividad reciente en las Béticas Occidentales (Hoya de Málaga). Geogaceta, 31: 135-138.

Capdevila, R., Boillot, G., Lepvrier, C., Malod, J.A., Mascle, G., 1980. Les formations cristallines du Banc Le Danois (marge nord-ibérique). CR Acad. Sci. Paris, D 291, 317–320.

Carballo, A., Fernandez, M., Torne, M., Jiménez-Munt, I., Villaseñor, A., 2015a. Thermal and petrophysical characterization of the lithospheric mantle along the Northeastern Iberia geo-transect. Gondwana Research, pp. 1430-1445. http://dx.doi.org/10.1016/j.gr.2013.12.012.

Carballo, A., Fernandez, M., Jimenez-Munt, I., Torne, M., Vergés, J., Melchiorre, M., Pedreira, D., Afonso, J.C., Garcia-Castellanos, D., Diaz, J., Villasenor, A., Pulgar, J.A., Quintana, L. (2015b), From the Norht-Iberian Margin to the Alboran Basin: a lithosphere geo-transect crossing the Iberian Plate (submitted).

Carbonell, R., Torne, M., García-Dueñas, V., Moya, R., Banda, E., 1997. The ESCI-Béticas: a seismic reflection image of the Betics orogen. Revista de la Sociedad Geológica de España., 8:503–512.

Carminati, E., Wortel, M.J.R., Meijer, P.T., Sabadini, R., 1998. The two stage opening of the western–central Mediterranean basins: a forward modeling test to a new evolutionary model. Earth and Planetary Science Letters 160, 667–679.

Carminati, E., Lustrino, M., Doglioni, C., 2012. Geodynamic evolution of the central and western Mediterranean: Tectonics vs. igneous petrology constraints. Tectonophysics, 579, 173–192, doi:10.1016/j.tecto.2012.01.026.

Carlson, R. L., 2003. Mantle wedge water contents estimated from seismic velocities in partially serpentinized peridotites. Geophysical Research Letters, 30(5), 1250, doi:10.1029/2002GL016600.

Casas Sainz, A., Faccenna, C., 2002. Tertiary compressional deformation of the Iberian plate. Terra Nova, 13.

Casas-Sainz, A. M., De Vicente, G., 2009. On the tectonic origin of Iberian topography.

Tectonophysics, 474, 214–235.

Casciello E., Fernandez M., Vergés J., Cesarano M., Torne M., 2014. The Alboran Domain in the Western Mediterranean evolution: the birth of a concept. Bulletin de la Société Géologique de France, in press.

Cavazza, W., Roure, F., Spakman, W., Stampfli, G.M., Ziegler, P.A. (Eds.), 2004. The TRANSMED Atlas — the Mediterranean Region from Crust to Mantle. Springer, Berlin Heidelberg. http://dx.doi.org/10.1007/978-3-642-18919-7.

Cebriá, J. M., Lopez-Ruiz, J., 1995. Alcali basalts and leucitites in an extensional intracontinental plate setting: The late Cenozoic Calatrava Volcanic Province (central Spain). Lithos, 35: 27-46.

Cebrià, J.M., Wilson, M., 1995. Cenozoic mafic magmatism in Western/Central Europe: a common European asthenospheric reservoir. Terra Nova Abstract Suppl. 7, 162.

Charroud, M., 1990. Evolution geodynamique de la partie Sud-Ouest du Moyen-Atlas durant le passage Jurassique-Cretace, le Cretace et le Paleogene: un exemple d'évolution intraplaque. These 3emecycle, Universite Mohammed V, Rabat.

Chertova, M. V., Spakman, W., Geenen, T., van den Berg, A.P., van Hinsbergen, D.J.J., 2014. Underpinning tectonic reconstructions of the western Mediterranean region with dynamic slab evolution from 3-D numerical modeling. Journal of Geophysical Research Solid Earth, 119, doi:10.1002/2014JB011150.

Chevrot, S., Villaseñor, A., Sylvander, M., PYROPE Working Group, 2014. High resolution of the Pyrenees and Massif Central from the data of the PYROPE and IBERARRAY Portable array deployments. Journal of Geophysical Research Solid Earth 119, 6399–6420. http://dx.doi.org/10.1002/2014JB010953

Christensen, N., Mooney, W., 1995. Seismic velocity structure and composition of the continental crust: A global view. Journal of Geophysical Research 100(B6), 9761–9788, doi:10.1029/ 95JB00259.

Clauser, C., Huenges, E., 1995. Thermal conductivity of rocks and minerals, in: Ahrens, T.J. (Ed.), A Handbook of Physical Constants: Rock Physics and Phase Relations. American Geophysical Union, pp. 105–126.

Collier, J.S., Buhl, P., Torne, M., Watts, A.B., 1994. Moho and lower crustal reflectivity beneath a young rift basin — results from a 2-ship, wide-aperture seismic-reflection

experiment in the Valencia Trough (western Mediterranean). Geophysical Journal International 118, 159–180.

Comas, M.C., Dañobeitia, J.J., Alvarez-Marrón, J., Soto, J.I., 1995. Crustal reflections and structure in the Alboran Basin: Preliminary Results of the SCI-Alboran Survey. P. Santanach (Ed). Revista de la Sociedad Geológica de España, 8, 75- 88.

Connolly, J.A.D., 1990. Multivariable phase diagrams: an algorithm based on generalized thermodynamics. American Journal of Science, 290, 666-718.

Connolly, J.A.D., 2005. Computation of phase equilibria by linear programming: A tool for geodynamic modeling and its application to subduction zone decarbonation. Earth and Planetary Science Letters, 236(1-2), 524–541, doi:10.1016/j.epsl.2005.04.033.

Connolly, J.A.D., 2009. The geodynamic equation of state: What and how. Geochemistry, Geophysics, Geosystems, 10(10), Q10014, doi:10.1029/2009GC002540.

Danobeitia, J.J., Arguedas, M., Gallart, F., Banda, E., Makris, J., 1992. Deep crustal configuration of the Valencia trough and its Iberian and Balearic borders from extensive refraction and wide-angle reflection profiling. Tectonophysics 203, 37–55.

Davies, J.H., Bunge, H.P., 2006. Are splash plumes the origin of minor hotspots? Geology 34, 349-352.

DeMets, C., Gordon, R.G., Argus, D.F., Stein, S., 1994. Effect of recent revisions to the geomagnetic reversal time scale on estimate of current plate motions. Geophysical Research Letters 21, 2191–2194.

Dercourt , J., Zonenshain , L. P., Ricou , L. E., 1986. Geological evolution of the Tethys belt from the Atlantic to the Pamir since the Lias. Tectonophysics, 123, 241–315.

Deverchere, J., Yelles, K., Domzig, A., Mercier de Lepinay, B., Bouillin, J.P., Gaulier, R., Bracene, V., Calais, E., Savoye, B., Kherroubi, A., Le Roy, P., Pauc, H., Dan, G., 2005. 15 Active thrust faulting offshore Boumerdes, Algeria, and its relation to the 2003 Mw 6.9 earthquake. Geophysical Research Letters 32. http://dx.doi.org/10.1029/2004GL021646.

De Vicente, G., Cloetingh, S., Muñoz-Martín, A., Olaiz, A., Stich, D., Vegas, R., Galindo-Zaldivar, J., Fernández-Lozano, J., 2008. Inversion of moment tensor focal mechanisms for active stresses around microcontinent Iberia: tectonic implications.

Tectonics 27, 1–22.

De Vicente, G., Vegas, R., 2009. Large-scale distributed deformation controlled topography along the western Africa–Eurasia limit: Tectonic constrains. Tectonophysics 474, 124–143. doi10.1016/j.tecto.2008.11.026.

De Vicente, G., Muñoz-Martín, A., 2013. The Madrid Basin and the Central System: a tectonostratigraphic analysis from 2D seismic lines. Tectonophysics 602, 259–285.

Díaz, J., Gallart, J., 2009. Crustal structure beneath the Iberian Peninsula and surrounding waters: A new compilation of deep seismic sounding results. Physics Earth and Planetary Science Letters 173, 181-190, http://dx.doi.org/10.1016/j.pepi. 2008.11.008.

Díaz, J., Gil, A., Gallart, J., 2013. Uppermost mantle seismic velocity and anisotropy in the Euro-Mediterranean region from Pn and Sn tomography. Geophysical Journal International. http://dx.doi.org/10.1093/gji/ggs016.

Doglioni, C., Gueguen, E., Sàbat, F., Fernandez, M., 1997. The Western Mediterranean extensional basins and the alpine orogen. Terra Nova 9 (3), 109–112.

Domzig, A., Le Roy, C., Yelles, K., Deverchere, J., Bouillin, J.-P., Bracene, R., Mercier de Lepinay, B., Le Roy, P., Calais, E., Kherroubi, A., Gaullier, V., Savoye, B., Pauc, H., 2006. Searching for the Africa–Eurasia Miocene boundary offshore western Algeria (MARADJA'03 cruise). Comptes Rendus Geoscience 338, 80–91.

Duee, G., Hervouet, Y., Laville, E., De Luca, P., Robillard, A., 1977. L àccident nord moyen-atlasique dans la region de Boulemane (Maroc): une zone de coulissement synsedimentaire. Annales de la Societe Geologique du Nord, serie 2, 145–162.

Du Dresnay, R., 1988. Recent data on the geology of the Middle Atlas (Morocco). In: Jacobshagen, V. (Ed.), The Atlas System of Morocco. Springer-Verlag, Berlin, pp. 293–320.

Duggen, S., Hoernle, K., van den Bogaard, P., Harris, C., 2004. Magmatic evolution of the Alboran region; the role of subduction in forming the western Mediterranean and causing the Messinian salinity crisis. Earth and Planetary Science Letters, 218(1-2): 91-108.

Duggen, S., Hoernle, K.A., Hauff, F., Klugel, A., Bouabdellah, M., Thirlwall, M.F., 2009. Flow of Canary mantle plume material through a subcontinental lithospheric corridor beneath Africa to the Mediterranean. Geology, v. 37, p. 283–286, doi:

10.1130/G25426A.1.

Dutour, A., Ferrandini, J., 1986. Nouvelles observations neotectoniques dans le Haut Atlas de Marrakech et le Haouz central (Maroc). Apports sur l'evolution récente d'un segment du bati atlasique.-Rev. Géol. dyn. Geogr. phys., 26(5): 285-297, Paris.

El Harfi, A., Lang, J., Salomon, J., 1996. Le remplissage continental cénozoïque du bassin d'avant-pays de Ouarzazate: Implications sur l'évolution géodynamique du Haut-Atlas central (Maroc), C. R. Acad. Sci., Ser. II, 323, 623–630.

El Kochri, A., Chorowicz, J., 1995. Oblique extension in the Jurassic trough of the central and eastern High Atlas (Morocco). Can. J. Earth Sci. 33, 84 – 92.

Eaton, D.W., Darbyshire, F., Evans, R.L., Grütter, H., Jones, A.G., Yuan, X., 2009. The elusive lithosphere–asthenosphere boundary (LAB) beneath cratons. Lithos 109, 1–22.

ECORS Pyrenees team, 1988. The ECORS deep reflection seismic survey across the Pyrenees. Nature 311, 508–511. Faccenna, C., Piromallo, C., Crespo-Blanc, A., Jolivet, L., Rossetti, F., 2004. History of subduction and back-arc extension in the central Mediterranean. Geophysic Journal International 145, 809–820.

Ehsan, S. A., Carbonell, R., Ayarza, P., Martí, D., Jesús Martínez-Poyatos, D., Simancas, J., Azor, A., Ayala, C., Torne, M., Pérez-Estaún A., 2014. Lithospheric Velocity Model across the Southern Central Iberian Zone (Variscan Iberian Massif): the ALCUDIA Wide-Angle Seismic Reflection Transect. Tectonics, accepted.

Engdahl, E.R., van der Hilst, R., Buland, R., 1998. Global teleseismic earthquake relocation with improved travel times and procedures for depth determination. Bulletin of the Seismological Society of America 88, 722-743.

Engvik, A. K., Austrheim, H., Erambert, M., 2001. Interaction between fluid flow, fracturing and mineral growth during eclogitization, an example from the Sunnfjord area, Western Gneiss Region, Norway. Lithos, 57(2), 111–141.

Faccenna, C., Piromallo, C., Crespo-Blanc, A., Jolivet, L., Rossetti, F., 2004. Lateral slab deformation and the origin of the western Mediterranean arcs. Tectonics, 23(1), doi:10.1029/2002TC001488.

Faccenna, C., Becker, T.W., 2010. Shaping mobile belts by small-scale convection. Nature 465, 602-605.

Fedan, B., 1988. Evolution geodynamique d'un bassin intraplaque sur decrochements (Moyen Atlas, Maroc) durant le Meso-Cenozoique. These Sciences, Universite Mohammed V, Rabat.

Fernández Casals, M.J., 1976. Estudio meso y microtectónico de la zona de tránsito paleozoico-metamórfica de Somosierra (Sistema Central, España). Ph.D.Thesis Univ. Compultense de Madrid.

Fernandez, M., Torne, M., Zeyen, H., 1990. Lithospheric thermal structure in NE Spain and North-Balearic basin. Journal of Geodynamics 12, 253–267.

Fernandez, M., Marzan, I., Correia, A., Ramalho, E., 1998. Heat flow, heat production, and lithospheric thermal regime in the Iberian Peninsula. Tectonophysics 291, 29–53. http://dx.doi.org/10.1016/S0040-1951(98)00029-8.

Fernandez, M., Marzán, I., Torne, M., 2004. Lithospheric transition from the Variscan Iberian Massif to the Jurassic oceanic crust of the Central Atlantic. Tectonophysics 386, 97–115.

Fernández-Viejo, G., Gallart, J., Pulgar, J. A., Gallastegui, J., Dañobeitia, J. J., Córdoba, D., 1998. Crustal transition between continental and oceanic domains along the North Iberian margin from wide angle seismic and gravity data. Geophysical Research Letters, v. 25, no. 23, p. 4249-4252.

Fernández-Viejo, G., Gallart, J., Pulgar, J.A., Córdoba, D., Dañobeitia, J.J., 2000. Seismic signature of Variscan and Alpine tectonics in NW Iberia: Crustal structure of the Cantabrian Mountains and Duero basin, Journal of Geophysical Research. Solid Earth (1978–2012), 105(B2), 3001–3018.

Fernández-Viejo G., Gallastegui, J., 2005. The ESCI-N Project after a decade: a synthesis of the results and open questions. Trabajos de Geología, Univ. de Oviedo, 25, pp. 9-25.

Fernández-Viejo, G., Pulgar, J.A., Gallastegui, J., Quintana, L., 2012. The Fossil Accretionary Wedge of the Bay of Biscay: Critical Wedge Analysis on Depth-Migrated Seismic Sections and Geodynamical Implications. The Journal of Geology 120, 315–331. doi:10.1086/664789.

Ferrer, O., Roca, E., Benjumea, B., Munoz, J. A., Ellouz, N., MARCONI TEAM, 2008. The deep seismic reflection MARCONI-3 profile: role of extensional Mesozoic structure during the Pyrenean contractional deformation at the eastern part of the Bay

of Biscay. Marine and Petroleum Geology, 25, 714–730, http://dx.doi.org/10.1016/j.marpetgeo.2008.06.002.

Fischer, K.M., Ford, H.A., Abt, D.L., Rychert, C.A., 2010. The lithosphere–asthenosphere boundary. Annual Review of Earth and Planetary Sciences 38, 551–575. http://dx.doi.org/10.1146/annurev-earth-040809-152438.

Forte, A., Quéré, S., Moucha, R., Simmons, N.A., Grand, S.P., Mitrovica, J.X., Rowley, D.R., 2010. Jointseismic-geodynamic-mineral physical modelling of African geodynamics : a reconciliation of deep-mantle convection with surface geophysical constraints. Earth and Planetary Science Letters 295, 329-341.

Foucher, J.E., Mauffret, A., Steckler, M., Brunet, M.E., Maillard, A., Rehanlt, J.E., Alonso, B., Desegaulx, E., Murillas, J., Ouillon, G., 1992. Heat flow in the Valencia trough: geodynamic implications. Tectonophysics 203, 77–97.

Frizon de Lamotte, D., Saint-Bezar, B., Bracène, R., Mercier, E., 2000. The two steps of the Atlas building and geodynamics of the western Mediterranean. Tectonics 19, 740–761.

Frizon de Lamotte, D., Crespo-Blanc, A., Saint-Bezar, B., Comas, M., Fernandez, M., Zeyen, H., Ayarza, P., Robert-Charrue, C., Chalouan, A., Zizi, M., Teixel, A., Arboleya, M.L., Alvarez-Lobato, F., Julivert, M., Michard, A., 2004. TRASNSMED-transect I (Betics, Alboran Sea, Rif, Moroccan Meseta, High Atlas, Jbel Saghro, Tindouf basin). In: Cavazza, W., Roure, F., Spakman, W., Stampfli G.M., Ziegler, .M., (eds) 2004. The TRANSMED Atlas- the Mediterranean region from Crust to Mantle. Springer, Berlin Heildelberg.

Früh-Green, G. L., Connolly, J. A., Plas, A., Kelley, D. S., Grobéty, B., 2004. Serpentinization of oceanic peridotites: implications for geochemical cycles and biological activity. Geophysical Monograph Series, 144, 119–136.

Fullea, J., Fernandez, M., Zeyen, H., Vergés, J., 2007. A rapid method to map the crustal and lithospheric thickness using elevation, geoid anomaly and thermal analysis. Application to the Gibraltar Arc System and adjacent zones. Tectonophysics 430, 97–117. doi:10.1016/j.tecto.2006.11.003

Fullea, J., Fernandez, M., Zeyen, H., 2008. FA2BOUG—a FORTRAN 90 code to compute Bouguer gravity anomalies from gridded free air anomalies: application to the Atlantic–Mediterranean transition zone. Computers & Geosciences 34, 1665–1681.

Fullea, J., Fernandez, M., Afonso, J.C., Vergés, J., Zeyen, H., 2010. The structure and evolution of the lithosphere–asthenosphere boundary beneath the Atlantic–Mediterranean Transition Region. Lithos 120 (1–2), 74–95. http://dx.doi.org/10.1016/j.lithos.2010.03.003.

Gaite, B., Ugalde, A., Villaseñor, A., 2014. Development of a 3D velocity Model for Improving the Location of Potentially Induced Earthquakes in the Gulf of Valencia. 76th EAGE Conference and Exhibition, doi:10.3997/2214-4609.20140574.

Gallart, J., Olivera, C., Correig, A.M., 1985. Reconocimiento sísmico de la Cerdafia (Pirineos Orientales), Primeros resultados. Rev. Geofis., 41, 81-90.

Gallart, J., Vidal, N., Dañobeitia, J.J., the ESCI-Valencia Trough Working Group, 1994. Lateral variations in the deep crustal structure at the Iberian margin of the Valencia trough imaged from seismic reflection methods. Tectonophysics 232, 59–75.

Gallart, J., Vidal, N., Dañobeitia, J.J., 1995. Multichannel seismic image of the crustal thinning at the NE Iberian margin combining normal and wide angle reflection data. Geophysical Research Letters, 22, 489–492.

Gallart, J., Fernández-Viejo, G., Díaz, J., Vidal, N., Pulgar, J.A., 1997. Deep structure of the transition between the Cantabrian Mountains and the north Iberian Margin from wide-angle ESCI-N data. Revista de la Sociedad Geológica de España, 8 (4) (1995), 365–382.

Gallastegui, J., 2000. Estructura cortical de la Cordillera y Margen Continental Cantabricos: Perfiles ESCI-N, Trabajos Geol., 22, 9 – 234.

Gallastegui, J., Pulgar, J.A., Gallart, J., 2002. Initiation of an active margin at the North Iberian continent-ocean transition. Tectonics 21, 15–1 15–14.

Garcia-Castellanos, D., Fernàndez, M., Torne, M., 2002. Modeling the evolution of the Guadalquivir foreland basin (southern Spain). Tectonics, 21(3), 1018, doi:10.1029/2001TC001339.

Garcia-Castellanos, D., 2007. The role of climate in high plateau formation. Insights from numerical experiments. Earth and Planetary Science Letters 257, 372-390, doi:10.1016/j.epsl.2007.02.039.

Garcia-Castellanos, D., Villasenor, A., 2011. Messinian salinity crisis regulated by competing tectonics and erosion at the Gibraltar arc. Nature 480, 359–363.

Gibbons, W., Moreno , T. 2002. The Geology of Spain. Geological Society, London.

Gil, A., Gallart, J., Diaz, J., Carbonell, R., Torne, M., Levander, A., Harnafi, M., 2014. Crustal structure beneath the Rif Cordillera, North Morocco, from the RIFSIS wide-angle reflection seismic experiment. Geochemistry, Geophysics, Geosystems, 15, 4712–4733, doi:10.1002/2014GC005485

Gómez-Ortiz, D., Tejero-Lopez, R., Babın-Vich, R., Rivas-Poncé, A, 2005. Crustal density structure in the Spanish Central System derived from gravity data analysis (central Spain). Tectonophysics, 403, 131 – 149.

Gomez, F., Barazangi, M., Bensaid, M., 1996. Active tectonism in the intracontinental Middle Atlas Mountains of Morocco: synchronous crustal shortening and extension. Journal of the Geological Society of London 153, 389–402.

Gomez, F., Allmendinger, R., Barazangi, M., Er-Raji, A. and Dahmani, M., 1998. Crustal shortening and vertical strain partitioning in the Middle Atlas Mountains of Morocco. Tectonics, 17, 520–533.

Görler, K., Helmdach, F.-F., Gaemers, P., Heissig, K., Hinsch, W., Mädler, K., Schwarzhans, W., Zucht, M., 1988. The uplift of the central High Atlas as deduced from Neogene continental sediments of the Ouarzazate province, Morocco, in the Atlas System of Morocco, edited by V. Jacobshagen, pp. 361–404. Springer-Verlag, New York.

Griffin, W.L., O'Reilly, S.Y., Ryan, C.G., 1999. The composition and origin of sub-continental lithospheric mantle. In: Fei, Y., Berkta, C.M., Mysen, B.O. (Eds.), Mantle Petrology: Field observations and High-pressure Experimentation: a Tribute to Francis R. (Joe) Boyd. Geochemical Society Special Publication, vol. 6, pp. 13–45.

Griffin, W.L., O'Reilly, S.Y., Afonso, J.C., Begg, G., 2009. The composition and evolution of lithospheric mantle: a reevaluation and its tectonic implications. Journal of Petrology. http://dx.doi.org/10.1093/petrology/egn033.

Grose, C., Afonso, J.C., 2013. Comprehensive plate models for the thermal evolution of oceanic lithosphere. Geochemistry, Geophysics, Geosystems, 14,9, doi:10.1002/ggge.20232.

Gueguen, E., Doglioni, C., Fernandez, M., 1998. On the post-25 Ma geodynamic evolution of the Western Mediterranean. Tectonophysics 298, 259–269.

Gunnell, Y., Zeyen, H., Calvet, M., 2008. Geophysical evidence of a missing lithospheric root beneath the Eastern Pyrenees: consequences for post-orogenic uplift and associated geomorphic signatures. Earth and Planetary Science Letters 276, 302–313.

Hailwood, E. A., Mitchell, J. G., 1971. Paleomagnetic and radiometric dating results from Jurassic intrusions in south Morocco. Geophysical Journal of the Royal Astronomical Society, 24, 351–364,.

Hamilton, E. L., 1978. Sound velocity-density relations in sea-floor sediments and rocks. J. Acoust. Soc. Am., 63, 366-377.

Harmand, C., Cantagrel, J.M., 1984. Le volcanisme alcalin Tertiaire et Quaternaire du Moyen Atlas (Maroc): Chronologie K/Ar et cadre géodynamique, J. Afr. Earth Sci., 2, 51–55.

Hatzfeld, D., Frogneaux., M., 1981. Intermediate depth seismicity in the western Mediterranean unrelated to subduction of oceanic lithosphere. Nature, 292, 443–445.

Hinz, K., 1972. Results of seismic refraction investigations (Project Anna) in Western Mediterranean, south and north of the island of Mallorca. Bulletin Centre De Recherches Pau-SNPA 6 (2), 405–426.

Hoernle, K., Zhang, Y.S., Graham, D., 1995. Seismic and geochemical evidence for large-scale mantle upwelling beneath the eastern Atlantic and western and central Europe. Nature 374, 34–39.

Hofmeister, A.M., 1999. Mantle values of thermal conductivity and the geotherm from phonon lifetimes. Science 283, 1699–1706.

Holland, T., Powell, R., 1998. An internally consistent thermodynamic data set for phases of petrological interest. Journal of Metamorphic Geology 16, 309-344.

Holland, T., Powell, R., 2001. Calculation of phase relations involving haplogranitic melts using an internally consistent thermodynamic dataset. Journal of Petrology, 42, 673–683.

Huismans, R.S., Beaumont, C., 2007. Roles of lithospheric strain softening and heterogeneity in determining the geometry of rifts and continental margins. Geological Society, London, Special Publications 282, 111–138. doi:10.1144/SP282.6.

Hung, S.-H., Dahlen, F.A., Nolet, G., 2001. Wavefront healing: a banana-doughnut perspective. Geophysical Journal International 146 (2), 289–312.

Hyndman, R. D., Shearer, P. M., 1989. Water in the lower continental crust: modelling magnetotelluric and seismic reflection results. Geophysical Journal International, 98(2), 343–365.

Jagoutz, E., Palme, H., Baddenhausen, H., Blum, K., Cendales, M., Dreibus, G., Spettel, B., Lorenz, V., Wanke, H., 1979. The abundance of major, minor and trace elements in the Earth's mantle as derived from primitive ultramafic nodules. Proc. Lunar and Planetary Science Conference 10th, pp. 2031–2205.

Jammes, S., Huismans, R.S., Muñoz, J.-A., 2014. Lateral variation in structural style of mountain building: controls of rheological and rift inheritance. Terra Nova 26, 201–207. doi:10.1111/ter.12087.

Jiménez-Díaz, A., Ruiz, J., Villaseca, C., Tejero, R., Capote R., 2012. The thermal state and strength of the lithosphere in the Spanish Central System and Tajo Basin from crustal heat production and thermal isostasy. Journal of Geodynamics, 58, pp. 29–37.

Jiménez-Munt, I., M. Fernàndez, Vergés, J., Afonso, J.C., Garcia-Castellanos, D., Fullea, J., 2010. Lithospheric structure of the Gorringe Bank: insights into its origin and tectonic evolution. Tectonics, 29, pp. 1–16. ttp://dx.doi.org/10.1029/2009TC002458.

Jiménez-Munt, I., Fernàndez, M., Vergés, J., Garcia-Castellanos, D., Fullea, J., Pérez-Gussinyé, M., Afonso, J.C., 2011. Decoupled crust–mantle accommodation of Africa–Eurasia convergence in the NW Moroccan margin. Journal of Geophysical Research 116, B08403.http://dx.doi.org/10.1029/2010JB008105

Kennett, B.L.N., Engdahl, E.R., Buland, R., 1995. Constraints on seismic velocities in the Earth from travel times. Geophysical Journal International 122, 108–124.

Lavier, L. L., Manatschal., G 2006. A mechanism to thin the continental lithosphere at magma-poor margins. Nature, 440(7082), 324–328, doi:10.1038/nature04608.

Laville, E., Lesage, J.-L., Séguret, M., 1977. Geometrie, cinématique (dynamique) de la tectonique atlasique sur le versant sud du Haut Atlas marocain: Aperçu sur les tectoniques hercyniennes et tardi-hercyniennes. Bulletin de la Société Géologique de France,19, 527–539.

Laville, E., Petit, J.P., 1985. Role of synsedimentary strike-slip faults in the formation

of the Moroccan Triassic basins. Geology 12, 424–427.

Lachenbruch, A.H., Morgan, P., 1990. Continental extension, magmatism and elevation: formal relations and rules of thumb. Tectonophysics 174, 39–62.

Le Roux, V., Bodinier, J.-L., Tommasi, A., Alard, O., Dautria, J.-M., Vauchez, A., Riches, A.J.V., 2007. The Lherz spinel lherzolite: refertilised rather than pristine mantle. Earth and Planetary Science Letters 259, 599–612.

Legendre, C.P., Meier, T., Lebedev, S., Friederich, W., Viereck-Götte, L., 2012. A shear wave velocity model of the European upper mantle from automated inversion of seismic shear and surface waveforms. Geophysical Journal International 191, 282–304. http://dx.doi.org/10.1111/j.1365-246X.2012.05613.x.

López Casado, C., Sanz de Galdeano, C., Molina Palacios, S., Henares Romero, J., 2001. The structure of the Alboran Sea: An interpretation from seismological and geological data. Tectonophysics, 338, 79–95.

Lustrino, M., Wilson, M., 2007. The circum-Mediterranean anorogenic Cenozoic igneous province. Earth-Science Reviews 81, 1–65.

Lustrino, M., Duggen, S., Rosenberg, C.L., 2011. The central–western Mediterranean: anomalous igneous activity in an anomalous collisional tectonic setting. Earth-Science Reviews 104, 1–40.

Manatschal, G., Lavier, L., Chenin, P., 2015. The role of inheritance in structuring hyperextended rift systems: Some considerations based on observations and numerical modeling. Gondwana Research 27, 140–164. doi:10.1016/j.gr.2014.08.006.

Mancilla, F., Stich, D., Morales, J., Julì, J., Diaz, J., Pazos, A., Córdoba, D., Pulgar, J. A., Ibarra, P., Harnafi, M., Gonzalez-Lodeiro, F., 2012. Crustal Thickness variations in northern Marocco. Journal of Geophysical Research 117, B02312.

Mancilla, F., Diaz, J., 2015. High resolution Moho topography map beneath Iberia and Northern Morocco from Receiver Functions analysis. Tectonophysics (accepted pending revision).

Makris, J., Demnati, A., Klussmann, J., 1985. Deep seismic soundings in Morocco and a crust and upper mantle model deduced from seismic and gravity data. Annales Geophysicae 3, 369–380.

Martí, J., Mitjavila, J., Roca, E., Aparicio, A., 1992. Cenozoic magmatism of the Valencia trough (western Mediterranean): relationships between structural evolution and volcanism. Tectonophysics 203, 145–165.

Martínez Catalán, J. R., Arenas, R., Díaz García, F., Rubio Pascual, F. J., Abati, J., Marquınez, J., 1997. Variscan exhumation of a subducted Paleozoic continental margin: The basal units of the Ordenes Complex, Galicia, NW Spain, Tectonics, 15, 106 – 121.

Martínez Poyatos, D., Carbonell, R., Palomeras, I., Simancas, J.F., Ayarza, P., Martí, D., Azor, A., Jabaloy, A., González Cuadra, P., Tejero, R., Martín Parra, L.M., Matas, J., González Lodeiro, F., Pérez-Estaún, A., García Lobón, J.L., Mansilla, L., 2012. Imaging the crustal structure of the Central Iberian Zone (Variscan Belt): The ALCUDIA deep seismic reflection transect. Tectonics 31, 1–21.

Marzán Blas, I., 2000. Régimen térmico en la Península Ibérica. Estructura litosférica a través del Macizo Ibérico y el Margen Sur-Portugués. Tesis Doctoral Universidad de Barcelona (192 pp.).

Matte, P., 1986. Tectonics and plate tectonics model for the Variscan Belt of Europe, Tectonophysics, 126, 329 – 374.

Matte, P., 2001. The Variscan collage and orogeny (480-290 Ma) and the tectonic definition of the Armorica microplate: A review, Terra Nova, 13, 122 – 128.

Mauffret, A., 2007. The Northwestern (Maghreb) boundary of the Nubia (Africa) Plate. Tectonophysics, 429, 21–44.

Medialdea, J., Maldonado, A., Alonso, B., Díaz, J.I., Farrán, M., Giró, S., Vázquez, A., Sainz-Amor, E., 1986. Mapa geológico de la plataforma continental española y zonas adyacentes. E. 1: 200.000. Memoria y Hoja nos 41 y 42. Tarragona. Instituto Geológico y Minero de España. Madrid, 78 pp.

Michard-Vitrac, A., Albarede, F., Dupuis, C., Taylor Jr., H.P., 1980. The genesis of Variscan (hercynian) plutonic rocks: inferences from Sr, Pb and O studies on the Maladeta igneous complex, Central Pyrenees, Spain. Contributions to Mineralogy and Petrology 72, 57–72.

McDonough, W.F., Sun, S., 1995. The composition of the Earth. Chemical Geology 120, 223–253.

McKenzie, D.P., 1978. Some remarks on the development of sedimentary basins. Earth

and Planetary Science Letters 25–32.

McKerrow, W. S., Mac Niocaill, C., Ahlberg, P. E., Clayton, G., Cleal, C. J., Eagar, G., 2000. The Late Palaeozoic relations between Gondwana and Laurussia, in Orogenic Processes: Quantification and Modelling in the Variscan Belt, edited by W. Franke et al., Geol. Soc. Spec. Publ., 179, 9 – 20.

Medialdea, J., Maldonado, A., Alonso, B., Díaz, J.I., Farrán, M., Giró, S., Vázquez, A., Sainz-Amor, E., 1986. Mapa geológico de la plataforma continental española y zonas adyacentes. E. 1: 200.000. Memoria y Hoja nos 41 y 42. Tarragona. Instituto Geológico y Minero de España. Madrid. 78 pp.

Medina, F., Cherkaoui, T., 1991. Focal mechanisms of the Atlas earthquakes, and tectonic implications. Geologische Rundschau, 80, 639–648.

Mendia, M.S., Ibarguchi, J.I.G., 1991. High-grade metamorphic rocks and peridotites along the Leiza Fault (Western Pyrenees, Spain). Geologische Rundschau, 80, 93–107.

Michard, A., Chalouan, A., Feinberg, H., Goffé, B., Montingny, R., 2002. How does the Alpine belt end between Spain and Morocco. Bulletin de la Société Géologique de France 173, 3–15.

Mickus, K., Jallouli, C., 1999. Crustal structure beneath the Tell and Atlas Mountains (Algeria and Tunisia) through the analysis of gravity data. Tectonophysics 314, 373–385.

Monna, S., Cimini, G., Montuori, C., Matias, L., Geissler, W.H., Favali, P., 2013. New insights from seismic tomography on the complex geodynamic evolution of two adjacent domains: Gulf of Cadiz and Alboran Sea. Journal of Geophysical Research 118(4), 1587–1601, http://dx.doi.org/10.1029/2012JB009607.

Morgan, P., Ramberg, I.B., 1987. Physical changes in the lithosphere associated with thermal relaxation after rifting. Tectonophysics, 143, 1–11.

Morel, J.-L., M. Zouine, Poisson, A., 1993. Relations entre la subsidence des bassins moulouyens et la création des reliefs atlasiques (Maroc): Un exemple d'inversion tectonique depuis le Néogene. Bulletin de la Societe Geologique de France, 93 (1), t. 164, 79–91.

Morel, J.-L., Zouine, M., Andrieux, J., FaureMuret, A., 2000. De´formations néogenes et quaternaires de la bordure nord haut atlasique (Maroc): Role du socle et

conséquences structurales. Journal of African Earth Sciences, 30, 119–131.

Muñoz, J.A., Martínez, A., Vergés, J., 1986. Thrust sequences in the eastern Spanish Pyrenees. Journal of Structural Geology 8 (3/4), 399–405.

Muñoz, J.A., 1992. Evolution of a continental collision belt: ECORS—Pyrenees crustal balanced section. In: McClay, K.R. (Ed.), Thrust Tectonics. Chapman and Hall, London, pp. 235–246.

Muñoz, J.A., 2002. The Pyrenees, in the geology of Spain. In: Gibbons, W., Moreno, T. (Eds.). Geological Society of London, pp. 370–385.

Nance, R.D., Gutiérrez-Alonso, G., Keppie, J.D., Linnemann, U., Murphy, J.B.,Quesada, C., Strachan, R.A., Woodcock, N.H., 2012. A brief history of the Rheic Ocean. Geoscience Frontiers, v. 3, 125-135.

Natali, C., Beccaluva, L., Bianchini, G., Ellam, R.M., Siena, F., Stuart, F.M., 2013. Carbonated alkali-silicate metasomatism in the North Africa lithosphere: evidence from Middle Atlas spinel-lherzolites, Morocco. Journal of South American Earth Sciences 41, 113–121.

Palomeras, I., Carbonell, R., Ayarza, P., Fernàndez, M., Simancas, J.F., Martinez-Poyatos, D., González Lodeiro, F., Pérez-Estaún., A., 2011. Geophysical model of the lithosphere across the Variscan Belt of SW-Iberia: Multidisciplinary assessment, Tectonophysics, 508(1–4), 42–51, doi:10.1016/j.tecto.2010.07.010.

Palomeras, I., Thurner, S., Levander, A., Liu, K., 2014. Finite-frequency Rayleigh wave tomography of the western Mediterranean: Mapping its lithospheric structure. Geochemistry, Geophysics, Geosystems, 15, 140–160, doi:10.1002/2013GC004861.

Pascal, G., Torné, M., Buhl, P., Watts, A.B., Mauffret, A., 1992. Crustal and velocity structure of the València trough (western Mediterranean), Part II. Detailed interpretation of five Expanded Spread Profiles. Tectonophysics 203, 21–35.

Pavlis, N.K., Holmes, S.A., Kenyon, S.C., Factor, J.K., 2008. An Earth Gravitational Model to Degree 2160: EGM 2008, presented at Session G3: “GRACE Science Applications”. EGU, Vienna.

Pedreira, D., Pulgar, J.A., Gallart, J., Dıaz, J., 2003. Seismic evidence of Alpine crustal thickening and wedging from the western Pyrenees to the Cantabrian Mountains (north Iberia), J. Geophys. Res., 108(B4), 2204, doi:10.1029/2001JB001667.

Pedreira, D., Pulgar, J. A., Gallart, J., Torné, M., 2007. Three-dimensional gravity and magnetic modeling of crustal indentation and wedging in the western Pyrenees-Cantabrian Mountains. Journal of Geophysical Research, 112, B12405, doi:10.1029/2007JB005021.

Pedreira, D., Afonso, J.C., Pulgar, J.A., Gallastegui, J., Carballo, A., Fernàndez, M., García-Castellanos, D., Jiménez-Munt, I., Semprich, J., 2015. Geophysical-petrological modeling of the lithosphere beneath the Cantabrian Mountains and the North-Iberian margin: geodynamic implications. Lithos (accepted).

Pérez-Estaún, A., Bea, F. (eds), 2004. Macizo Ibérico. In: J.A. Vera (ed), Geología de España, SGE-IGME, Madrid, 19-230.

Pérez Estaún, A., Martínez Catalán, J.R., Bastida, F., 1991. Crustal thickening and deformation sequence in the footwall to the suture of the Variscan belt of northwest Spain. Tectonophysics, 191, 243-253.

Pérez-Gussinyé, M., Reston, T.J., 2001. Rheological evolution during extension at nonvolcanic rifted margins: onset of serpentinization and development of detachments leading to continental breakup. Journal of Geophysical Research: Solid Earth (1978–2012) 106, 3961–3975.

Pérez-Gussinyé, M., Watts, A.B., 2005. The long-term strength of Europe and its implications for plate-forming processes. Nature, 436(7049), 381–384.

Piromallo, C., Morelli, A., 2003. P wave tomography of the mantle under the Alpine–Mediterranean area. Journal of Geophysical Research 108 (B2), 2065. http://dx.doi.org/10.1029/2002JB001757.

Platt, J. P., Allerton, S., Kirker, A., Mandeville, C., Mayfield, A., Platzman, E.S., Rimi, A., 2003. The ultimate arc: Differential displacement, oroclinal bending, and vertical axis rotation in the External Betic-Rif arc. Tectonics, 22 (3), 1017, doi:10.1029/2001TC001321.

Poudjom Djomani, Y.H., O'Reilly, S.Y., Griffin, W.L., Morgan, P., 2001. The density structure of subcontinental lithosphere through time. Earth and Planetary Science Letters 184, 605–621.

Pous, J., Ledo, J., Marcuello, A., Daignieres, M., 1995. Electrical resistivity model of the crust and upper mantle from a magnetotelluric survey through the central Pyrenees. Geophysical Journal International 121, 750–762.

Pulgar, J.A., Pérez Estaún, A., Gallart, J., Álvarez Marrón, J., Gallastegui, J., Alonso, J.L., ESCI-N Group., 1995. The ESCI-N2 deep seismic reflection profile: a traverse across the Cantabrian Mountains and adjacent Duero basin. Revista de la Sociedad Geológica de España, 8, 383-394.

Pulgar, J. A., Gallart, J., Fernández-Viejo, G., Pérez-Estaún, A., Alvarez-Marrón, J., ESCIN Group 1996. Seismic image of the Cantabrian Mountains in the western extension of the Pyrenees from integrated ESCIN reflection and refraction data. Tectonophysics, 264(1-4), 1–19.

Pulgar, J. A., A. Pérez-Estaún, J. Gallart, J. Alvarez-Marrón, J. Gallastegui, J. L. Alonso, and E. Group (1997), The ESCI-N2 deep seismic reflection profile: a traverse across the Cantabrian Mountains and adjacent Duero basin, Rev. Soc. Geol. España, 8(4), 383–394.

Quesada, C., Fonseca, P., Munha, J., Oliveira, J. T., Ribeiro, A., 1994. The Beja-Acebuches Ophiolite (Southern Iberia Variscan fold belt): Geological characterization and geodynamic significance, Bol. Geol. Min., 105, 3 – 49,

Quintana, L., 2012. Extensión e Inversión Tectónica en el sector central de la Región Vasco-Cantábrica (Cantabria-Vizcaya, norte de España). Unpublished PhD Thesis, Universidad de Oviedo, Spain, 560 pp, 2 maps and 5 cross-section plates.

Quintana, L., Pulgar, F.J., Alonso J.L., 2015. Displacement transfer from borders to plate interior along a mid-crustal detachment: a crustal transect across the Iberian plate. Tectonophysics (accepted pending revision).

Raffone, N., Chazot, G., Pin, C., Vannucci, R., Zanetti, A., 2009. Metasomatism in the lithospheric mantle beneath Middle Atlas (Morocco) and the origin of Fe- and Mg-rich Wehrlites. Journal of Petrology 50, 197–249.

Ramdani, F., 1998. Geodynamic implications of intermediate-depth earthquakes and volcanism in the intraplate Atlas mountains (Morocco). Physics of the Earth and Planetary Interiors, 108, 245–260.

Ribeiro, A., Pereira, E., Dias, R., 1990a. Part IV Central Iberian Zone, allochthonous sequences, in Pre-Mesozoic Geology of Iberia, edited by R. D. Dallmeyer and E. Martínez-García, pp. 220 –236, Springer-Verlag, New York.

Ribeiro, A., Kullberg, M.C., Manupella, G., Phipps, S., 1990b. A review of Alpine tectonics in Portugal: foreland detachment and cover rocks. Tectonophysies, 184,

357-366.

Rimi, A., Fernandez, M., Manar, A., Matsushima, J., Okubo, Y., Morel, J.L., 2005. Geothermal anomalies and analysis of gravity, fracturing and magnetic features in Morocco. World Geothermal Congress Antalya, Turkey, vol. 2, pp. 4–290.

Roca, E., Sans, M., Cabrera, L., Marzo, M., 1999. Oligocene to Middle Miocene evolution of the Central Catalan margin (North-western Mediterranean). Tectonophysics 315, 209–229.

Roca, E., Frizon de Lamotte, D., Mauffret, A., Bracène, R., Vergés, J., Benaouali, N., Fernandez, M., Muñoz, J.A., Zeyen, H., 2004. TRANSMED transect II. In: Cavazza, W., Roure, F., Spakman, W., Stampfli, G.M., Ziegler, P. (Eds.), The TRANSMED Atlas—the Mediterranean Region from Crust to Mantle. Springer, Berlin Heidelberg.

Roca, E., Muñoz, J.-A., Ferrer, O., Ellouz, N., 2011. The role of the Bay of Biscay Mesozoic extensional structure in the configuration of the Pyrenean orogen: Constraints from the MARCONI deep seismic reflection survey. Tectonics 30, TC2001. doi:10.1029/2010TC002735.

Rodríguez Fernández, L.R., Bellido, F., Díez Montes, A., Gallastegui, G., González Clavijo, E., López Olmedo, F., Marín, C., Martín Parra, L.M., Martín Serrano, A., Matas, J., Montes, M., Nozal, F., Roldán, F., Rubio, F., 2004. Mapa Geológico de España, E:1:2,000,000. IGME.

Rosenbaum, G., Lister, G.S., Duboz, C., 2002. Reconstruction of the tectonic evolution of the western Mediterranean since the Oligocene. Journal of the Virtual Explorer, 8, 107–130.

Rubie, D.C., 1990. Role of kinetics in the formation and preservation of eclogites, in Eclogite Facies Rocks, edited by D. A. Carswell, pp. 111–140, Blakie, Glasgow.

Rudnick, R. L., Fountain, D. M., 1995. Nature and composition of the continental crust: a lower crustal perspective. Reviews of Geophysics, 33(3), 267–309.

Rudnick, R.L., Gao, S., 2003. Composition of the continental crust, in: Rudnick, R.L., Holland, H.D., Turekian, K.K. (Eds.). Treatise on Geochemistry, Vol. 3: the Crust. Elsevier, Oxford, pp. 1–64.

Ruiz, M., 2007. Caracterització estructural i sismotectònica de la litosfera en el domini Pirenaico-Cantàbric a partir de mètodes de sísmica activa i passiva. PhD Thesis, Universidad de Barcelona, 1–354.

Ruiz, M., Díaz, J., Gallart, J., Pedreira, D., Pulgar, J.A., 2015. Seismic structure of the North Iberian continental margin from wide-angle data of MARCONI survey. In prep.

Ruiz-Constan, A., Pedrera, A., Galindo-Zaldívar, J., Pous, J., Arzate, J., Roldn-García, F.J., Marin-Lechado, C., Anahnah, F., 2012. Constraints on the frontal crustal structure of a continental collision from an integrated geophysical research: The central-western Betic Cordillera (SW Spain). Geochemistry, Geophysics, Geosystems, 13 (8), art. no. Q08012.

Sàbat, F., Muñoz, J.A., Santanach, P., 1988. Transversal and oblique structures at the Serres de Llevant thrust belt (Mallorca Island). Geologische Rundschau 77, 529–538.

Sàbat, F., Roca, E., Muñoz, J.A., Vergés, J., Santanach, P., Masana, E., Sans, M., Estévez, A., Santisteban, C., 1997. Role of extension and compression in the evolution of the eastern margin of Iberia: the ESCI-València trough seismic profile. Revista de la Sociedad Geológica de España 8, 431–448.

Sandwell, D.T., Smith, W.H.F., 1997. Marine gravity from Geosat and ERS 1 satellite altimetry. Journal of Geophysical Research 102, 10,039–10,054.

Schettino, A., Turco, E., 2010. Tectonic history of the western Tethys since the Late Triassic. Geological Society of America Bulletin 123, 89–105. http://dx.doi.org/10.1130/B30064.1.

Schaer, J.P., 1987. Evolution and structure of the High Atlas of Morocco. In: Schaer, J.P., Rodgers, J. (Eds.). The Anatomy of Mountain Ranges. Princeton University Press, New Jersey, pp. 107–127.

Schmid, S.M., Bernoulli, D., Fügenschuh, B., Matenco, L., Schefer, S., Schuster, R., Tischler, M. and Ustaszewski, K., 2008. The Alpine-Carpathian-Dinaridic orogenic system: correlation and evolution of tectonic units. Swiss Journal of Geosciences, 101(1): 139-183.

Semprich, J., Simon, N. S. C., Podladchikov Y. Y., 2010. Density variations in the thickened crust as a function of pressure, temperature, and composition. International Journal of Earth Sciences (Geol Rundsch), 99(7), 1487–1510, doi:10.1007/s00531-010-0557-7.

Sibuet, J.C., Collette, B.J., 1991. Triple junctions of Bay of Biscay and North Atlantic: New constraints on the kinematic evolution. Geology, 19, 522-525.

Sibuet, J.C., 2004. Pyrenean orogeny and plate kinematics. Journal of Geophysical Research, 109(B8), doi:10.1029/2003JB002514.

Silva, J. B., Oliveira, J. T., Ribeiro, A., 1990. Part VI South Portuguese Zone, structural outline, in Pre-Mesozoic Geology of Iberia, edited by R. D. Dallmeyer and E. Martínez-García, pp. 348 – 362, Springer-Verlag, New York.

Simancas, J. F., Martínez Poyatos, D., Expósito, I., Azor, A., González lodeiro, F., 2001. The structure of a major suture zone in the SW Iberian Massif: The Ossa-Morena/Central Iberian contact, Tectonophysics, 332, 295 – 308.

Simancas, J.F., Carbonell, R., González Lodeiro, F., Pérez-Estaún, A., Juhlin, C., Ayarza, P., Kashubin, A., Azor, A., Martínez-Poyatos, D., Almodóvar, G. R., Pascual, E., Sáez, R., Expósito, I., 2003. Crustal structure of the transpressional Variscan orogen of SW Iberia: SW Iberia deep seismic reflection profile (IBERSEIS), Tectonics, 22(6), 1062, doi:10.1029/2002TC001479.

Smith, W.H.F., Sandwell, D.T., 1997. Global Sea Floor Topography from Satellite Altimetry and Ship Depth Soundings. Science 277, 1956–1962. doi:10.1126/science.277.5334.1956

Spakman, W., Wortel, M.J.R., 2004. A tomographic view on western Mediterranean geodynamics. In: Cavazza, W., Roure, F., Spakman, W., Stampfli, G.M., Ziegler, P. (Eds.), The TRANSMED Atlas—the Mediterranean region from crust to mantle. Springer, Berlin Heidelberg, pp. 31–52.

Srivastava, S., Roest, W. R., Kovacs, L. C., Okay, G., Levesque, S., Verhoef, J., Macnab, R., 1990. Motion of Iberia since the late Jurassic: Results from detailed aeromagnetic measurements in the Newfoundland basin. Tectonophysics, 184, 229–260.

Stich, D., Ammon, C.J., Morales, J., 2003. Moment tensor solutions for small and moderate earthquakes in the Ibero–Maghreb region. Journal of Geophysical Research 108 (B3), 2148. http://dx.doi.org/10.1029/2002JB002057.

Suriñach, E., Vegas, R., 1988. Lateral inhomogeneities of the Hercynian crust in central Spain. Physics of the Earth and Planetary Interiors 51, 226–234.

Talwani, M., Worzel, J., Landisman, L., 1959. Rapid computations for two-dimensional bodies with application to the Mendocino submarine fracture zone. Journal of Geophysical Research 64, 49 – 59.

Teixell, A., Arboleya, M.L., Julivert, M., Charroud, M., 2003. Tectonic shortening and topography of the central High Atlas (Morocco). Tectonics, 22, 1051, doi:10.1029/2002TC001460.

Teixell, A., Ayarza, P., Zeyen, H., Fernàndez, M., Arboleya, M.L., 2005. Effects of mantle upwelling in a compressional setting: the Atlas Mountains of Morocco. Terra Nova, 17: 456-461.

Tejero, R., Ruiz, J., 2002 .Thermal and mechanical structure of the central Iberian Peninsula lithosphere. Tectonophysics, 350, pp. 49–62.

Termier, H., 1936. Etudes geologiques sur le Maroc central et le Moyen Atlas septentrional. Notes et Memoires du Service de Mines et Carte Geologique du Maroc 33, p. 1566.

Thybo, H., Artemieva, I.M., 2014. Moho and magmatic underplating in continental lithosphere. Tectonophysics 609, 605–619.

Torné, M., De Cabissole, B., Bayer, R., Casas, A., Daignières, M., Rivero, A., 1989. Gravity constraints on the deep structure of the Pyrenean belt along the ECORS profile. Tectonophysics 165, 105–116.

Torne, M., Pascal, G., Buhl, P., Watts, A.B., Mauffret, A., 1992. Crustal structure of the Valencia Trough (Western Mediterranean). Part 1. A combined refraction/wide angle reflection and near-vertical reflection study. Tectonophysics 203, 1–20.

Torné, M., Banda, E., Fernàndez, M., 1996. The Valencia Trough: geological and geophysical constraints on basin formation models. In: Ziegler, P.A., Horvàth, F. (Eds.), Peri-Tethys Memoir 2: Structure and Prospects of Alpine Basins and Forelands. Mémoires Muséum National d'Histore Naturelle, 170, pp. 103–128.

Torne, M., Fernandez, M., Comas, M.C., Soto, J., 2000. Lithospheric structures beneath the Alboran Basin: Results from three-dimensional gravity modeling and tectonic relevance. Journal of Geophysical Research 105, 3209–3228.

Torne, M., Fernandez, M., Vergés, J., Ayala, C., Salas, M.C., Jiménez-Munt, I., Buffet, G.G., 2015. Crustal and mantle lithospheric structure of the Iberian Peninsula deduced from potential field and thermal modeling. Tectonophysics (accepted pending revision).

Torres Roldán, R.L., Poli, G., Pecerillo, A., 1986. An Early Miocene arc-tholeiitic magmatic dike event form the Alboran Sea. Evidence for preocolisional subduction

and back-arc crustal extension in the westernmost Mediterranean. Geologische Rundschau, 7: 219-234.

Tugend, J., Manatschal, G., Kusznir, N.J., Masini, E., Mohn, G., 2014. Formation and deformation of hyperextended rift systems: Insights from rift domain mapping in the Bay of Biscay-Pyrenees. Tectonics, in press, 10.1002/2014TC003529.

Tunini, L., Jiménez-Munt, I., Fernandez, M., Vergés, J., Villaseñor, A., 2014. Lithospheric mantle heterogeneities below the Zagros Mountains and the Iranian Plateau: a petrological-geophysical study. Geophysical Journal International, Volume 200, Issue 1, p.596-614.

Turner, S. P., Platt, J.P., George, R.M.M., Kelley, S.P., Pearson, D.G., Nowell, G.M., 1999. Magmatism associated with orogenic collapse of the Betic-Alboran domain, SE Spain. Journal of Petrology, 40 (6), 1011–1036.

Van Hinsbergen, D. J. J., Vissers, R.L.M., Spakman, W., 2014. Origin and consequences of western Mediterranean subduction, rollback, and slab segmentation. Tectonics, 33, 393–419, doi:10.1002/tect.20125.

Vegas, R., Vazquez, J.T., Suriñach, E., Marcos, A., 1990. Model of distribuited deformation, block rotations and crustal thickening for the formation of the Spanish central System. Tectonophysics, 184, 367-378.

Vera, J.A., 2004. Geología de España, Sociedad Geológica de España-Instituto Geológico y Minero de España. Madrid, pp. 884.

Vergés, J., Fernàndez, M., 2012. Tethys–Atlantic interaction along the Iberia–Africa plate boundary: the Betic–Rif orogenic system. Tectonophysics 579, 144–172. http://dx.doi.org/10.1016/j.tecto.2012.08.032.

Vergés, J., Fernàndez, M., 2006. Ranges and basins in the Iberian Peninsula: their contribution to the present topography. Geological Society, London, Memoirs 32, 223–234.

Vergés, J., Sàbat, F., 1999. Constraints on the western Mediterranean kinematic evolution along a 1,000-km transect from Iberia to Africa. In: Durand, B., Jolivet, L., Horváth, F., Séranne, M. (Eds.), On the Mediterranean Basins: Tertiary Extension within Alpine orogen. Geological Society London Special Publications, 134, pp. 63–80.

Vergés, J., Millan, H., Roca, E., Muñoz, J.A., Marzo, M., Cirés, J., den Bezemer, T.,

Zoetemeijer, S., Cloethingh, R., 1995. Eastern Pyrenees and related foreland basins: Pre-, syn- and post-collisional crustal-scale cross-sections. Marine and Petroleum Geology 12, 903–916.

Vidal, N., Gallart, J., Danobeitia, J.J., 1998. A deep seismic transect from the NE Iberian Peninsula to the Western Mediterranean. Journal of Geophysical Research 103, 12381–12396.

Vielzeuf, D., 1984. Relations de phases dans le faciès granulite et implications géodynamiques: l'exemple des granulites des Pyrénées. Université de Clermont-Ferrand II.

Vilà, M., Fernandez, M., Jiménez-Munt, I., 2010. Radiogenic heat production variability of some common lithological groups and its significance to lithospheric thermal modeling. Tectonophysics 490, 152–164.

Villaseca, C., Downes, H., Pin, C., Barbero, L., 1999. Nature and composition of the lower continental crust in Central Spain and the granulite-granite linkage: Inferences from granulitic xenoliths. Journal of Petrology 40, 1465–1496.

Villaseca, C., Ancochea, E., Orejana, D., Jeffries, T., 2010. Composition and evolution of the lithospheric mantle in central Spain: inferences from peridotite xenoliths from the Calatrava volcanic field. Geological Society of London. Special Publication, 337, 125-152.

Villaseñor, A., Spakman, W., Engdahl, E.R., 2003. Influence of regional travel times in global tomographic models. Geophysical Research Abstracts. EAE03-A-08614, EGS-AGU-EUG Joint Assembly, Nice, France, vol. 5.

Vissers, R. L. M., Meijer, P. T., 2012. Iberian plate kinematics and Alpine collision in the Pyrenees. Earth-Science Reviews, 114(1-2), 61–83, doi:10.1016/j.earscirev.2012.05.001.

Vosteen, H.-D., Schellschmidt, R., 2003. Influence of temperature on thermal conductivity, thermal capacity and thermal diffusivity for different types of rock. Physics and Chemistry of the Earth, Parts A/B/C 28, 499–509. doi:10.1016/S1474-7065(03)00069-X.

White, R. W., Powell, R., Holland, T. J. B., 2001. Calculation of partial melting equilibria in the system $Na_2O$-CaO-$K_2O$-FeO-MgO-$Al_2O3$-$SiO_2$-$H_2O$ (NCKFMASH). Journal of Metamorphic Geology, 19, 139–153.

Wilson, M., Bianchini, G., 1999. Tertiary–Quaternary magmatism within the Mediterranean and surrounding regions. London Geological Society, Special Publication 156, 141–168.

Wilson, M., Downes, H., 1992. Mafic alkali magmatism associated with the European Cenozoic rift system. Tectonophysics 208, 173-182.

Wilson, M., Downes, H., 2006. Tertiary-Quaternary intra-plate magmatism in Europe and its relationship to mantle dynamics. In: Stephenson, R., Gee, D. (Eds.) European lithosphere dynamics. Geological Society of London Memoir 32, 137-146.

Wilson, M., Patterson, R., 2001. Intraplate magmatism related to short-wavelength convective instabilities in the upper mantle: evidence from the Tertiary–Quaternary volcanic province of western and central Europe. In: Ernst, R.E., Buchan, K.L. (Eds.), Mantle Plumes: Their Identification Through Time. Geological Society of America Special Paper, vol. 352, pp. 37–58.

Working Group for Deep Seismic Sounding in the Alboran Sea, Crustal Seismic profiles in the Alboran sea: Preliminary results, 1974. Pure and Applied Geophysics, 116, 67-180.

Zeyen, H., Fernandez, M., 1994. Integrated lithospheric modelling combining thermal, gravity, and local isostasy analysis: application to the NE Spanish geotransect. Journal of Geophysical Research 99, 18089–18102.

Zeyen, H., Ayarza, P., Fernandez, M., Rimi, A., 2005. Lithospheric structure under the western African-European plate boundary: A transect across the Atlas Mountains and the Gulf of Cadiz, Tectonics, 24, TC2001, doi:10.1029/2004TC001639.